Photochemical Electron Transfer Across Surfactant Vesicle Bilayers

a thesis presented by

COLIN JOHN GRUBB

to the Faculty of Science of the University of St. Andrews

in application for the Degree of

DOCTOR OF PHILOSOPHY

St. Andrews

November 1995

DECLARATION

I, Colin John Grubb, certify that this thesis has been composed by myself, that it is a record of my own work, and has not been submitted in any previous application for a higher degree.

Signed: Date: 4/3/96

I was admitted to the Faculty of Science in the University of St. Andrews under Ordinance General No. 12 on 1 October 1992 and as a candidate for the higher degree of Doctor of Philosophy on 1 October 1992.

Signed:..... Date: 4/3/96

CERTIFICATION

I hereby certify that Colin John Grubb, B.Sc. has spent twelve terms of research work under my supervision, and that he has fulfilled the conditions of the Resolution and Regulations appropriate to the degree of Doctor of Philosophy.

Signed: Date: 5th March 1996

D.J. Cole-Hamilton

Supervisor

LIBRARY DECLARATION

In submitting this thesis to the University of St. Andrews, I understand that I am giving permission for it to be made available for use in accordance with regulations of the University Library for the time being in force, subject to any copyright vested in the work not being affected thereby. I also understand that the title and abstract will be published, and that a copy of the work may be made and supplied to any *bona fide* library or research worker.

Signed:.... ..... Date:..... ..

ACKNOWLEDGEMENTS

I would like to take this opportunity to pay very special thanks, to my supervisor, Prof. David J. Cole-Hamilton who was a source of untiring enthusiasm, patience and guidance as well as his "always look on the bright side of life" attitude. In addition, my thanks goes to Dr. Mike Green, BP Chemicals, Sunbury, for valuable discussions and for providing an insight into R & D within the chemical industry.

Thanks also go to :

Dr. Mike Whittlesey and Prof. Robin Perutz, York University for providing and aiding me with Laser Flash Photolysis Studies and to everyone in the inorganic section for making me so welcome.

Dr. Alasdair Christie, St. Andrews University, for providing the equipment and the assistance to allow me to perform the electrochemical studies.

Prof. Robert Hay and Prof. David Gani, St. Andrews University, for allowing me unlimited access to their u.v-visible spectrophotometers.

Dr. Christopher Glidewell, St. Andrews University, for performing the MOPAC calculations and the patience in providing me with the relevant information.

Mr. John Mackie, St. Andrews University, for providing invaluable advice and assistance with regards to the SEM studies.

Prof. Richard Cammack, Kings College London for the kind donation of the enzyme Hydrogenase.

Dr. Nigel Botting, St. Andrews University, for helpful discussions concerning the organic chemistry and enzyme studies associated with this project.

The technical staff of the School of Chemistry, in particular, Jim Bews (Computing), Colin Smith (Glassblowing), Colin Miller (GCMS), Sylvia Smith (CHN), Melanja Smith (NMR) and Caroline Horsburgh (Equipment Lender) and Marjorie Parker for the Jethro Tull collection, with a special thanks to Ian Patterson for chauffeuring me between Dundee and St. Andrews while my hand was healing

The DCH group, in particular, Dr. Charles Lindall, Dr. Jason Nash, Dr. Mike Simpson, Peter Pogorzelec and the rest of the group. To Will "not another presentation to listen too" Weston for being an excellent colleague and a good friend over the last three years.

Finally, let me express a special gratitude to my family who have continually provided support and encouragement as well as showing great tolerance throughout my time as student and without whom this would not have been possible.

List of commonly used symbols

C	Capacitance
C_{dl}	Double layer capacitance
c_o^{σ}, c_R^{σ}	Surface concentrations of O and R
c_O^{∞}, c_R^{∞}	Bulk concentrations of O and R
D	Diffusion coefficient
E	Applied potential
E_e	Equilibrium potential
E_e^{θ}	Standard equilibrium potential
E_p	Peak potential
I	Current density
I_{dl}	Double layer charging current
I_p	Peak current density
i	Current
n	Number of electrons
O	Oxidised species
R	Reduced species
R	Resistance
R_u	Uncompensated solution resistance
T	Temperature (K)
t	Time
α_C, α_A	Transfer coefficients for the cathodic and anodic processes
δ	NMR chemical shift
ε	Extinction Coefficient
η	Overpotential
υ	Sweep rate

Constants

Faraday constant	F	=	96485 C mol^{-1}
Gas constant	R	=	8.314 51 $JK^{-1}mol^{-1}$

ABBREVIATIONS

ACES	(2-[2-Amino-2-oxoethyl]amino)ethanesulfonic acid
ADA	N-[2-Acetamido]-2-iminoacetic acid
BES	2-[bis(2-Hydroxyethyl)amino]ethanesulfonic acid
BisTris	2-bis[2-hydroxyethyl]amino-2-[hydroxymethyl]-1,3-propanediol
BisTrispropane	[1,3-bis[tris(hydroxymethyl)methylamino]propane
AQDS	disodium-9,10-anthraquinone-1,5-disulphonate
$AQDSH_2$	disodium-9,10-hydroquinone-1,5-disulphonate
ATP	Adenosine triphosphate
BFDN	4,7-benzofurazandicarbonitrile
BTDB	dibutyl ester of 2,1,3-benzothiadiazole-4,7-dicarboxylic acid
BTDE	diethyl ester of 2,1,3-benzothiadiazole-4,7-dicarboxylic acid
BTDN	2,1,3-benzothiadiazole-4,7-dicarbonitrile
CTAB	cetyltrimethylammonium bromide
DMF	Dimethylformamide
DODAB	Dioctadecylammonium bromide
EDTA	ethylenediaminetetraacetate
HEPES	N-[2-Hydroxyethyl]piperazine-N-[2-ethanesufonic acid]
MES	4-morpholineethanesulphonic acid
MOPS	3-[N-Morpholino]propanesulfonic acid
MOPSO	3-[N-Morpholino]-2-hydroxypropanesulfonic acid
MV^{2+}	methylviologen (paraquat)
NADH	nicotinamide adenine dinucleotide
NHE	Hydrogen Electrode
PIPES	1,4-piperazinediethanesulfonic acid
$[Ru(bpy)_3]^{2+}$	*tris* (2,2'-bipyridine)ruthenium(II)
SEM	Scanning Electron Microscopy
SCE	Saturated Calomel Electrode
TEM	Transmission Electron Microscopy
TEOA	Triethanolamine
TES	(N-tris[hydroxymethyl]methyl-2-aminoethanesulfonic acid
Trizma	tris[hydroxymethyl]aminoethane

Chapter 1

Solar Energy Conversion

Chapter 2

Studies of 2,1,3-benzothiadiazole-4,7-dibutylester (BTDB) in Micellar and Non-aqueous Systems

Chapter 3

TEM and Photo-assisted Electron Transfer Studies Across Synthetic Vesicle Bilayers

Chapter 4

Kinetic Studies on Vectorial Electron Transfer Across DODAB Vesicles Using BTDB

Chapter 5

Studies of Benzofurazan-4,7-dicarbonitrile (BFDN) in a Micelle and Vesicle System

Chapter 6

EXPERIMENTAL

Abstract

Diethyl (BTDE) and dibutyl (BTDB) esters of 2,1,3-benzothiadiazole-4,7,-dicarboxylic acid are effective as combined chromophores and electron transfer catalysts in the photochemical transfer of electrons from suitable donors to anthraquinones. The less electron withdrawing nature of the ester groups than of -CN has improved the redox potential and by altering the nature of the ester R group, we can tailor other properties into the molecule such as increasing solubility in the lipophilic environment of the micellar core or vesicle bilayer by increasing the length of the R group.

The stability of the radical anions obtained by reduction decreases in the order $BTDN^{-\cdot}$>$BTDE^{-\cdot}$>$BTDB^{-\cdot}$; correlating inversely with their reducing power. The more transient nature of $BTDB^{-\cdot}$ is compensated for by its more favourable redox, micelle-partition and light absorption properties. The rate of onward electron transfer from all the radical anions is sufficient for it to dominate over the radical decomposition. The rate of electron transfer is the same for each chromophore and this is interpreted in terms of charge compensating diffusion of OH^- or H^+ across the vesicle as being the overall rate determining process. Mechanistic studies have highlighted that transmembrane electron transfer is affected by the diffusion of the radical anion. Attempts will be made to couple the transmembrane electron transfer with the production of H_2.

Kinetic studies carried out on the electron transfer from MES to AQDS in a micellar system mediated by BTDB show that the reaction is first order in [BTDB], light intensity (with saturation at high I) and [MESH] at low concentration. It tends to zero order at higher [MESH] and is zero order in [AQDS] and [H^+] between pH 6.5 and 10. A mechanism is proposed in which the BTDB acts as a chromophore and electron transfer catalyst and the rate determining step is transfer of the electron from $BTDB^{-\cdot}$ to AQDS.

The system can be modified to allow transfer of electrons across a vesicle

bilayer constructed from simple surfactant molecules (DODAB). It is shown that the initial rate of electron transfer depends upon the overall surface area of the vesicle present in solution but that the yield is determined by the availability of MES^- within the inner water pools of the vesicles. For unilamellar vesicles, all of the MES^- present within them is available for reaction but for multilamellar vesicles only the MES^- within the outer bilayer is available.

Kinetic studies upon the vesicular system indicates similar results to those obtained in the micelles except that at higher BTDB concentration the reaction is zero order in all reagents except H^+. This suggests that some process other than electron transfer must be rate determining. Since the rate increases with $[H^+]$, we assume that charge compensating flow of H^+ across the vesicle bilayer is rate determining.

Attempts to couple the transbilayer electron transfer to H_2 production were unsuccessful.

Studies were also carried out on benzofurazan-4,7-dicarbonitrile (BFDN) but it proved to be a less effective electron transfer agent in the micelle system than BTDN or BTDB and was ineffective for electron transfer across the vesicles. Some possible explanations for this behaviour are discussed.

Chapter 1
Solar Energy Conversion

1.0 Introduction

World annual consumption of energy is presently at the enormous value of 4^{18} kJ. and continues to increase, doubling every 15 — 20 years.[1] At the same time the reserves of fossil fuels that now make the main contribution to the energy balance are recognised as limited. It is anticipated that in the near future the energy demands of the world will be satisfied mainly through the growth of coal extraction, and its processing, as well as nuclear sources of electrical energy and heat. Both of these are generally agreed to have the raw material resources for at least the next century.

However, a rapid increase of coal and nuclear fuel use can create some environmental problems, for example, from coal, measures are required to prevent air and water pollution from sulphur oxides, carcinogenic and other toxic substances. The problem of nuclear fission was highlighted after Chernobyl, regarding safety as well as the social consequences. It must be remembered that fissile materials are themselves neither renewable nor available in unlimited amounts. Nuclear fusion has great potential as an inexhaustible supply of energy but is probably decades away from fruition. The raw material of the 20th century, oil, has produced substantial economies but has a limited lifetime as a major source of energy.

These facts have led scientists to search for renewable sources of energy which may be exploited on a commercial basis. Most renewable energy options rely on a net input of energy into the earth. Since the sun is our only external energy source, harnessing its energy is the main objective of almost all alternative energy strategies. The only exceptions being the tides' whose energy is derived from the kinetic energy of the Earth's rotation via the gravitational attraction between the moon and the earth and geothermal energy which can't be described as renewable since the heat largely arises from natural underground decay of radioactive nuclei. These forms of energy are unlikely to make more than a relatively small contribution to the total

energy balance.

Therefore, from a long term prospective, the interest in solar-energy conversion may not be caused by the threat of an energy crisis, rather it may come from a critical situation in ecological terms. The view that solar-energy in all its forms seems to be the most promising source of energy, agrees with the prognosis of the International Energy conference that by the year 2020 as much as 10 — 15% of the world's energy consumption will be provided by solar-energy conversion.[2]

The most important advantage of solar-energy is its ecological purity in offering the opportunity for achieving energy cycles without pollution of the environment and additional heating of the earth. The other forms of non-renewable energy production in contrast would inevitably lead to additional heating of the Earth *via* the greenhouse effect thus necessitating the reduction in consumption of hydrocarbon fossil fuels.

1.1 The Power of Solar-Energy

Solar-energy is continuously received by the earth in amounts largely exceeding the needs of our civilisation. The energy falling on the earth annually is 2.2×10^{22} kJ per year, corresponding to an average power of 10^{17} watts. The present consumption of primary energy in all forms by mankind is 2×10^{17} kJ. per year, corresponding to an average consumption per person of 2000 watts.[2] Therefore, solar-energy input exceeds present use by a factor of 10^4. About 35% of solar-energy (1.2×10^{21} kJ) is lost by reflection from the earth's surface and atmosphere. In addition, absorption processes in the atmosphere, mainly by H_2O and CO_2, remove a large proportion of the IR region of the sun's energy so that the main energy available at sea level is in the visible region.[3] (Figure 1.0)

The rest of the energy is absorbed by the oceans and seas ($\sim 1.76 \times 10^{21}$ kJ) and land ($\sim 7.6 \times 10^{20}$ kJ). A proportion of the energy absorbed $\sim 1.44 \times 10^{18}$ kJ/yr is converted into chemical energy via photosynthesis but only a small portion of this energy is utilised : $\sim 3.2 \times 10^{16}$ kJ/yr as fuels and materials and $\sim 1.6 \times 10^{16}$ kJ/yr as food.[2]

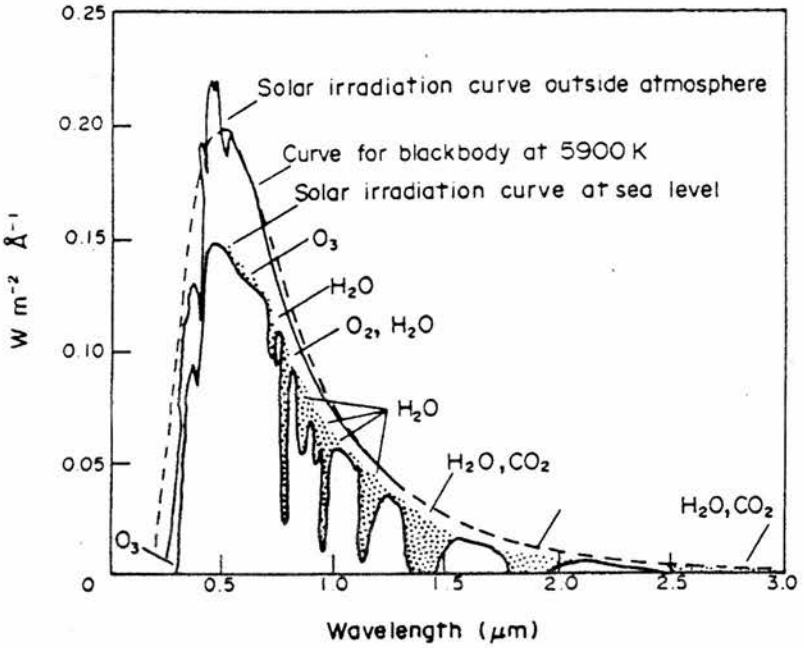

Figure 1.0 : Spectral distribution curves related to the sun. Shaded area indicates absorption at sea level due to the atmospheric constituents shown.[4]

However, solar-energy has several drawbacks:[4]

(i) The density of the solar-energy flux (ca. 1 kWm^{-2} on a clear day with the sun directly overhead).

(ii) Wide wavelength spread

(iii) The energy flux is dependent on the weather and season.

(iv) Conversion of the light energy into a form convenient for use.

It has however been shown that, in theory, it is possible to provide the energy needs of the whole world provided that solar energy can be stored in a usable form and the storage process has an efficiency of 10%. At this efficiency level the available solar-energy would still exceed future requirements by a factor of 150.

Currently, it is possible to convert solar-energy into three principal, more readily usable energy forms: thermal, electrical and chemical.[5,6] Firstly, solar panels, where collection units consisting of a blackened absorber surface, enclosed by one or two layers of silvered glass, absorb the incident radiation and convert the light into heat. The absorbed energy can be transferred to water flowing in or beneath the plate up to a temperature of 50°C with an efficiency of 40%. By using absorbers which are

selective in the visible region and mirror concentrators, temperatures exceeding 100°C can be produced.[7]

The second method is the conversion of solar radiation into electricity by means of a photovoltaic cell which at present is the most sophisticated technical development in solar-energy devices.[7] The silicon cell was developed for powering space vehicles and satellites and is still the most efficient and reliable way of converting solar energy, with efficiencies of about 10% which can be improved if gallium arsenide is employed (>20%). However, with high production costs and the difficulty in interfacing with high power electrical circuits, the use of photovoltaic cells may never be economical other than for special applications.

Thirdly, it may be possible to use photobiological and photochemical methods which set out to convert solar-energy into a gaseous or liquid fuel on a renewable basis. Photobiological processes by "energy forming" are well established. The energy stored in biological materials is made available for direct use in combustion, for example, biomass or as other fuels. In Brazil, petroleum for motor cars is augmented by the addition of 20% ethanol obtained by fermentation of sugar.[8] Unfortunately, the efficiency of such processes, is much less than the previous two methods, rarely exceeding 1%. Furthermore, photobiological systems require energy expenditures in the form of fertilisers, irrigation and harvesting followed by processing.

Therefore, the aim is to develop a process evolved purely on photochemical lines but which is simpler than photosynthesis and produces directly the product required. With this aim in mind the scientific community set out to develop a method for converting solar energy into chemical fuels. The advantage of this method is that it deals with the difficulty related to the dependence of the solar-energy flux on season and weather, by producing energy in a concentrated and versatile form which can be readily stored for use, for example, at night.

Endergonic reactions are considered to be the most promising routes to solar energy conversion. These sunlight induced catalytic reactions involve the conversion

of solar-energy to the form of chemical energy that is stored in a variety of chemical fuels.[2] Mechanistically, there are two different ways of obtaining chemical fuels with solar-energy:

(1) via photocatalytic processes in which the light quanta directly induce endergonic photochemical reactions.

(2) via thermochemical catalytic processes in which reactions that are endergonic at ambient temperatures are thermally driven at high temperature using the heat from the sun.

1.2 Why Hydrogen ?

As indicated above, most of the solar energy arriving on the earth is in the form of light, so that the most efficient of the above processes will be photocatalytic. In this review, we shall concentrate on these and especially on the photocatalytic cleavage of water into hydrogen and oxygen, the former being used as a fuel.

$$H_2O \longrightarrow H_2 + {}^1/_2O_2 \qquad (1)$$

Solar hydrogen production from water has a number of extremely attractive properties.[4] Due to its small weight, the energy storage of H_2 per gram, 119 000J/g^{-1}, is very high. It is, for example, three times higher than the storage capacity of oil (40 000 J/g^{-1}). There is a high abundance of water, making it cheap, while on burning, the water is regenerated which means that no raw material is consumed. Hydrogen can be easily stored and transported, with feasibility studies suggesting that natural gas pipelines in the United States could be converted for the transport of hydrogen gas. A number of manufacturers have demonstrated the feasibility of hydrogen powered aircraft and motor cars. Another factor in the favour of hydrogen as a pure chemical fuel is the value attached to it by the chemical industry.

On combustion, hydrogen is essentially non-polluting, the oxides of nitrogen that can be produced when hydrogen burns in air can be reduced to a minimum by efficient carburation. On the otherhand, the combustion of coal in power stations forms greenhouse gases along with the oxides of sulphur which lead to acid rain and nuclear energy produces large quantities of spent radioactive fuel which has to be

stored for thousands of years before becoming safe.

The main disadvantage of hydrogen is the belief that hydrogen is a highly dangerous commodity with it being associated with explosions, for example, R101 airship. These actual dangers are oversimplified because for a massive explosion to occur hydrogen has to be mixed with oxygen in a 2:1 ratio. Even with such a possibility there is an advantage to be sought from hydrogen through the very low density of the gas which causes explosions to go upwards, therefore limiting damage on the ground. Fires and explosions arising from petroleum fumes are much more dangerous, as they tend to stay at ground level while incinerating everything nearby. There has been extensive material written on the background to a hydrogen based economy.[9-12]

1.3 Photocatalytic Systems for Water Cleavage

Outside living organisms, the process of water cleavage does not occur upon illumination by solar light because water, like other raw materials that we would like to convert into fuel, for example, carbon dioxide and nitrogen, cannot be electronically excited by solar radiation. The electronic absorption spectrum does not overlap the emission spectrum of the sun. Therefore, to accomplish the goal of developing the conversion of solar-energy photochemically, it is necessary to develop photocatalytic systems involving photocatalysts that promote the chemical steps. A photocatalyst is a substance that upon absorption of light photons induces chemical transformations of the reactants via repeated intermediate interaction with the reaction participants while being regenerated after each reaction cycle.[1]

Developments in the use of photocatalytic systems for water cleavage into molecular hydrogen and oxygen are already achieving success. These systems are conventionally divided into two types: (a) Semiconductor and (b) Molecular Photocatalytic systems.

1.3(a) Semiconductor Systems

A number of different approaches are possible with semiconductors as the photoconverter. The two most common methods are[13] (1) where the semiconductor particle acts as an electron relay, this light harvesting unit suitable for water splitting is shown in figures 1.1 and 1.2.

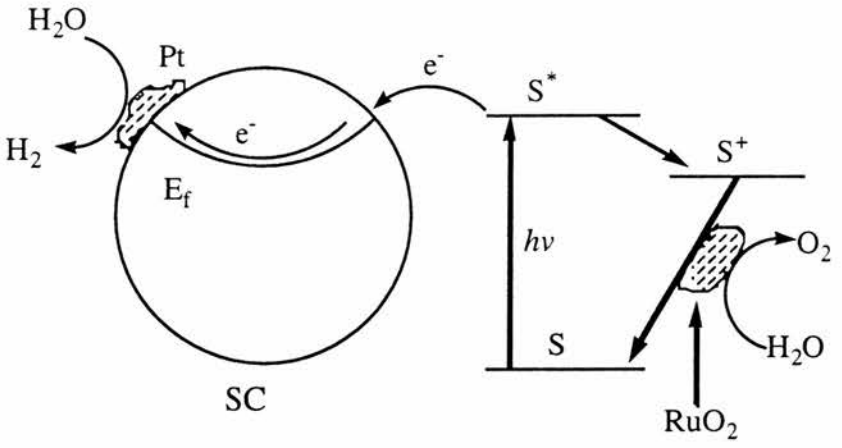

Figure 1.1 : Water splitting scheme using an adsorbed sensitiser and a semiconductor.

Here the photosensitiser (S) is absorbed onto the semiconductor particle (SC). Charge injection from the excited state S* to the conduction band of the SC occurs, following which, the electron (e^-) is channelled to a catalytic site for H_2 evolution. The RuO_2 codeposited on the particle mediates O_2 generation from S^+ and H_2O while regenerating S. For examples in this area see the work by Tabata[14] and Sakata.[15] The second case is shown in Figure 1.2 ;

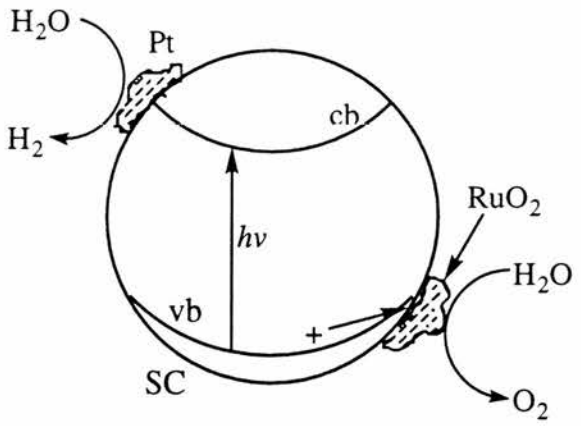

Figure 1.2 : Water cleavage process using a semiconductor particleas the light harvesting unit.

In the second type of system, the SC particle acts as the light harvesting unit. Irradiation with $h\nu$ greater than the band gap generates electron/hole pairs (e^-/h^+) that separately migrate to the particle surface where water reduction and oxidation occur, mediated by surface absorbed redox catalysts. However, no practical examples of this type have been reported.

The advantage of such systems is that the water splitting takes place on a single SC particle, thus avoiding bulk phase diffusion of the reactants. Many different strategies have been considered for the generation and stabilisation of these colloids which include aqueous polymers/polyelectrolytes, non-aqueous solvents and self-organised assemblies.[16-18] Systems of this type have been developed with the efficiency of several percent of solar light conversion into the chemical energy of a hydrogen plus oxygen pair. More detailed information is given in selected reviews by Kamat,[19] Hurst[20] and Hoffman[21] and in the pioneering work by Fujishima and Honda.[22] It is expected that in the near future the efficiency of semiconductor photocatalytic systems for water cleavage will be substantially increased.

1.3(b) Photocatalytic Systems

Molecular photocatalytic systems are based on modelling the scheme of natural photosynthesis on which we are all dependent for food, oxygen and fossil fuels by duplicating the self organisation and reproductive nature of photosynthesis.

Natural photosynthesis in plants and bacteria utilises the sun's energy in primarily converting the light quanta from sunlight into chemical energy in the form of carbohydrates. The basic process involves photoinduced electron transfer across thylakoid membranes using chlorophyll as the photocatalyst. The oxidation of water occurs in the inner surface of the membrane (Photosystem II) and then starts the vectorial transfer of electron to photosystem I located at the outer surface of the membrane where the reduction of carbon dioxide to carbohydrate occurs.[23,24]

A related approach is often used in the design of photocatalytic systems.[25,26] The first stage involves the photosensitiser absorbing light and being promoted to the

excited state.

$$S + h\nu \longrightarrow S^* \qquad (2)$$

The second stage of the cleavage reaction involves a photoinduced charge separation with electron transfer from the excited photosensitiser S* to an acceptor A (oxidative quenching):

$$S^* + A \longrightarrow S^+ + A^- \qquad (3)$$

or to a photosensitiser from a donor D (reductive quenching):

$$S^* + D \longrightarrow S^- + D^+ \qquad (4)$$

Dihydrogen and dioxygen which are the final stable products of water cleavage are formed *via* subsequent dark catalytic processes of water reduction and oxidation by A^- or S^- ($2e^-$ reduction) and D^+ or S^+ ($4e^-$ oxidation) species respectively if they have the appropriate redox potentials.

$$2S^- (\text{or } A^-) + 2H_2O \xrightarrow{CAT_1} 2S (\text{or } A) + H_2\uparrow + 2OH^- \qquad (5)$$

$$4D^+ (\text{or } S^+) + 2H_2O \xrightarrow{CAT_2} 4D (\text{or } S) + O_2\uparrow + 4H^+ \qquad (6)$$

Mechanistically, this pathway is rather similar to the scheme of light to chemical energy conversion during photosynthesis; the difference being, in plants the energy is in the form of carbohydrates and not dihydrogen as in water cleavage.

The redox catalysts in the equations above are needed to overcome the high kinetic barriers associated with multielectron transfer. The thermodynamics of converting photochemical energy to chemical energy are shown in figure 1.3, where S is the sensitiser and A is the electron relay.[27] The excited state of the sensitiser is a better electron donor (oxidant) as well as a better electron acceptor (reductant) than the ground state S. Absorption of light ($h\nu$) can drive a redox reaction nonspontaneously and result in the storage of energy, ΔG, in S^+ and A^-. In the scheme, S^* acts as an

electron donor but may just as well accept an electron from A which could function as an electron donor.

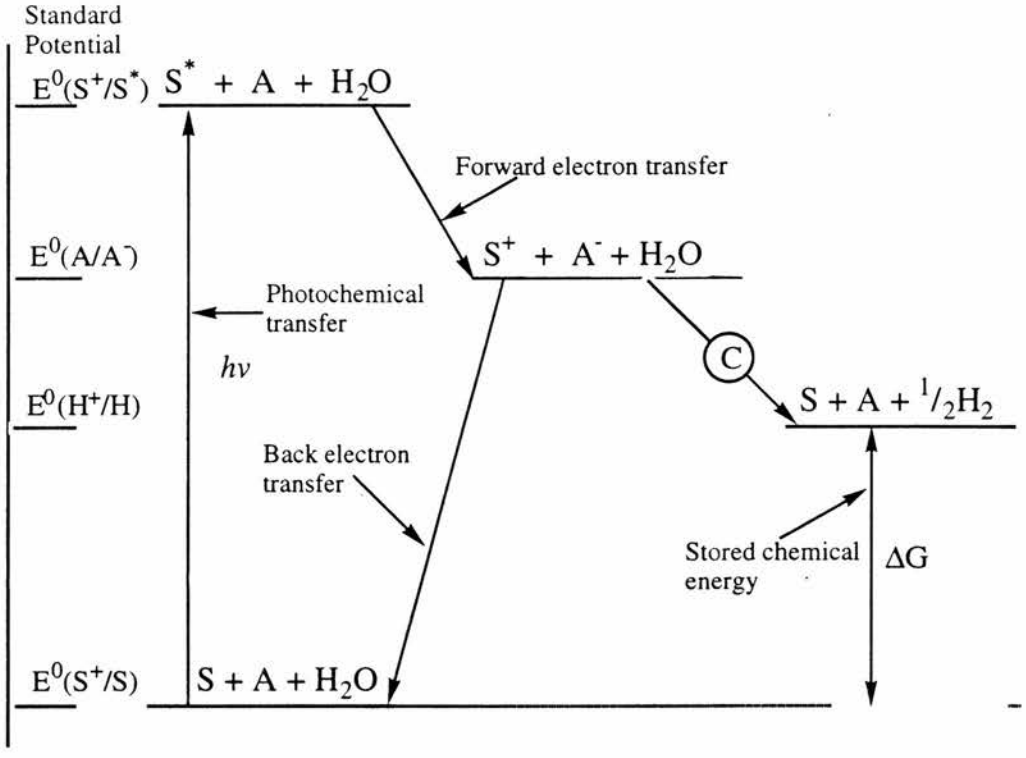

Figure 1.3 : A non-spontaneous light-driven redox reaction which results in energy storage.

In addition, the reactions (5) and (6) are thermodynamically the most favoured and may therefore be affected photochemically over the broadest range of wavelengths of the solar spectrum. Since, ΔG = 1.23 eV per electron for reaction (1), light of λ<1000 nm would be effective, corresponding to a threshold energy of 119 kJ/N$h\nu$ so that about 33% of the energy in the solar spectrum could in principle be stored.[27,3] However, when conversion efficiency factors are taken into account, the thresholds are shifted to shorter wavelengths: $\lambda \leq 600$ nm and $\lambda \leq 900$ nm for one $h\nu$/electron and two $h\nu$/electron, respectively. If free radical intermediates are involved, the threshold wavelengths are substantially shorter (< 370 nm) and efficiencies will not exceed 12%. For a schematic representation of the above information, see figure 1.4, showing the threshold energies and wavelengths for dissociation of water by one, two and four electron processes.[4] Light of any wavelength shorter than the threshold

should be capable of inducing the reaction. However, all photon energy in excess will be transformed into heat.

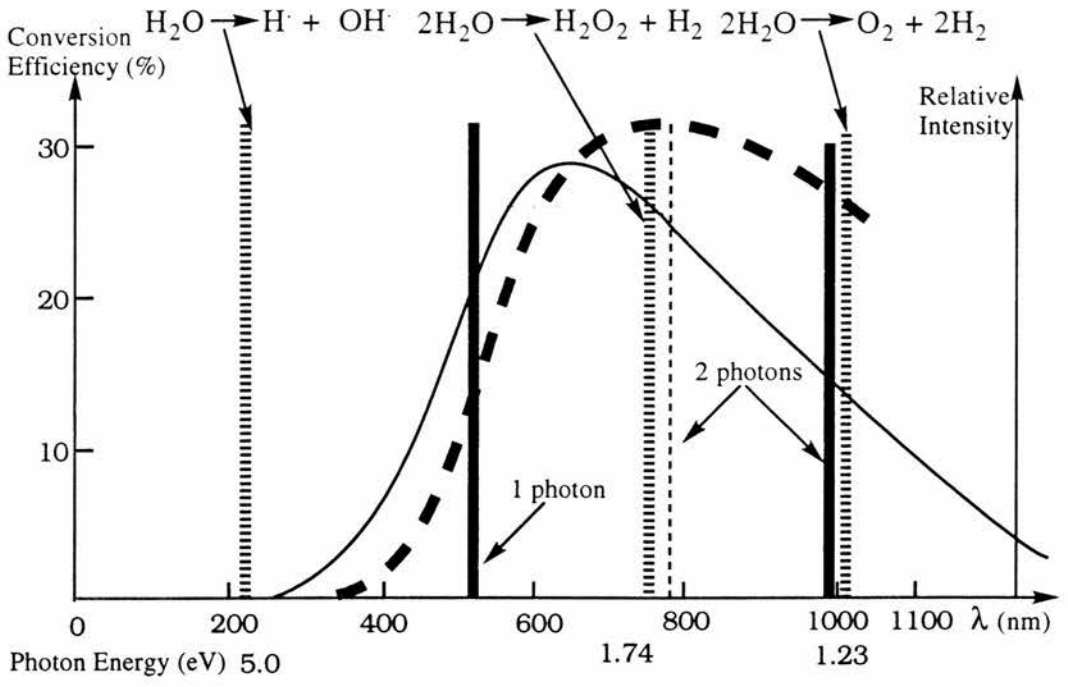

Figure 1.4 : Schematic representation of solar spectral distrubution (—) with theoretical threshold energies and wavelengths (≣) for water dissociation by one, two and four electron processes and solar energy conversion efficiency (▬ ▬) with threshold wavelengths at sea level, the energies (▬) required for water decomposition using one or two photons per H_2O molecule and the threshold wavelengths (- - -) taking into account thermodynamic losses.

It is unlikely that simple homogenous systems, as shown above, would find application in artificial devices that convert sunlight to chemical energy[13] because of two disadvantages: (a) the light driven electron transfer processes are diffusion controlled and (b) there is no kinetic barrier to inhibit the back electron transfer reaction which degrades photons to heat (Figure 1.3).

1.4 Control of Back Electron Transfer

The problem of differentiating the rates of back electron transfer and chemical reaction of radical ions can be addressed in one of two ways[29] : either the rate of the reaction, of the radicals anions can be increased or the rates of back electron transfer between the components can be suppressed.

The factors influencing the rate of back electron transfer are similar to those which have been demonstrated to influence forward electron transfer.[30] Such as the relationship between rate and energetics, the dependence of the rate of electron transfer on the distance separating the donor and acceptor, the solvation of the components of the radical ion pair and the mode and identity of solvent or spaces separating the participants in the electron transfer reaction.

Back electron transfer has an appreciable thermodynamic driving force, with rates exceeding that of diffusion control so that kinetic suppression of back electron transfer often becomes the limiting factor in the ability of the chemist to observe well defined chemistry derived from photoinduced electron transfer. To control the relative rates for a given set of reagents, the most common approach involves, controlling polarity and spatial inhomogeneity of the medium. To see how electron transfer reactions might be controlled by the reaction medium, we can look to photosynthesis.[31] In nature, to inhibit the recombination of oxidising and reducing agents, the reaction centres are spatially organised by biomembranes diminishing undesirable charge recombinations.

However, an alternative approach to this problem without the use of membranes has been to design dye molecules and substrates so that redox products have the same charge and hence electrostatically repel one another.[4] Most success has been achieved using positively charged chromophores such as ruthenium (II) tris-2,2-bipyridyl ($[Ru(bpy)_3]^{2+}$), zinc(II) tetrakis-N-methyl-4-pyridyl porphyrine ($[ZnTMPyP]^{4+}$) and multipositively charged viologen acceptors such as paraquant (MV^{2+}).

1.5 Self-organised Assemblies[33]

The design of artificial self-assemblies is based on the ability of some molecules, which contain both hydrophobic and hydrophilic groups, to form molecular assemblies of definite structure in solution. Effective charge separation and the formation of definite molecular assemblies has been demonstrated in surfactant micelles and vesicles.

1.5.1 Micelles[33-37]

Single tailed surfactant molecules form spherical micelles in water above a surfactant concentration called the critical micelle concentration (cmc) and because of this, upon dilution, the micelles can be destroyed. The spherical structure contains a nonpolar (hydrophobic) inner core which is separated from the surrounding polar solution by a shell of water soluble moieties comprising of positive, neutral or negative surfactant head groups and their accompanying solution shells, see figure 1.5.

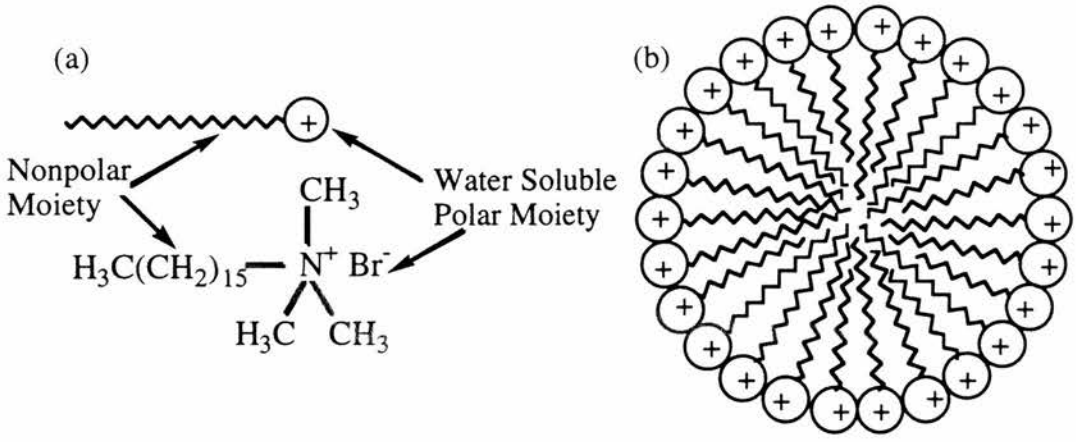

Figure 1.5 : (a) Surfactant molecule of cetyltrimethylammonium bromide
(b) Representation of CTAB assembly in cross section.

In some cationic surfactant systems, at higher surfactant concentrations, some surfactants will associate into rod like micelles called, cylindrical micelles. In addition, the transition from spherical to cylindrical micelles can be brought about by the addition of salt or acid where the salt or acid screens the electrostatic repulsion between surfactant head groups, and allows for the formation of the lower mean curvature cylindrical microstructures. The restricted volume of the micellar core can be used to create catalysts of a predetermined size, for example, semiconductor particles. The most extensively studied systems are the alkyltrimethylammonium halides and the alkylpyridinium halides where halide anions associate only moderately with surfactant cations and micellar growth is gradual.

The two most common uses of micelles in photochemical systems are : Firstly, in the solubilisation of hydrophobic species e.g. where [ZnTPP] in TritonX-100

micelles could act as a chromophere in the photochemical reduction of MV^{2+} by ethanethiol or triethanolamine.[38] Hydrogen was produced if hydrogenase or colloidal platinum was added. Secondly, they can retard back electron transfer reactions between products produced in a photochemical redox reaction e.g. the 1000 fold reduction in the rate of back electron transfer between methyltetradecylviologen cation ($C_{14}MV^{+}$) and $[Ru(bipy)_3]^{3+}$ formed on photolysis of $C_{14}MV^{2+}$ and$[Ru(bipy)_3]^{2+}$ in the presence of cetyltrimethylammonium chloride (CTAC) micelles rather than in the free solution.[39] Another role of the micelles is to inhibit the ground state complexation between electron donor or acceptor and chromophore.[40]

1.5.2 Vesicles[40-43]

The component surfactants employed in forming vesicles, have two long alkyl chains attached to a polar head group which can be positive, negative or neutral in charge. Most investigations to date have been concerned with the surfactant vesicles of dialkyldimethylammonium halide and dialkylphosphates whose structures are shown below in figure 1.6.

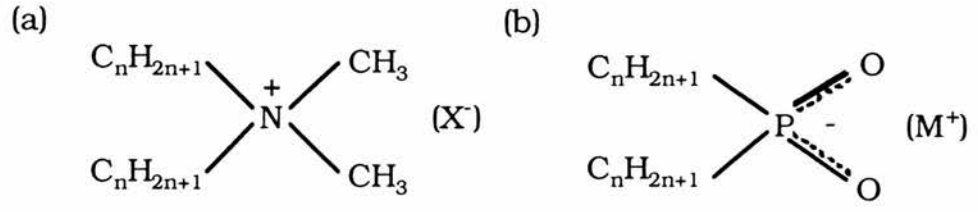

Figure 1.6 : (a) dioctadecyldimethylammonium halide
(b) dihexadecylphosphate

The structure, resulting from dissolving these species in water, is analogous to a liposome formed from similar orientation of naturally occurring phospholipids but surfactant vesicles are chemically stable as well as being easy to prepare and functionalise. The bilayer membrane separates an inner aqueous compartment from the bulk aqueous phase thus providing a physical barrier for generated species during photoinduced redox electron transfer (Figure 1.7).

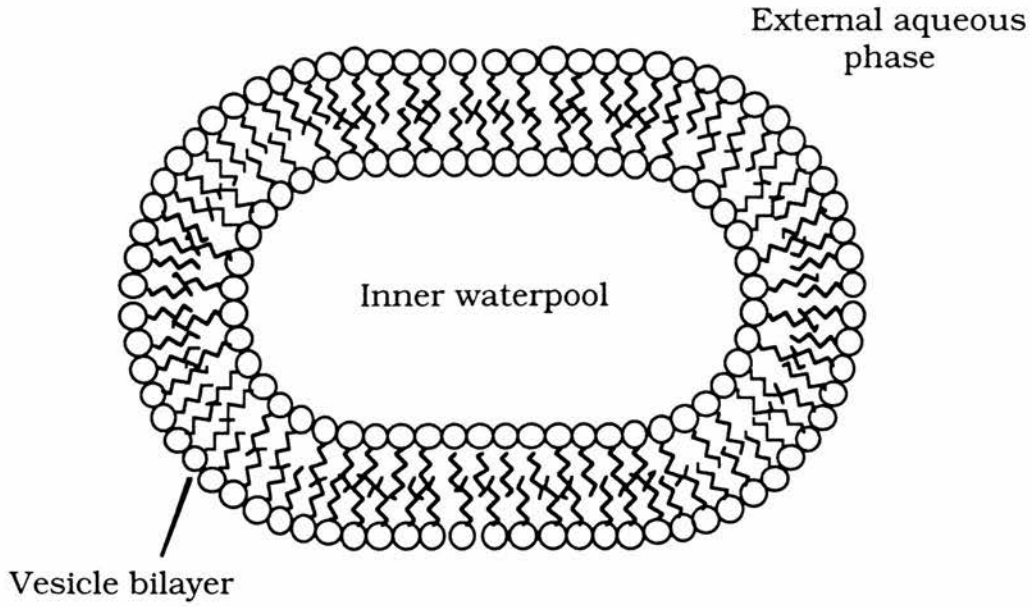

Figure 1.7 : Idealized representation of a lipid vesicle assembly in cross section. ○ hydrophobic headgroup, ∿∿ hydrophilic hydrocarbon tails. (two per headgroup)

The ability of these organised assemblies to allow kinetic control of photosensitised charge separation because of their high surface charge density and to allow transbilayer charge transport makes them ideal models for artificial photosynthesis. However, charge separation may be affected by the structural parameters of the vesicles[44,45] such as counterions, headgroups, hydrocarbon tail length, addition of salts and soluble alcohols or cholesterol. The vesicle bilayer also allows for different concentrations of reagents or separate locations, since operative catalysts can be placed in the inner and external phases. In addition, the restricted volume of the inner aqueous phase can be used to create catalysts of a predetermined size but unfortunately, it is impossible to alter the inner aqueous phase once the vesicles are formed. Polar solutes remain in the inner aqueous phase, or external water phase but like micelles, may be electrostatically bound or repelled by appropriate vesicle surface charge. Also, hydrophobic molecules can be dissolved in the vesicle hydrocarbon bilayers or a polar group can be attached to a long hydrocarbon chain and thus fix its position within the bilayer.

In principle, therefore, electron transfer may be possible across the bilayer which minimises short circuits between reduced and oxidised species participating in equations (9) and (10). Furthermore, the ability to generate a system in which the generation of hydrogen and oxygen are in separate compartments, enhances the practical utilisation of such a system. However, in practical terms, problems arise due to the diffusion of oxygen across the membrane followed by the subsequent inhibition of the hydrogen evolution process. These difficulties are unlikely to be solved with the use of microscopic mono or bilayer membranes for photoinduced charge separation. The problem being, the prevention of a small non-polar molecule diffusing across a membrane 30 — 50 Å thick. Therefore, better isolation of individual redox reactions is needed. This might be achieved by using a structural membrane (Figure 1.8) which can be prepared by the absorption, into millipore membranes, of complexes between dioctadecyldimethylammonium cations and sulphonated polystyrene anions.[46] Such membranes have been shown to contain bilayers and to exhibit many properties similar to those of DODAB vesicles.[47-49] They are however, multilayer in character with polymer chains between the bilayers and are much thicker than a simple bilayer. Alternatively, monolayers of positively charged surfactant adsorbed onto the outer surfaces of an absorbent paper might serve a similar purpose as a structural membrane. Therefore, the use of vesicles as models, allows scientists to model all the steps of the water splitting reaction, and put them together in a simple, well defined, system; before tackling the problems associated with electron transport across the greater distances of structural membranes.

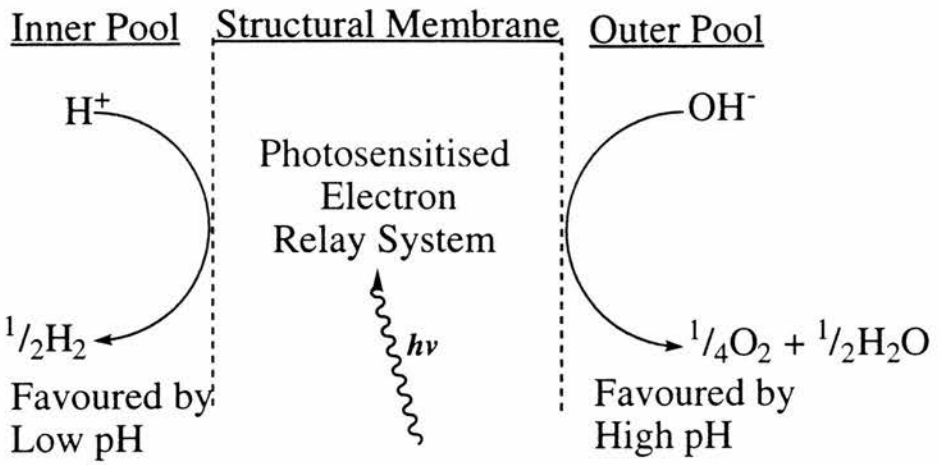

Figure 1.8 : Diagram of a water splitting photochemical cell with the redox reaction linked by a membrane based electron relay system.

Another feature of membranes is their ability to set-up a pH gradient across the bilayer. Studies by Fendler[50] have shown hydrogen ion concentrations in vesicle interiors along with proton and hydroxide ion permeability's across the bilayers of dioctadecyldimethylammonium chloride (DODAC), using flouresence probes. Positively charged 2-aminopyridine hydrochloide and negatively charged trisodium 8-hydroxy-1,3,6-pyrenetrisulfonate, pyranine, were used for cationic DODAC and anionic DHP vesicles, respectively. Electrostatic repulsions between the similarly charged probes and vesicle surfaces cause the probes to locate in the middle of the aqueous interiors. Free probes were separated from the entrapped probes by gel filtration. In the absence of cholesterol, protons and hydroxide ions instantaneously permeate the vesicles. Fendler also showed that in cholesterol containing DODAC vesicles, proton and hydroxide permeabilities became measurably slow and a pH gradient across the bilayer could be maintained for some time.[51-54] Tabushi *et al,* showed electron transport and the setting up of a pH gradient across a modified artificial liposome.[53]

The significance of the pH levels in both compartments can be explained by looking at the thermodynamics of "water splitting".[4] The dissociation of water into hydrogen and oxygen (1) is a highly endoergonic reaction (8).

$$H_2O_{(l)} \longrightarrow H_{2(g)} + {}^1/_2O_{2(g)} \qquad \Delta G^0 = 238 kJmol^{-1} \qquad (8)$$

Standard electrode potentials (E°) and corresponding values of ΔG^θ for one-electron and multi-electron reduction and oxidation processes involving water and its reaction products have been collected.[17] In energy terms, the most favourable redox reactions are the two-electron reduction (9) and the four electron oxidation (10).

$$2H^+ + 2e^- \longrightarrow H_2 \qquad E = -0.41V \text{ (pH7)} \qquad (9)$$

$$H_2O \longrightarrow O_2 + 4H^+ + 4e^- \qquad E = +0.82V \text{ (pH7)} \qquad (10)$$

The potential difference for water decomposition is independent of pH and fixed at 1.23 V. The half cell reactions are dependent on pH for hydrogen and oxygen evolution from solution and this dependence is presented graphically in figure 1.9.[14]

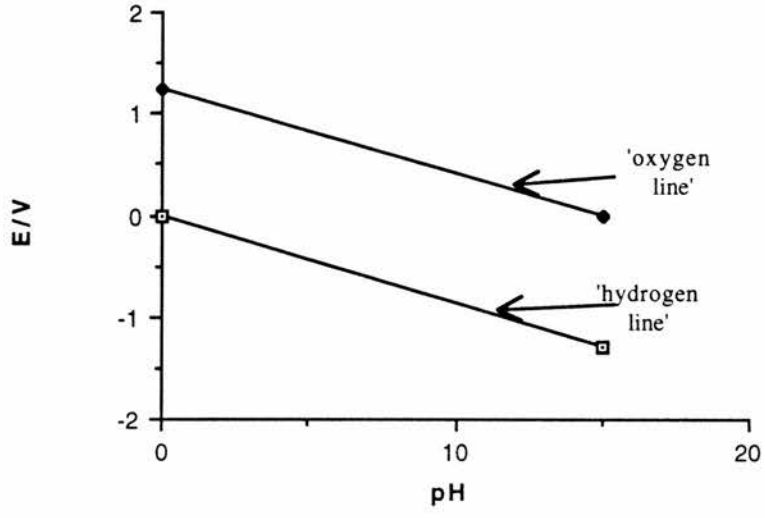

Figure 1.9 : Variation of electrode potentials with pH for hydrogen and oxygen production from water.

Consequently, a redox couple having a potential either below the 'hydrogen line' or above the 'oxygen line' at a given pH is thermodynamically capable of either reducing or oxidising water respectively. This variation in redox potential with pH means that, by changing the pH of a solution, the water half-cell potentials can be altered to bring them within access of an oxidant or reductant. There are other factors

such as kinetics and mechanisms which must be considered and a major objective is the coupling of the oxidative and reductive cycles.

Hydrogen production is favoured at low pH whilst oxygen production is favoured at high pH. An ideal system for water decomposition would therefore involve a two compartment system in which the pH's are different and remain so. Using vesicles, this is, in priciple possible, since the bilayer electron transfer must be accompanied by H^+ flow in the same direction and OH^- flow in the opposite direction in order to prevent build up of electrochemical potential across the bilayer. This means that the pH differential will be retained so as to favour H_2 and O_2 production in the different compartments.

The mechanism by which hydrogen would be produced is given in figure 1.10, where the photocatalyst (PC) is within the bilayer environment,[54] the sacrificial electron donor (D) is in the inner aqueous phase, the electron relay (R) and catalyst (CAT) are in the external aqueous phase. The PC upon illumination is excited and gains an electron through interaction with D, the radical anion of PC carries the electron across the membrane then transfers the electron to R, before the PC returns to the ground state and is ready to repeat the process. Molecule R acts as a relay to the proton source, usually in the presence of a catalyst (CAT) to produce hydrogen gas. The catalyst functions both to accumulate electrons to provide the necessary electrochemical potential and the number of electrons necessary for the reduction of water and to serve as a gas evolution site, see figure 1.10. Alternatively, the photocatalyst in the excited state donates an electron to R to repeat the whole process above, with the photocatalyst being reconverted by the transfer of an electron from the sacrificial donor.

These type of systems[23] are called photoactive, where the photocatalyst not only participates in photochemical and dark reactions with substances which are located in the water phases, but also serves as a carrier across the membrane. The other type of system is photopassive where the photocatalyst is located outside the membrane.

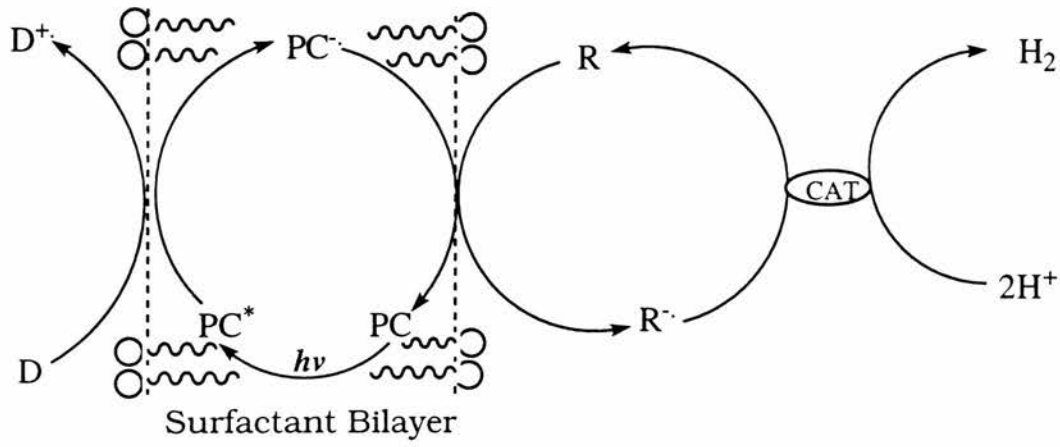

Figure 1.10 : Schematic representation of the redox catalytic cycle in the photoreduction of water to H_2 by visible light irradiation of a four component system by reductive quenching.

There are several possible mechanisms for the transport of electrons across the vesicle bilayer. These include (a) the exchange of a surfactant molecule with an electrostatically bound photocatalyst (PC) from the inner surface, to the outer surface of the vesicle by the so called 'flip-flop' mechanism,[53,57] (b) self exchange of the electron from an excited PC bound near the inner surface of the bilayer to a ground state PC near the outer surface *via* a series of PC molecules within the bilayers, (c) electron tunnelling across the vesicle bilayer where electron transfer from the PC and electron acceptor occurs over a distance of 50 Å. However, the distance for this process may be smaller than the thickness of the bilayer because the PC and electron acceptors are able to penetrate a certain distance inside the membrane, (d) diffusion of the PC across the mebrane i.e. the PC acting as the electron carrier.

1.6 Photo-assisted Transmembrane Electron Transfer in Photoactive Systems

1.6.1 Natural Membranes

Early studies involved the use of zwitterionic (phospholipid) liposomes and the electron transfer agent was usually a photosensitive metal complex.[58,59,60] For example, ferrocene was found to transfer electrons from external ascorbate ion to entrapped ferricyanide.[61] A marked increase in the rate of this electron transfer reaction occurs with the addition of a proton carrier (Vitamin K), and is attributed to the ability of this substance to increase proton transfer and hence neutralise any charge accumulation generated by electron transfer across the bilayer. Biological cytochrome c[52,53] or synthetic mediators can promote similar reactions.[63,64]

The observation of vectorial photoinduced electron transfer across the membranes of phopholipid vesicles was first reported in 1976 by Mangel[65] (Figure 1.11). By incorporating chlorophyll as a sensitiser and β-carotene as an electron mediator into the bilayer of phosphatidylcholine vesicles, Mangel effected electron transfer from waterpool-entrapped ascorbate to 'external' Fe^{3+}. Spectroscopic data indicated that some chlorophyll aggregates were present in the vesicle bilayer and he also showed that the chlorophyll aggregates may play an important role in the conversion of photonic energy to electronic energy.

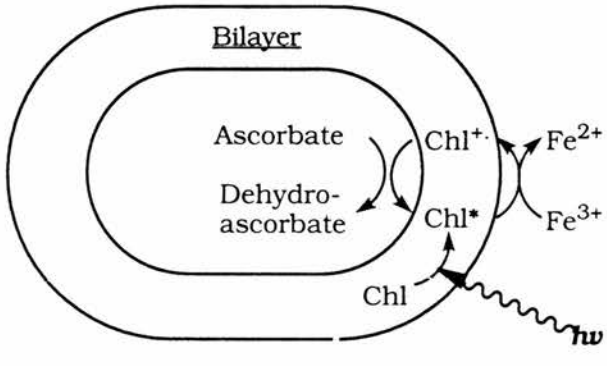

Figure 1.11 : Photo-assisted mediation of electrons across phospholipid vesicle bilayer between ' internal' ascorbate and 'external' $FeCl_3$.

Kurihara[66] *et al.* showed that chloropyll itself could act catalytically as both sensitiser and electron mediator in the photo-assisted transport of electrons across

phosphatidylcholine bilayers between 'internal' ascorbate and 'external' Cu^{2+}, without requiring β-carotene or other proposed electron carriers.

Ford and Tollin[67] employed laser flash and steady state photolysis to carry out detailed kinetic studies on the reaction processes involved in the photo-assisted, chlorophyll-mediated, transport of electrons across phosphatidylcholine vesicle bilayers from 'external' EDTA to 'internal' methyl viologen (MV^{2+}), see figure 1.12.

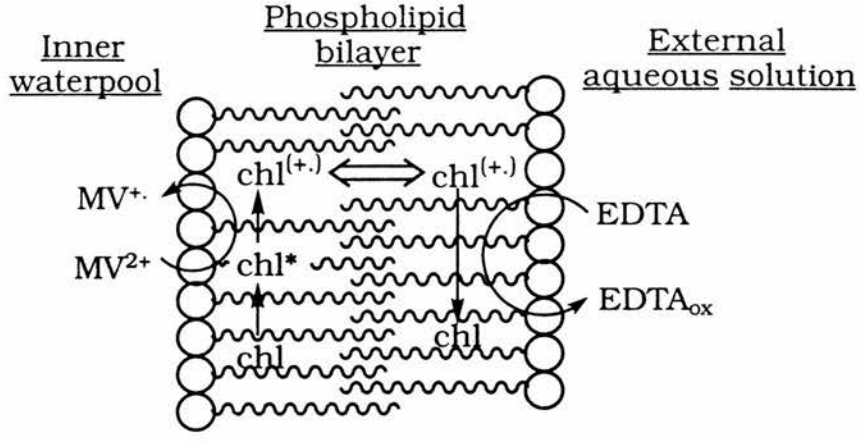

Figure 1.12 : Proposed mechanism for photo-assisted, chlorophyll mediated electron transport across a vesicle bilayer from EDTA to methyl viologen.

In an extension of this work, Ford and Tollin[68] reported a similar rate of electronic transfer across the bilayer of phosphotidylcholine/chlorophyll *a* vesicles separating a water soluble napthaquinone acceptor in the inner waterpools from an 'external' thiol donor. They concluded that the inherent asymmetry of chlorophyll distribution in the vesicle bilayer favoured net photo-assisted transfer into the vesicles. It is believed that the electron transfer in both cases occured via self-exchange of $[chlorophyll]^{+\cdot}$ on the inner surface with chlorophyll on the outer surface of the liposome, rather than by electron tunnelling or diffusion.

Interestingly, the reverse was found to be true when chlorophyllin *a* [69] a water soluble saponification product of chlorophyll *a*, with a similar photochemical reactivity,[70,71] was used as a membrane-bound sensitiser/mediator in phosphatidylcholine vesicle bilayers separating 'internal' ascorbate from 'external'

methyl viologen. Diffusion of chlorophyllin was proposed as the mechanism of electron transport across the bilayer, since chlorophyllin possesses no long alkyl chain and is mobile across the bilayer.[72]

Photochemical electron transfer across similar liposomes from ascorbate ion to MV^{2+} is observed using chlorophyllin, a water-soluble chlorophyll derivative[27] or various zinc porphyrins.[73] It has been proposed that some of these reactions proceed by a biphotonic process with a photon being absorbed on each side of the liposome (Figure 1.13).[74]

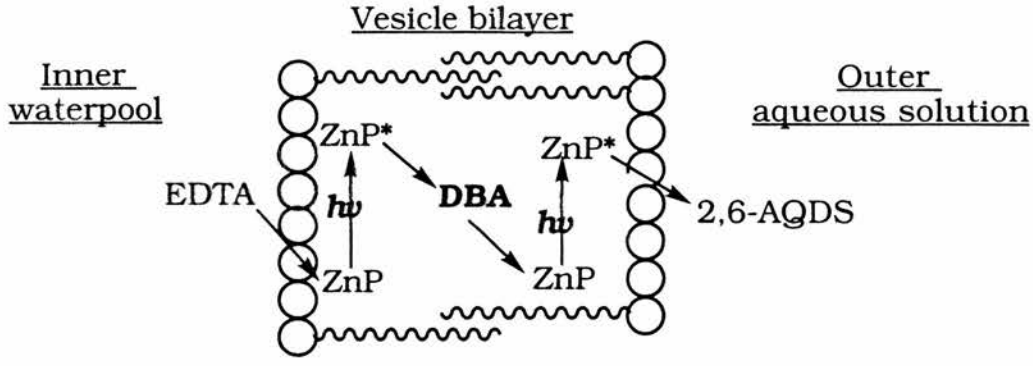

Figure 1.13 : Proposed two-quantum mechanism of transbilayer electron transport by ZnP{5.10.15-tris(4-pyridyl)-20-[4-(dodecylpyridinium)] porphinato zinc} in the presence of the elctron mediator DBA.

Parmon and co-workers found that neutral zinc tetraphenylporphyrin acts both as a chromophore and as a mediator for the transfer of electrons from internal EDTA or NADH to external MV^{2+}.[58,75] However, in the latter case they found that higher quantum yields were obtained if $[Ru(bipy)_3]^{2+}$ was entrapped in the inner water pool as an additional chromophore. Derivatives of $[Ru(bipy)_3]^{2+}$ incorporated into the bilayer, promote rapid (several orders of magnitude faster than diffusion) electron transfer from internal EDTA to external MV^{2+} as found by Laane.[64]

Coutts and Paterson[76] constructed an asymmetric vesicle system based on natural products. Where flavin mononucleotide acted as an electron source, when dissolved in the inner waterpool of unsaturated phosphatidylcholine vesicles, for 'external' cytochrome c^{III} in the presence of light when either coenzyme Q_{10} or

vitamin K_1 were present in the vesicle bilayer. The proposed mechanism by which this proceeded involved diffusion across the bilayer (Figure 1.14)

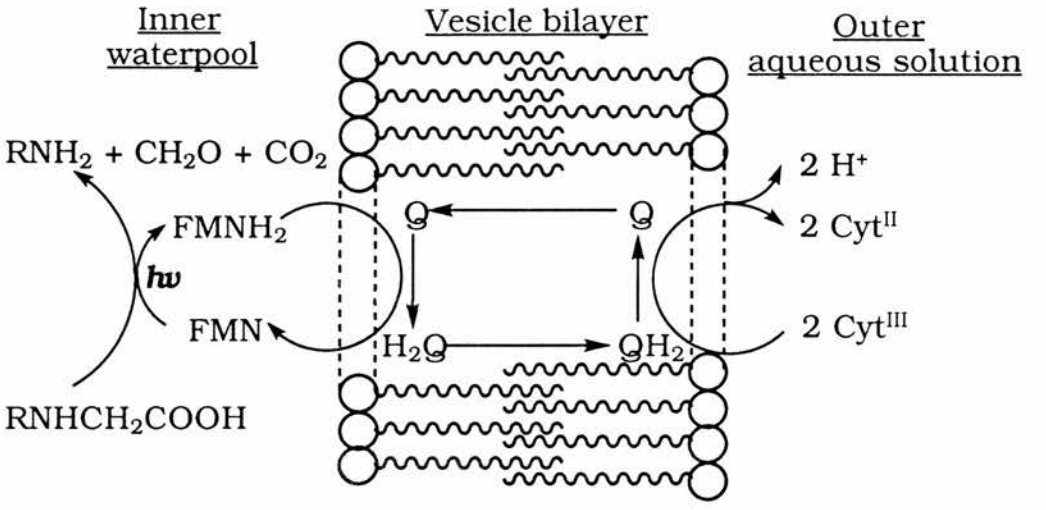

Figure 1.14 : Model of photochemically activated transbilayer electron/proton transport mediated by Q_{10}.

Willner and associates,[77] introduced the use of charged interfaces to effectively prevent the complex formation of oppositely charged donors and acceptors. Colloid particles of SiO_2 were employed to prevent the ground state complex between Rose bengal (Rb^{2-}) and methyl viologen (MV^{2+}) whereby the [Rb^{2-}...MV^{2+}] complex is separated through the selective association of MV^{2+} to the negatively charged colloid surface. Subsequently, developing a colloidal-based sytem that effectively hydrogenates ethylene. This concept has been extended by Armitage and O'Brien[76,79,80] by preventing complex formation of a tricationic cyanine and the hydrophobic triphenylbenzylborate anion using a phosphatidylcholine membrane. The important feature of the system is the binding of both donor and acceptor within the membrane, leading to vectorial photoinduced electron transfer upon red light irradiation. Schuster[81] and co-workers also demonstrated efficient photoinduced electron transfer from similar anionic triphenylalkylborates to cationic cyanine dyes by using low polarity organic solvents.

Nango[82] and co-workers while studying the effect of distance and orientation

in electron transfer reactions of biological processes involving porphyrin pigments, reported the first system in which covalently-linked manganese porphyrin dimers ($MnTTP\text{-}(CH_2)_n\text{-}MNP(COOMe)_3$, n= 2,3) with spacer methylene groups enhanced electron transfer in S-cyanoethylated keratin (SCEK) liposomal membranes from indigotetrasulfonic acid to potassium ferricyanide. The porphyrin dimers being fixed in the keratin membrane.

Lymar and Hurst[83] reported that the organic ion 1-methyl-4-cyanopyridinium (MCP^+) can serve the dual function of oxidative quencher of sensitisers and transmembrane electron carrier in vesicle organised photoredox systems. Under steady-state illumination in either the Soret or Q bands of the porphyrin ($ZnTPPS^{4-}$), one electron reduction of the entrapped acceptor ($Co(bpy)_3^{3+}$) occurred. However, reduction was not recorded unless all system components were present, see figure 1.15.

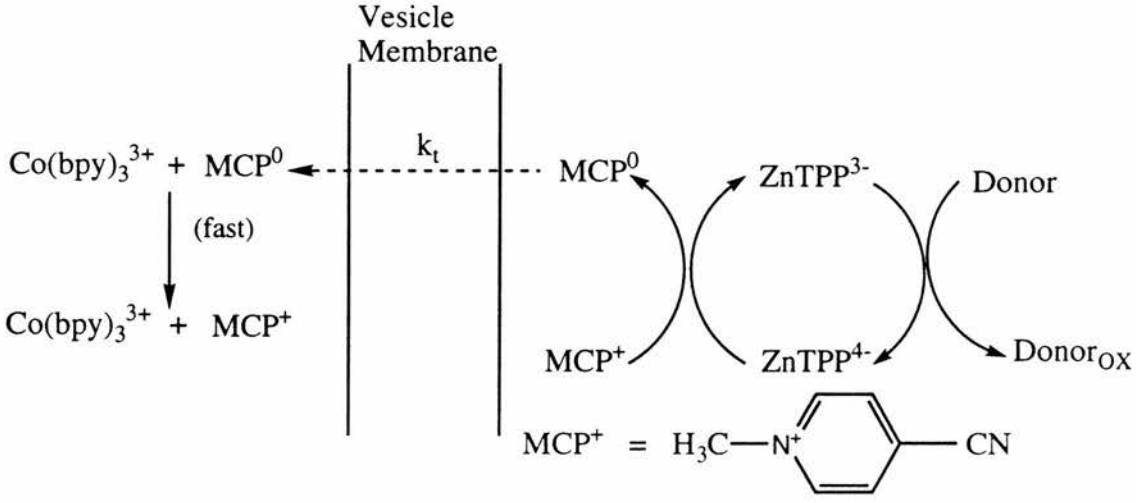

Figure 1.15 : Reaction scheme for photoinduced electron transfer mediated by MCP^+.Trethanolamine, dithiothreitol or $Fe(CN)_6^{4-}$.

Recent research by Hammarstrom *et al.* [84,85,86] on transmembrane electron transfer in lecithin vesicles mediated by interfacially bound cetyl-methylviologen ($C_{16}MV^+$) and the subsequent reduction of ferricyanide, showed that the mechanism for viologen electron transfer across interfaces involves disproportionation

(Figure 1.16). This supported the work of Lymar and Hurst[87] who reported, in contrast to earlier conclusions[88] that transmembrane redox reaction mediated by dimethylviologen (MV^{2+}) in dihexadecylphophate vesicles also proceeded by a disproportionation mechanism (k_d).

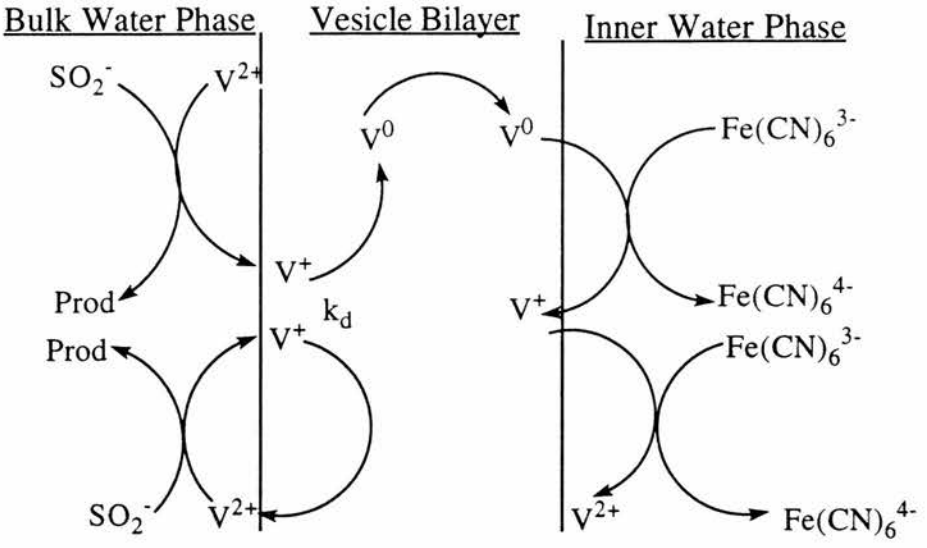

Figure 1.16 : Proposed disproportionation mechanism for transmembrane electron transfer by viologen. Direction of electron transfer is inward from dithionite to ferricyanide.

1.6.2 Synthetic Membranes

An unusual example, in which the electron transfer mediator was a surface-active viologen molecule with the metal sensitiser in the aqueous phase has been reported.[88] Reports[89] of unmediated electron transfer across a bilayer were subsequently shown to be in error[90] because it was found that $MV^{+\cdot}$ was diffusing through the vesicle bilayer and the redox reaction was in fact occuring at the outer surface of the vesicles. This proposed mechanism can be seen below in figure 1.17.

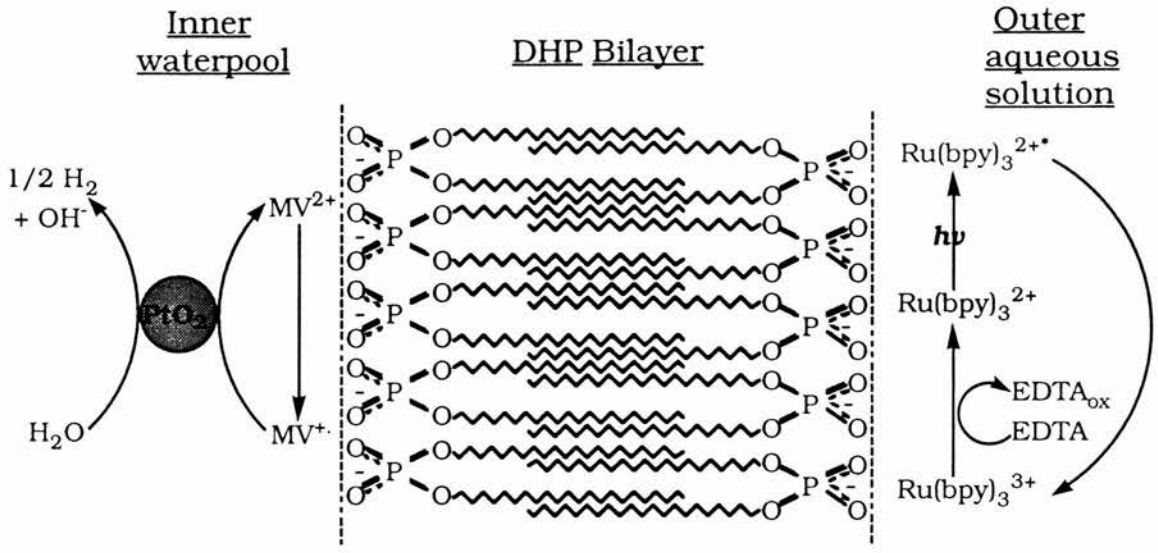

Figure 1.17 : Originally proposed model for transmembrane electron transfer.

It has been stated that, with high concentrations of CdS embedded in the bilayer, electrons can be transferred to MV^{2+} inside dihexadecylphosphate vesicles but even in this case the analysis was hampered by the diffusion of $MV^{+\cdot}$ through the vesicle.[92] A model for this proposed electron transfer mechanism can be seen below in figure 1.18.

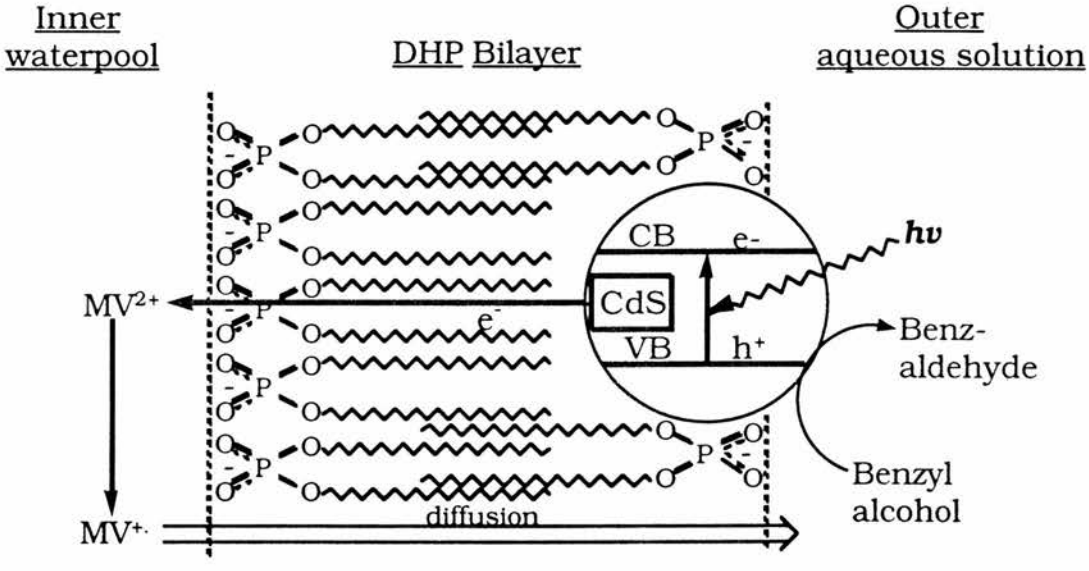

Figure 1.18 : Proposed mechanism for electron transfer across DHP vesicle bilayer from embedded CdS to 'internal' MV^{2+}.

For a more detailed review of photoinduced electron-transfer across bilayer membranes, see J.N. Robinson and D.J. Cole-Hamilton.[92]

Cole-Hamilton[93,94] and co-workers during studies, seeking to identify possible neutral electron transfer catalysts for use in the photochemical decomposition of water, discovered a reaction in which the micelle fulfills its roles i.e. inhibition of ground state complexation and the retardation of back electron transfer while protecting a radical anion from the environment in which it was unstable. The compound was 2,1,3-benzothiadiazole-4,7-dicarbonitrile (BTDN) (Figure 1.19) which acted as a chromophore and an electron acceptor.

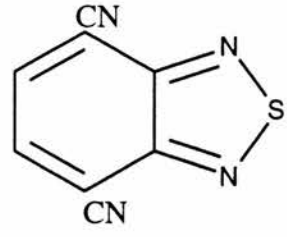

Figure 1.19 : 2,1,3-benzothiadiazole-4,7-dicarbonitrile

The radical anion of BTDN could be generated using photolysis in the presence of a suitable sacrificial electron donor such as ethylenediaminetetraacetate (EDTA) or 4-morpholineethanesulphonic acid (MESH) (Figure 1.20), taken up by the micelle (CTAB) and stabilised.

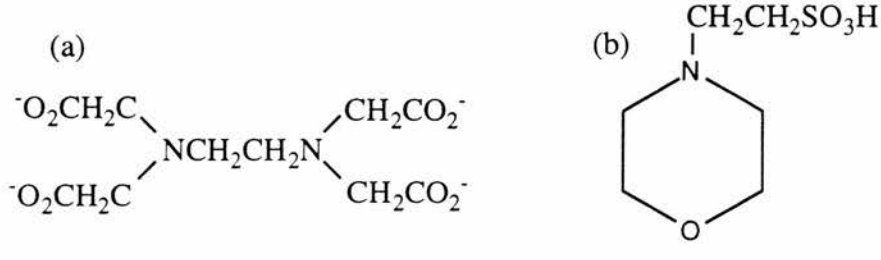

Figure 1.20 : (a) EDTA and (b) MESH

Robinson,[95] investigated the possibility that the radical anion of BTDN could act as a combined chromophore and an electron transfer catalyst towards other molecules, which led to the redox matched electron acceptor of disodium-9,10-anthraquinone-1,5-disulphonate (AQDS) (Figure 1.21) being used, where upon reduction by $BTDN^{-\cdot}$ formed the hydroquinone ($AQDSH_2$) which was an intense

yellow colour, allowing the reaction to be followed by uv-visible spectroscopy. The overall micellar electron transfer system is illustrated below in figure 1.22.

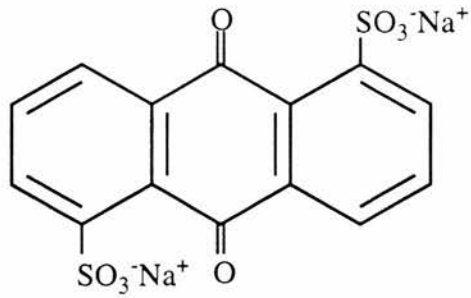

Figure 1.21 : Disodium-9,10-anthraquinone-2,6-disulphonate (AQDS).

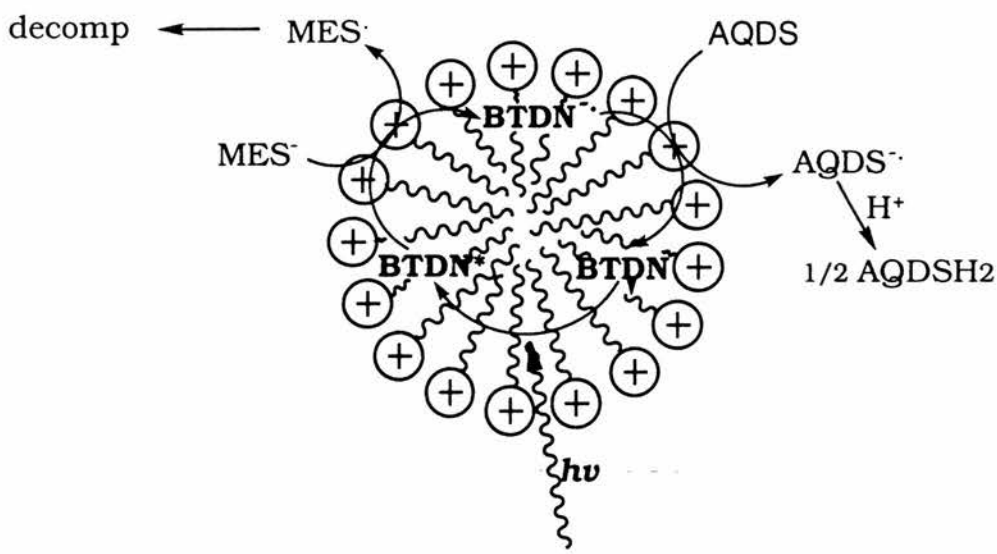

Figure 1.22 : Schematic representation of the photo-aassisted BTDN mediated electron transfer from MES to AQDS in the presence of CTAB micelles.

Robinson *et al.*[96,97] applied the main features of the micellar system to develop a practical system for the photochemical transfer of electrons across a surfactant vesicle bilayer (DODAB). The overall electron transfer process is shown below in figure 1.23 and is the first of its kind to be reported across simple surfactant vesicle bilayers.

In a key experiment, they photolysed the unsymmetrical vesicle system until *c.a.* 50% of the AQDS had been reduced. They then separated the vesicles from the bulk water by chromatography on a Sephadex column. The vesicle fraction contained

MESH and AQDS (BTDN was lost on the column) but reduction of AQDS did not occur on photolysis, confirming that AQDS had not diffused through the bilayer but was bound to the outer surface of the vesicle. On addition of BTDN to these vesicles, reduction of AQDS again occured on photolysis, confirming that the MES^- had remained inside the vesicles and that the vesicles had retained their integrity. Photolysis of the chromatographed fraction which contained the bulk water did not lead to reduction of AQDS, confirming that MES^- had not leaked out of the inner water pools.

Mechanistic studies suggest that electrons were transported across the vesicle bilayer by diffusion of $BTDN^{-\cdot}$ which is only stable in ordered assemblies such as vesicles or micelles, not in water, but in continuous photolysis experiments the overall rate of this process was determined by concomitant charge compensating diffusion of OH^- or H^+ across the bilayer.

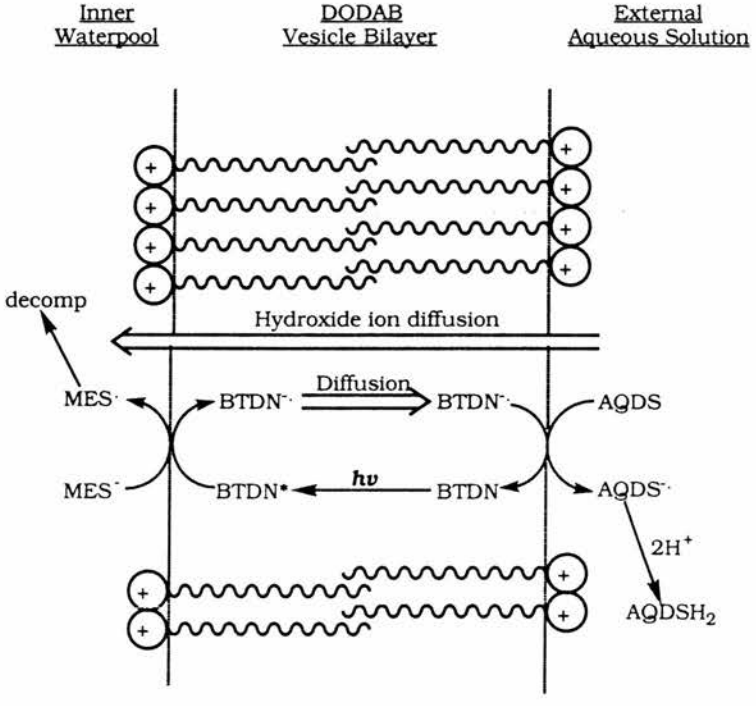

Figure 1.23 : Mechanism of electron transport across vesicle bilayers mediated by BTDN.

1.7 Present Studies

The system described above, containing BTDN, suffers from certain drawbacks which include :

(i) The main absorption of BTDN is 320 nm, so that only a small proportion of visible light can harnessed by it,[93,98]

(ii) The partition coefficient of BTDN between octanol and water is low [94] suggesting that it has low solubility in the bilayer,

(iii) the redox potential of BTDN is too low for H_2 evolution and

(iv) the presence of S may lead to poisoning of the colloidal platinum redox catalyst used for hydrogen evolution.[98]

In order to overcome some or all of these problems we have sought to study related molecules. By changing the substituents on the benzothiadiazole ring it should be possible to change the electronic properties so that the radical anion becomes more reducing. This should be achievable by increasing the electron density on the ring by initially substituting the cyano group with a less electron withdrawing group such as an ester function. This approach would also allow for the improvement of other properties, such as, providing better solubility in the bilayer and possibily increased electron delocalisation, which is why the dibutyl ester of 2,1,3-benzothiadiazole-4,7-dicarboxylic (BTDB) has been synthesised (Figure 1.24). We have also replaced the thiadiazole ring with a furazan ring because the oxygen of the furazan ring should not lead to poisoning of the platinum catalyst.

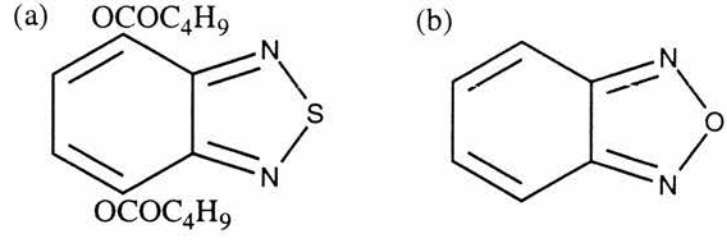

Figure 1.24 : (a) BTDB and (b) Benzofurazan

The replacement of the cyano group for an ester will make the radical anion more reducing and perhaps allow the reduction of H^+ at near neutral pH. Although

the anthraquinone is used to accept electrons in the system described by Julian N. Robinson,[10,12] it is not suitable for hydrogen production. We propose to attempt to couple the radical anion directly to hydrogen production by using a suitable redox catalyst such as colloidal platinum. However, this may not be successful because of the presence of the sulphur atom in the thiadiazole ring poisoning the colloidal platinum catalyst. Therefore, we shall try the enzyme, hydrogenase which has been used in the presence of thiols with great success for hydrogen production.[99] Alternatively, the use of the furazan compound may also aid hydrogen production since it does not contain sulphur and may be more compatible with colloidal platinum catalysts. It may be necessary to employ a further electron transfer catalyst such as methyl viologen.

Oxygen production in a coupled redox system has proved difficult[4] in that we know of catalysts, such as RuO_2 and ruthenium red that will aid oxygen evolution[100] but little is known about the mechanisms by which they operate. In the system we propose there is a possibility that water (or OH^-) can act as a donor to the chromophore.[101] Therefore, it will be necessary to establish if OH^- is the electron donor and to identify whether O_2 or H_2O_2 is the other product.

One attraction of this system under investigation, is that the charge accumulation caused by the transfer of electrons across the vesicle bilayer is neutralised by the transport of OH^- and/or H^+.[102] It has previously been shown that the overall rate determining process is this charge compensating diffusion of H^+ and/or OH^- across the vesicle.[96] This will set up a potential gradient across the bilayer so that high pH is produced on the oxygen producing side of the bilayer whilst low pH is produced on the hydrogen side. A similar process has been reported by Bhaduri and Sharma[103] where OH^- acted as an electron donor to an anionic carbonylcluster of platinum through a liquid membrane. The process being driven by a pH gradient across the membrane.

However, studies will first have to be performed on BTDB in a micellar (CTAB) environment before progressing onto the surfactant vesicle bilayer system.

References

1. K.I. Zameraev, V.N. Parmon. '*Energy resources through Photochemistry and Catalysis*', M Gratzel (Ed.), Academic Press, 1983, Chap. 5.
2. V.N. Parmon and K.I. Zameraev '*Photocatalysis - Fundamentals and Applications*', N. Serpone and E. Pelizzetti (Eds.), Wiley, 1989, Chap 17.
3. J.R. Bolton, A.F. Haught and R.T. Ross, '*Photochemical Conversion and Storage of Solar Energy*', J.S. Connolly (Ed), Academic Press, New York, 1981, p.297.
4. D.J. Cole-Hamilton and D.W. Bruce, '*Comprehensive Coordination Chemistry*', G.Wilkinson, R.D.Gillard and J. A. McCleverty Eds., Pergamon Press. Oxford, 1987, vol. 6, p.487 and refs. therein.
5. A. Mills, The University of Wales Science and Technology Reveiw 1988, **4**, 39.
6. '*Solar Power and Fuels*' Ed. J.R. Bolton, Acedemic Press, London 1977, p.53.
7. '*Light, Chemical Change and Life: A source book in photochemistry*', Ed., J.D. Coyle, R.R. Hill and D.R. Roberts, Open University Press, Milton Keynes, 1982.
8. M. Calvin, *Int. S. Energy Research*, 1977, **1**, 299.
9. L.B. McGown and J.O'M. Bockris, '*How to Obtain Abundant Clean Energy*', Plenum, New York, 1980.
10. J.O'M. Bockris, '*Energy Options*', Taylor and Francis, London, 1980.
11. C.A. McAuliffe, '*Hydrogen and Energy*', MacMillan, London, 1980.
12. J.R. Bolton (Ed), '*Solar Power and Fuels*', Academic, NewYork, 1976.
13. N. Serpone, '*Photochemical Energy Conversion*', J.R. Norris Jr. and D. Meisel, Eds., Elsevier Publishing Co., p.297, 1989.
14. S. Tabata, H. Nishida, Y. Masaki and K. Tabata, *Catal. Lett.*, 1995, **34**, 245 and refs. therein.
15. Y. Sakata, Y. Hirata, K. Miyahara, H. Imamura and S. Tsuchiya, *Chem. Lett.*, 1993, 2381.
16. R. Rossetti, J.L. Ellison, J.M. Gibson and L.E. Brus, *J. Chem. Phys.*, 1984, **80**, 4464.
17. J.J. Ramsden, S.E. Webber and M. Gratzel. *J.Phys., Chem.* 1985, **89**, 2740.
18. R. Rafaeloft, Y.M. Tricot, F. Norne and J.H. Fendler, *J.Phys.Chem.*, 1985, **89**, 533.
19. P.V. Kamat, '*Prog. Reaction Kenetics*', 1994, **19**, 277 and refs. therein.

20. J.K. Hurst, '*Kinetic and Catalysis in Microheterogeneous Systems*', M. Gratzel and K. Kalyanasundaram Eds., Marcel Dekker, New York, 1991 and refs. therein.
21. M.R. Hoffman, S.T. Martin, W. Choi and D.W. Bahneman, *Chem.Rev.*, 1995, **95**, 69, and refs. therein.
22. A. Fujishima and K. Honda, *Nature* (London), 1972, **238**, 37.
23. H.T. Witt, *Photosynth. Res.*, 1991, **29**, 53.
24. H.T. Tien, *Prog. Surf. Sci.*, 1989, **30**, 1.
25. S.V. Lymar, V.N. Parmon and K.I. Zamaraev, *Topics in Current Chemistry*, 1991, **159**, 3.
26. J.S. Connolly (ed), '*Photochemical Conversion and Storage of Solar Energy*', Academic Press, New York, 1981.
27. J.-M. Lehn, ref. 26, p. 161.
28. P. Mitchell, 1966, **41**, 445.
29. M.A. Fox, *Topics in Current Chemistry*, 1991, **159**, 68.
30. M.A. Fox, *Adv. Photochem*, 1986, **13**, 237.
31. J. Deisenhofer, O. Epp, K. Miki, R. Huber and H. Michel, *J. Biol.*, 1984, **180**, 385.
32. D. Meisel and M.S. Mathson, '*Photocatalysts - Funamentals and Apllications,* N. Serpone and E. Pelizzetti Eds., 1989, Chap. 12, p. 385.
33. J.H. Fendler and E.J. Fendler, '*Catalysis in Micellar and Macromolecular Systems*', Academic Press, New York, 1975.
34. P.K. Vinson, *Proc. Ann. Meet Elec. Microsc. Soc. Amer.*, 1988, **46**, 112.
35. S. Miyagashi, H. Kurimoto and T. Asakawa., *Bull. Chem. Soc. Jpn.*, 1995, **68**, 135.
36. Z. Lin, J.J. Cai, L.E. Scriven and H. T. Davis, *J. Phys. Chem.*, 1994, **98**, 5984.
37. P.K. Vinson, J.R. Bellare, H.T. Davis, W.G. Miller and L.E. Scriven, *J. Coll. Intf. Sci.*, 1991, 142.
38. I. Okura and N. Kim-Thuan, *J. Mol. Catal*, 1979, **6**, 227.
39. P.-A. Brugger and M. Gratzel, *J. Am. Chem. Soc.*, 1983, **102**, 2461.
40. '*The Porphyrins*', ed. D. Dolphin, Academic Press, New York, 1978 and refs. therein.
41. J.H. Fendler, '*Membrane Mimetic Chemistry*', Wiley, New York, 1982.
42. J.H. Fendler, *J. Photochem.*, 1981, **17**, 303.
43. J.H. Fendler, *Acc. Chem. Res.*, 1980, **13**, 7.
44. T. Hiff and L. Kevan, *J. Phys. Chem.*, 1989, **93**, 1572.
45. P. Bratt, Y.S. Kang, L. Kevan, H. Nakamura and T. Matsuo, *J. Phys. Chem.*, 1991, **95**, 6399.

46. T. Kunitake, N. Kimizuka, N. Higashi and N. Nakashima, *J. Am. Chem. Soc.*, 1984, **106**, 1978 and refs. therein.
47. T. Kunitake, A. Tsuge and N. Nakashima, *Chem. Lett.*, 984, 1783.
48. N. Nakshima, K. Ymashuta, T. Jorobata, K. Tamaka, K. Nakano and M. Takgi, *Anal. Sci.*, 986, **2**, 589.
49. N. Nakashima, K. Nakayma, M. Kunitake and O. Manabe, *J. Chem. Soc., Chem. Commun.*, 1990, 887.
50. K. Kano and J.H. Fendler, *Biochim. Biophys. Acta.*, 1978, **509**, 289.
51. C.D. Tran, P.l Klahn, A. Romero and J.H. Fendler, *J. Am. Chem. Soc.*, 1978, **100**, 1622.
52. R.A. Moss, S. Bhattachyra and S. Chatterjee, *J. Am. Chem. Soc.*, 1989, **111**, 3680.
53. I.M. Caccovia, M.K. Kauramuro, M.A.K. Krutman and H. Chaimovich, *J. Am. Chem. Soc.*, 1989, **111**, 365.
54. R.A. Moss, S. Swarup and H. Zhang, *J. Am. Chem. Soc.*, 1988, **110**, 2914.
55. I. Tabushi, T. Nishiya, M. Shimomura, T. Kuniotake, H. Inokuchi and T. Yagi, *J. Am. Chem. Soc.*, 1984, **106**, 219.
56. I. Tabushu, I. Hamacki and Y. Kobuke, *J. Chem. Soc. Perkin Trans.*, I, 1989, 383
57. A.J. Bard and M.A. Fox, *Acc. Chem. Res.*, 1995, **28**, 141.
58. V.N. Parmon, S.V. Lymar, I.M. Tsuerhov and K.I. Zamaraev, *J. Mol. Catal.*, 1983, **21**, 353.
59. W.E. Ford and G. Tollin, *Photochem. Photobiol.*, 1982, **35**, 809.
60. Y. Toyoshima, M. Norino, H. Motoki and M. Sukigara, *Nature* (London), 1977, **265**, 187.
61. P. Hinkle, *Biochim. Biophys, Res. Commun.*, 1970, **41**, 1375.
62. I. Tabushi and T. Nishya, *J. Am. Chem. Soc.*, 1981, **103**, 6893.
63. L.Y.C. Lee and J.K. Hurst, *J. Am. Chem. Soc.*, 1984, **106**, 7411.
64. C. Laane, W. E. Ford, J.W. Otvos and M. Calvin, *Proc. Natl. Acad. Sci, USA.*, 1981, **78**, 2017.
65. M. Mangel, *Biochim. Biophys. Acta.*, 1979, **430**, 459.
66. K. Kurihara, M. Sukigara and Y. Toyoshima, *Biochim. Biophys. Acta.*, 1979, **547**, 117.
67. W.E. Ford and G. Tollin, *Photochem., Photobiol.*, 1982, **35**, 809.
68. W.E. Ford and G. Tollin, *Photochem., Photobiol.*, 1983, **38**, 441.
69. G. Oster, S.B. Broyde and J.S. Bellin, *J. Am Chem Soc.*, 1964, **86**, 1309.
70. D. Brune and A.S. Peitro., *Arch. Biochim. Biophys.*, 1970, **141**, 371.
71. S. Hidaka, E. Matsuomota and F. Toda, *Bull. Chem. Soc. Jpn.*, 1985, **58**,

207.

72. S. Hidaka and F. Hoda, *Chem. Lett.*, 1983, 1333.
73. T. Katagi, T. Yamamura, T. Saito and Y. Sasaki, *Chem. Lett.*, 1981, 1451.
74. T. Matsuo, *Pure Appl. Chem.*, 1982, **54**, 1693.
75. K.T. Zamaraev, S.V. Lymar, M.T. Khramov and V.N. Parmon, *Pure Appl. Chem.*, 1988, **60**, 1039.
76. D. Coutts and R. Patterson, *J. Membrane Sci.*, 1986, **27**, 275.
77. I. Willner, Y. Eichen and E.S. Joselevich, *J. Phys. Chem.*, 1990, **94**, 3092.
78. B. Armitage, D.F. O'Brien, *J. Am. Chem. Soc.*, 1991, **113**, 9678.
79. B. Armitage, D.F. O'Brien. *J. Am. Chem. Soc.*, 1992, **114**, 7396.
80. P.J. Clapp, B. Armitage, P. Rossa and D.F. O'Brien, *J. Am. Chem. Soc.*, 1994, **116**, 9166.
81. S. Chatterjee, P.D. Davis, P. Gottschalk, M.E. Kurz, B. Saurwein, X. Yang, G.B. Schuster, *J. Am Chem. Soc.*, 1990, **112**, 6329.
82. K. Iida, M. Nango, M. Hikita, T. Tajima, T. Kurihara, K. Yamashita, K. Tsuda, T. Dewa, J. Komiyama, M. Nakata, and Y. Ohtsuka, *Chem. Lett.*, 1994, 1157.
83. S.V. Lymar and J.K. Hurst, 10th International Conference on Photochemical Conversion and Storage of Solar Energy, Book of Abstracts. G. Calzaferri, Ed. 1994.
84. L. Hammarstrom, M. Almgren and T. Norrby, *J. Phys. Chem.*, 1992, **96,** 5017.
85. L. Hammarstrom, M. Almgren, J. Lind, G. Merenyi, T. Norrby and B. Akermark, *J. Phys. Chem.*, 1993, **97**, 10083.
86. L. Hammarstrom, H. Berglund and M. Almgren, *J. Phys. Chem.*,1994, **98**, 9588.
87. S.V. Lymer and J.K. Hurst, *J. Phys. Chem.*, 1994, **98**, 989.
83. J.K. Hurst, L.Y.C. Lee and M. Gratzel, *J. Am. Chem. Soc.*, 1983, **105**, 7048.
88. M.S. Tunuli and J.M. Fendler, *J. Am. Chem. Soc.*, 1981, **103**, 2507.
89. L.Y.C. Lee, J.K. Hurst, M. Polite, K. Kurimara and J.M. Fendler, *J. Am. Chem. Soc.*, 1983, **105**, 370.
90. Y.M. Tricot and J. Manassen, *J. Phys. Chem.*, 1988, **92**, 5231.
91. O. Horvath and J.H. Fendler, *J. Phys. Chem.*, 1992, **96**, 9591.
92. J.N. Robinson and D.J. Cole-Hamilton, *Chem. Soc. Rev.*, 1991, **20**, 49.
93. C. Dainty, D.W. Bruce, D.J. Cole-Hamilton and P. Camilleri, *J. Chem. Soc. Chem. Commun.*, 1984, 1324.
94. P. Camilleri, A. Dearing, D.J. Cole-Hamilton and P. O'Neil, *J. Chem. Soc. Perkin, Trans 2*, 1986, 569.

95. J.N. Robinson, D.J. Cole-Hamilton, P. Camilleri, C. Dainty and V. Maxwell, *J. Chem. Soc. Faraday Trans.*, 1989, **85**, 3385.
96. J.N. Robinson, D.J. Cole-Hamilton and P. Camilleri, *J. Chem. Soc. Chem. Commun.*, 1988, 1410.
97. J.N. Robinson, D.J. Cole-Hamilton, M.K. Whittlesey and P. Camilleri, *J. Chem. Soc. Faraday Trans.*, 1990, **86**, 2897.
98. J. N. Robinson, PhD. Thesis, University of St Andrews 1989.
99. I. Okura, *Coord. Chem. Rev.*, 1985, **68**, 53 and refs. therein
100. M. Kareko, G.J. Yao and A. Kira, *J. Chem. Soc. Chem. Commun.*, 1989, 1338.
101. J.N. Robinson, R. Becker and D.J. Cole-Hamilton unpublished observations.
102. '*Biochemistry, A Problems Approach*', Ed. W.B. Woods, J.A. Wilson, R.M. Benbow and L.E. Hood, Benjamin / Cummings, Melono Park, California, 2nd Edn., 1981; '*Principles of Biochemistry*', A.L. Lehninger, CBS Publishers, New Delhi, 1st Indian Edn., 1984.
103. S. Bhaduri and K. Sharma, *J.Chem. Soc. Chem. Commun.*, 1992, 1593.

Chapter 2

Studies of 2,1,3-benzothiadiazole-4,7-dibutylester (BTDB) in Micellar and Non-aqueous Systems

2.1 Introduction

As indicated from the previous chapter, the aim of the research detailed in this thesis, was to investigate the ability of the dibutyl ester of 2,1,3-benzothiadiazole (BTDB) to perform as an improved photochemical mediator over BTDN for the electron transfer between morpholineethanesulphonic acid (MESH) and disodium-9,10-anthraquinone-1,5-disulphonate (AQDS) in a micellar and vesicle environment. The structures of the various components of the system are given below in figure 2.0:

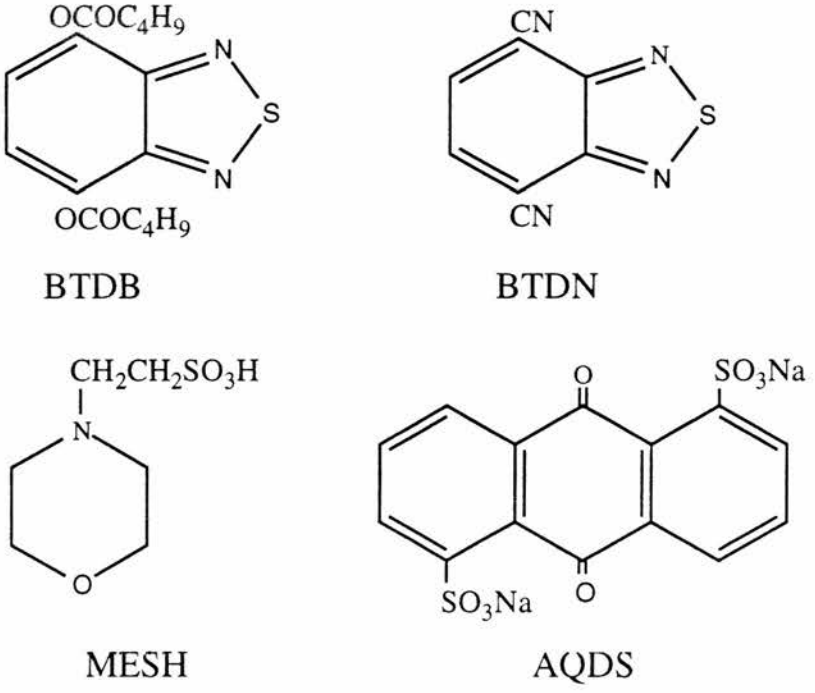

Figure 2.0 : Structures of chromophores, electron donor and electron acceptor.

2.1 Synthesis of BTDB

The previously reported method[1] for the synthesis of BTDB was *via* a dipotassium salt of benzothiadiazole, synthesised by the reaction of 4,7-dibromo-2,1,3-

benzothiadiazole with excess potassium. The dipotassium salt was then reacted with n-butylchloroformate to give the dibutyl ester. However, there was little evidence of the formation of BTDB and doubts were raised as to the exact nature of the product formed.

Therefore, we decided to pursue the synthesis of BTDB in a similar manner to that of BTDE (diethyl ester) which involved the hydrolysis of 2,1,3-benzothiadiazole-4,7-dicarbonitrile (BTDN) (Section 6.9.3) to the 4,7-dicarboxylic acid. Subsequent reaction with thionyl chloride gave the acid chloride and further reaction with alcohol to yield the diester, see figure 2.1.

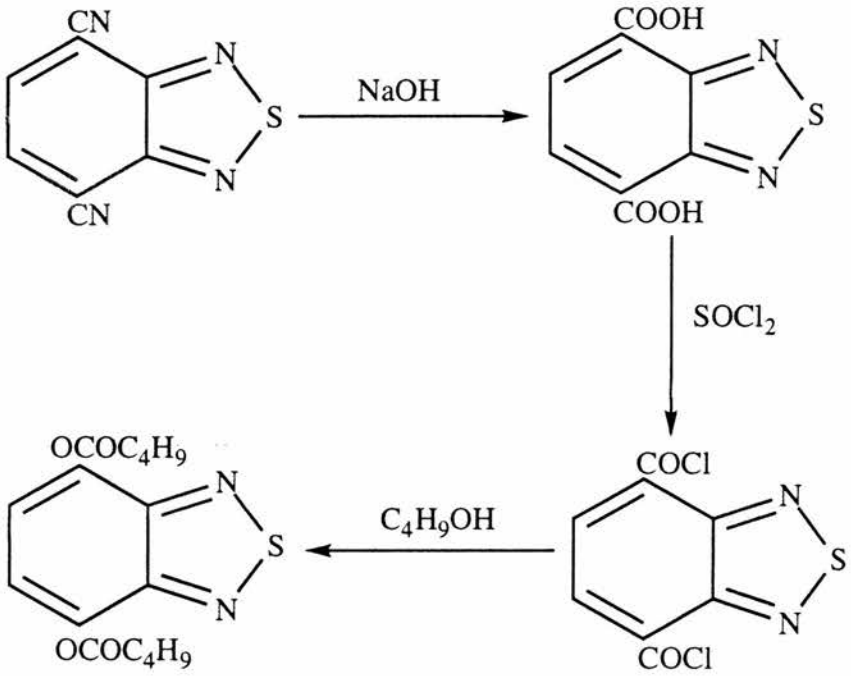

Figure 2.1 : Formation of BTDB from BTDN.

The problem previously encountered[1] with this method was the separation of butanol from BTDB which is a (red - orange) oil. We overcome this by adding petroleum ether to the solution and on removal of it *in vacuo*, BTDB was obtained free from the butanol. The petroleum ether appearing to form an azeotropic mixture with the alcohol.

The BTDB at this stage was not completely pure and it was necessary to

chromatograph in petroleum ether, with BTDB absorbed onto alumina. The impurities were eluted to leave BTDB absorbed on the alumina, washing with diethyl ether removed the BTDB and, on removal of the diethyl ether *in vacuo*, BTDB of high purity was recovered. The melting point for BTDB must be close to room temperature because crystals have been observed in the oil after two weeks of sitting in the sample container. BTDB has been fully characterised by g.c.m.s., accurate mass analysis, elemental analysis and ^{1}H and ^{13}C spectroscopy (Figures 2.3 and 2.4). See figure 2.2 for the mass spectrum of BTDB, showing a weak molecular ion peak with an m/e value of 336 which would be expected.

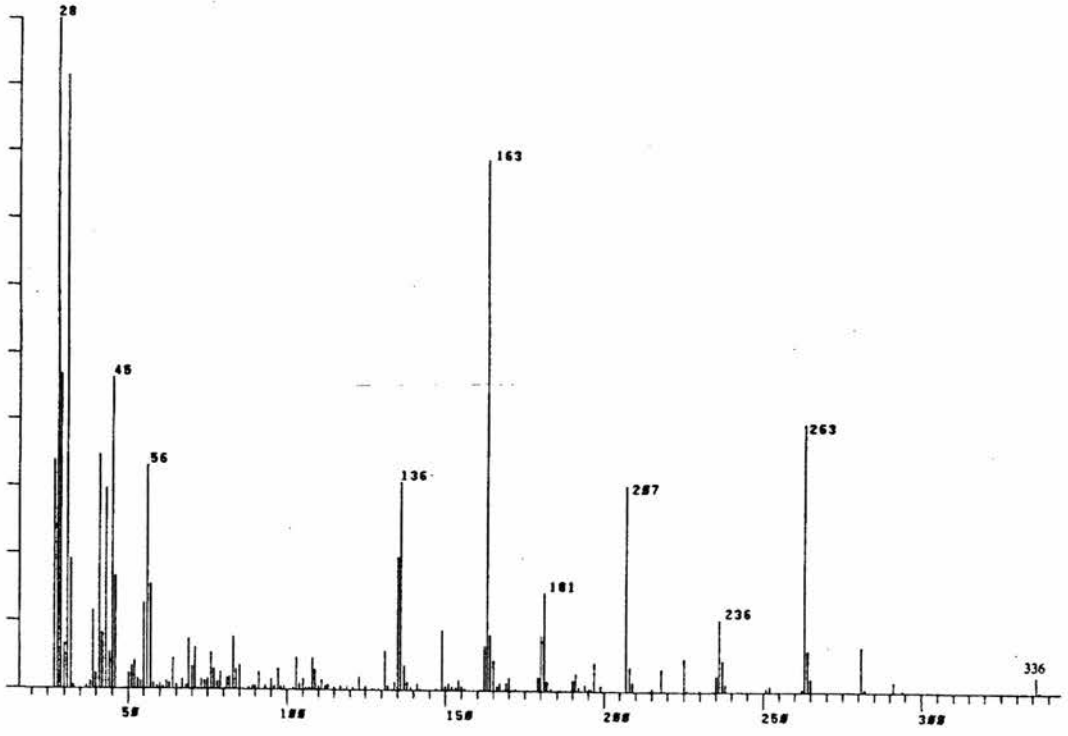

Figure 2.2 : Mass Spectrum of BTDB.

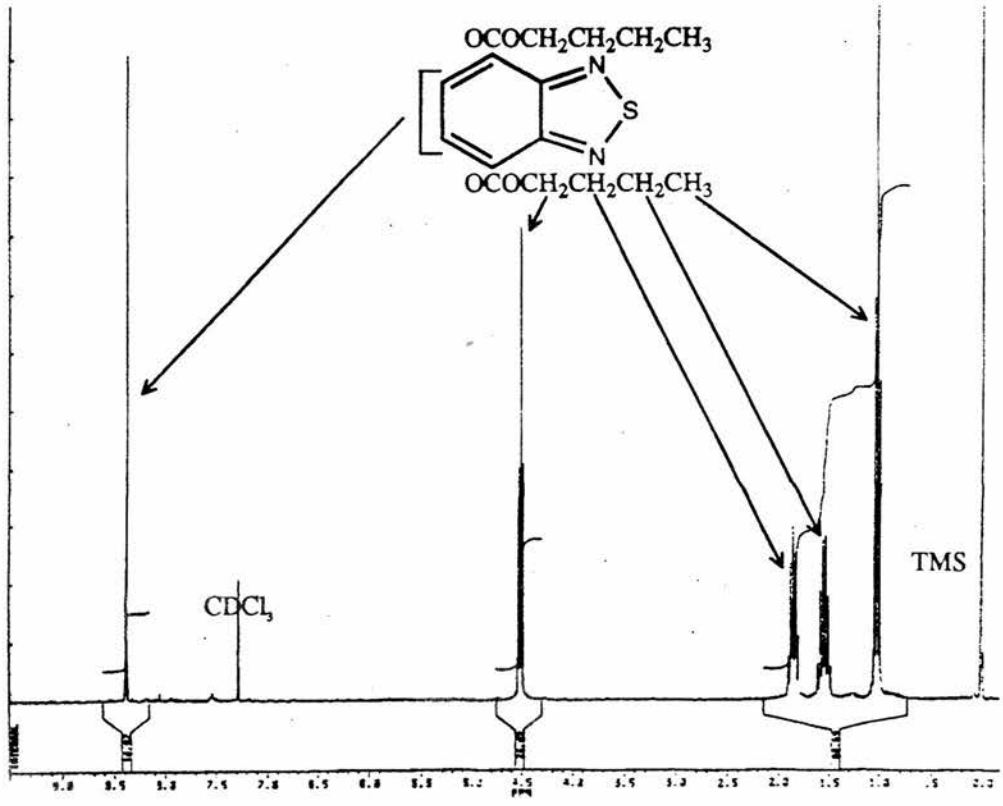

Figure 2.3 : ^{1}H n.m.r. spectrum of BTDB in $CDCl_3$

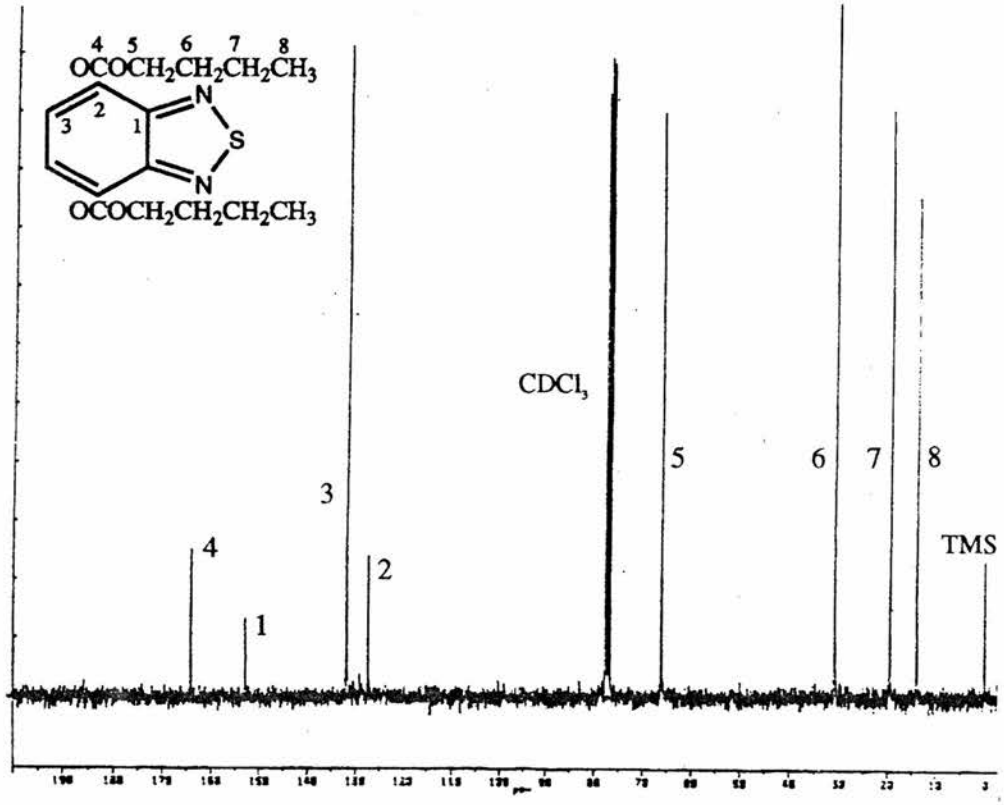

Figure 2.4 : ^{13}C n.m.r. spectrum of BTDB in $CDCl_3$

2.2 U.V.-Visible Spectroscopy

These spectra showed that BTDB has enhanced light absorbing properties over both BTDN and BTDE, in the visible region of the spectrum. This can be seen by examining the extinction coefficients (ε) obtained for each compound at 325 and 400 nm respectively. See table 2.1, below.

Chromophore	$\varepsilon_{325}/10^4 dm^3 mol^{-1} cm^{-1}$	$\varepsilon_{400}/10^4 dm^3 mol^{-1} cm^{-1}$
BTDN	1.8	0.02
BTDE	1.5	0
BTDB	1.8	0.08

Table 2.1: Extinction Coefficients for BTDN, BTDE and BTDB at 325 and 400 nm.

The fact that BTDB possesses a much broader shoulder into the visible region (Figure 2.5) than for BTDN. An absorbance into the visible region is not observed for BTDE. This is important if BTDB is to be used for solar energy conversion.

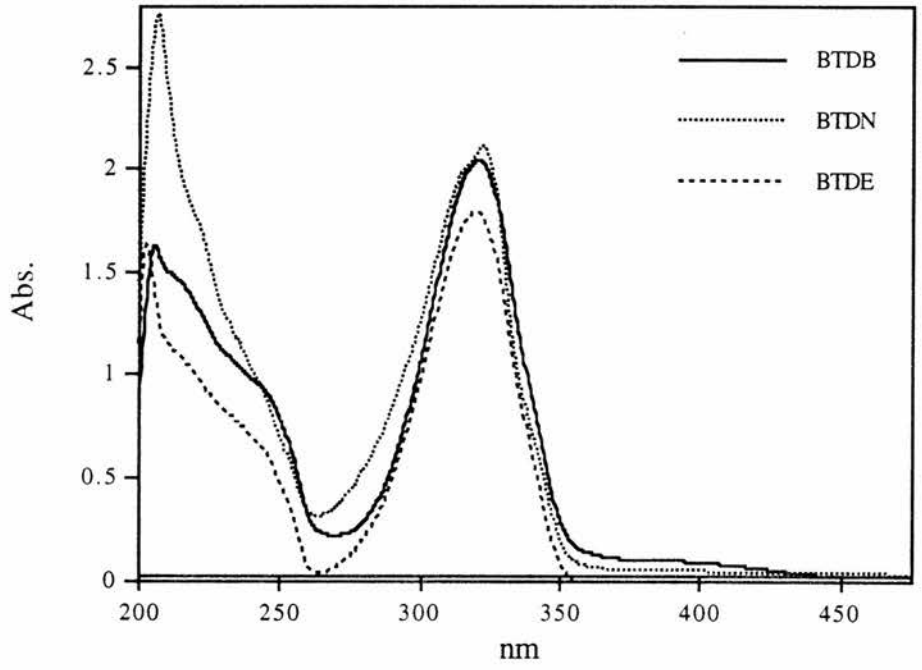

Figure 2.5 : U.v.-visible spectrum of BTDB, BTDN and BTDE in ethanol.

2.3 Partition Coefficients

This experiment was used as an indication of how the chromophores would partition between the hydrocarbon chains of the vesicle and water, thus indicating in which environment the majority of the chromophore would be found, either in the hydrophobic interior of the micelle and vesicle or in the bulk aqueous phase.

Partition coefficients between octan-1-ol and water for each chromophore were measured using uv-visible spectroscopy. The partition coefficient is a constant which can be measured in a heterogeneous system with two or more phases in equilibrium. The ratio of the activities (or concentrations) of the same molecular species in the two or more phases is a constant at a constant temperature. The figures quoted are the ratio of units of chromophore in octanol to the units in water. Previous studies[1] have shown, that BTDE is less soluble than BTDN in octanol. For BTDB, the greater lipophilicity of the butyl groups over the ethyl groups should improve the solubility of BTDB in the octan-1-ol. A value of 400 for BTDB does indeed show that BTDB does have improved solubility in octan-1-ol over BTDN and BTDE, see table 2.2 below. This means that BTDB should be found predominately in the micellar environment or within the vesicle bilayer.

Chromophore	BTDN	BTDE	BTDB
Partition Coeff. (Octanol:Water)	9	6.3	400

Table 2.2 : Partition Coefficients for BTDN, BTDE and BTDB.

A more direct indication of the enhanced solubility of BTDB in the hydrophobic environment was given by the observation that when the vesicles containing BTDB were eluted down a Sephadex column to remove the vesicles from the bulk aqueous phase in which they were produced, the absorbance of BTDB was virtually unchanged from that recorded before passage through the column. In contrast, BTDN was completely removed from the vesicles under these conditions (Table 2.3).

Chromophore	BEFORE	AFTER
BTDN	0.440	0
BTDB	0.550	0.545

Table 2.3 : Effect of GPC on retention of chromophore within the vesicle bilayer (Abs. 320 nm)

2.4 Photolysis Studies in a Micellar Environment

Intermolecular electron transfer studies were carried out with a view to investigating the efficiency of $BTDB^{-\cdot}$ as a combined chromophore and electron transfer catalyst by enhancing the rate of production of the reduced form of the disodium-9,10-anthraquinone-1,5-disulphonate (AQDS) by MES^-. $BTDB^{-\cdot}$ has a shorter lifetime than $BTDN^{-\cdot}$, owing to the ester groups not withdrawing electrons to the same degree as the cyano groups. The electron withdrawal aids in the stabilisation of the radical anion. However, even under conditions where $BTDN^{-\cdot}$ has a short lifetime, the radical anions could still enhance the rate of production of the reduced form of AQDS. Therefore, we have investigated the efficiency of BTDB for these reactions despite its short lifetime.

To determine that the reaction of AQDS reduction is enhanced by BTDB, continuous photolysis experiments were performed. These were complicated by the fact that photochemical electron transfer occurs from the electron donor (MESH), to the anthraquinone derivative, in the presence of the CTAB micelles, but without BTDB being present. In this reaction, the anthraquinone absorbs light to give an excited state which then receives an electron from MES^- (sacrificial electron donor) to form the radical anion of the anthraquinone. This radical anion then goes on to disproportionate and protonate to form the hydroquinone (Figure 2.6).

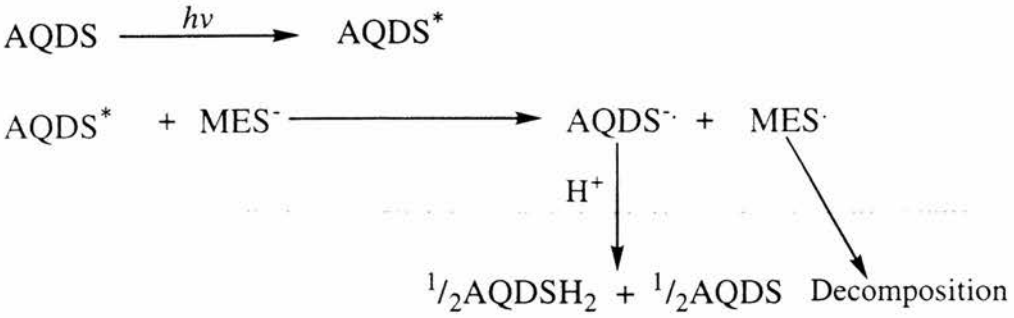

Figure 2.6 : Reaction scheme between MES^- and AQDS.

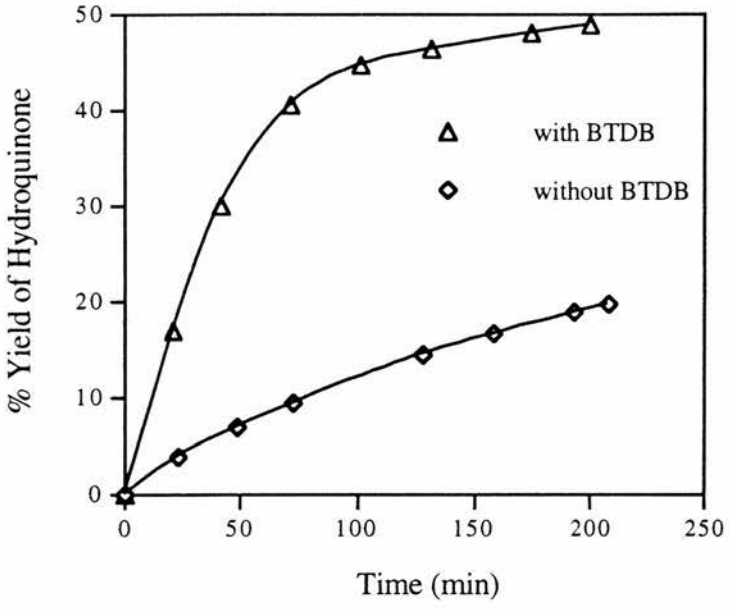

Figure 2.7 : Production of $AQDSH_2$ from AQDS and MES^- in the presence of CTAB while in the presence and absence of BTDB at pH 6.5.

Figure 2.7, shows that BTDB causes a marked enhancement in the rate of formation of the hydroquinone ($AQDSH_2$) in the heterogeneous system, showing that enhanced electron transfer does occur, despite the transient nature of $BTDB^{-}\cdot$, suggesting that the forward electron transfer to AQDS is highly efficient. A reaction scheme for this photo-assisted electron transfer using BTDB can be seen in figure 2.8.

On photolysis with BTDB, the solution went from being a very pale yellow to producing a bright yellow colour, confirming the presence of $AQDSH_2$. Yields of

1,5-$AQDSH_2$ were determined from the absorbance of the solution at 392 nm (ε = 17500 $dm^3mol^{-1}cm^{-1}$). By photolysing AQDS in the presence of, excess MESH, CTAB and BTDB until the generation of $AQDSH_2$ at ~392 nm ceased. and using the Beer-Lambert equation, the extinction coefficient could be determined (Section 6.2.1(ii)).

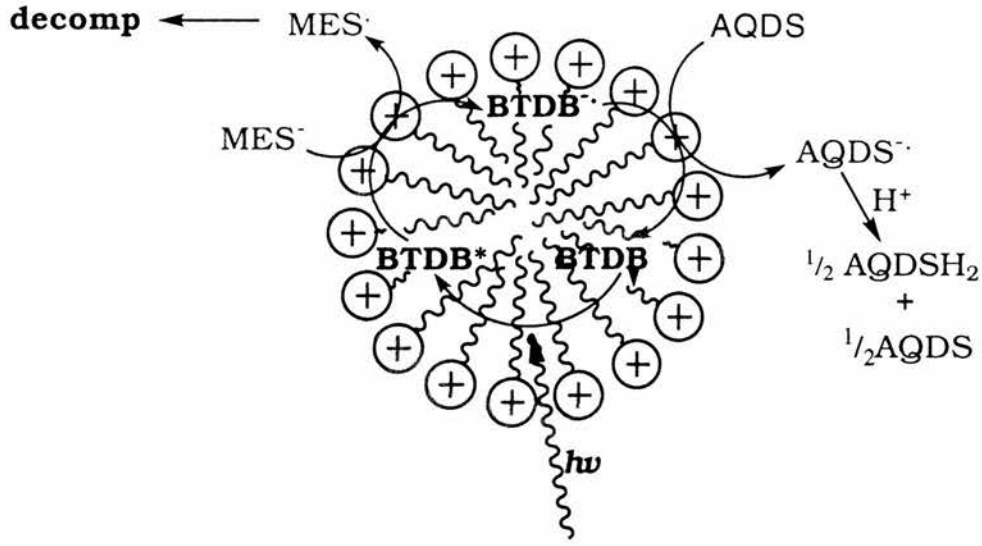

Figure 2.8 : Schematic representation of the photo-assisted BTDB-mediated electron transfer from MES^- to AQDS in the presence of CTAB micelles.

2.5 The Effect of Individual Reagents on the Rate of Conversion of AQDS to $AQDSH_2$

2.5.1 Light Intensity

This set of experiments was performed to study the influence the different reagents of the reaction have on the the overall rate of conversion.

The first reagent to be studied was light intensity. Variations were achieved by the use of metal gauzes of different mesh size acting as light filters. The percentage of light allowed to pass through the filter was determined by using an I.R. machine, see section 6.1.10. The gauzes finally used transmitted 33, 52, 58 and 73% of the light. All other reagents remained constant as described in the experimental section 6.2.1(iii). The results are presented graphically in figure 2.9 — 2.13.

Figure 2.9, shows the yields of $AQDSH_2$ involving two competing reactions (1) BTDB catalysed reduction and (2) MES^- reduction of AQDS, as mentioned in the previous section. Initial rates were then plotted against light intensity, (Figure 2.10).

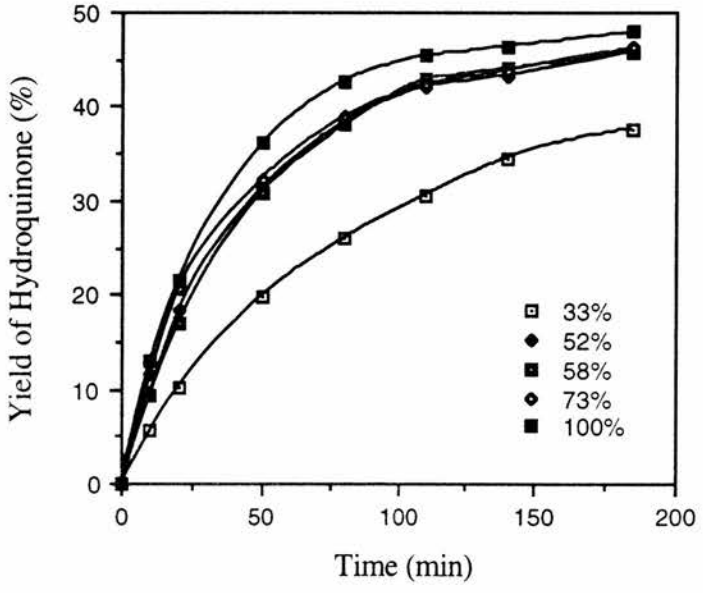

Figure 2.9 : Production of $AQDSH_2$ from AQDS in the presence of CTAB, MES^- and BTDB while varying light intensity at pH 6.5.

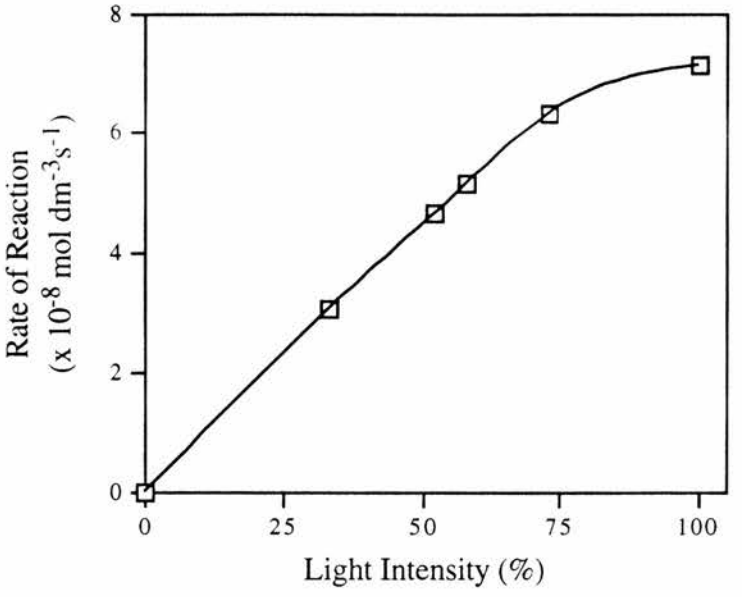

Figure 2.10 : Changes in rates of reaction of AQDS reduction caused by changes in light intensity in the presence of CTAB, MES^- and BTDB at pH 6.5.

In order to obtain data, solely on the BTDB promoted reaction, we have also studied the reaction in the absence of BTDB (Figures 2.11 and 2.12).

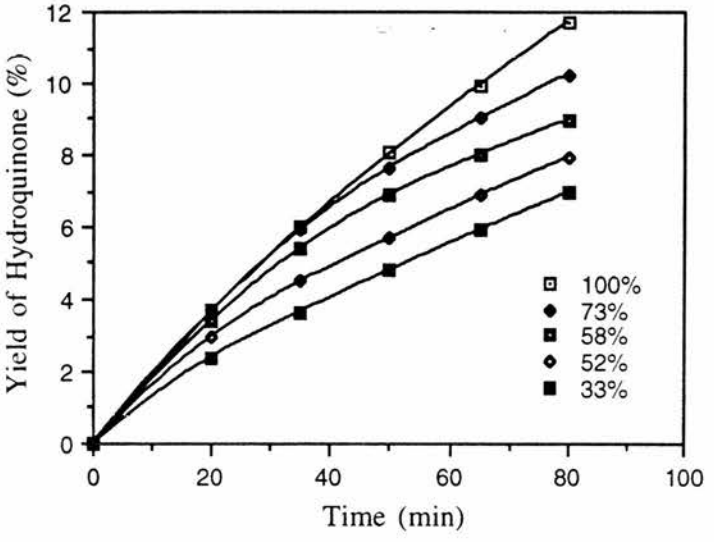

Figure 2.11 : Production of $AQDSH_2$ from AQDS in the presence of CTAB and MES^- in the absence of BTDB at pH 6.5 while varying light intensity.

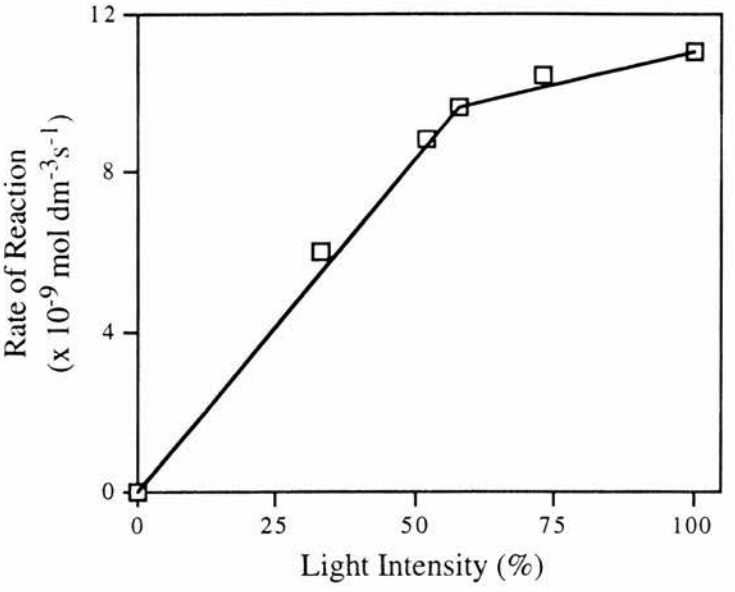

Figure 2.12 : Rates of reaction for the reduction of AQDS by MES^- only in the presence of CTAB and the absence of BTDB at pH 6.5 while changing light intensity.

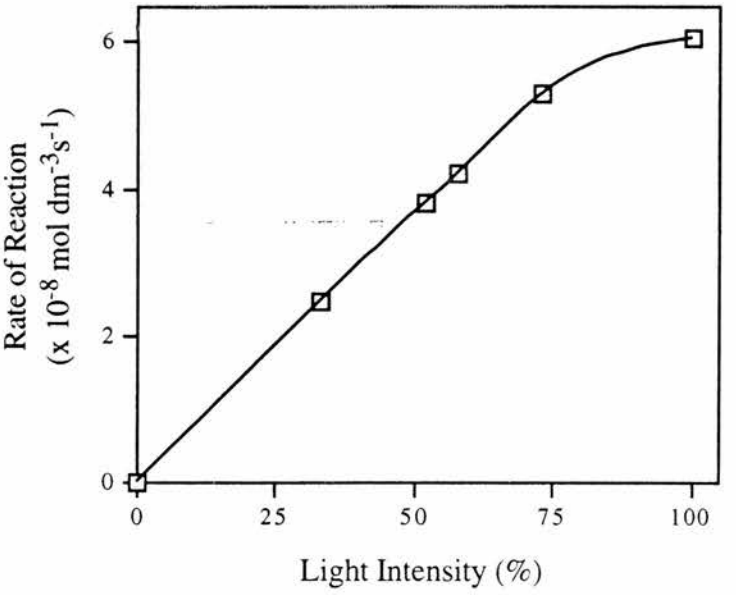

Figure 2.13 : Variation in rates of reaction with light intensity for $AQDSH_2$ production from AQDS by BTDB without the competing reaction of AQDS reduction by MES^-, in CTAB at pH 6.5.

By subtracting the rates of reaction obtained in figure 2.12 from those in figure 2.10, we obtain the graph in figure 2.13, showing the actual rates of reaction for the BTDB catalysed reduction of AQDS only. The rate has first order dependence up to 75% of total light intensity but shows saturation at higher values.

2.5.2 [MESH]

The next reagent to be studied was the sacrificial electron donor (MESH) and the effect its concentration had upon the rate of conversion. The concentrations used were 0.025, 0.05, 0.075 and 0.1 mol dm^{-3}. Controls were run where BTDB was absent from the reaction mixture. For method see section 6.2.1 (iv).

Once again, the results are presented graphically. In figures 2.14 and 2.15 the yields for $AQDSH_2$ for the two competing reactions and in the absence of BTDB are shown respectively. From figures 2.14 and 2.15 the initial rates were calculated and plotted against [MESH] (Figures 2.16 and 2.18).

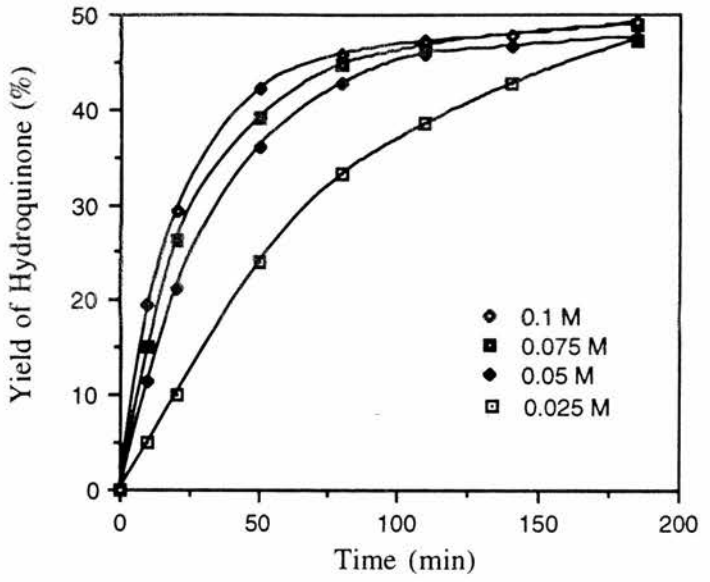

Figure 2.14 : Production of $AQDSH_2$ from AQDS in the presence of CTAB and BTDB while varying [MESH] at pH 6.5.

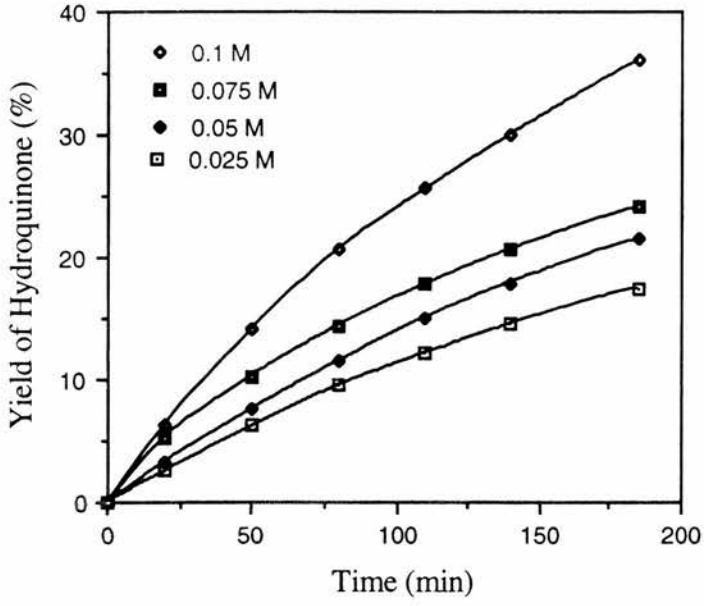

Figure 2.15 : Production of $AQDSH_2$ from AQDS in the presence of CTAB and absence of BTDB while varying [MESH] at pH 6.5.

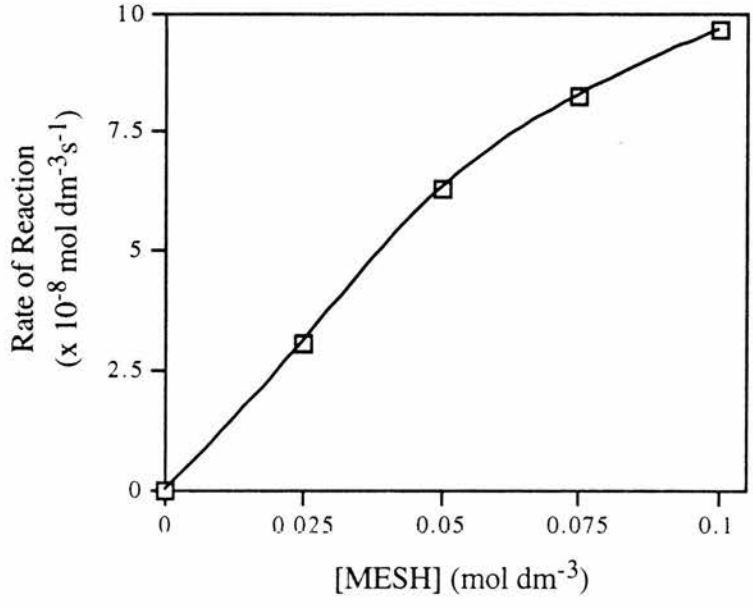

Figure 2.16 : Varying Rates of Reaction caused by changing the [MESH] in the presence of BTDB and CTAB at pH 6.5.

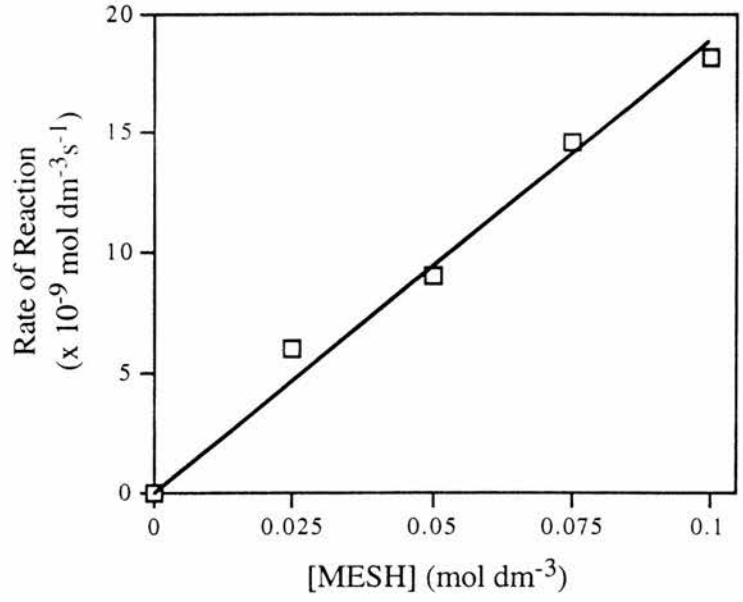

Figure 2.17 : Varying Rates of Reaction caused by changes in [MESH] in the absence of BTDB but in the presence of CTAB at pH 6.5.

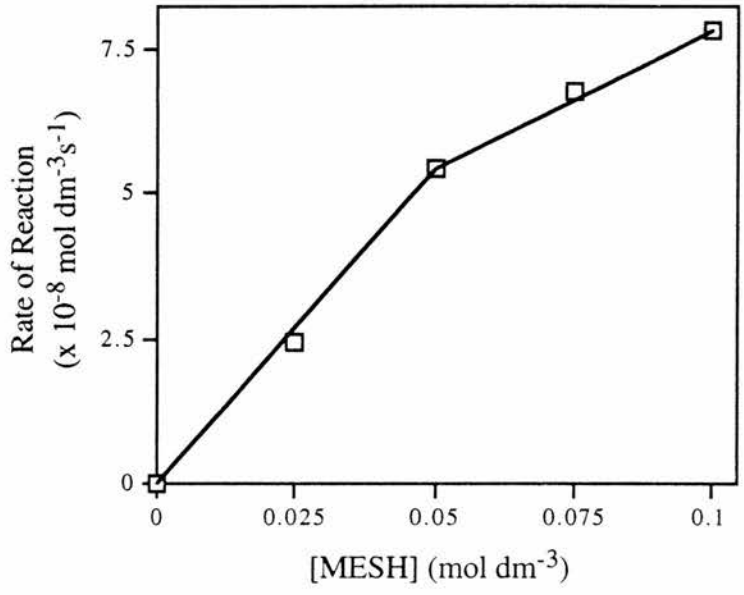

Figure 2.18 : The dependence of initial with [MESH] rates of reaction for the BTDB catalysed reduction of AQDS without the competing reduction of AQDS by MES^-, in CTAB at pH 6.5.

The values shown in figure 2.18 were calculated by subtracting the rates in figure 2.17 from those in figure 2.16 and shows the rates of reaction for the BTDB catalysed reduction of AQDS, without the competing reaction with MES^-. Once again, first order dependence is observed at low [MESH] but this tends towards zero order at higher [MESH].

2.5.3 [BTDB]

This set of experiments was concerned with the effect that [BTDB] has on the overall rate of conversion from AQDS to $AQDSH_2$ (section 6.2.1 (v)). The results are presented graphically in figure 2.19. As shown previously, there are two photochemical processes occuring simultaneously when BTDB is present. Therefore, to try and gain a more accurate picture of the BTDB enhanced reaction, we subtracted the percentage conversion values obtained for the reduction of AQDS by MES^- in the absence of BTDB, from the values obtained in the presence of BTDB. These subtracted values are presented graphically in figure 2.20. From figures 2.19 and 2.20, we were able to determine the initial rate at t = 0 and hence the kinetics involved in the system. These rates are presented in figures 2.21 and 2.22 and show a simple first order dependence on [BTDB].

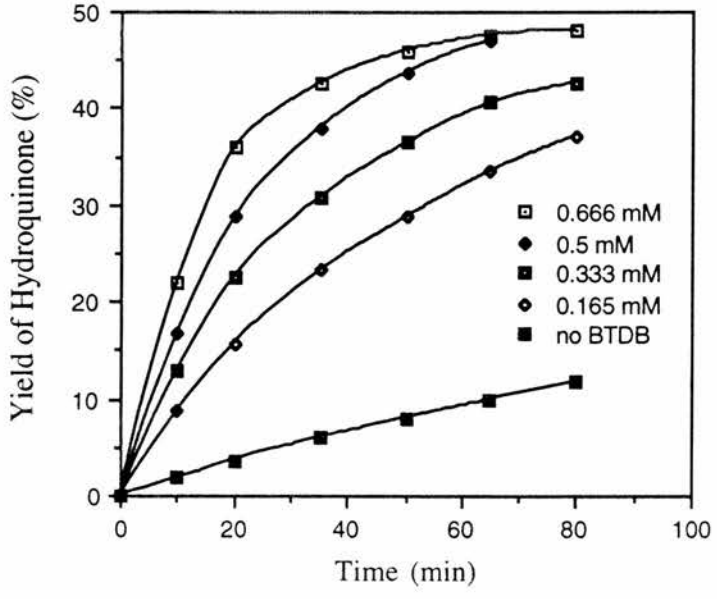

Figure 2.19 : Production of $AQDSH_2$ from AQDS in the presence of CTAB and MES^- while varying [BTDB] at pH 6.5.

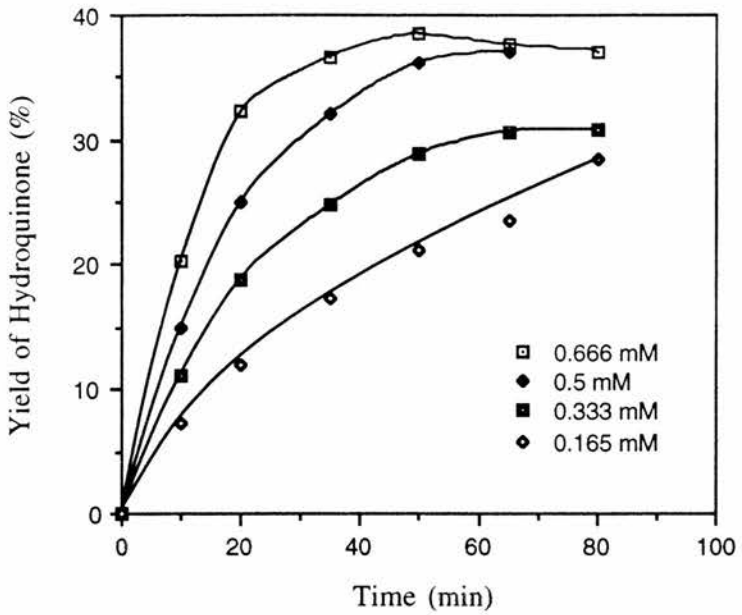

Figure 2.20 : Reduction of AQDS to $AQDSH_2$ minus the direct influence of MES^- reducing AQDS in the presence of CTAB and BTDB at pH 6.5.

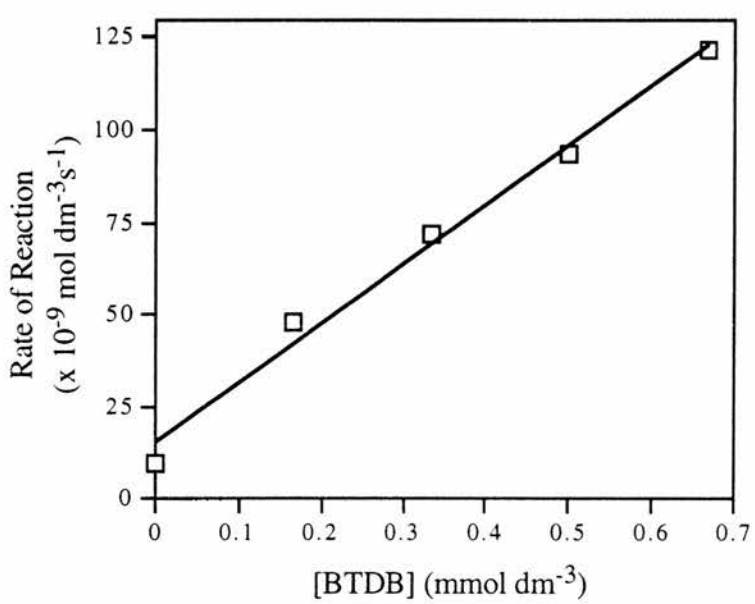

Figure 2.21 : Varying rate of reaction caused by the presence of two reduction processes while varying [BTDB] in the presence of CTAB and MES^- at pH 6.5.

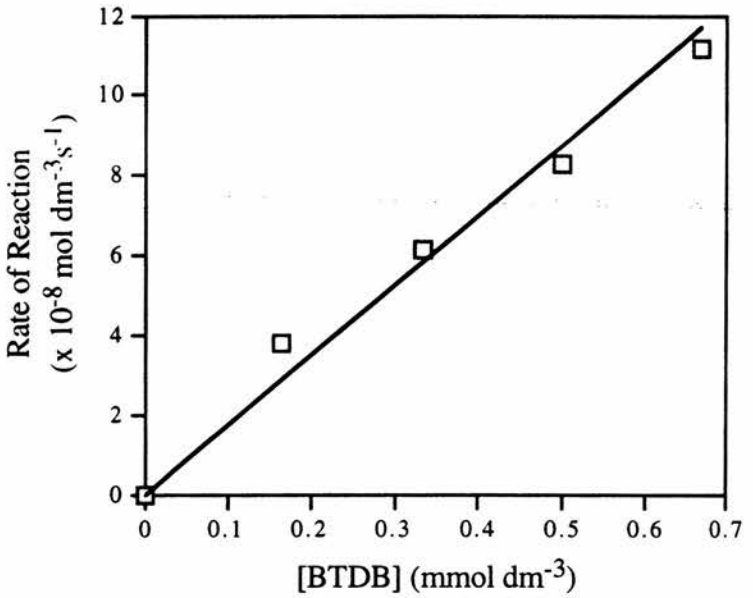

Figure 2.22 : Overall rates of reaction for $AQDSH_2$ production from AQDS catalysed by BTDB while varying [BTDB] without the competing reaction of AQDS reduction by MES^-, in CTAB at pH 6.5.

2.5.4 pH

The next effect studied was pH. As the optimum pH for MES^- is 6.5[1], a pH range (4 — 12) was employed and the production of $AQDSH_2$, at each pH, is presented graphically in figure 2.23. The initial rates are plotted against pH in figure 2.25 and show that the initial rate is essentially independent of pH between pH 6.5 and 10.

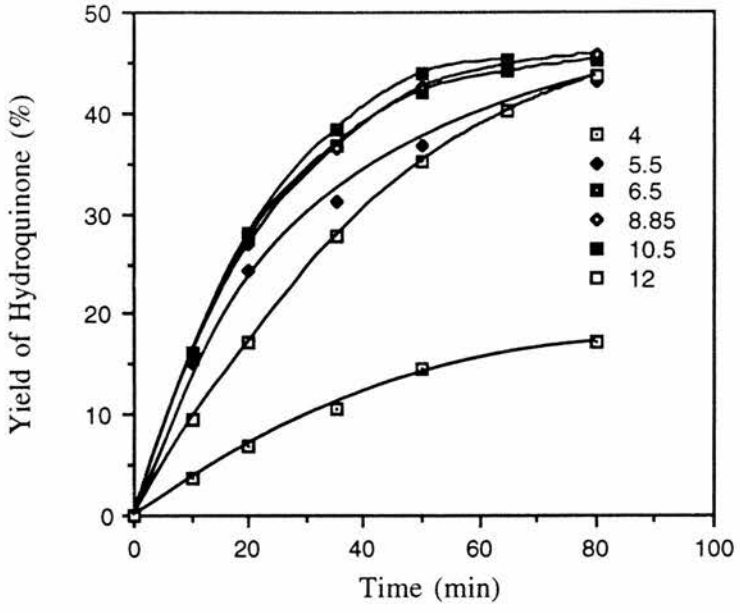

Figure 2.23 : Production of $AQDSH_2$ while varying pH in the presence of CTAB, MESH and BTDB.

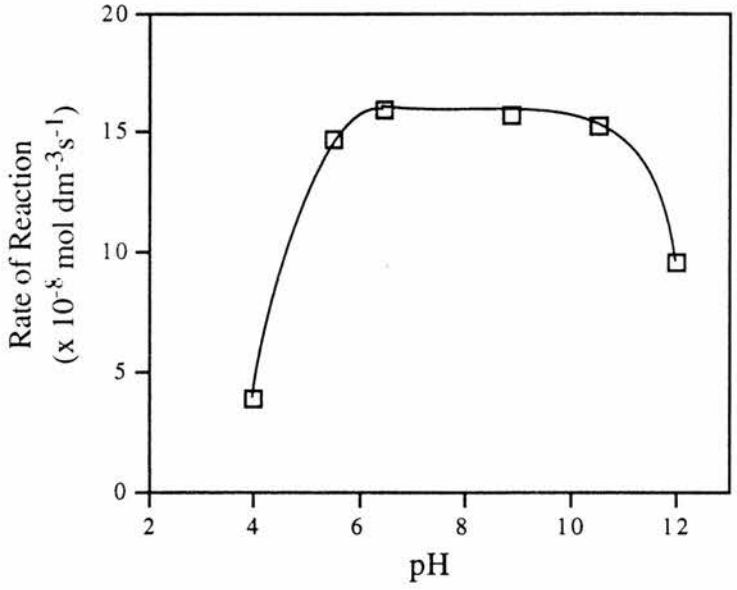

Figure 2.24 : Varying rates of reaction caused by changes in pH in the presence of CTAB, MESH and BTDB.

2.5.5 [AQDS]

The effect of [AQDS] was the penultimate to be studied. As with previous reagents a range of concentrations was utilised; 0.083, 0.165, 0.33, 0.495 and 0.66 mmol dm^{-3} (section 6.2.1 (viii)). The yields and the initial rates obtained are presented graphically in figures 2.25 and 2.26, respectively.

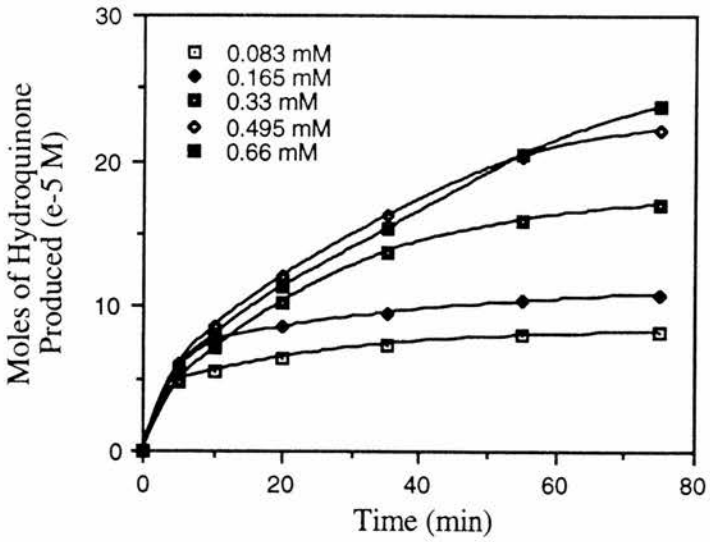

Figure 2.25 : Production of $AQDSH_2$ from AQDS while varying [AQDS] in the presence of CTAB, MES^- and BTDB at pH 6.5.

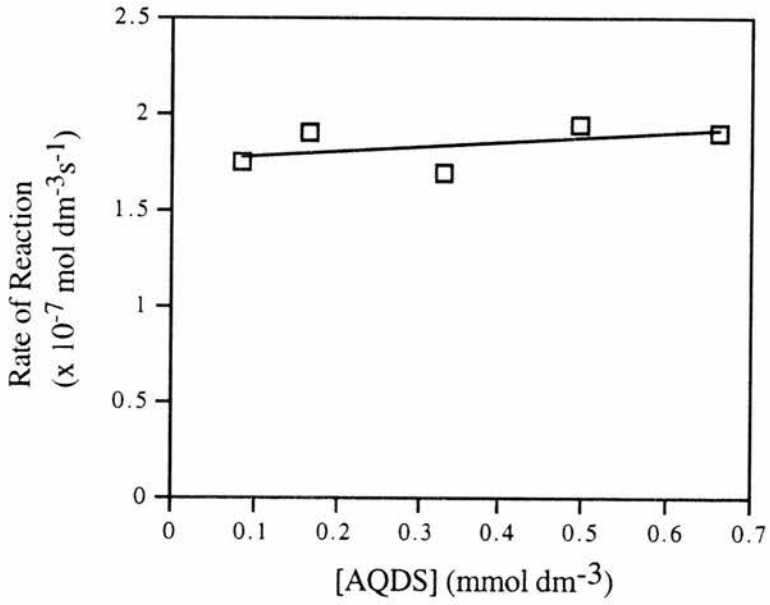

Figure 2.26 : Different rates of reaction caused by varying [AQDS] in the presence of CTAB, MES^- and BTDB at pH 6.5.

2.5.6 [CTAB]

The effect of [CTAB] on the reduction of AQDS was last to be studied. A range of concentrations was employed, from CTAB being absent through the c.m.c. (0.034% w/w) up to 0.8% w/w. For method see section 6.2.1 (vi). The yields of $AQDSH_2$ obtained are presented in figure 2.27 and from this data, the initial rates were calculated, plotted and displayed in figure 2.28. For comparison, a similar study involving BTDN is shown in figure 2.29.

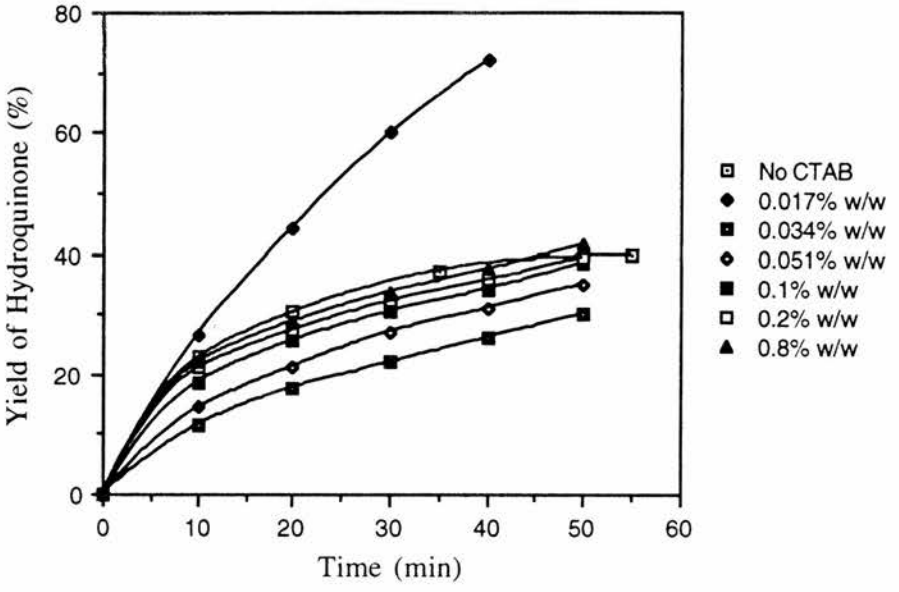

Figure 2.27 : Production of $AQDSH_2$ from AQDS while varying [CTAB] in the pesence of BTDB, MES^- at pH 6.5.

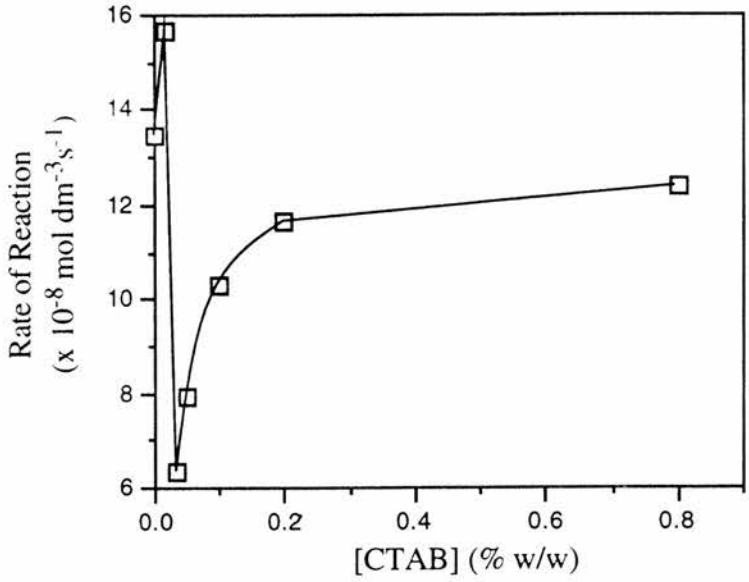

Figure 2.28 : Different rates of reaction caused by varying [CTAB] in the presence of MES^-, BTDB at pH 6.5.

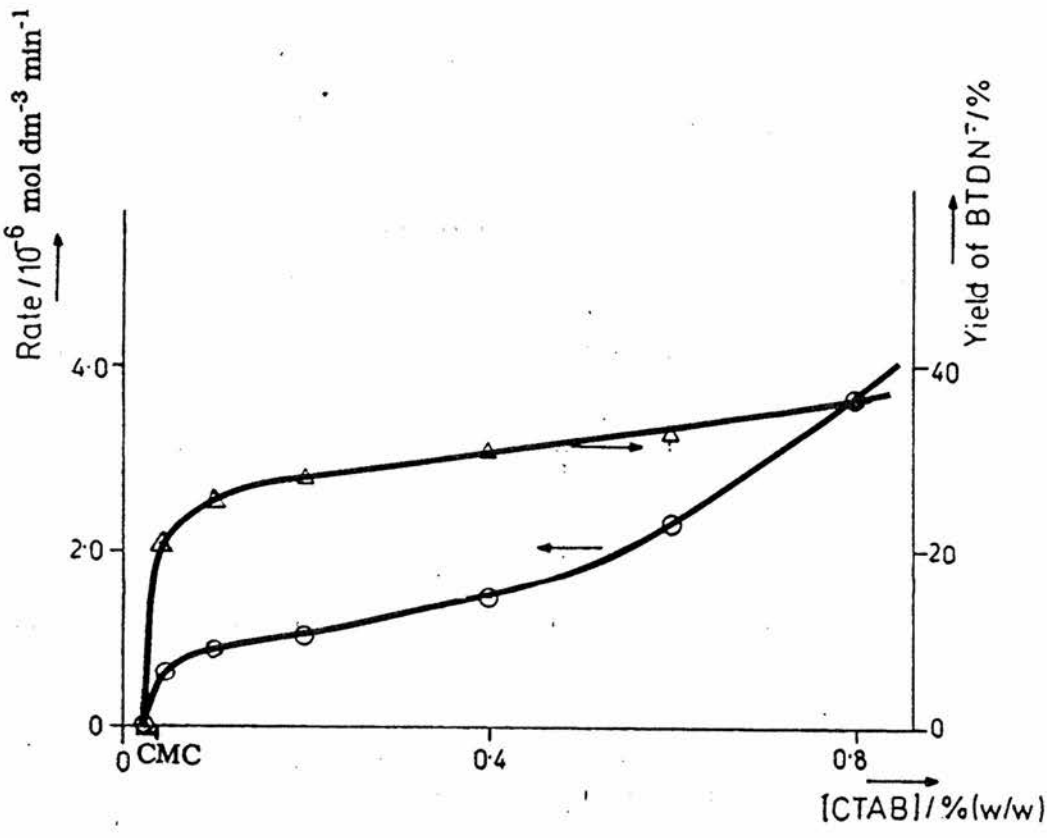

Figure 2.29 : Dependence of the initial rate (0) and maximum yield (Δ) of $BTDN^{\cdot-}$ on the formation of [CTAB].

2.6 DISCUSSION

Before discussing the results presented in the previous section concerning the effects the individual reagents have on the production of $AQDSH_2$, we shall first propose an overall reaction mechanism for the reduction of AQDS by BTDB and subsequently derive a rate expression for the reaction, see figure 2.30 below. It is assumed that the rates of decomposition of $MES^{\cdot}$ and the disproportionation and protonation of $AQDS^{-\cdot}$ are fast compared with the other reaction steps.

$$BTDB + I \xrightarrow{k_1} BTDB^*$$

$$BTDB^* \xrightarrow{k_2} BTDB$$

$$BTDB^* + MES^- \xrightarrow{k_3} BTDB^{-\cdot} + MES^{\cdot} \xrightarrow{\text{Fast}} \text{Decomposition}$$

$$BTDB^{-\cdot} + AQDS \xrightarrow{k_4} BTDB + AQDS^{-\cdot} \xrightarrow[H^+]{\text{Fast}} {}^1/_2AQDSH_2 + {}^1/_2AQDS$$

$$\text{Rate} = k_4\,[BTDB^{-\cdot}][AQDS]$$

$$\frac{d[BTDB^{-\cdot}]}{dt} = k_3\,[BTDB^*][MES^-] - k_4\,[BTDB^{-\cdot}][AQDS] = 0$$

$$\frac{d[BTDB^*]}{dt} = k_1 I[BTDB] - k_2[BTDB^*] - k_3[BTDB^*][MES^-] = 0$$

$$\text{Rate} = k_3[BTDB^*][MES^-] = k_4[BTDB^{-\cdot}][AQDS]$$

$$[BTDB^*] = \frac{k_1 I[BTDB]}{k_2 + k_3[MES^-]}$$

$$\therefore \text{RATE} = \frac{k_3\,k_1 I[BTDB][MES^-]}{k_2 + k_3[MES^-]}$$

Figure 2.30 : The reaction mechanism and the rate law expression for the enhanced reduction of AQDS by BTDB in the presence of CTAB and MES^-.

From the final rate expression we can make the following predictions about the order of the reaction with respect to individual reagents:

(1) 1st order with respect to Light Intensity (I),

(2) 1st order with respect to [BTDB],

(3) 1st order with respect to [MES^-] at low [MES^-] and zero-order at high [MES^-].

(4) Independent of [AQDS]

2.6.1 [BTDB]

The effect of [BTDB] on the formation of $AQDSH_2$ is shown in figure 2.21. This shows a straight line with non-zero intercept indicating that the reaction is first order in [BTDB] but that another reaction occurs which does not involve BTDB. This is a slower reaction in which AQDS acts as the chromophore and accepts an electron into the excited state from MES^-. This reaction has been studied separately (Figure 2.19) and allowances can be made for it by subtracting the results obtained when there was no BTDB present in solution (Figure 2.19) from those where BTDB was present. These corrected results are displayed in figure 2.20 and from the initial rates (Figure 2.22), confirm the first order dependence of the rate of $AQDSH_2$ production on [BTDB], consistent with the proposed mechanism.

2.6.2 [MESH]

As for varying BTDB, it is necessary to correct the data obtained for varying [MESH] by subtracting the data obtained in the absence of BTDB. This corrected data is shown in figure 2.18. First order behaviour is observed for [MESH] below 0.05 mol dm^{-3} but the reaction tends to zero order at higher [MESH]. This result is completely consistent with the proposed mechanism.

2.6.3 Light Intensity

After correcting for the reaction between MES^- and BTDB in the absence of BTDB, the dependence of the initial rate of production of $AQDSH_2$ upon light intensity is

shown in figure 2.13. As expected from the rate expression, the reaction shows first order dependence at low light intensity but less than first order at higher light intensity. This type of behaviour is not unusual for photochemical reactions and usually arises because the number of molecules present in the solution is finite. If all are excited, further increases in light intensity cannot excite further molecules so that no further increase in rate is observed. We assume that in our experiments we are moving towards this situation at higher light intensities.

2.6.4 pH

From the results obtained when studying the influence of pH on the enhanced reduction of AQDS by BTDB, we observe that the highest yields are obtained at pH 6.5 — 10.5 (Figure 2.23). This can be more clearly shown when the initial rates were plotted against pH (Figure 2.24) which shows that the rate of reaction below 6.5 and above 10.5 is slower than the rate observed between 6.5 and 10.5 which is relatively constant, showing zero order dependence.

The structure of MES- is similar to that of an amino acid which means that MESH is amphoteric. Therefore, below pH 6.15, MESH predominately exists as a neutral protonated species (Figures 2.32 and 2.33) but MES^- with a net negative charge is still present which is why a reaction is still observed at these lower pH's. Between the pH's of 6.5 and 10.5, the MESH exists predominately with a negative charge (Figures 2.32 and 2.33) until 100% converted at pH 9.5. This would indicate that the reduction of AQDS by BTDB is independent of $[MES^-]$ as the rate of reaction between pH 6.5 and 10.5 is relatively constant.. At pH's greater than 10.5 the speciation graph (Figure 2.33) shows no formation of any other species. Therefore, we assume that a reaction between BTDB and OH^- is occuring and reducing the number of BTDB molecules available to perform the reaction. A similar reaction occured for BTDN where it formed a Miesenheimer complex.[1]

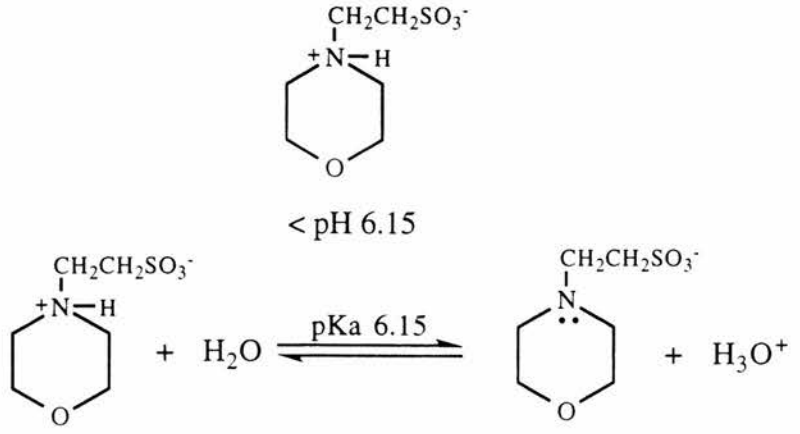

Figure 2.32 : Reaction schemes showing the effect of pH on the structure of MESH.

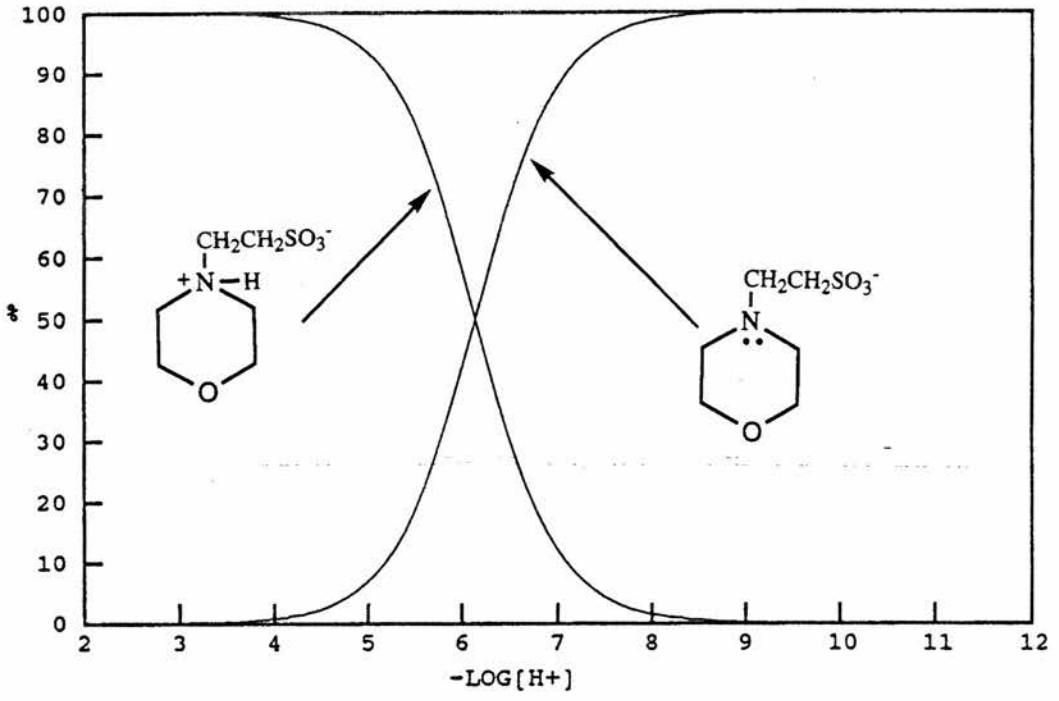

Figure 2.33 : Speciation graph for MES.

2.6.5 [AQDS]

As predicted by the proposed mechanism, the reaction is zero-order in AQDS.

2.6.6 [CTAB]

The effect of [CTAB] concentration on the initial rate of generation of [$AQDSH_2$] is shown in figure 2.28. With no CTAB present, the rate is relatively high and it

increases on addition of small amounts of CTAB but drops dramatically once the c.m.c is reached before rising slowly at higher [CTAB]. A similar observation was recorded by Robinson *et al.* when studying the reduction of AQDS by BTDN in a micellar environment.[2]

In the absence of CTAB, it is expected that the two reagents for the electron transfer event, $BTDB^{-\cdot}$ and AQDS (which is dinegative), will electrostatically repel one another so that electron transfer will be inhibited and most of the production of $AQDSH_2$ will thus be *via* the unpromoted reaction between $AQDS^*$ and MES^-. On addition of small amounts of CTAB, it seems probable, that the positive headgroups of the CTAB may act as an 'assembly point' for $BTDB^{-\cdot}$ and AQDS to come together so that the promoted reaction becomes more important and with the unpromoted reaction continuing, there was an increase in the rate of production of $AQDSH_2$.

As micelles form at the c.m.c., spatial separation occurs between the BTDB (inside the hydrophobic environment of the micelle) and the AQDS (outside the micelle) so that the rate drops. Upon increasing the [CTAB] from the c.m.c. we observed an increase in the rate of production of $AQDSH_2$. This increase in the rate was probably due to an increase in the [BTDB] solubilised within the hydrophobic envionment of the micelle. This allows a greater concentration of $BTDB^{-\cdot}$ to be produced which was reflected in the increase in the initial rate of production. The rate becoming almost constant reflects that the micelles have probably solubilised the majority of the BTDB from the aqueous solution.

Overall, this dependence of the initial rate of generation of $AQDSH_2$ from MES and AQDS in the presence of BTDB appears to be consistent with the reaction scheme proposed (Figure 2.29) for [BTDB], [MESH], [AQDS] and light intensity. The dependence upon [CTAB] can be explained in terms of the uptake of BTDB by the micelles.

2.7 Attempted Photochemical Generation of $BTDB^{-\cdot}$

Having demonstrated that BTDB could act as an electron transfer agent, we attempted to generate $BTDB^{-\cdot}$ *via* a number of different methods. The first was by photolysis, simply omitting AQDS from the reaction described above.

The experiment was performed in a buffered aqueous solution of BTDB along with MES^- at pH 6.5 in the presence of CTAB, under an argon blanket. CTAB was employed to help stabilise the radical anion. Upon photolysis a green/yellow colouration appeared, with an absorption maximum at 400 nm along with a corresponding reduction in the intensity of the absorption from BTDB at 320 nm. On addition of air, the colouration remained. When the experiment was repeated in air the colouration appeared again but slower than under an inert atmosphere. Therefore, the green/yellow species appears as a function of the period of photolysis.

Continuous photolysis of BTDB and TEOA in acetonitrile also led to a steady increase in the absorbance peak at 400 nm corresponding to the formation of the green/yellow species. Control experiments were performed and in an aqueous environment it was essential to have the micelle and electron donor present. When in acetonitrile, it was necessary to have the electron donor present. The green species was not ESR active and appeared to be a stable decompositon product. Attempts to isolate the unknown species or to identify it by n.m.r. spectroscopy were unsuccessful because of the low concentration of BTDB in solution.

2.8 Electron Spin Resonance Studies

Esr studies were performed on an aqueous buffered CTAB solution of BTDB in the presence of TEOA and MES. However, no esr signal was recorded which would indicate that any radical anion species was extremely short lived. Similar results were observed on photolysis of BTDB in acetonitrile. These observations appear to be in contrast with those from the cyclic voltammetry studies performed in acetonitrile (Section 2.10) but confirm that the green/yellow product observed in the continuous photolysis studies is not a radical.

2.9 Laser Flash Photolysis studies on BTDB in a CTAB Environment

Since $BTDB^{-\cdot}$ appears to be very short lived, we attempted laser flash photolysis studies. These studies were concerned with attempting to characterise $BTDB^{-\cdot}$ spectroscopically by studying the decay and lifetime of the radical anion within a micellar environment in the presence of air and argon and in the presence and absence of AQDS.

2.9.1 Observation of $BTDB^{-\cdot}$

A solution containing MES, BTDB and CTAB was subjected to a flash from a Xe-HCl laser and the maximum absorbance measured at various wavelengths betwen 350 and 750 nm. The absorbances were plotted to obtain a visible spectrum of the transient (Figure 2.34) which was very similar to that of $BTDN^{-\cdot}$ which has been isolated and characterised by ESR spectroscopy.[1,3] Therefore, the spectrum obtained in figure 2.34 is an accurate representation of the spectrum that would be achieved if the radical anion of BTDB could be isolated and studied by uv-visible spectroscopy.

The absorbance at 380 nm was recorded over time (Figure 2.35) and showed a single exponential decay back to the baseline. This decay arises from reaction with O_2 *via* the reaction sequence shown below and has a first order rate constant of $6.6 \times 10^4\ s^{-1}$ (Table 2.4).

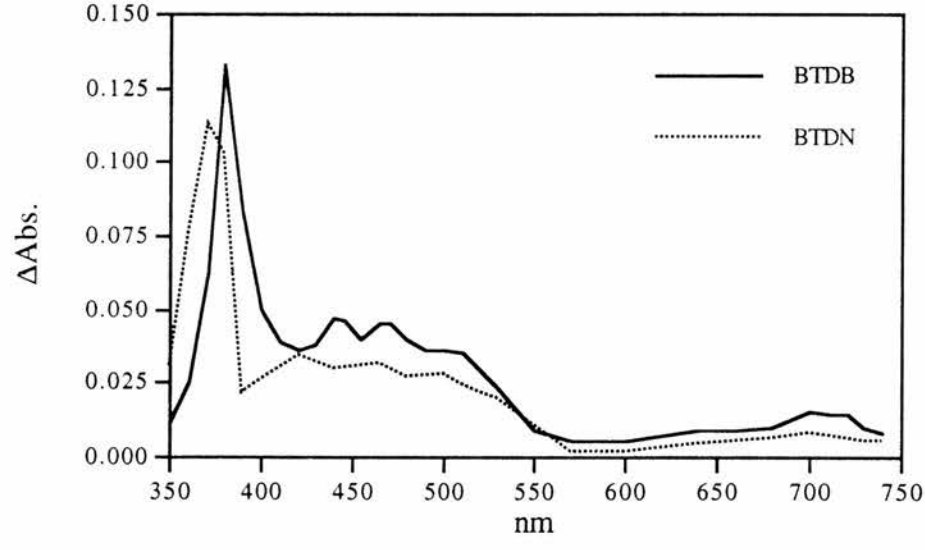

Figure 2.34 : Spectrum of transient species obtained on the photolysis of BTDB in air, in the presence of CTAB and MES^- at pH 6.5.

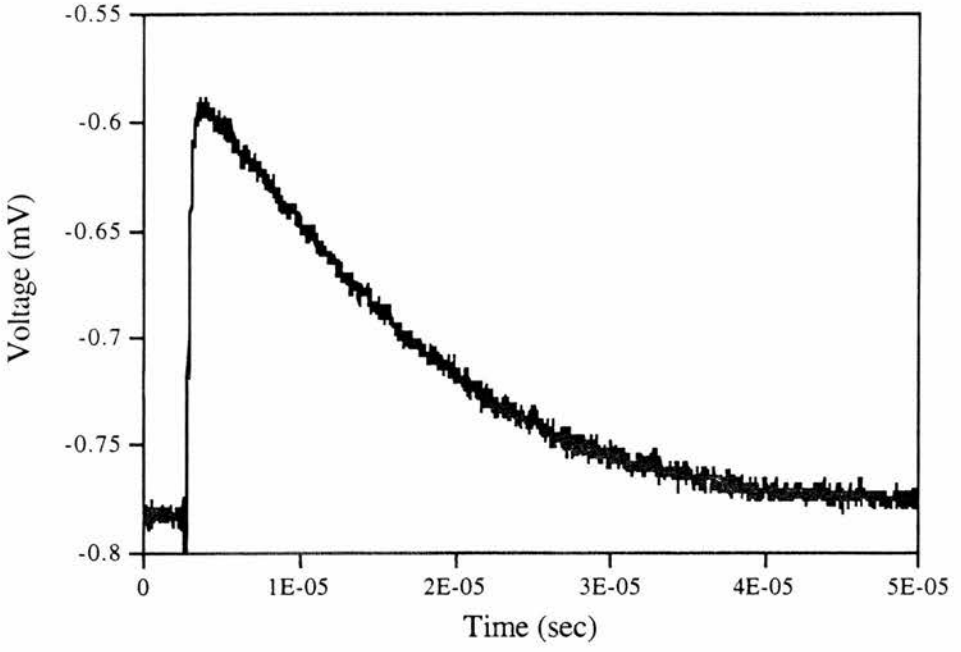

Figure 2.35 : Laser flash photolysis decay trace for $BTDB^{-\cdot}$ at 380 nm in air in the presence of CTAB and MES at pH 6.5.

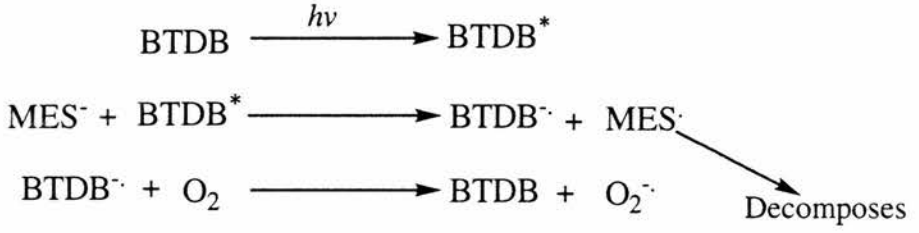

Figure 2.36 : Reactions of BTDB in CTAB with MES^- at pH 6.5 in Air.

The formation of the superoxide and the subsequent regeneration of the BTDB (Figure 2.36) would be predicted on the basis of the large difference in the redox potentials of BTDB and O_2 (E = -155 mV).[4]

2.9.2 Under Argon

When a similar experiment was repeated under argon, we again observed the growth of the radical anion. However, monitoring at 380 nm, no decay of the signal was observed, rather, there was a small increase in the absorbance over the next 30 μs

(Figure 2.35). This profile suggested that the radical anion decays to produce a species which has a larger extinction coefficient at 380 nm than that of the radical anion. In addition, it was observed that the solution became turquoise in colour.

To compare with the experiment performed in air, the sample used for the laser flash photolysis experiments under argon was left open to the air. After 30 and 50 minutes the sample was re-photolysed and the decay recorded at 380 nm. The half life was longer and the rate of the decay was slower after 30 minutes (Figure 2.38) than was observed for the sample in air which would indicate that the solution was not completely saturated with air. After 50 minutes (Figure 2.39), the rate of decay and half life were identical to those of the sample in air. These results indicate that the reaction with O_2 is very much faster than the reaction that $BTDB^{-\cdot}$ undergoes in the presence of argon. This was confirmed upon passing O_2 through the sample for 5 minutes thus ensuring saturation. The initial rate increased 4-fold, indicating (a) that the decay observed in the presence of air arises from the reaction with O_2 and (b) that this reaction is first order in the presence of O_2 (Table 2.4).

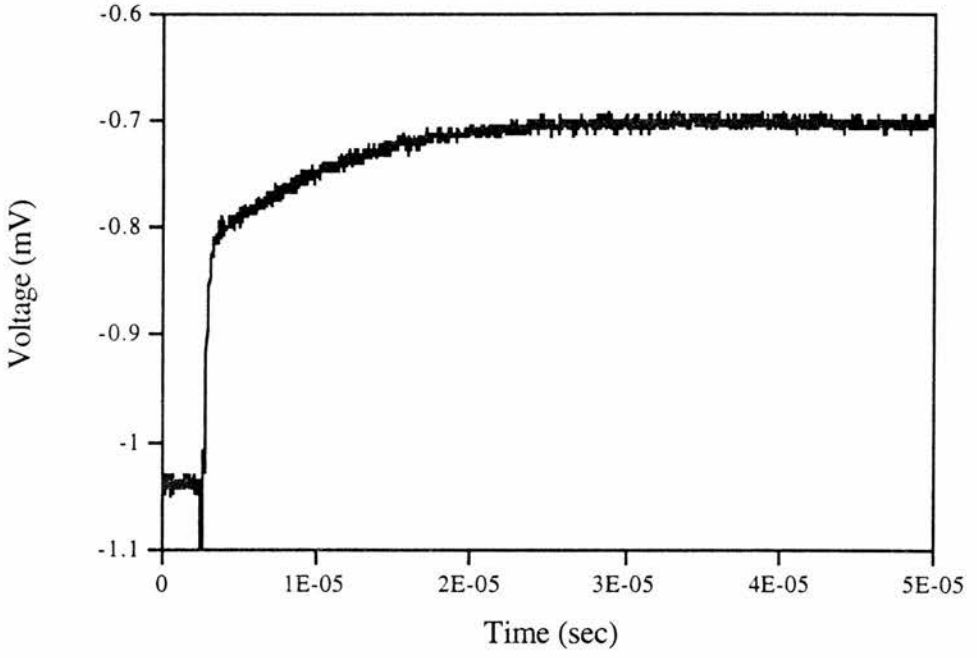

Figure 2.37 : Laser flash photolysis spectrum for BTDB at 380 nm under an argon blanket in the presence of CTAB and MES^- at pH 6.5.

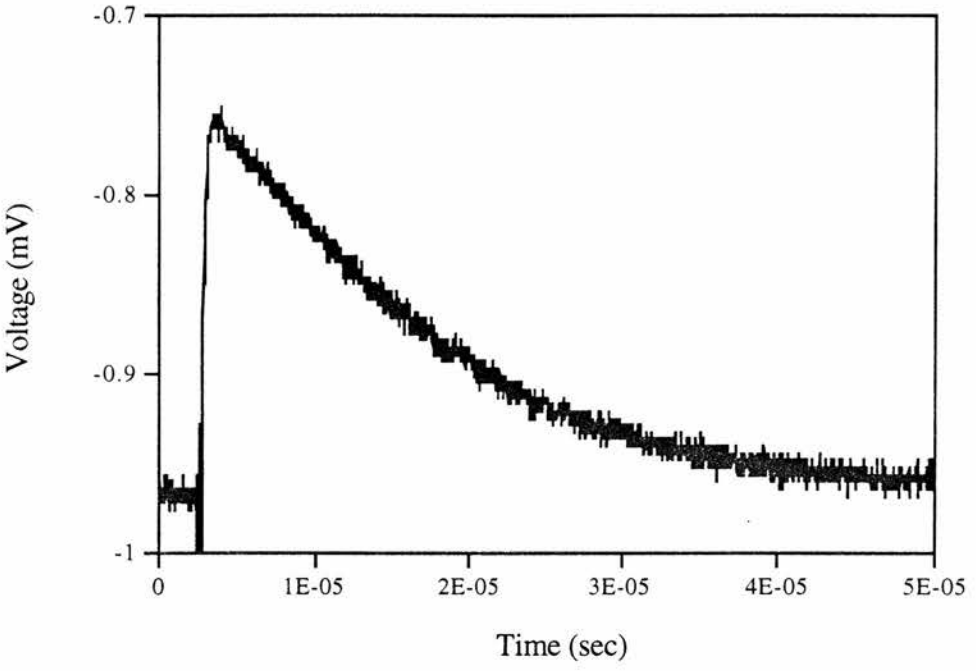

Figure 2.38 : Laser flash photolysis decay spectrum for the argon sample of BTDB at 380 nm in the presence of CTAB and MES^- at pH 6.5 after being left open to the air for 30 minutes.

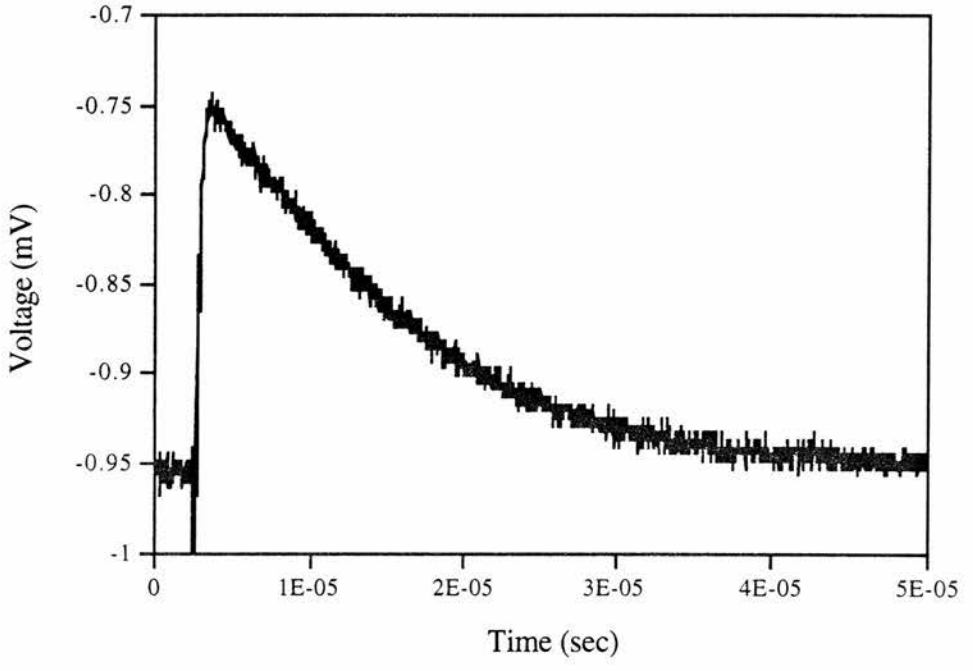

Figure 2.39 : Laser flash photolysis decay spectrum for the argon sample of BTDB at 380 nm in the presence of CTAB and MES^- at pH 6.5 after being left open to the air for 50 minutes

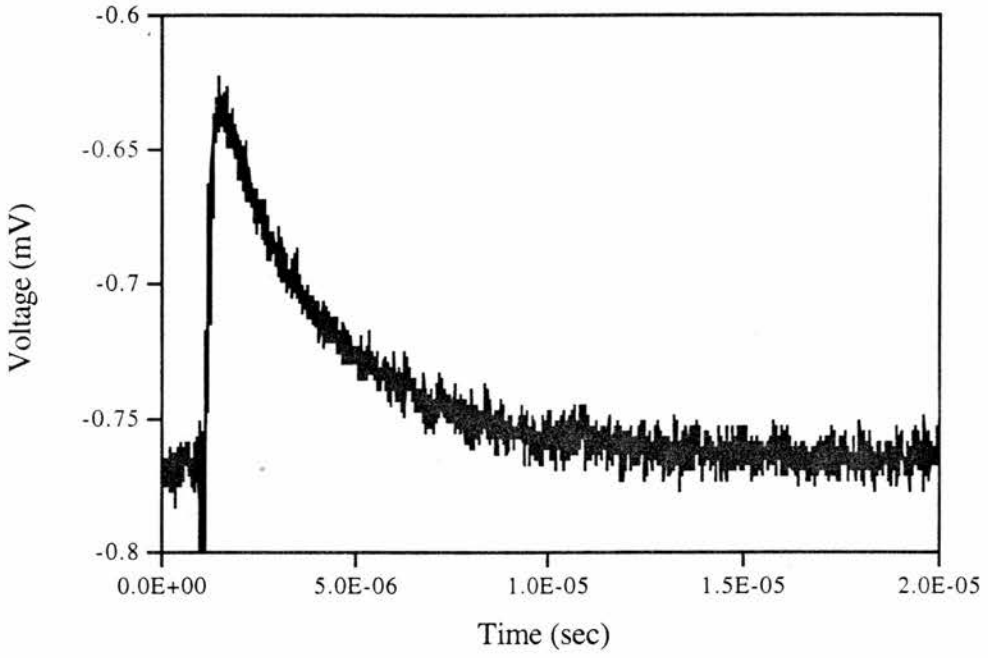

Figure 2.40 : Laser flash photolysis decay spectrum for BTDB in the presence of CTAB and MES^- at 380 nm saturated with O_2 at pH 6.5.

Sample	ΔAbs at 380 nm	k_{Obs} (s^{-1})	$t_{1/2}$ (μs)
Air	0.123	7.4 x 10^4	9.4
Argon	0.141	Growth Observed	
Air after 30 mins	0.107	6.5 x 10^4	10.7
Air after 50 mins	0.102	7.6 x 10^4	9.1
O_2 for 5 mins	0.081	3.27 x 10^5	2.1

Table 2.4 : Rate of decay and half-life for $BTDB^{-\cdot}$ at 380 nm, in CTAB with MES^- at pH 6.5 in the presence of air, argon and O_2.

In order to measure the decay of $BTDB^{-\cdot}$ directly, we monitored the reaction at 510 nm, where the turquoise species does not absorb and we observed a first-order decay of the radical anion. ΔAbs. recorded for the BTDB sample in air was the same as the argon sample, indicating that the concentration of $BTDB^{-\cdot}$ being produced was identical, with $BTDB^{-\cdot}$ being clearly consumed because after 50 flashes, ΔAbs. for the growth of $BTDB^{-\cdot}$ was reduced. The rate of decay, however, remained essentially the same (Table 2.5).

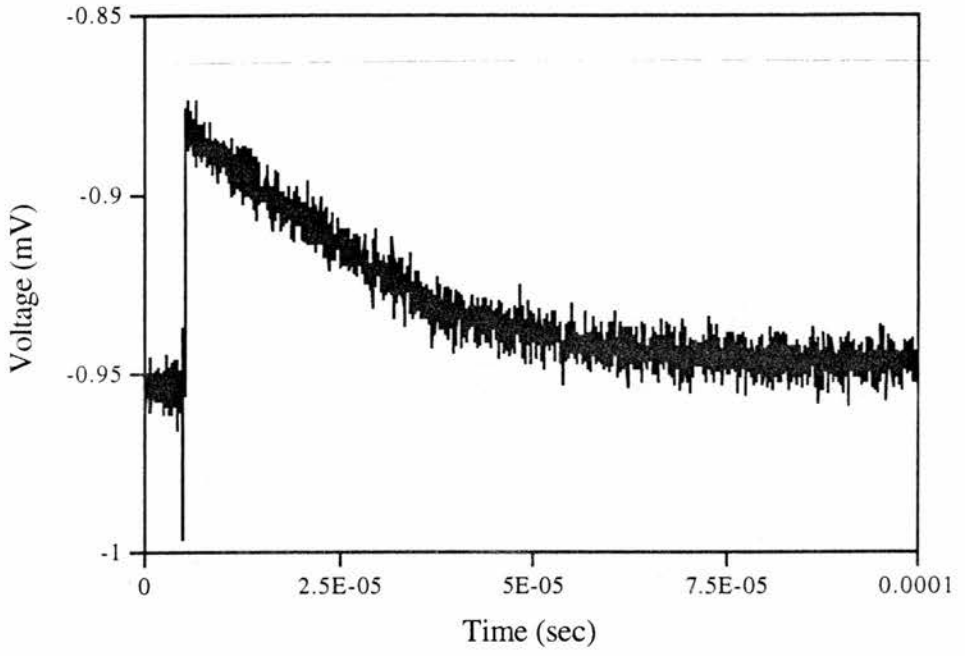

Figure 2.41 : Laser flash photolysis decay spectrum for BTDB in air at 510 nm in the presence of CTAB and MES^- at pH 6.5.

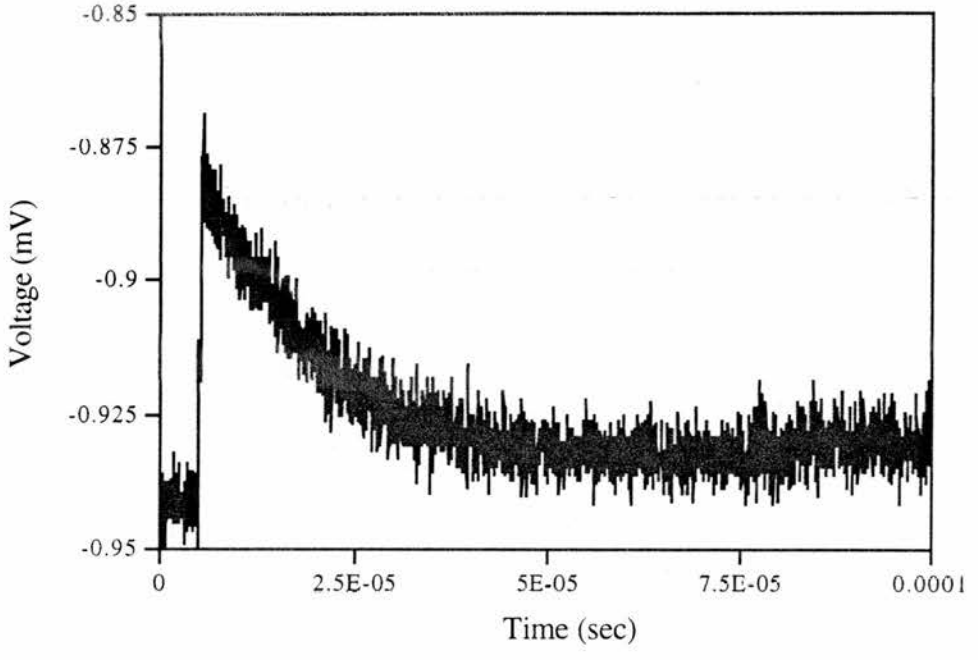

Figure 2.42 : Laser flash photolysis decay spectrum for BTDB in argon at 510 nm in the presence of CTAB and MES^- at pH 6.5.

Sample	ΔAbs at 510 nm	k_{Obs} (s^{-1})	$t_{1/2}$ (μs)
Air	0.035	6.6×10^4	10.5
Argon	0.035	3.5×10^4	19.8
Argon (after 50 flashes)	0.025	3.3×10^4	21.0

Table 2.5 : Rate of decay and half-life for $BTDB^{-\cdot}$ at 510 nm, in CTAB with MES^- at pH 6.5 under an atmosphere of air and argon.

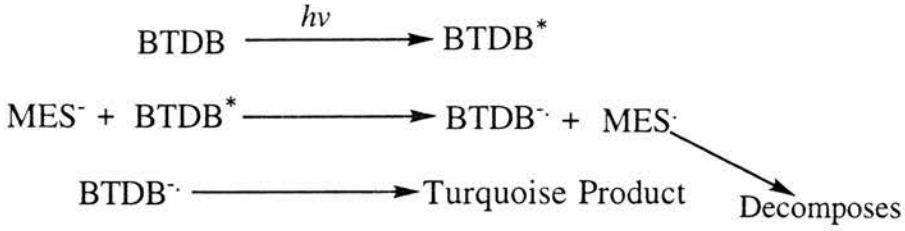

Figure 2.43 : Reactions of BTDB in CTAB with MES^- under an argon blanket.

We can conclude that, under an argon atmosphere, $BTDB^{-\cdot}$ exists twice as long as it does in air and reacts to form the turquoise product.

2.9.3 In the presence of AQDS under Argon

To gain a more accurate insight into the reaction of $BTDB^{-\cdot}$ within our system, we added AQDS to the solution being photolysed. For this set of experiments we observed not only a decay but also the growth of a species at 380 nm. The initial decay observed was not the decay of $BTDB^{-\cdot}$ because the time taken for the decay was 1 ms which is too long based on the previous studies. This was confirmed upon monitoring the decay of $BTDB^{-\cdot}$ at 510 nm where we observed a first order decay which was faster than the rate observed when AQDS was not present in solution.

We can assume from these results that with AQDS present in solution, $BTDB^{-\cdot}$ was not reacting with itself nor with a decomposition product from $MES^{\cdot}$, to form a new species but was reacting with $AQDS^*$ to subsequently produce $AQDSH_2$. This was confirmed by u.v.-visible spectroscopy where we observed a growth at 392 nm for $AQDSH_2$ and a decrease in the concentration of AQDS. In addition, the solution became bright yellow in colour, confirming the presence of $AQDSH_2$.

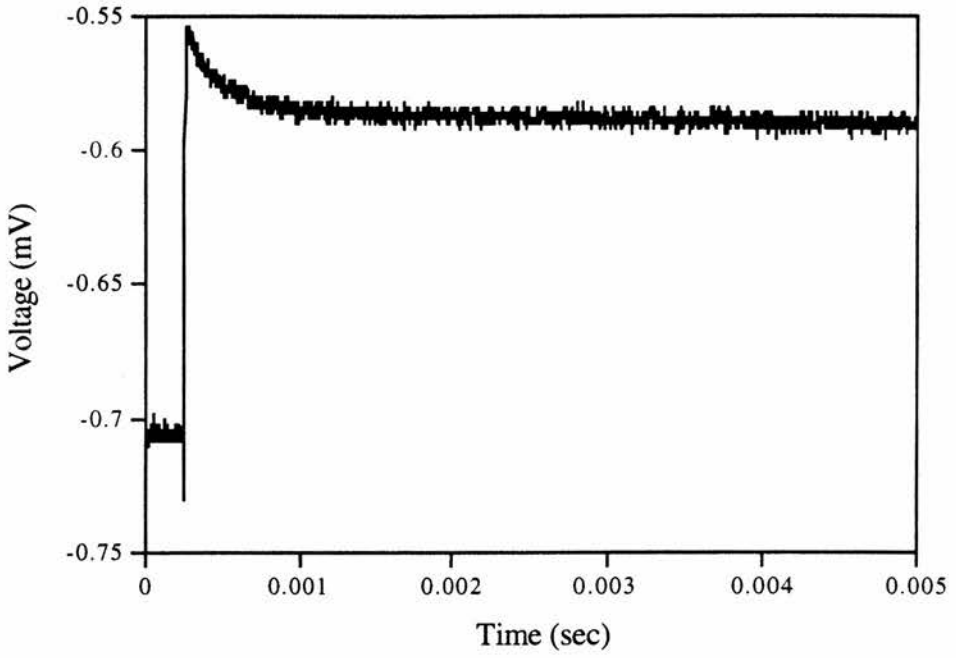

Figure 2.44 : Decay Trace of $AQDS^{-\cdot}$ at 380 nm with AQDS present in CTAB with MES^- and AQDS at pH 6.5

2.10 Cyclic Voltammetry

Cyclic voltammetry is a very powerful technique for the probing of electroactive species and is particularly useful in the initial studies of a new system. Many experiments can be carried out within a few minutes and the results are presented in a form which can be rapidly analysed in a qualitative manner. The theory and practice of cyclic voltammetry is described extensively in the literature.[5,6]

The E-t wave form used in cyclic voltammetry is shown in figure 2.46. The potential of the working electrode, controlled against the reference electrode, is swept from a starting potential E_1 to a second potential at E_2.

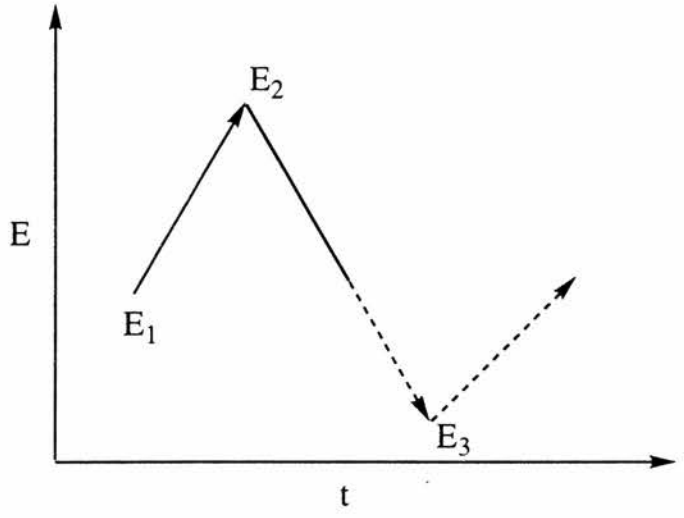

Figure 2.45 : A possible potential-time profile used in cyclic voltammetry.

On reaching E_2 the sweep is reversed and the electrochemical characteristics of the products and/or intermediates of the forward sweep are then probed. When the potential returns to E_1, the sweep may be either terminated, continued on to a potential, E_3, or reversed again. Single or multiple cycles can be formed at varying scan rates, while the current is monitored as a function of potential.

2.10.1 Reversible Reactions

A reversible reaction is one where the rate of charge transfer is fast relative to the rate of mass transport and both the *O* and *R* are stable. A typical cyclic voltammogram (CV) for a reversible process is shown in figure 2.47, where *O* and *R* are soluble

species. The ratio of surface concentrations of *O* and *R* is given by the Nernst equation, below;

$$E_e = E_e^{\theta} + \frac{RT}{nF} \ln \frac{c_o^{\sigma}}{c_R^{\sigma}} \qquad 2.0$$

where E_e is the equilibrium potential, E_e^{θ} the standard potential of the couple *O/R*, and c_o^{σ} and c_R^{σ} are the surface concentrations of *O* and *R*, respectively. From equation 2.0, it is seen that the standard potential is equal to the equilibrium potential when the surface concentrations of *O* and *R* are equal.

Hence as the potential is swept cathodically the surface concentration of reactant must decrease, and the concentration gradient then increases, followed by an increase in the cathodic current. Due to the relaxation effect of diffusion, the concentration gradient now begins to decrease resulting in a corresponding decrease in current.

On reversing the sweep, the product *R* continues to be formed until the potential reaches the charge transfer equilibrium and begins to reoxidise back to *O*, with a corresponding anodic current flowing. The magnitude of the current increases, as before, until the surface concentration of *R* is depleted and the current becomes diffusion controlled. Solution of Fick's second law for species *O* and *R*, with the relevant experimental boundary conditions, reveals the exact form of the CV for a reversible process. The *Randles - Sevcik equation* [7-9] shows that under planar diffusion control, the peak current density is;

$$\left|I_p\right| = 0.4463nF\left(\frac{nF}{RT}\right)^{1/2} c_i^{\infty} D^{1/2} \upsilon^{1/2} \qquad 2.1$$

where I_p is the peak current for either the cathodic or anodic process and υ is the sweep rate. Thus, it is evident that a plot of I_p against $\upsilon^{1/2}$ should be linear and pass through the origin for such a reversible process. Further, the peak positions, E_p, are independent of υ. The ratio of peak height I_p^A / I_p^C is unity. This however, often falls below this since, the species R will diffuse away from the surface before

reoxidation can occur. The peak separation for a perfect reversible system should be 59/*n* mV where *n* is the number of electrons transferred.

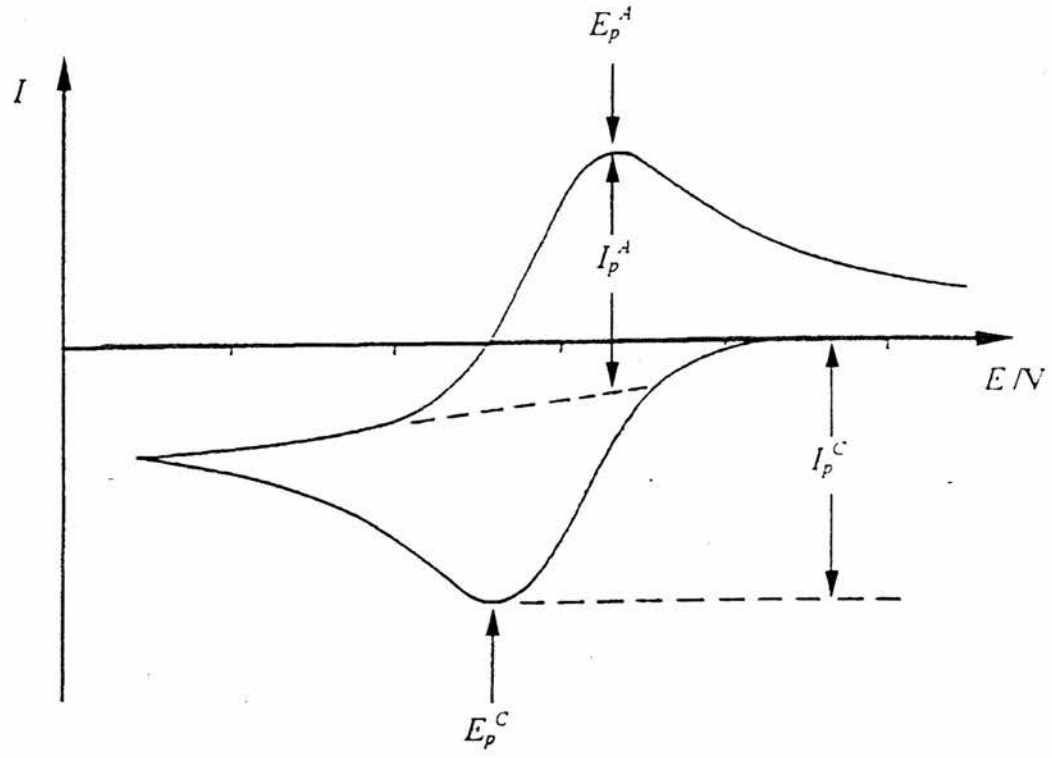

Figure 2.46 : Typical cyclic voltammogram for a reversible process, for the reaction $O + e \rightleftharpoons R$. Initially there is only *O* present in solution before sweeping cathodiclly.

It is common for a process that is reversible at low sweep rates to become irreversible at higher ones after having passed through a region known as quasi-reversible at intermediate values. Thus, transition from reversiblity occurs when the relative rate of the electron transfer with respect to that of mass transport is insufficient to maintain Nernstian equilibrium at the electrode surface.

In the quasi-reversible region both forward and back reactions make a contribution to observed current. This change from reversible to quasi reversible and finally irreversible behaviour can be readily seen from a plot of I_p as a function of $\upsilon^{1/2}$ where I_p increases with $\upsilon^{1/2}$ but is not proportional to it. Further, ΔE_p is greater than 59/*n* mV and increases with increasing υ. Also, E_p^c shifts negatively with increasing υ.

2.10.2 Irreversible Reactions

In the case of an irreversible process, the rate of charge transfer is insufficient to maintain Nernstian equilibrium at the surface. At low potential sweep rates the rate of charge transfer may be fast relative to mass transport and a reversible CV is observed. As the sweep rate is increased, the rate of mass transport increases and becomes comparable with charge transfer rate, resulting in peak separation.

The solution to Fick's second law for the peak current density of a totally irreversible system[9] is given by

$$|I_p| = 0.282 \frac{\pi^{1/2}F^{3/2}}{(RT)^{1/2}} n(\alpha_C n_\alpha)^{1/2} c_o^\infty D_o^{1/2} \upsilon^{1/2} \qquad 2.2$$

where n_α is the number of electrons transferred up to, and including, the rate determining step. The peak current density is therefore a function of the square root of the sweep rate, as in the reversible case. A reverse peak is absent in such a system, although lack of the anodic wave may also be due to a fast following chemical reaction. In addition, I_p^C varies proportionally to $\upsilon^{1/2}$ and E_p^C shifts cathodically with increasing υ.

2.10.3 The ec Reaction

An ec reaction implies an electron transfer process followed by a chemical step. The electron transfer may be reversible, quasi-reversible or irreversible and the chemical step may be reversible or irreversible and of first or higher order.[9,10]

When the electron transfer is totally irreversible the chemical step will have no effect on the shape of the voltammogram. However, when the charge transfer process is reversible, the effect of the chemical reaction will be most noticeable on the reverse sweep where R is oxidised. If the rate of the chemical reation is fast, R is rapidly removed from near the electrode and at low sweep rates no anodic peak will be observed. As the sweep rate is increased, a reverse peak becomes apparent, until at high enough rates the voltammogram assumes reversible behaviour. The chemical reaction has the effect of shifting the cathodic peak potential positive of the value

obtained for the reversible electron transfer reaction.

For a reversible charge transfer, I_p^A / I_p^C is less than one but tends to unity as υ is increased and $I_p^C / \upsilon^{1/2}$ decreases slightly with increasing υ.

2.10.4 Experimental Problems Associated with Cyclic Voltammetry

(i) Double Layer Charging Effects[6]

In addition to the Faradaic current (the current due to the electrochemical reation), there is double layer charging current contribution given by $I_{dl} = C_{dl}\upsilon$, where $I_{total} = I_{Faradaic} + I_{dl}$, υ is the sweep rate and C_{dl} is the double layer capacitance. Whilst $I_{Faradaic}$ is proportional to $\upsilon^{1/2}$, I_{dl} is proportional to υ, C_{dl} is usually between 20 and 40 $\mu F\ cm^{-2}$, therefore, at $100mVs^{-1}$ I_{dl} will be between 2 and $4\mu Acm^{-2}$ and this is usually small by comparison with the Faradaic current. However, at $100Vs^{-1}$, I_{dl} increases to between 2 and 4 $mA\ cm^{-2}$ and is no longer negligible. Thus, the double layer charging current distorts the voltammograms at high sweep rates, and if C_{dl} varies over the potential range the effect is increased. This effect imposes one of the major limitations on the maximum value of the sweep rate. A good approach to eliminate the problem of the double layer charging current is to use a microelectrode, where the charging current density decreases as the electrode is made smaller. Corrections for double layer can be made by subtracting the double layer charging current from the I-E curve for the test solution without the electroactive species (assuming the double layer/potential curve is unchanged by the presence of the electroactive species).

(ii) Uncompensated solution resistance[6]

The voltage observed at the working electrode is changed from the applied voltage E to $E-iR_u$, where R_u is the uncompensated solution resistance, and since i varies during a scan, the sweep is no longer linear and results in the decrease of peak heights and an increase in peak separation. The behaviour is very similar to that expected for a slow electron transfer step, so the iR_u drop problem is often mistaken for this. Great care

must therefore be taken to ensure iR_u drop is not affecting the system under study, or is at least minimised, before performing the experiment. This was achieved by incorporating a Luggin capillary and/or by electronically applying iR_u compensation during the experiment.

2.11 Microelectrodes

2.11.1 Introduction

The implementation of microelectrodes in research first began in the late 1960's at the University of Southampton by Martin Fleischmann and co-workers.[11] Other research groups began utilising microelectrodes in the early 1980's, demonstrating their ability in electroanalytical and biochemical studies (e.g. Wightman, Osteryoung and others).[12-18]

A microelectrode is an electrode with at least one dimension small enough that its properties are a function of its size. Most microelectrodes have radii in the range 0.5 — 25 μm. They may be manufactured in many different forms, for example, disk, hemisphere, band or ring, although typically the electrode is used in the form of a disk due to ease of preparation. Currents measured at such electrodes, range from pA to nA and require the amplification of the current and for the cell to be housed in a Faraday cage to prevent stray fields causing interfering currents. Three major consequences arise from the reduction in size of the electrode :

(i) mass transport rates to and from the electrode are increased due to non-planar diffusion, resulting in high current densities.

(ii) ohmic losses, which are the product of electrode current and solution resistance (iR), are reduced due to the greatly diminished current, often in the order of nA, e.g. a solution resistance of 1MΩ would result in a 1mV loss at 1nA. The current is proportional to a^2 (where a is the radius of the electrode surface) so when the radius decreases so does the current. Microelectrodes may therefore be used in a situation where it is impractical to add supporting electrolyte. This also means that dynamic electrochemistry can be carried out

without the need for a third electrode, i.e. the reference can also act as the counter.

(iii) The voltage at the microelectrode may be changed quickly, allowing high rate constants and short lived species to be probed.

2.12 Calibration of Electrochemical Cell

The electrode material selected for the macroelectrode was glassy carbon (3 mm diameter) and carbon fibre (8 μm diameter) for the microelectrode. Carbon was chosen over platinum as it was found to provide the widest electrochemical range over which the solvent, supporting electrolyte and buffer were stable. The calibration of the electrochemical cell was achieved by employing ferrocene and potassium ferrocyanide as internal standards for the non-aqueous and aqueous systems, respectively. The standard reduction potentials were +0.614 V vs. SCE and +0.677 V vs. Ag/AgCl for potassium ferrocyanide and ferrocene, respectively, comparing similarly with literature values.[19]

2.12.1 Results from Cyclic Voltammetry studies

(i) Aqueous System

These experiments were concerned with showing that (a) the redox potential for BTDB was, as expected, significantly more negative than for BTDN and (b) to define the chemical processes each of the chromophores undergoes and relate them to stability of the radical anion. All peak positions were referenced against a saturated calomel electrode (+241.5 mV vs NHE) and by using the Hickling equation,[20] we determined that the process involved one electron transfer.

Firstly, each of the chromphores was studied in an acetate buffered solution (0.14 M, pH 6.5) without the presence of CTAB (Section 6.4 (v)). Due to the nature of the cyclic voltammograms recorded for BTDB and BTDE, the peak positions are only reported, (Table 2.6).

	Redox Couple (1)		Redox Couple (2)	
Chromophore	$E^{C}_{p_1}$ (mV)	$E^{A}_{p_1}$ (mV)	$E^{C}_{p_2}$ (mV)	$E^{A}_{p_2}$ (mV)
BTDB	-1008	-850	Decomposition of Solvent	
BTDE	-971	-790	Decomposition of Solvent	
BTDN	-752	-669	-1097	No Peak Observed

Table 2.6 : Showing the peak positons for BTDB, BTDE and BTDN in acetate buffer solution (pH 6.5, 0.14 M) recorded against SCE (+241.5 mV v NHE) at 100 mVs^{-1} using a glassy carbon working electrode (3 mm diameter).

The peak positions are only presented because of the nature of the anodic wave observed at $E^{A}_{p_1}$ which did not allow an accurate E^{θ} to be determined. This was a result of the electrochemical processes that BTDB and BTDE underwent in the aqueous system. The CV's produced for BTDB (Figure 2.48) and BTDE show the absence of an anodic wave at low sweep rates which suggests an irreversible process but could also be due to a fast following chemical reaction eg. decomposition of the radical anion. Further tests indicated that the cathodic peak current was proportional to $\upsilon^{1/2}$ and the cathodic peak potential shifted negatively upon increasing sweep rate which supported the initial observation that the process was irreversible. However, upon increasing sweep rate, the anodic peak became more apparent which indicated that an ec reaction may be occurring. The absence of an anodic wave at the low sweep rates supports the flash photolysis studies that shows $BTDB^{-\cdot}$ as being extremely short lived and supports the explanation as to why it was not possible to record an ESR spectrum of $BTDB^{-\cdot}$. A reaction scheme for BTDB in an aqueous environment is shown in figure 2.47.

$$BTDB + 1e^{-} \rightleftharpoons BTDB^{-\cdot}$$

$$BTDB^{-\cdot} \longrightarrow \text{Unknown Product}$$

Figure 2.47 : Reaction scheme for BTDB in an aqueous environment during cyclic voltammetry studies.

In contrast, the first redox couple for BTDN showed reversibility, reflecting

the greater stability of $BTDN^{-\cdot}$. The peak positions were independent of υ and the ratio of the peak heights was almost unity. The second redox couple showed no reversibility and an anodic wave did not appear upon increasing υ, suggesting that the second electrochemical process was irreversible. The presence of the second cathodic wave has been shown to be linked to the formation of a dimer or dianion species of BTDN.[1] The irreversible peak represents the reduction of this dimeric or dianionic species forming an unstable dianion which decays to yield the monomer radical anion once again.

In addition, we observe the influence the less electron withdrawing ester groups have on the peak positions by making the species more reducing since they are more electron rich. In comparison, the electron poor BTDN, is less reducing as a result of the cyano groups being electron withdrawing . Further, the higher electron density on BTDB and BTDE destabilises the radical anion so that reoxidation can only be observed at faster sweep rates. As expected, there was very little difference between the diethyl and dibutyl ester species in terms of peak potentials and electrochemical behaviour. An example of the cyclic voltammograms produced for BTDB and BTDN in the aqueous system are shown in figure 2.48.

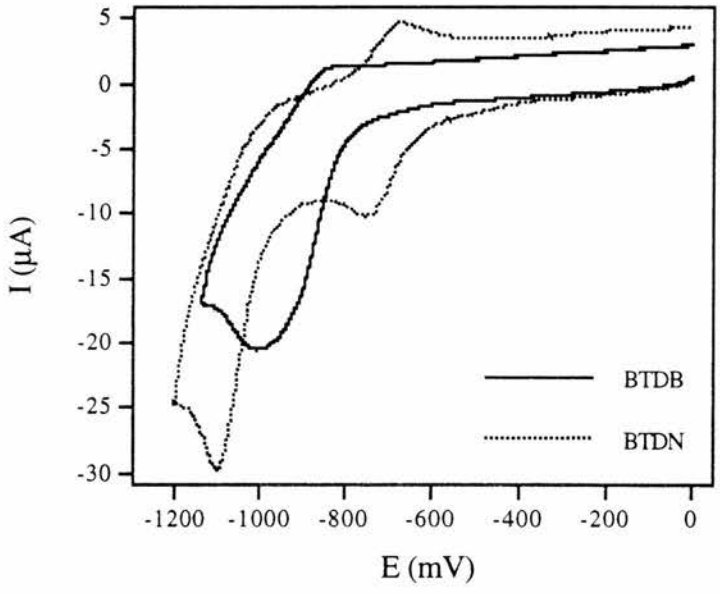

Figure 2.48 : CV of an aqueous buffered solution (pH 6.5) of BTDB and BTDN in the absence of CTAB at 100 mVs^{-1} (Ref. SCE (241.5 mV vs NHE).

(ii) Micellar System

These studies were concerned with studying the effect that CTAB had on the peak potentials for the three chromophores and if the micelle was able to stabilise the radical anion which would be reflected in a change in the electrochemical processes that occurred compared with those in the aqueous system (without CTAB). The results obtained are presented in table 2.7. All peak positions were referenced against a saturated calomel electrode (+241.5 mV vs NHE) and by using the Hickling equation,[20] we determined that the process involved one electron transfer.

	Redox Couple (1)		Redox Couple (2)	
Chromophore	$E^{C}_{p_1}$ (mV)	$E^{A}_{p_1}$ (mV)	$E^{C}_{p_2}$ (mV)	$E^{A}_{p_2}$ (mV)
BTDB	-744	-666	-1151	No Peak Observed
BTDE	-711	-617	-1085	No Peak Observed
BTDN	-569	-475	-884	-794

Table 2.7 : Showing the peak positons for BTDB, BTDE and BTDN in the presence of CTAB at pH 6.5, recorded against SCE (+241.5 mV vs NHE) at 100 mVs^{-1} using a glassy carbon working electrode (3 mm diameter).

The results presented in table 2.7 show that the peak potentials for each chromophore have shifted anodically and in doing so, have shown that BTDB (Figure 2.49) and BTDE also undergo a second electrochemical process similar to that observed for BTDN in the aqueous system. The second process for BTDB and BTDE was not detected in the aqueous system (without CTAB) because it occured at a potential below which the solvent was electrochemically stable. However, despite this discovery, just as in the aqueous system both BTDB and BTDE undergo similar electrochemical processes for the first redox couple.

The second redox couple cannot be the formation of $BTDB^{2-}$ from $BTDB^{-\cdot}$ since the latter has too short a lifetime to be present at any significant concentration once the reduction potential of the second couple is achieved. However, it may correspond to a reduction of a decomposition product of $BTDB^{-\cdot}$.

The anodic shift of the peak potential ($E_{p_1}^{C}$) for all three chromophores could be a result of surface interactions between the micelle and the electrode. Covering the electrode surface will be water molecules through electrostatic adsorption which makes the electrode surface hydrophilic and an overpotential will have to be applied to overcome the additional energy barrier for electron transfer, since from partition coefficient studies BTDB was found to be hydrophobic. The micelles reduce this energy barrier with a subsequent decrease in the overpotential and allow the redox reactions to occur at less negative potentials. An alternative explanation may involve the solvation of each chromophore. If less energy is required to lose or partially lose the micelle solvent sheath than that of water then a lower overpotential would be expected for charge transfer to occur. The degree of anodic shift is greater for BTDB and BTDE than for BTDN and could be related to the improved partition coefficient for BTDB.

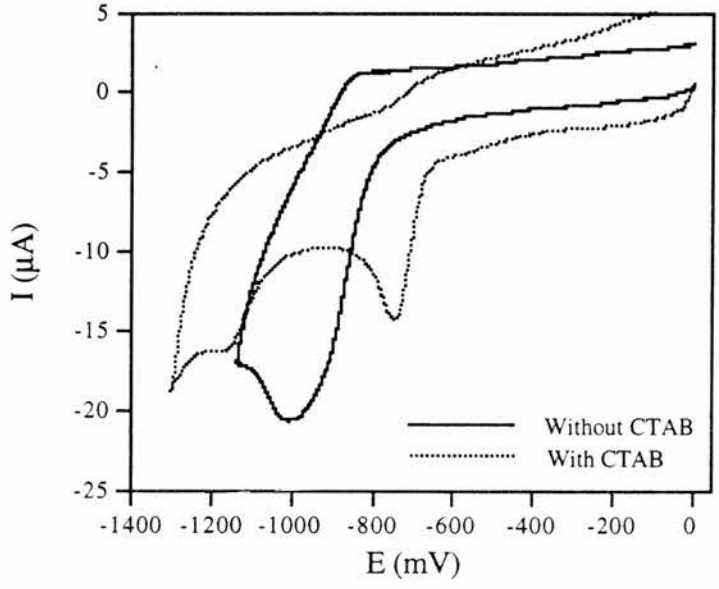

Figure 2.49 : Cyclic voltammograms for BTDB at 100 mVs^{-1} in the presence and absence of CTAB at pH 6.5 referenced to SCE (241.5 vs NHE)

(iii) Non-Aqueous System

Acetonitrile was employed because it allowed the three chromophores to be dissolved in solution at higher concentrations than was attainable in the aqueous systems while allowing an extended potential window to be used. These studies may also provide further evidence, that the radical anion for each of the chromophores predominately resides within the hydrophobic environment of the micelle. All peak positions were referenced against a Ag/AgCl electrode (+222 mV vs NHE) and by using the Hickling equation,[20] we determined that the process involved one electron transfer.

	Redox Couple (1)		Redox Couple (2)	
Chromophore	$E^{C}_{p_1}$ (mV)	$E^{A}_{p_1}$ (mV)	$E^{C}_{p_2}$ (mV)	$E^{A}_{p_2}$ (mV)
BTDB	-902	-826	-1504	-1428
BTDE	-895	-826	-1500	-1424
BTDN	-606	-530	-1436	-1352

Table 2.8 : Showing the peak positons for BTDB, BTDE and BTDN in acetonitrile, recorded against Ag/AgCl (+222 mV v NHE) at 100 mVs^{-1} using a glassy carbon working electrode (3 mm diameter).

All three chromophores undergo chemically reversible and quasi-reversible electrochemical processes where both redox couples for all three chromophores showed electrochemical reversibility at low sweep rates but upon increasing the sweep rate the separation between the peaks began to increase which indicates quasi-reversibility. Figure 2.50 shows selected cyclic voltammograms for BTDB, showing the reversibility at 50 mVs^{-1} and the quasi-reversibility at higher sweep rates for both redox couples.

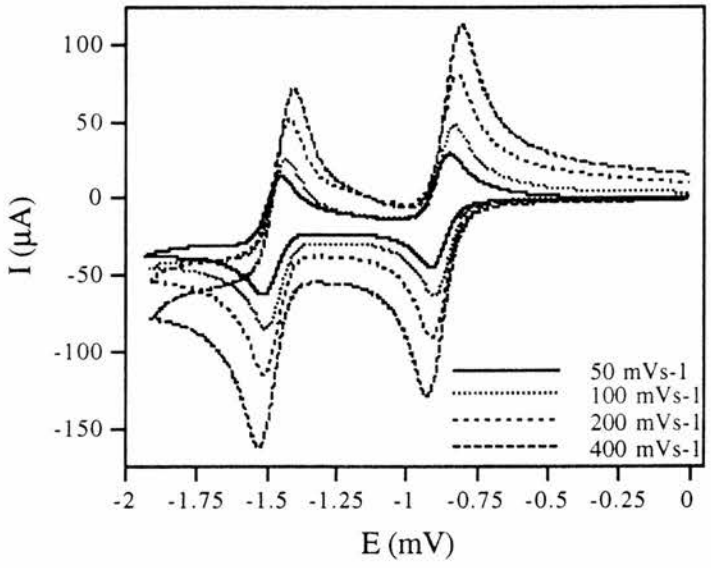

Figure 2.50 : Successive cyclic voltammograms for BTDB in acetonitrile at increasing sweep rates referenced against Ag/AgCl (222 mV vs NHE).

Microelectrodes were also employed in an attempt to clarify the electrochemical processes that the chromophores were undergoing. The experiments showed that at sweep rates of less than 100 mVs^{-1} the chromophores underwent electrochemically reversible processes but as with the macroelectrode, upon increasing sweep rate the chromophores demonstrated quasireversibility. A typical cyclic voltammogram obtained when employing a microelectrode is shown in figure 2.51.

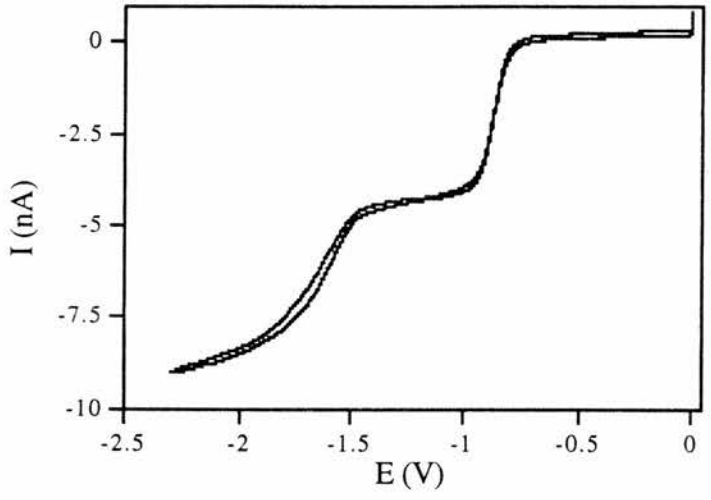

Figure 2.51 : Cyclic voltammogram for BTDB in acetonitrile at a carbon microelectrode (8μm) scanned at 100 mVs^{-1} referenced to Ag/AgCl (+222 mV vs NHE).

The studies with the microelectrode showed that the first redox couple is reversible at low sweep rates because the trace for the oxidation of the species follows the trace of the reductive process almost identically (Figure 2.51). This was confirmed by reversing the cathodic sweep after the second plateau had been produced, and as before, the traces for the cathodic and anodic sweep matched. Figure 2.52 presents the possible reactions occuring at each redox couple.

$$BTDB + 1e^- \rightleftharpoons BTDB^{\cdot-} \quad (E_{p1}^C)$$

$$BTDB^{\cdot-} + 1e^- \rightleftharpoons BTDB^{2-} \quad (E_{p2}^C)$$

$$BTDB^{2-} - 1e^- \rightleftharpoons BTDB^{\cdot-} \quad (E_{p2}^A)$$

$$BTDB^{\cdot-} - 1e^- \rightleftharpoons BTDB \quad (E_{p1}^A)$$

Figure 2.52 : Reaction scheme of the redox reactions for BTDB during cyclic voltammetry studies in acetonitrile.

These results suggest that $BTDB^{\cdot-}$ is stable in acetonitrile and can be further reversibly reduced to $BTDB^{2-}$. This was very different from the behaviour in the aqueous systems and suggests that the decomposition mechanism for $BTDB^{\cdot-}$ involves a reaction with water or protons.

These studies in acetonitrile support the theory that the micelles help to overcome the overpotential caused by the presence of solvent molecules around the electrode as the potentials obtained in acetonitrile have shifted cathodically, relative to micellar system, but are shifted anodically compared to those obtained in the aqueous system. It has been suggested[1] that the potentials obtained in acetonitrile should be similar to those obtained in a micellar environment or vice versa and would be evidence for the stabilisation of the radical anion of each of the chromophores within the micelle. The presence of the anodic waves for each of the chromophores suggests that the micelle is not fully protecting the radical anion from the aqueous environment and a solvation sheath of acetonitrile molecules around the reduced species may aid in their stabilisation.

Further investigations should involve studying the effects of concentration of chromophore and surfactant upon the electrochemical and redox potential as well as A.C. impedance studies to provide further evidence in support of the cyclic voltammetry studies in addition to determining rate constants and diffusion coefficients. It would also be interesting to attempt to detect $BTDB^{-\cdot}$ generated electrochemically in acetonitrile by ESR spectroscopy.

2.13 The Effect of the Chromophore upon the Reduction of AQDS

We have shown that BTDB has improved qualities over both BTDE and BTDN in terms of solubility within the hydrocarbon environment of the micelle, light absorbing properties and redox properties. A final experiment was necessary to quantify these improved individual characteristics in terms of improved yield and the rate of production of $AQDSH_2$. This was achieved by performing the reduction of AQDS in CTAB with MES and changing the chromophore (Section 6.2.1 (i)). The results of these experiments are presented in figure 2.53 and 2.54.

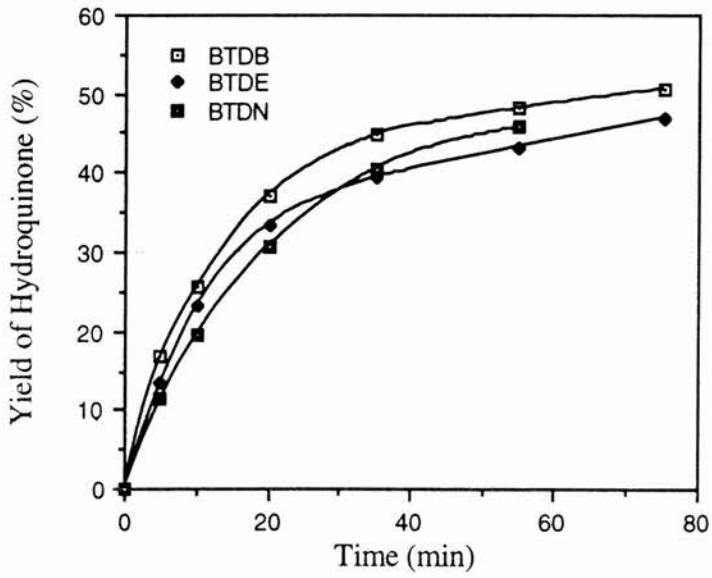

Figure 2.53 : The production of $AQDSH_2$ from AQDS in the presence of CTAB and MESH while varying the chromophore at pH 6.5.

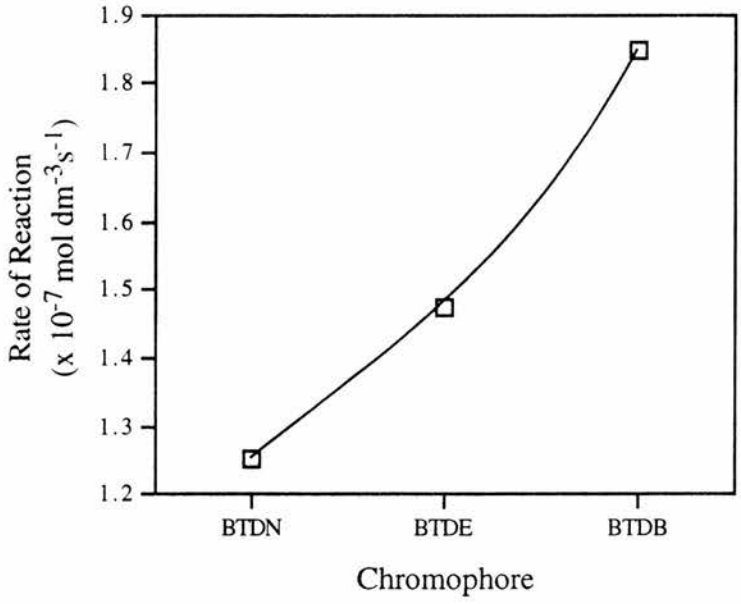

Figure 2.54 : Variation in the initial rates of reaction for $AQDSH_2$ production from AQDS while changing the chromophore in the presence of CTAB at pH 6.5.

The graphs shown in figures 2.53 and 2.54 confirm that the enhanced individual properies of BTDB have led to an improvement in the enhanced reduction of AQDS in a micellar environment. The next stage, involves studying the performance and ability of BTDB as an electron transfer agent within a surfactant vesicle bilayer. Before that can be determined, the preparation and subsequent morphology of the vesicle bilayers has to be investigated and this will be discussed in the next chapter.

References

1. J.N. Robinson, *Ph.D. Thesis*, University of St. Andrews, 1989.
2. J.N. Robinson, D.J. Cole-Hamilton, P. Camilleri, C. Dainty and V. Maxwell, *J. Chem. Soc. Faraday Trans.* 1, 1989, **85**, 3385.
3. P. Camelleri, A. Dearing, D.J. Cole-Hamilton and P. O'Neill, *J. Chem. Soc. Perkin Trans. II*, 1986, 569.
4. P.H. Wood, *FEBS Lett.*, 1974, **44**, 22.
5. *Instrumental Methods in Electrochemistry*, Southampton Electrochemistry Group, Ellis Harwood, Chichester, 1990.
6. *Electrochemical Methods*, A.J. Bard and L.R. Faulkner, John Wiley and Sons, New York, 1980.
7. J.E.B. Randles, *Trans. Faraday Soc.*, 1948, **44**, 327.
8. A. Sevcik, *Coll. Czech. Chem. Comm.*, 1958, **13**, 349.
9. R.S. Nicholson and I. Shain, *Anal. Chem.*, 1964, **36**, 706.
10. L. Nadjo and J.M. Saveant, *J. Electroanal. Chem.*, 1973, **48**, 113.
11. M. Fleischmann, S. Pons, D.R. Rolinson and P.P. Schmidt (Eds), *Ultramicroelectrodes*, Datatech Systems Inc., 1987.
12. R.M. Wightman, *Anal. Chem.*, 1981, **53**, 1125R, 1125A.
13. M.I. Montenegro, *Portugalie Electrochim. Acta.*, 1985, **3**, 165.
14. S. Pons and M. Fleischmann, *Anal. Chem.*, 1987, **59**, 1391A.
15. J.O. Howell, *Current Separations*, 1987, **8**, 2.
16. J. Robinson, *Chemical Kinetics*, 1989, **29**.
17. R.M. Wightman and D.O. Wipf, *Electroanal. Chem.*, 1989, **15**, 267.
18. A.M. Bond, K.B. Oldham and C.G. Zoski, *Anal. Chim. Acta.*, 1989, **216**, 177.
19. *Standard Potentials in Aqueous Solution*, A.J. Bard, R. Parsons and J. Jordan (Eds), Dekker, New York, 1985.
20. P.L. Allen and A. Hickling, *Trans. Faraday Soc.*, 1957, 1627.

Chapter 3

TEM and Photo-assisted Electron Transfer Studies Across Synthetic Vesicle Bilayers

3.1 Introduction

The formation of bilayer structures in simple surfactant dispersions has been inferred from their phase diagrams[1] for some time, but they were first recognised as potential membrane models by Gebicki and Hicks,[2,3] when shaking thin films of oleic and linoleic acids in aqueous buffers, yielded closed bilayers called ufasomes. Ufasomes, unfortunately were unstable outside the pH 6 — 8 range and retained substrates poorly. However, since the discovery by Kunitake[4,5] *et al.* and Fendler[6-10] *et al.* of the totally synthetic surfactant vesicles, dioctadecyldimethylammonium chloride and bromide (Figure 3.1), these dialkyldimethylammonium halide surfactants have been utilised as one of the simplest biological membrane models, providing an environment from which detailed insights can be gained of natural processes as a result of their formation and stabilities. These synthetic surfactant vesicles are defined as smectic mesophases of completely synthetic surfactant bilayers, allowing the compartmentalisation and organisation for the products of redox reactions, which are spatially separated in inner and outer aqueous phases and within the bilayer itself. They thus provide an attractive possibility for separating the sites of hydrogen and oxygen production in the photochemical decomposition of water.[11]

The surfactant vesicle dispersion being investigated was dioctadecyldimethylammonium bromide (DODAB) which is a quaternary ammonium salt with a cationic polar head and bromide as counterion, see figure 3.1,

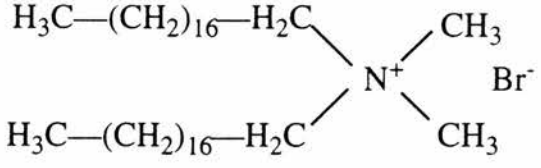

Figure 3.1 : Surfactant molecule of DODAB.

The formation of bilayer[12] vesicles is a spontaneous process in aqueous solution, resulting from the hydrophobic effect, which is a result of the low solubility of nonpolar molecules in water and the mainly entropic nature of the highly unfavourable free energy of solubilisation. It is unfavourable due to the reorientation or restructuring of water around nonpolar solutes or surfaces, since it disrupts the existing water structure and imposes a new (more ordered) structure on the surrounding water molecules.

Hydrophobic interactions are the major driving force for formation of the vesicles, with water molecules being released from the hydrocarbon tails of the amphiphiles as these tails form the nonpolar interior of the bilayerm which results in a large entropy increase. In addition, Van der Waals forces between hydrocarbon tails as well as favourable electrostatic and hydrogen bonding interactions between the polar head groups and the surrounding water molecules, results in a large gain in free energy for vesicle formation over micelles. Therefore, vesicles are formed at concentrations of several orders of magnitude below the critical micelle concentration (cmc) of the single chain surfactant analogues.

The final vesicle structure depends on the nature of the surfactant and the length of the alkyl chains. Where an alkyl chain length is greater than dioctadecyl this would give a lamellar structure and the longer the chain length of the alkyl groups, the more tightly the surfactant vesicles pack.[14] Vesicles, once formed cannot be destroyed upon dilution and do not disintegrate for weeks.[15,16] However, on prolonged standing, vesicles undergo fusion which involves neutralisation of charges on the exterior of vesicles just as in the case of liposomes.[17]

The high kinetic stability can only be exhibited over a relatively narrow range of solution conditions, for example, electrolyte concentrations in excess of 10^{-2} M, the presence of oxyanions or polyions and low concentrations of multicharged counterions all tend to precipitate surfactant vesicles.[18] This is because both cationic and anionic surfactant vesicles are osmotically active. Where the electrolyte concentration is greater in the external aqueous solution than within the internal aqueous solution

(hyperosmolar) they shrink.[8] The occurrence of osmotic shrinkage is the consequence of much faster water effusion from the vesicles than solute infusion into them. Under ideal conditions, vesicles behave like perfect osmometers where they are completely impermeable to solute but completely permeable to water. Alternatively, in hypoosmolar solutions the vesicles swell.[8]

Therefore, particular care is required for their preparation, handling and usage since both ionic strength and pH can strongly affect their size and permeabilities. The need for increase bilayer stability in conjunction with controllable permeability and morphology has led to the development of polymerised surfactant vesicles.[20,21,22]

3.2 Molecular Geometry

Amphiphilic molecules such as surfactants associate in aqueous solution and at solid interfaces to form a variety of structures.[23] At thermodynamic equilibrium, the geometry of an amphiphile molecule in the aggregate is given by the optimal area *a*, i.e. the surface area occupied per head group when the total interfacial energy per molecule in the aggregate is at a minimum; the volume of the hydrocarbon chain or chains *v*, and the maximum effective length that the chains can assume *l*. From the self assembly model and the molecular geometry it is possible to determine the nature, shape and size of the aggregate into which the amphiphilic molecules can pack.[23]

Amphiphiles that form planar bilayers are those with small head group areas and rigid, bulky hydrocarbon regions. For planar bilayers the value of *v/al* lies close to 1 with the critical packing shape being cylindrical. For a bilayer to curve (vesicles), the amphiphiles in the outer monolayer must be able to pack into truncated cones approaching a cylinder and the *v/al* value is smaller than 1 but larger than 0.5 (Figure 3.2). The ability to pack into a truncated cone is made possible by the larger head groups and the two hydrocarbon chains having a large surface area. For DODAC in water the *v/al* value is 0.64 whereas in 0.01M NaCl the v/al value is 0.81.[24,25] This is due to the *a* value decreasing, therefore, *v/al* becomes close to 1 indicating formation of planar bilayers.[26] The decrease in the surface area is caused by the ions of the salt

screening the repulsive charges between the hydrophobic head groups, thus reducing the effective head group area which makes the head groups effectively smaller. Therefore, for DODAC, the curved bilayer tends towards a planar bilayer structure. However, the self assembly model cannot predict tilting or interdigitation of the hydrocarbon chains.[27]

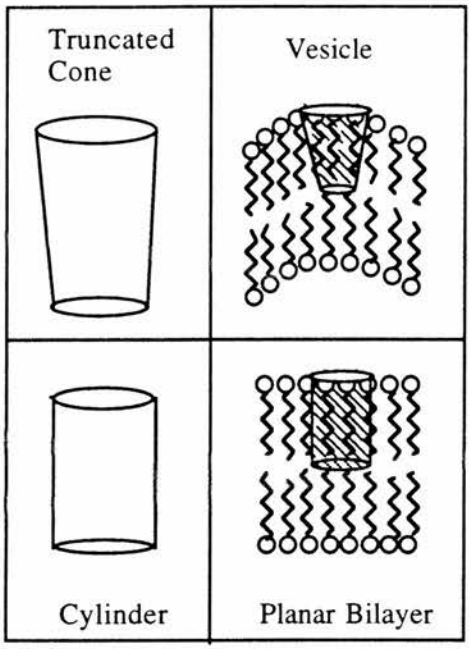

Figure 3.2 : Molecular geometry required to form vesicles and bilayers

3.3 Physical and Functional Properties

3.3.1 Preparation methods

There are five methods of preparation for DODAB vesicles[27-31]: (1) by injection into an alcohol or ether solution; (2) dialytic detergent removal; (3) chloroform vapourisation; (4) sonication in a bath; (5) sonication with a probe. The first two methods, yield cloudy suspensions containing small amounts of vesicles and the third, produces large unilamellar vesicles (d = 1000 — 2000 Å). The fourth yields vesicles which are multilamellar[7] (d = 1750 — 5000 Å) and the final method produces, small unilamellar vesicles (d = 200 — 500 Å), large unilamellar vesicles (d = 600 — 1500 Å) and multilamellar vesicles[6,8,29] (Figure 3.3) To study vectorial photoinduced electron transfer, the small unilamellar vesicles are typically used[32] and therefore, we employed sonic dispersal with a probe.

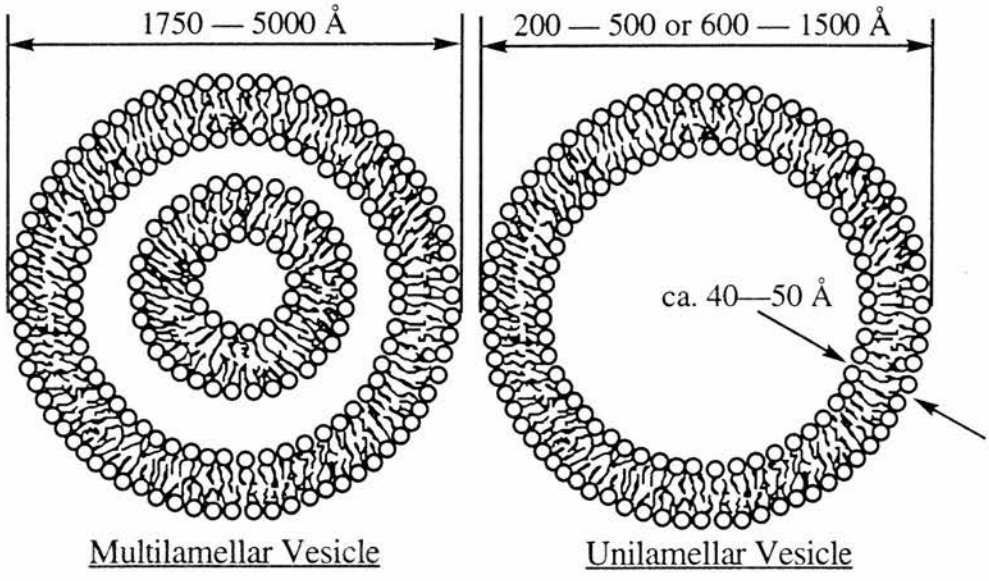

Figure 3.3 : A model of the structures for vesicles

3.3.2 Bilayer Packing and Physical State

The solution for sonication has to be heated above the maximum phase transition temperature because at lower temperatures only a heterogeneous dispersion of solid surfactant of high turbidity is produced. On raising the temperature, the surfactant went into solution where a decrease in the turbidity was observed. Both multi and single compartment vesicles undergo distinct structural changes at certain temperatures, these do not affect the gross structural features of the vesicle[33] i.e. they remain roughly spherical, closed smectic mesophases of surfactant bilayers.

For DODAB vesicles, phase transitions have been shown to occur at 30 and 36°C[11,27,34]. Below 30°C, DODAB vesicles consist of one-dimensional lamellae with the hydrocarbons fully extended and tilted.[35] Between 30 and 36°C, transformations from one to two dimensional arrangements occur with periodic undulations. At temperatures greater than 36°C, the hydrocarbon chains "melt" and revert to one dimensional lattice arrangements, somewhat separated from each other while assuming mobile, liquid like conformations (Figure 3.4). At these higher temperatures, large multilamellar vesicles are formed, which, in the melt state are easier to breakdown into unilamellar vesicles, which once formed, remain stable even when the temperature is lowered, to produce an opaque solution.

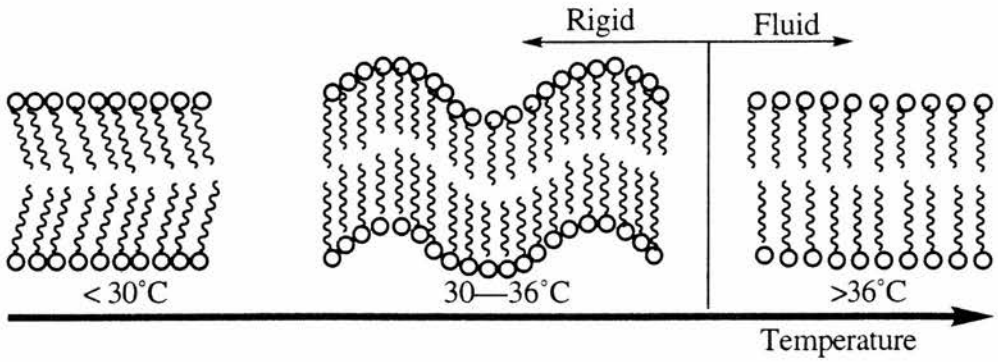

Figure 3.4 : Schematic representation of phase transitions for DODAB.

Unlike liposomes, another feature which can alter the packing arrangements in the highly charged surfactant vesicles is the considerably greater electrostatic head-group repulsions. If sonication was not performed, then shaking surfactant dispersions at high temperatures would yield extremely large nonuniform particles.[11] By increasing the sonication time at a given power setting or by increasing sonicating power over a fixed period, a decrease in the viscosity and turbidity was observed to give an optically transparent solution.

3.3 Structural Characterisation of DODAB

To study the above effects on vesicle formation and structure, transmission electron microscopy[8,4,36] (TEM), with negative staining, was employed, to substantiate the gross features of DODAB vesicles and to confirm the presence of closed vesicles. Negative staining has three principal applications for the examination of membranes[37]: (a) To give information about the structure, (b) To aid in the identification of a particular membrane in a mixture, (c) To give information on the extent to which a given membrane or membrane system is damaged.

An aqueous solution of an electron dense salt (uranyl acetate) was employed to surround the specimen which was then allowed to dry into a thin film to give, in effect, an amorphous electron dense glass in which the specimen was buried. The negative stain penetrated into the hydrophilic parts of the specimen and the resulting image in the electron microscope revealed the unpenetrated regions as relatively electron transparent

structures against an electron dense background. The pH of the uranyl acetate solution was approximately 4.2, but by the addition of ammonium acetate we raised the pH to around 6.0 which would have allowed a more direct comparison of the vesicles (pH 5.5 — 7.0) used in transmembrane electron transfer. Unfortunately, the addition of the ammonium acetate caused the vesicles to precipitate from solution.

Therefore, in the interpretation of the electron micrographs of surfactant vesicles much care was taken, since, both staining and pH are known to alter molecular arrangements. The next stage was to look at finding the optimum sonicating conditions, within the capabilities of the sonicator, that produced the greatest concentration of unilamellar vesicles.

3.3.1 Factors Affecting Unilamellar Vesicle Formation

We initially investigated the effect that the duration of sonication had on the production of unilamellar vesicles after 5 and 15 minutes. The electron micrographs obtained are shown in figures 3.5 and 3.6. In figure 3.5, we clearly observe that the vesicles are in the range of 1750 — 5000 Å-diameter which indicates a multilamellar structure. The vesicles are also strongly aggregated with no smaller unilamellar vesicles being present. Alternatively, in figure 3.6, we can still observe the presence of multilamellar vesicles but after the longer sonication time, the vesicles are not as aggregated and the concentration of large and small unilamellar vesicles (200 — 1500 Å) has greatly increased. This, demonstrates that, at longer sonication times, a greater number of multilamellar vesicles are able to be "broken" down to form unilamellar vesicles.

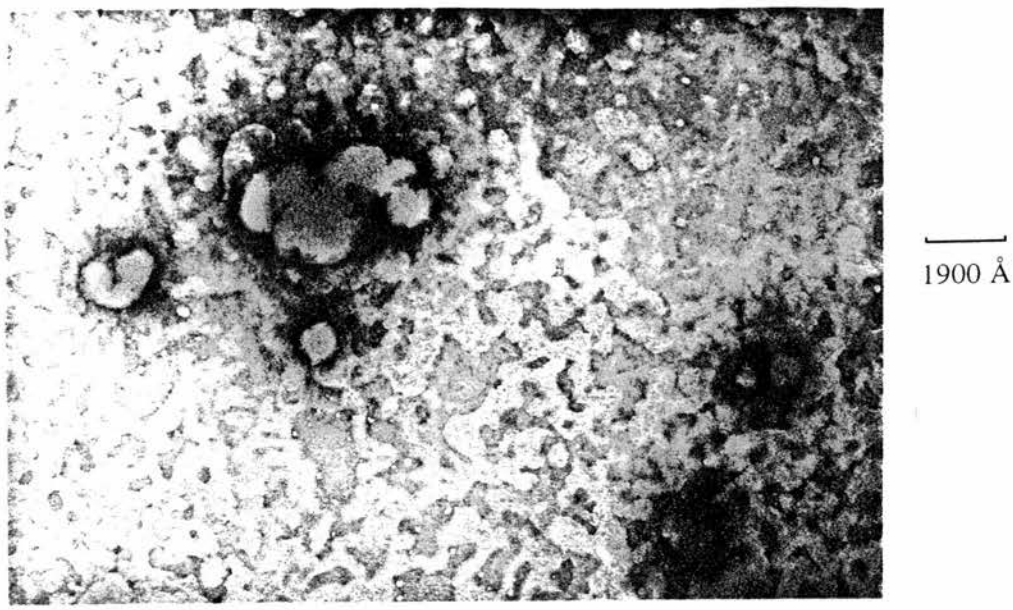

Figure 3.5 : Electron micrograph of DODAB vesicles sonicated after 5 minutes (x 52800).

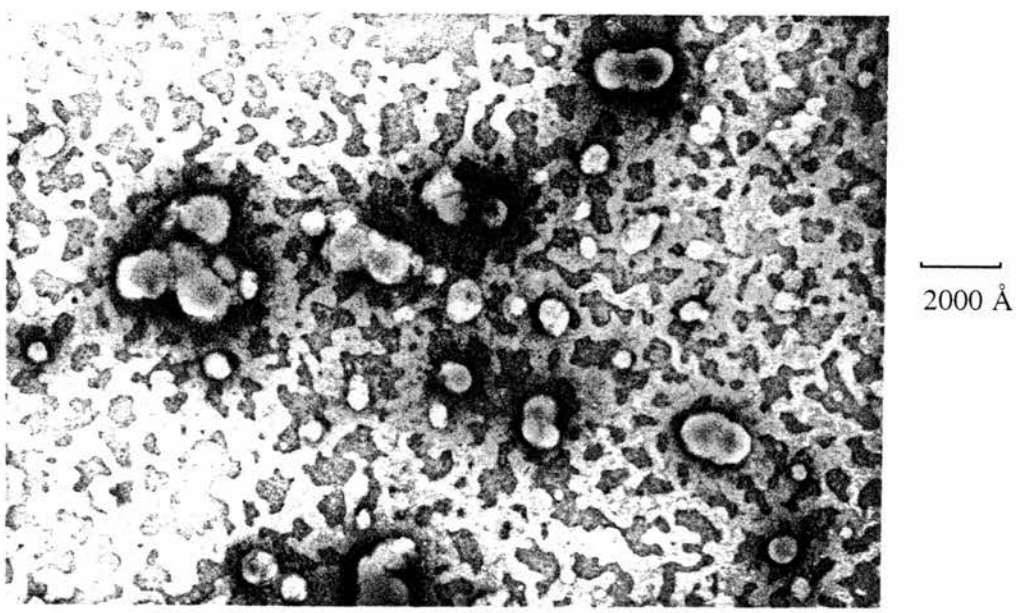

Figure 3.6 : Electron micrograph of DODAB vesicles sonicated after 15 minutes (x 50800).

We have been discussing the presence of multilamellar and unilamellar vesicles purely on the basis of size in the electron micrographs. We are however able to show electron micrographs of multilamellar, large unilamellar and small unilamellar vesicles in greater detail, (Figures 3.7, 3.8 and 3.9, respectively), confirming not only the size characteristics but also individual lipid architecture variations as shown in figure 3.2.

In figure 3.7, the individual bilayers in the multilamellar "onion ring" structure are clearly visible with the vesicle having an overall diameter of 1600 Å, with the individual layers roughly 40 Å thick. In figure 3.8, we observe a large unilamellar vesicle with a bilayer of 50 Å while the vesicle has an overall diameter of 1400 Å. Figure 3.9, shows a small unilamellar vesicle with an overall diameter of 450 Å and a bilayer thickness of 50 Å. The data, presented above, corresponds to the literature values given previously by Kunitake[4] and Tran.[6] Therefore, from these electron micrographs in figures 3.7, 3.8 and 3.9, we are able to support the observations in figures 3.5 and 3.6 with regards to multilamellar and unilamellar vesicle content.

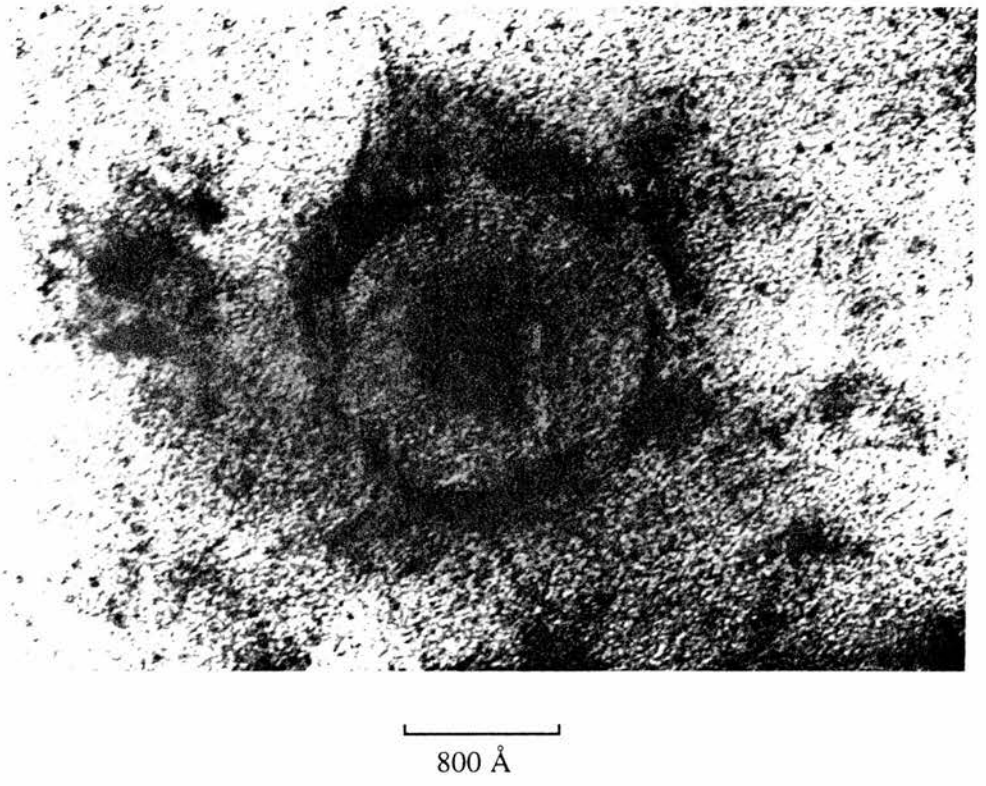

Figure 3.7 : Electron micrograph of a Multilamellar DODAB Vesicle (x 256000).

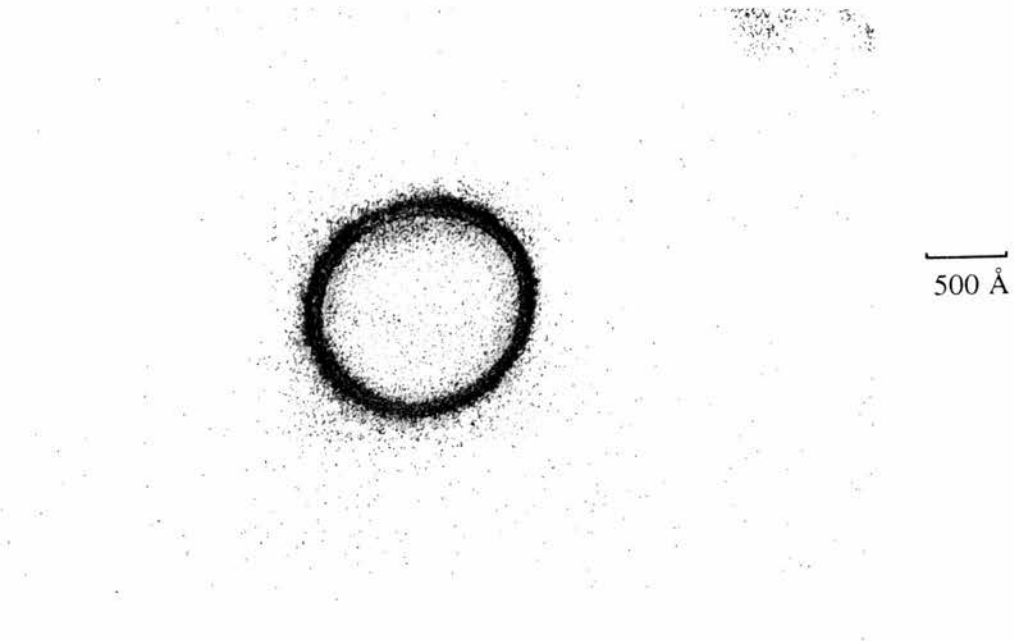

Figure 3.8 : Electron micrograph of a Large Unilamellar DODAB Vesicle (x 195500).

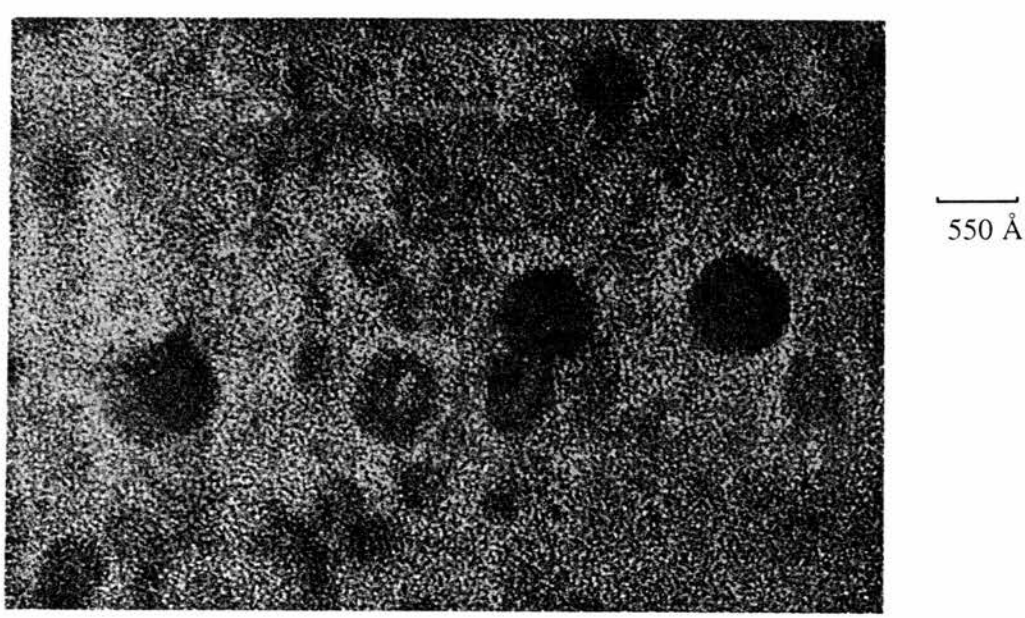

Figure 3.9 : Electron micrograph of Small Unilamellar DODAB Vesicle (x 185000).

3.3.2 Effect of Sonicating Power on Unilamellar Vesicle Formation

Next, we investigated the effect the power of sonication had on the formation of unilamellar vesicles. To study the effect in more detail, the sonicated solution was collected as individual fractions of 2 cm^3 volume after separation from the Sephadex column, in order to gain a better perception of the total vesicle content. The power settings of 10 and 12.5 microns were employed and the vesicles were prepared as in section 6.1.15. The solutions were again studied by transmission electron microscopy employing a negative stain, see section 6.1.15. The electron micrographs obtained for each fraction at both power settings are shown together in figure 3.10.

Figure 3.10 shows, that the vesicles formed at 10 microns, in the first four fractions (Figure 3.10 (1—4)(i)) were multilamellar and are one and half times larger and more aggregated, compared to the same vesicle fractions formed after sonication at 12.5 microns (Figure 3.10 (1—4)(ii)) where the vesicles were smaller and less aggregated. The multilamellar vesicles formed after sonication at 12.5 microns were smaller because at the higher power setting, more bilayers of the multilamellar vesicles have been 'broken down' to produce both large and small unilamellar vesicles in larger quantities. This observation was supported by there being nine vesicle containing fractions after sonicating at 12.5 microns (Figure 3.10 (1—9)(ii)), compared to only seven for 10 microns (Figure 3.10 (1—7)(i)), which shows that a greater number of unilamellar vesicles were formed after sonicating at 12.5 microns.

The large unilamellar vesicle content for the vesicle solution sonicated at 12.5 microns begins from fraction four (Figure 3.10 (3)(ii)). However, the large unilamellar vesicles were only shown to be present until fraction seven (Figure 3.10 (7)(ii)) and after fraction seven only small unilamellar vesicles were in solution. In comparison, the unilamellar vesicle content of the solution sonicated at 10 microns begins from fraction six (Figure 3.10 (6)(i)) which contains both large and small unilamellar vesicles. Small unilamellar vesicles were only to be found in fraction seven and in very low concentration as the electron micrograph shows (Figure 3.10 (7)(i)).

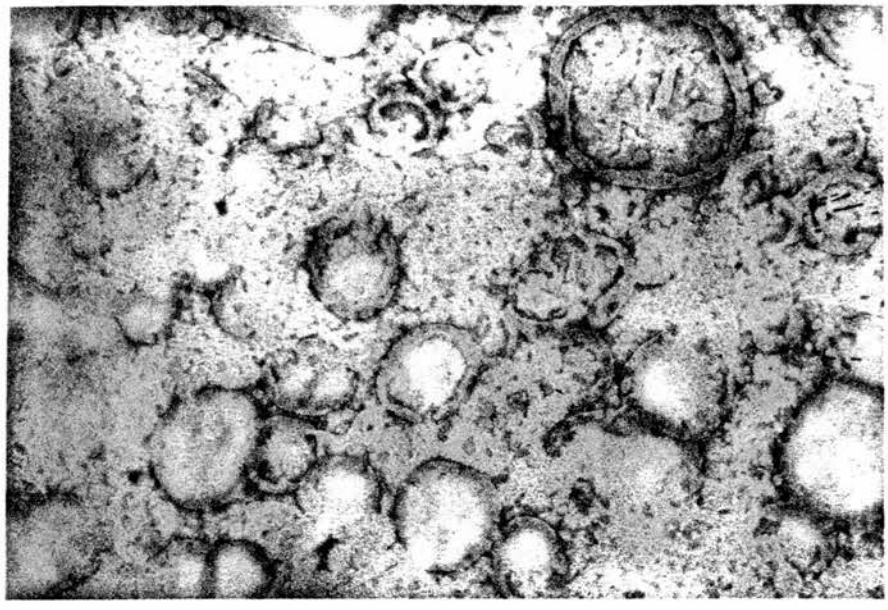

(i)

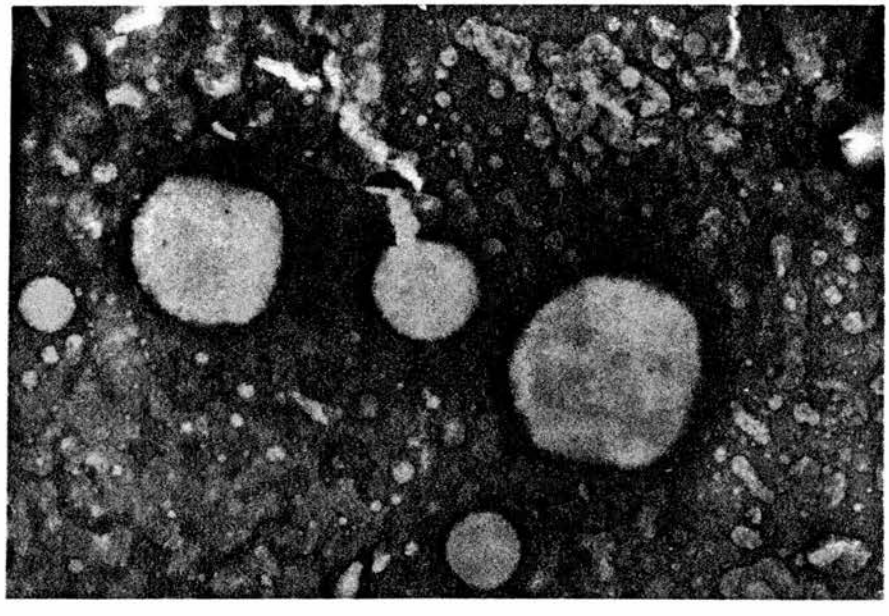

(ii)

Figure 3.10 (1) : Electron micrographs of DODAB vesicles in Fraction 1 after sonication at (i) 10 microns (x 65280) and (ii) 12.5 microns (x 65280).

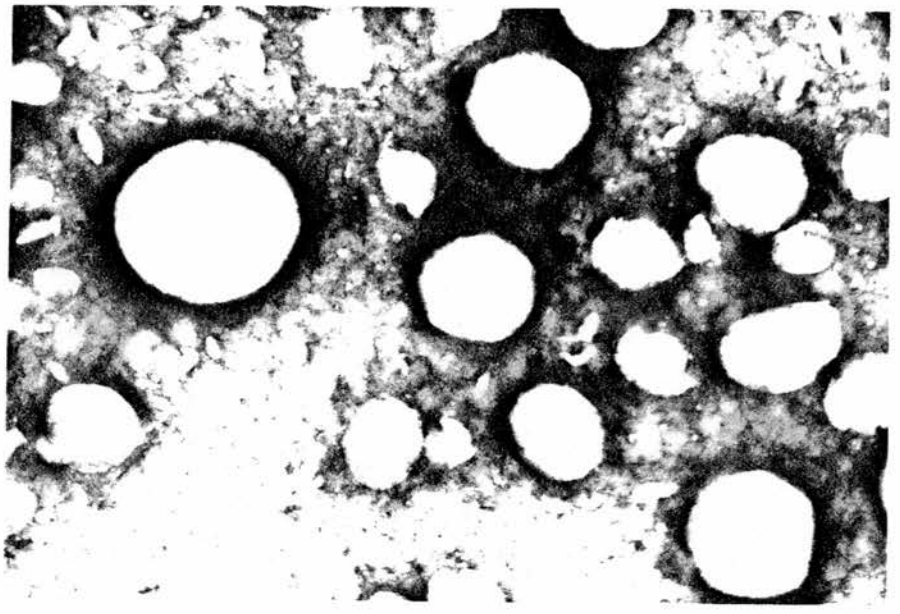

(i)

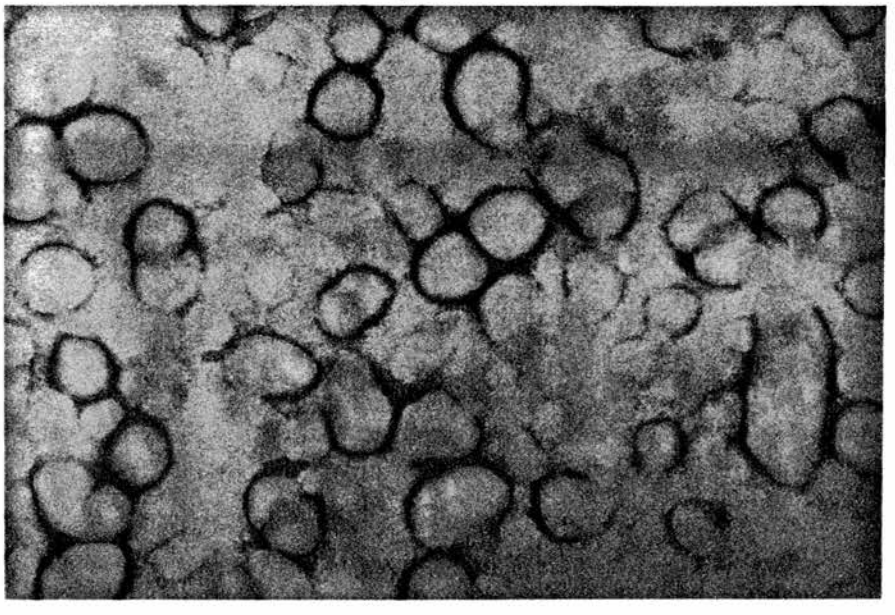

(ii)

Figure 3.10 (2) : Electron micrograhs of DODAB vesicles in Fraction 2 after sonication at (i) 10 microns (x 67200) and (ii) 12.5 microns (x 65280).

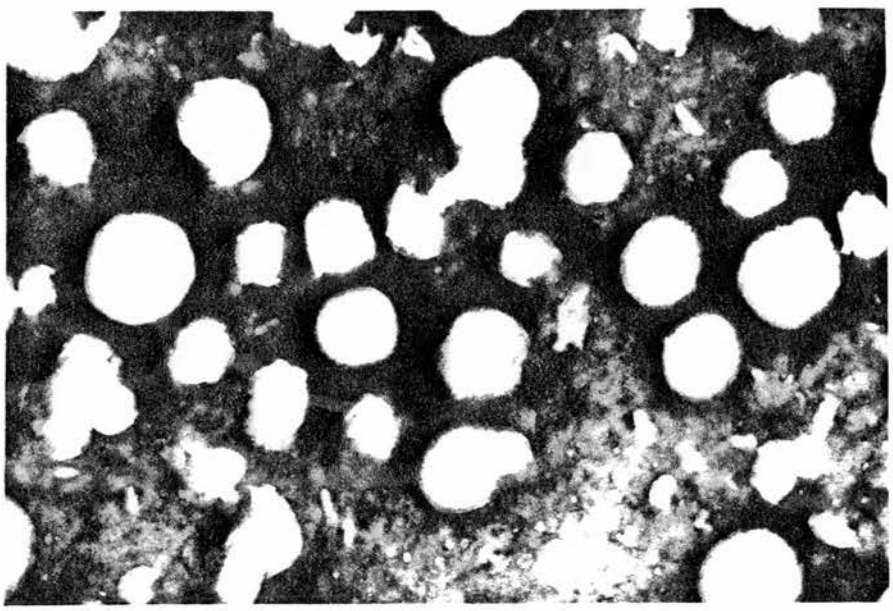

(i)

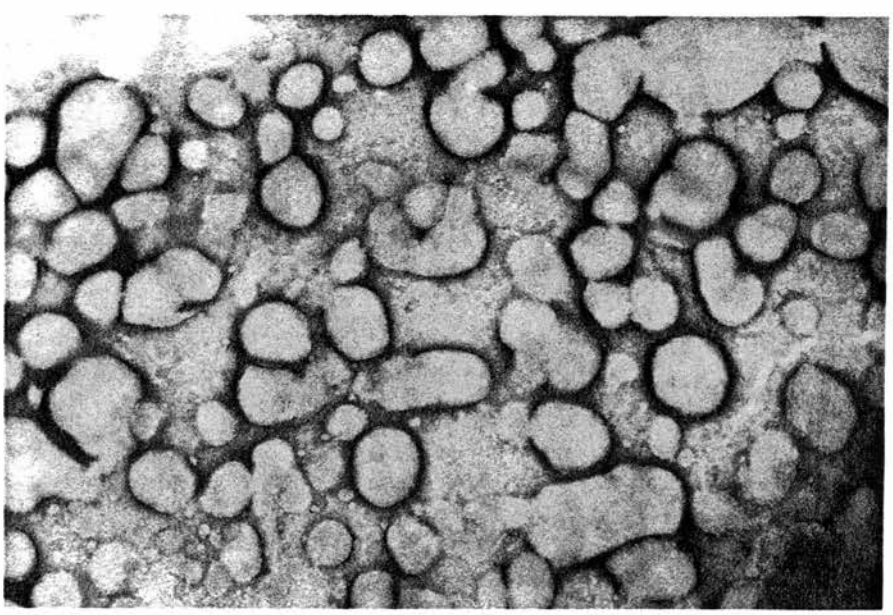

(ii)

Figure 3.10 (3) : Electron micrographs of DODAB vesicles in Fraction 3 after sonication at (i) 10 microns (x 65280) and (ii) 12.5 microns (x 69120).

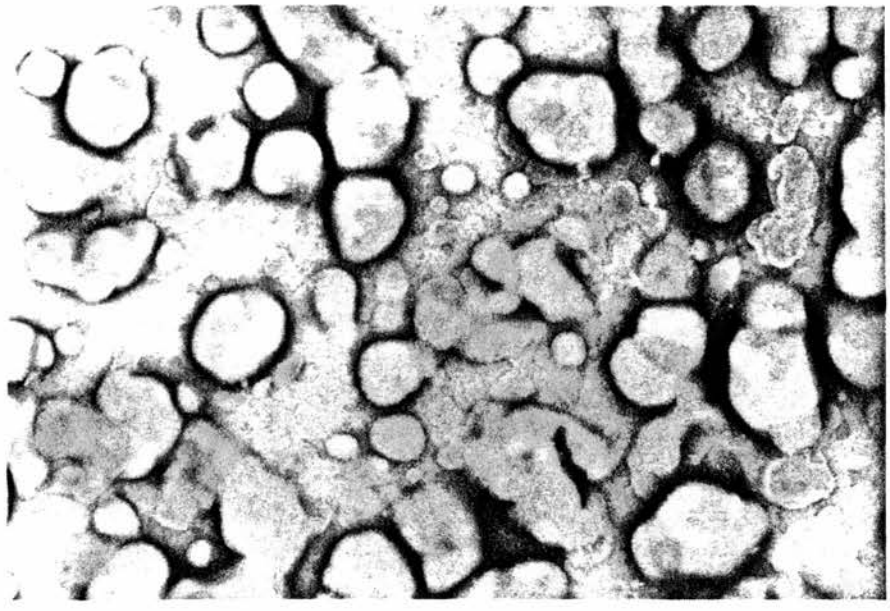

(i)

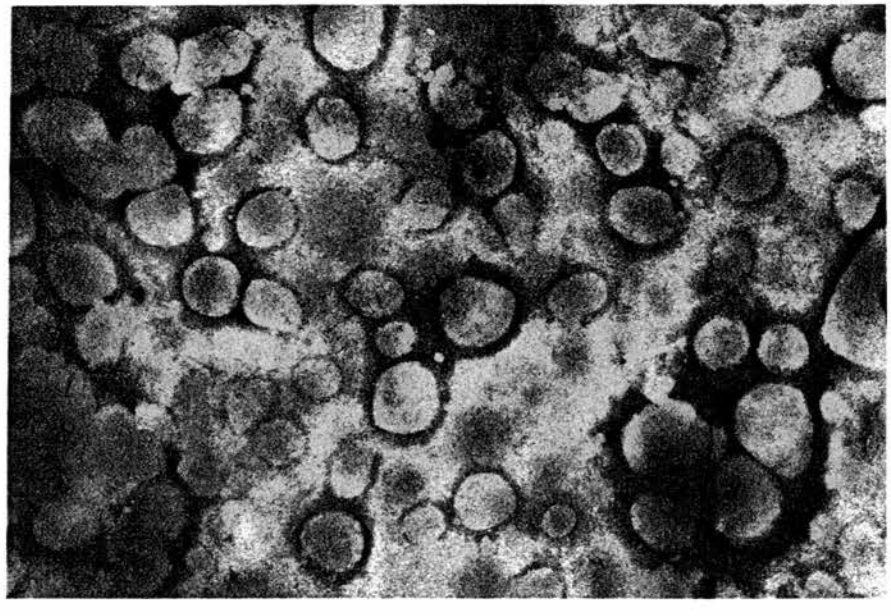

(ii)

Figure 3.10 (4) : Electron micrographs of DODAB vesicles in Fraction 4 after sonication at (i) 10 microns (65280) and (ii) 12.5 microns (x 69120).

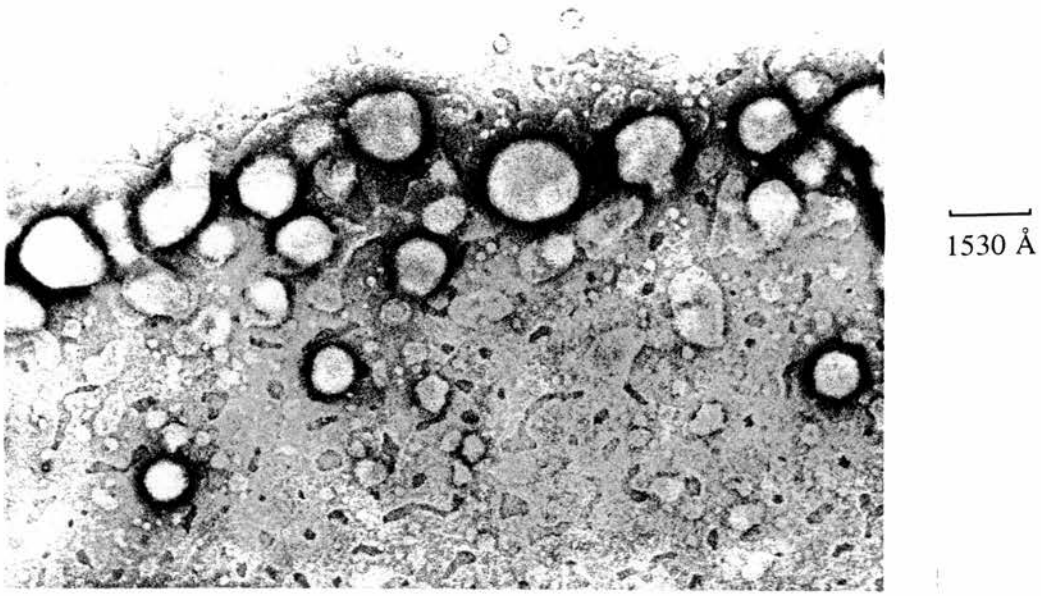

(i)

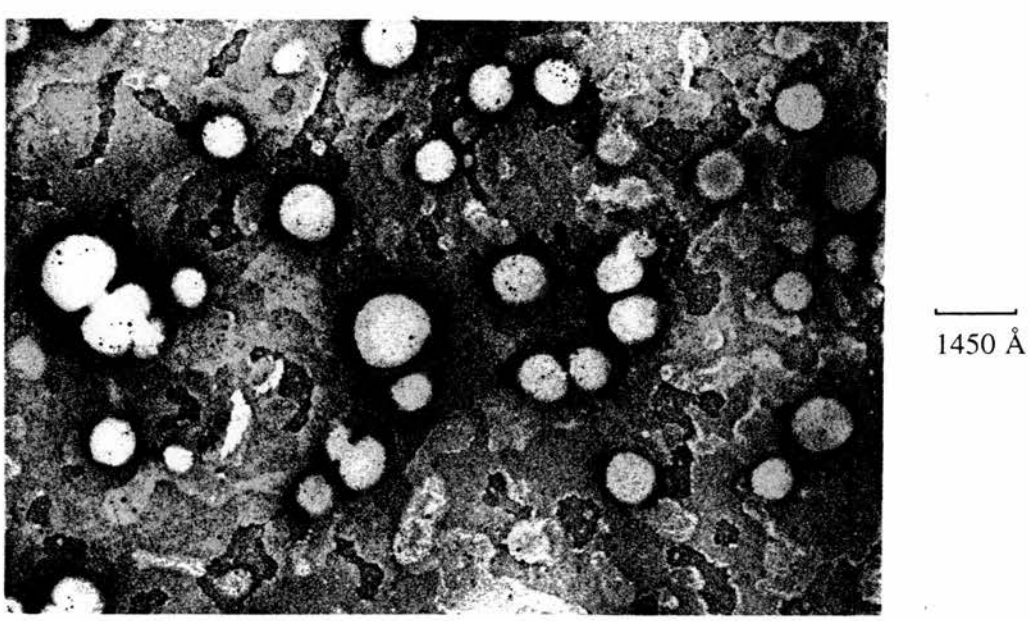

(ii)

Figure 3.10 (5) : Electron micrographs of DODAB vesicles in Fraction 5 after sonication at (i) 10 microns (x 65280) and (ii) 12.5 microns (x 69120).

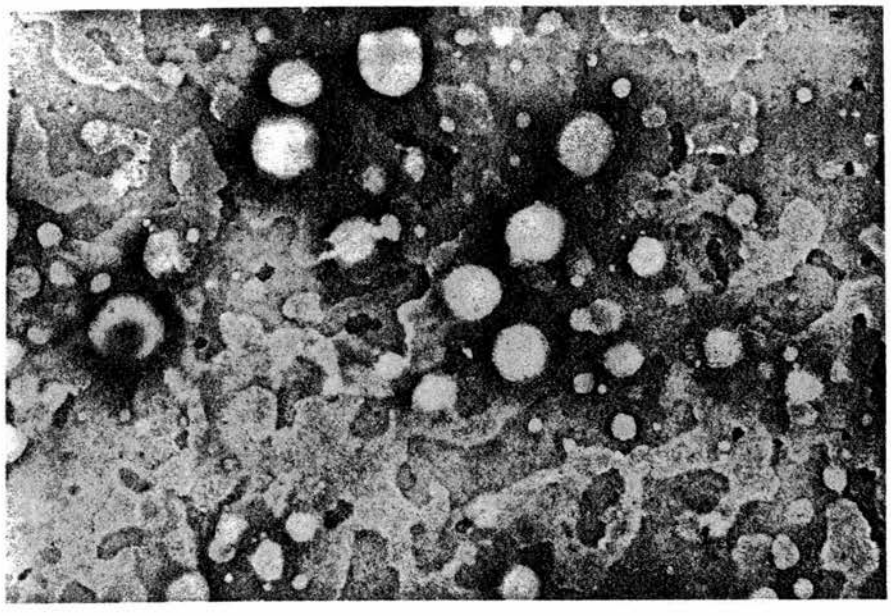

(i)

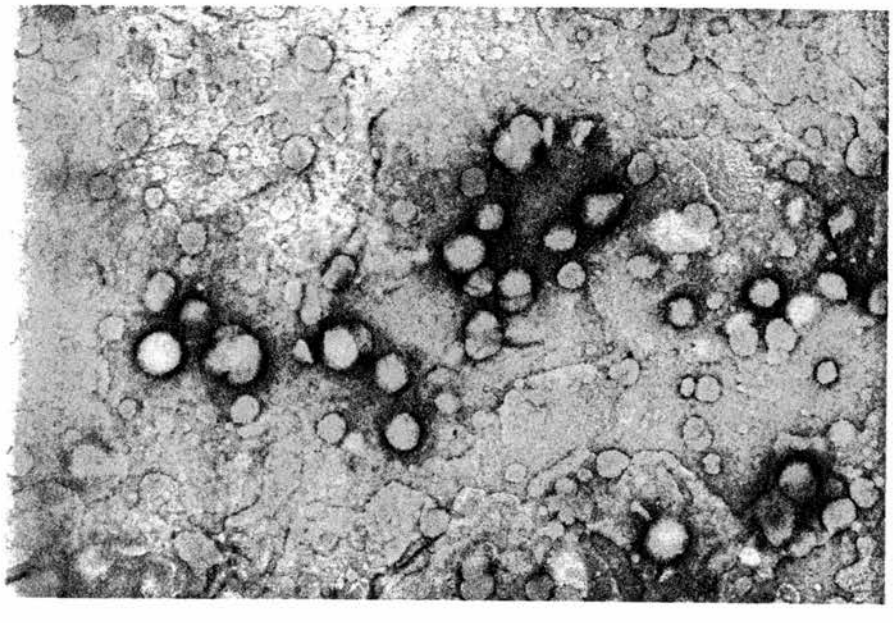

(ii)

Figure 3.10 (6) : Electron micrographs of DODAB vesicles in Fraction 6 after sonication at (i) 10 microns (x 65280) and (ii) 12.5 microns (x 69120).

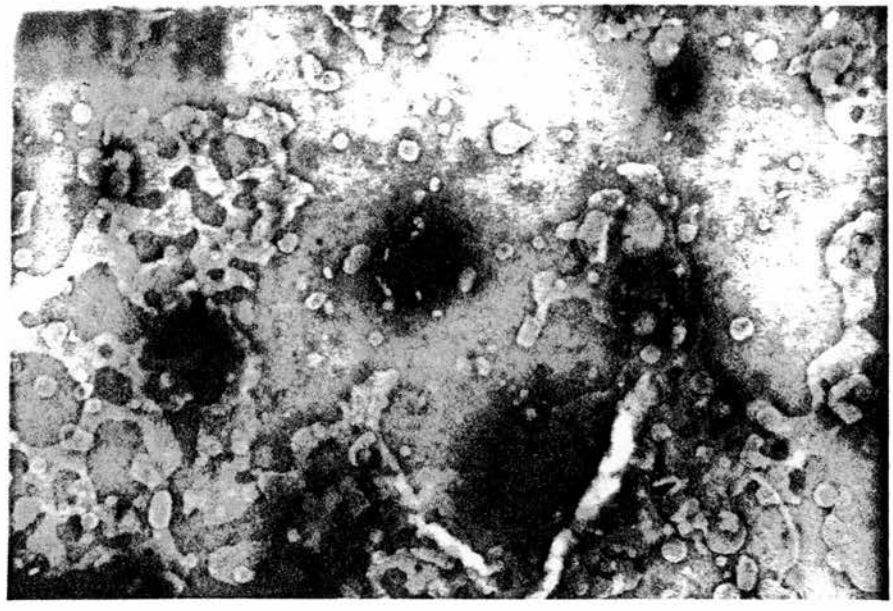

(i)

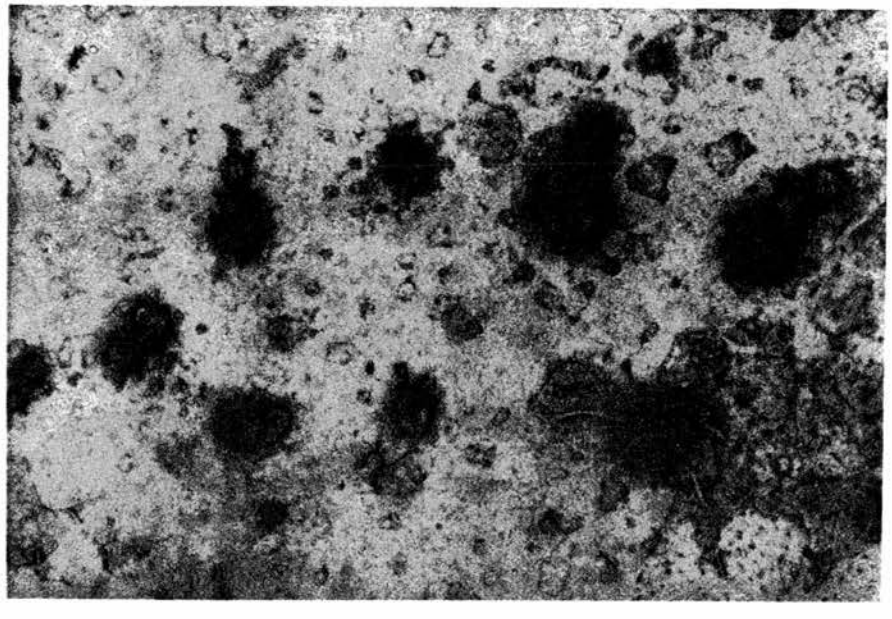

(ii)

Figure 3.10 (7) : Electron micrographs of DODAB vesicles in Fraction 7 after sonication at (i) 10 microns (x 61440) and (ii) 12.5 microns (x 57600).

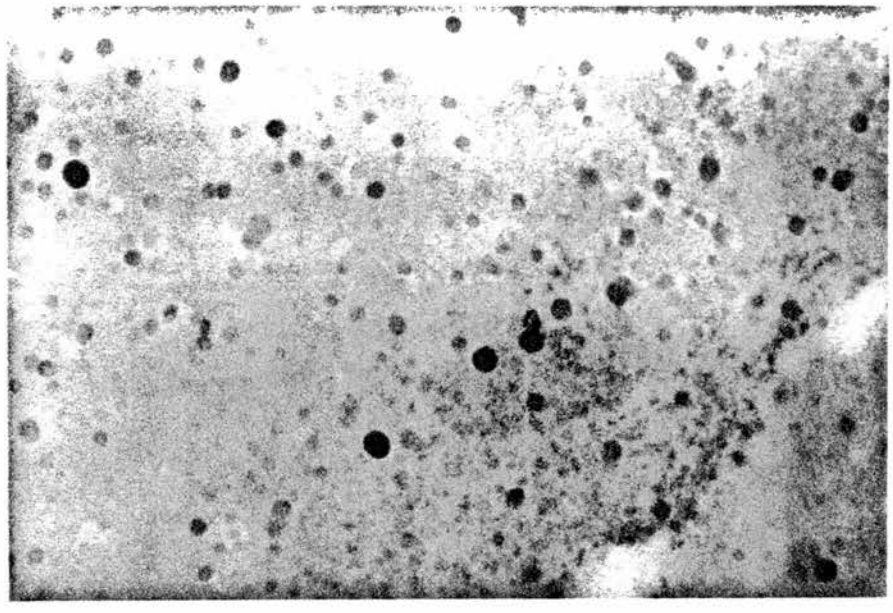

Figure 3.10 (8) (ii) : Electron micrograph of DODAB vesicles in fraction 8 after sonication at 12.5 microns (x 61440).

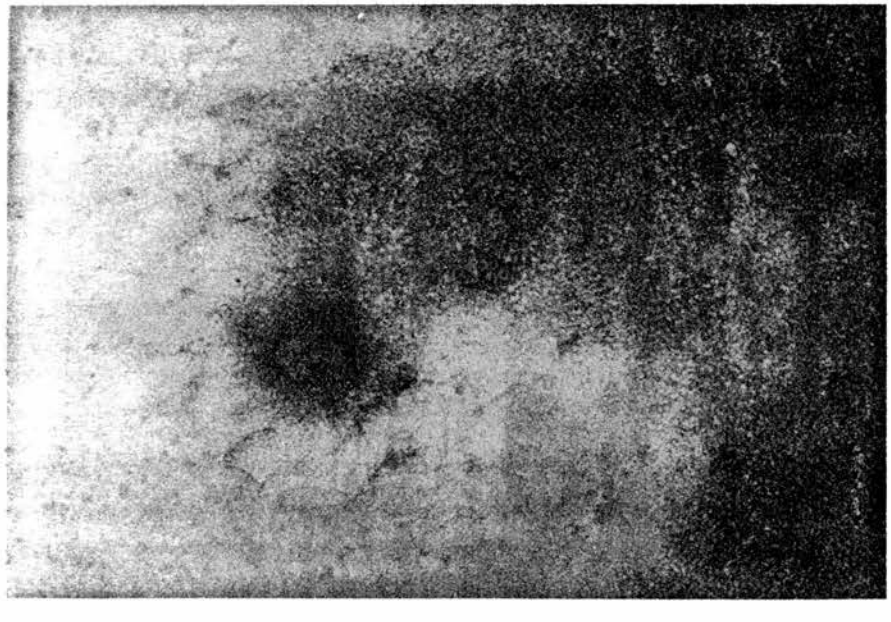

Figure 3.10 (9) (ii) : Electron micrograph of DODAB vesicles inFraction 9 after sonication at 12.5 microns (x 65280).

3.4 Photo-assisted Electron transfer Across Synthetic Vesicle Bilayers

As stated in chapter one, to mimic natural photosynthesis and obtain photoassisted transmembrane electron transfer in any 'artificial' system it is necessary to have a chromophore and electron mediator present. We have shown in the previous chapter that BTDB can act as a neutral chromophore and electron transfer catalyst in microheterogeneous systems containing CTAB micelles. Therefore, the potential of BTDB as a chromophore/mediator across a cationic membrane is of great interest.

Having now studied the vesicle environment, under various conditions, in which we want to demonstrate electron transfer, we require an asymmetric vesicle system where the inner aqueous phase is of a different composition from the outer aqueous phase. The ability of the vesicle bilayer to ensure separation of these two solutions is essential to prevent the leakage of species across the bilayer from the inner to the outer aqueous phases and vice versa. This ability was demonstrated by Robinson *et al.*[28] who showed genuine vectorial electron transport across DODAB vesicles, employing BTDN as the electron transfer catalyst, from entrapped MES^- to AQDS in the bulk water. The "leaking" of species has previously masked the unambiguous demonstration of transmembrane photoredox processes.[38]

3.4.1 Preparation of Asymmetric DODAB Vesicle System of BTDB

Positively charged vesicles of DODAB[43] in distilled water containing the sacrificial electron donor, MESH (0.05 mol dm^{-3}) and BTDB, were prepared by sonication at the various time and power settings used previously. Separation was achieved by passing the solution down a freshly prepared column of 'Sephadex G-50' (Section 6.2.2). The vesicle solutions were a mixture of unilamellar and multilamellar vesicles. The addition of the electron acceptor, AQDS to the surrounding solution, created an asymmetric system suitable for transmembrane processes. Fortunately, the multinegative charge of AQDS did not cause the DODAB vesicle to coagulate at the final concentration employed (0.165 mmol dm^{-3}). See figure 3.11, for a pictorial representation of the preparation of asymmetric DODAB vesicles.

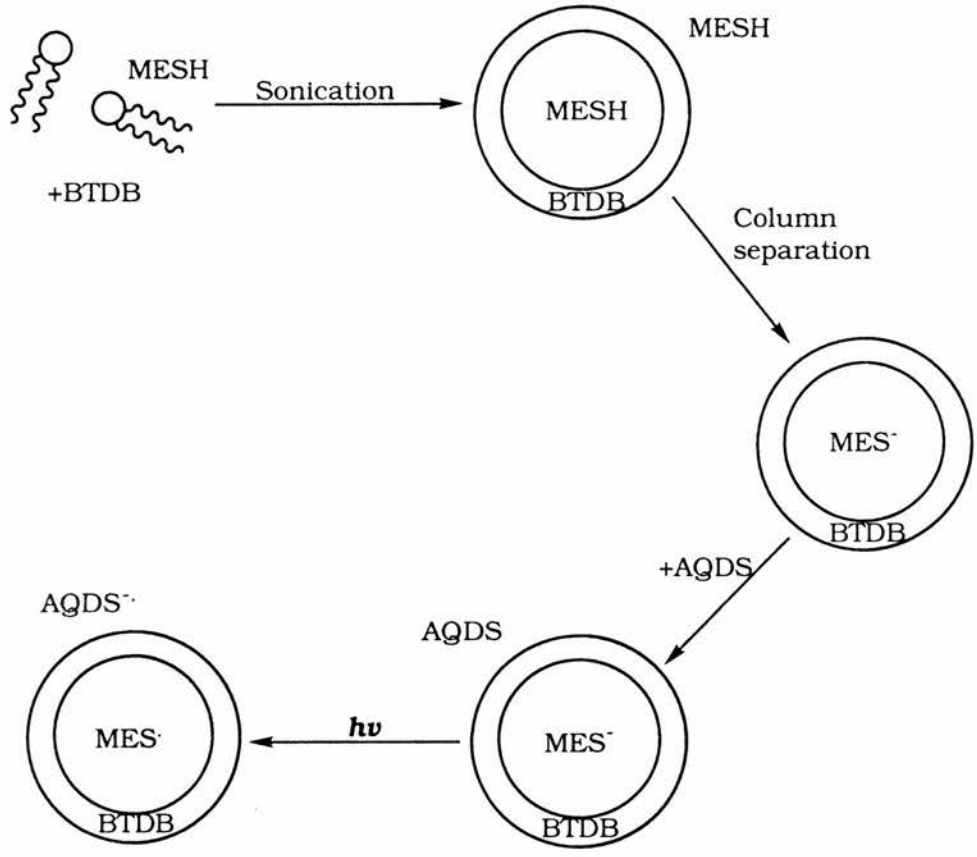

Figure 3.11 : Schematic representation of the procedure by which 'asymmetric' DODAB vesicles are formed.

Unlike previous preparations with BTDN and BTDE, BTDB was retained in the vesicle bilayer and not partitioned out on passage down the column. This was confirmed by recording the uv-visible spectrum before and after passage down the column. MESH was employed, as it was colourless, highly water soluble, possessed the necessary redox properties, and was uninegatively charged which would not cause coagulation of the vesicles.

In comparison to the dynamic nature of a CTAB micelle[33] the lipid architecture of a DODAB vesicle bilayer is highly ordered as shown in figure 3.6 and 3.7.[19,39] However, despite this important distinction the vesicle bilayer should perform the same role as CTAB in the photochemical generation and stabilisation of $BTDB^{-\cdot}$. Since BTDB has been found to act as a chromophore and electron mediator in the presence of micelles, it was hoped that BTDB may perform a similar role in the transfer of electrons across the bilayer of a DODAB vesicle.

3.4.2 Results and Discussion

The effect of BTDB on the production of $AQDSH_2$ generated on photolysis of the asymmetric DODAB vesicle system after sonicating for 5 and 15 minutes at 12.5 microns and collected as a total volume (12 cm^3) after gel chromatography are shown in figure 3.12. To demonstrate that MES^- or AQDS were not leaking across the membrane, the experiment was repeated with BTDB absent. The omission of BTDB resulted in there being no reduction of AQDS. Upon the addition BTDB to the solution and rephotolysis, $AQDSH_2$ was produced. This result demonstrated that BTDB was acting as an electron transfer catalyst between MES^- and AQDS and that neither MES^- nor AQDS were leaching across the bilayer unaided.

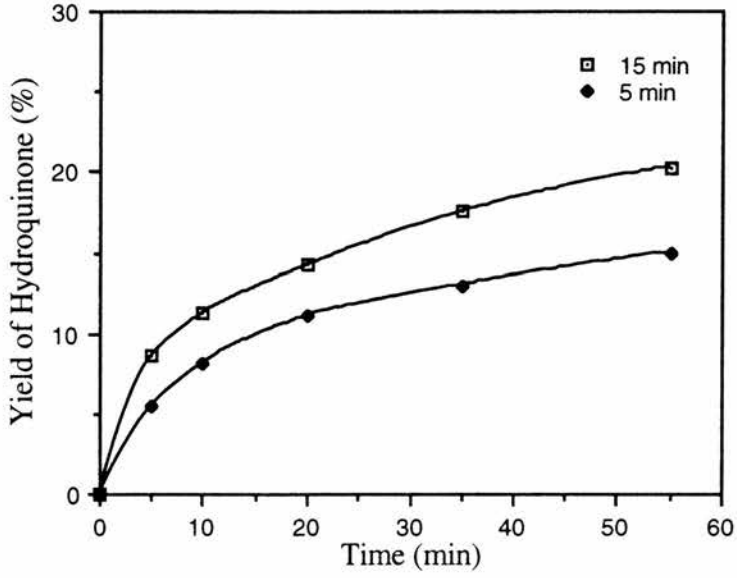

Figure 3.12 : Production of $AQDSH_2$ from AQDS, MES, BTDB and DODAB solutions sonicated for 5 & 15 minutes at pH 6.5.

The above experiment did not, however, rule out the possibility that BTDB was providing some photochemical transport mechanism by which, one or both of MES^- and AQDS could permeate the bilayer. To ensure that this was not happening, an experiment was performed (Figure 3.13), in which a vesicle solution was photolysed for 75 minutes. The solution was then chromatographed on a fresh Sephadex column in air (air oxidises $AQDSH_2$ back to AQDS), the fractions containing the vesicles and

the bulk water were collected. Uv-visible spectroscopy indicated that AQDS was present in both fractions, although most remained electrostatically bound to the vesicles. This was supported by the uv-visible spectrum of $AQDSH_2$ which showed the same red-shift in the presence of the DODAB vesicles as with CTAB micelles, which has been the result of electrostatic association of $AQDSH_2$ with the cationic surfactant headgroup.[6]

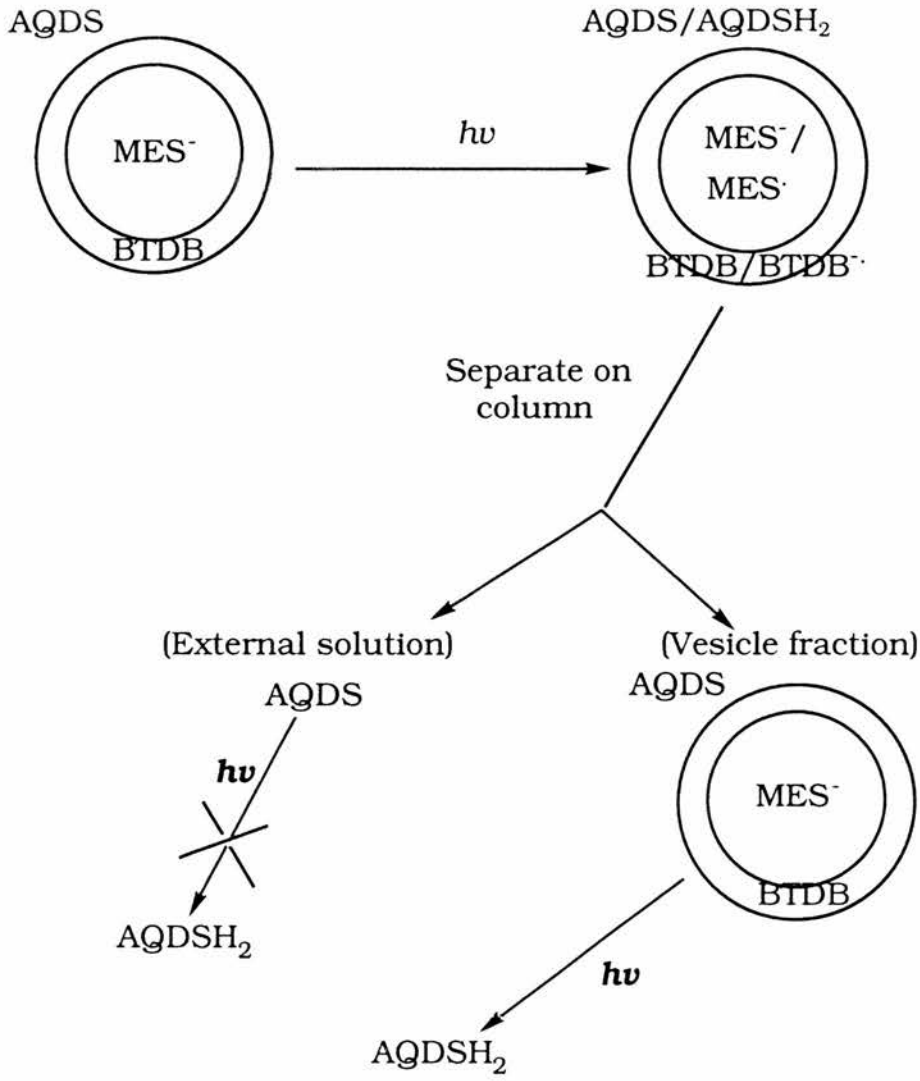

Figure 3.13 : Diagrammatic representation of the procedure by which 'asymmetric' DODAB vesicles were tested for leakage.

BTDB was found wholly in the vesicle containing solution and therefore, upon photolysis of the vesicle solution (vesicle), $AQDSH_2$ was produced as expected. Upon

photolysis of the external solution, no $AQDSH_2$ was produced, thereby showing no MES leaked through the bilayer, as in the previous chapter, we showed that MES^- can react with AQDS without the presence of BTDB or micelle. The results with the vesicle containing fraction confirmed that the vesicles had retained their integrity during photolysis. These results do not unequivically rule out the possibility that AQDS passes through the bilayer on photolysis. We assume that this is not the case, however, because in a similar experiment with BTDN, the BTDN was removed from the vesicles during the chromatography. In this case, no $AQDSH_2$ was produced on photolysis of the separated vesicles, which contained entrappped MES^- and confirmed that AQDS had not diffused through the bilayer but was bound to the outer surface of the vesicle.

Having shown that BTDB is solely responsible for transmembrane electron transfer then the result obtained in figure 3.12, where the rate of production of $AQDSH_2$ was quicker using the vesicle solution sonicated for 15 minutes, can be explained in terms of vesicle morphology and unilamellar vesicle concentration. The vesicle solution sonicated for only 5 minutes, contains only multilamellar vesicles as shown in figure 3.5. Between each bilayer of a multilamellar vesicle there is a trapped aqueous phase containing MES^- and having demonstrated that neither MES^- nor AQDS leak through the vesicle bilayer then the ability to transfer an electron from MES^- to AQDS will only occur on the outer bilayer. Therefore, the vesicle solution sonicated for 5 minutes possesses fewer bilayers across which transmembrane electron transfer can occur to reduce AQDS. Whereas, the vesicle solution sonicated for 15 minutes still contains multilamellar vesicles but in addition there are large and small unilamellar vesicles present which increases the number of bilayers across which electron transfer can occur thus increasing the amount of AQDS that can be reduced in the same time period.

By constructing a vesicle system in which the concentration gradient of electron donor and acceptor can be maintained throughout the duration of our experiments we have been able to demonstrate mediated electron transport across a synthetic surfactant vesicle bilayer.

3.5 The Effect of Vesicle Morphology on the Reduction of AQDS

Having now demonstrated transmembrane electron transfer, we next studied in more detail the link between vesicle morphology and the reduction of AQDS. The asymmetric vesicle environments were prepared as before (Section 6.2.2) but at different power settings of sonication as in section 3.3.2. The sonicated vesicle solutions were again separated into individual fractions, as the vesicle solution eluted from the gel chromatography column, similar to those used for the TEM studies of figure 3.10. AQDS was added and the resulting solution photolysed. The yields obtained for each fraction sonicated at 10 and 12.5 microns are presented in figure 3.13 and 3.14, respectively. To compare the effects between the two different solutions, and in particular between each fraction more closely, we selected the yields at 10 and 75 minutes for each fraction from both sonicated solutions and plotted them against the fraction number (Figures 3.15 and 3.16).

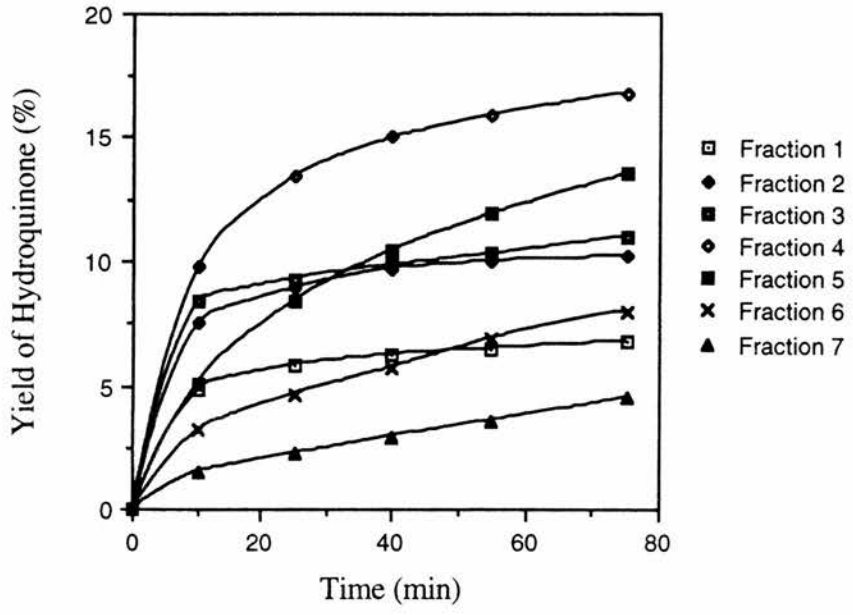

Figure 3.13 : Yields of $AQDSH_2$ from AQDS in the presence of BTDB, CTAB and MES^- at pH 6.5 for the vesicle fractions sonicated at 10 microns.

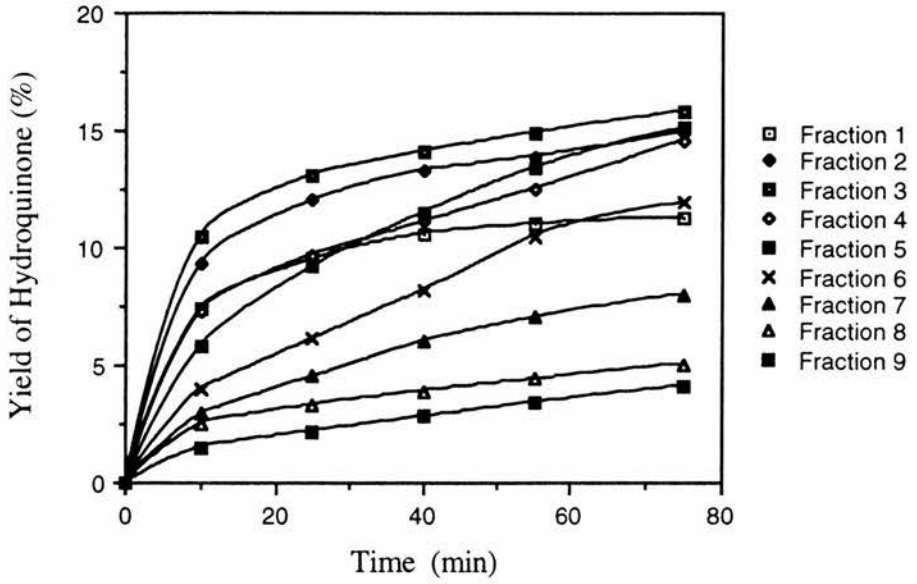

Figure 3.14 : Yield of $AQDSH_2$ from AQDS in the presence of BTDB, CTAB and MES^- at pH 6.5 for vesicle fractions sonicated at 12.5 microns.

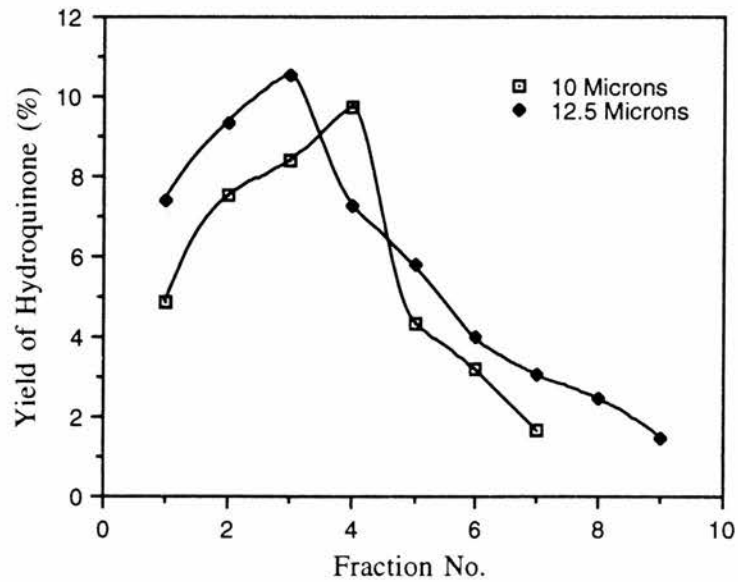

Figure 3.15 : Production of $AQDSH_2$ after 10 minutes from AQDS, MES^- and BTDB in DODAB for each fraction sonicated at 10 & 12.5 microns.

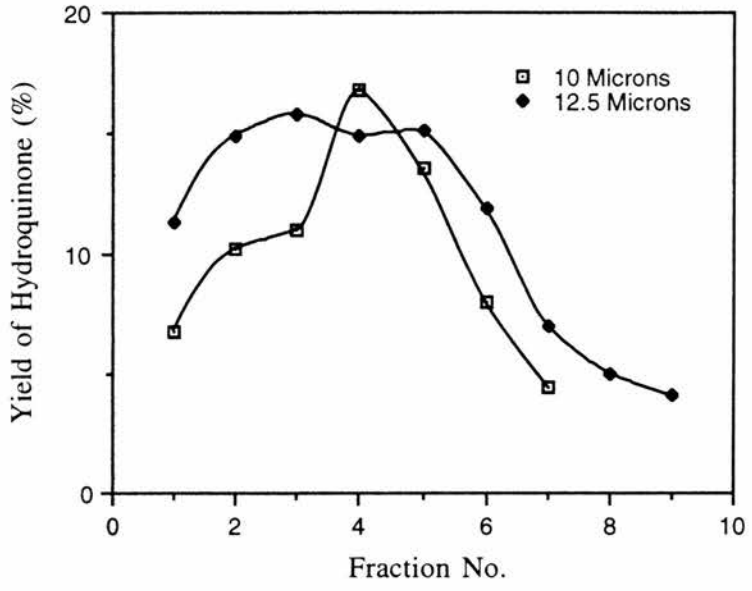

Figure 3.16 : Production of $AQDSH_2$ after 75 minutes from AQDS, MES^- and BTDB in DODAB for each fraction sonicated at 10 and 12.5 microns.

Examination of figures 3.13 and 3.14, suggest that after 10 minutes, for most fractions the production of $AQDSH_2$ was still proceeding at a reasonable rate but that after 75 minutes it had more or less stopped (there was still some growth of $AQDSH_2$ in the later fractions). As a first approximation, therefore, the yield after 10 minutes can be related to the rate of transmembrane electron transfer whilst that at 75 minutes can be related to the total yield of $AQDSH_2$. Since all else is equal, the rate should depend upon the total surface area of the vesicles in a particular preparation whereas, the total yield, which in these cases is presumably governed by the amount of MES^- available should depend upon the "total available volume" within the vesicles. Since there is no mechanism for electron transfer across more than one vesicle bilayer, the "total available volume" will be the sum of the volumes of any unilamellar vesicles and the outer bilayer of any multilamellar vesicle. To study the effect of surface area and volume of entrapped MES^- we calculated the surface area and the volume of entrapped MES^-, using the pictures in figure 3.10 as an example of the vesicle content present in each of the vesicle fractions.

Comparisons of yields after 10 minutes with surface area of vesicles, and of

yields after 75 minutes with available volume of the vesicles obtained using sonication at 10 and 12.5 microns, are shown in figures 3.17 — 3.19. The comparison is exceptionally good, with the graphs generally tracking one another closely. The main deviation is from the later fractions sonicated at 10 microns for 75 minutes. As indicated above, these are the fractions where significant $AQDSH_2$ productions is occuring so that they should not be volume limited.

For sonication at 10 microns, (Figures 3.17 and 3.18), from fractions 1 — 4, the vesicles were becoming smaller and their concentration increasing, thus causing an increase in the surface area. After fraction 4, the vesicles were becoming more dilute (Figure 3.10 (4 — 7)(i)), so that the surface area and the available volume both decrease.

Interestingly, for fractions 5 and 6, after 10 minutes the yield is below that for fraction 1 but after 75 minutes it is higher (Figure 3.18). The total surface area of the vesicles is higher in fraction 1, but because these were largely multilamellar and there were many more unilamellar vesicles in fractions 5 and 6, the 'available volume' is higher in fractions 5 and 6 than in fraction 1. Therefore, over time, the reaction within fractions 5 and 6 is able to proceed and produce for longer.

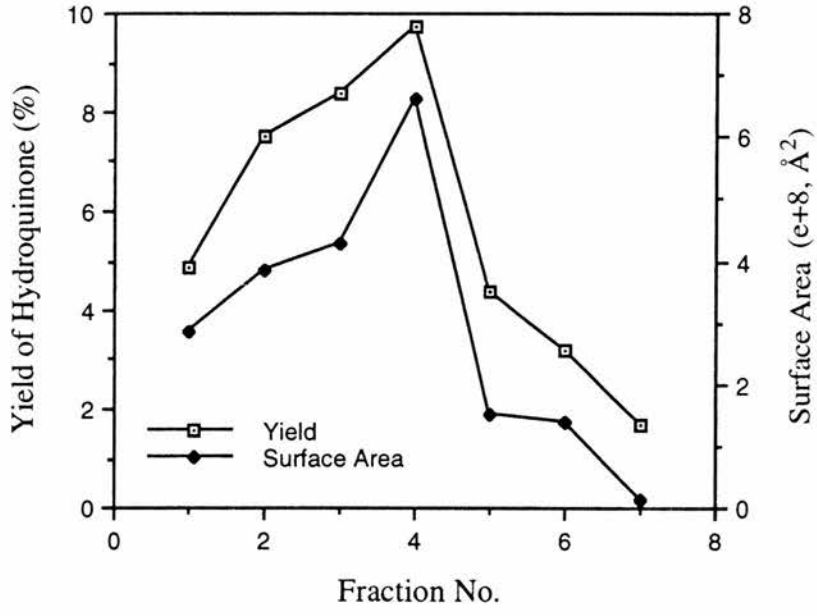

Figure 3.17 : Surface area of vesicles and yield at 10 mins for fractions sonicated at 10microns.

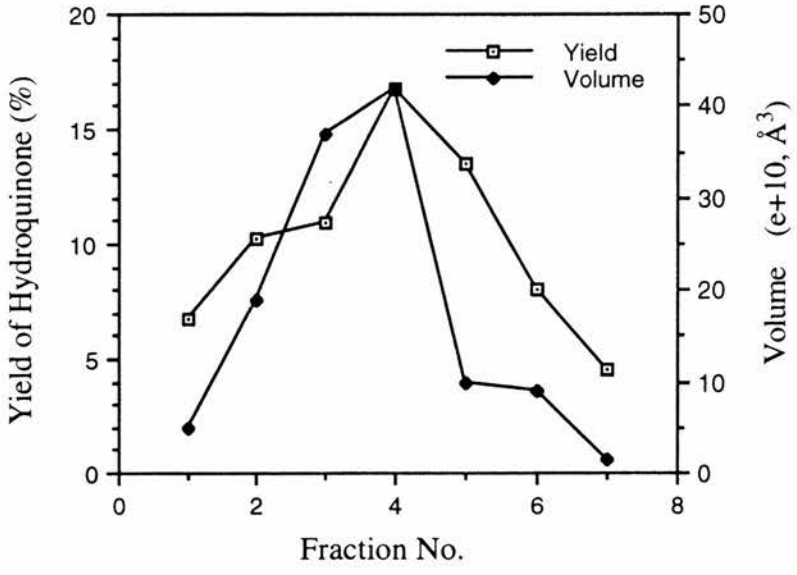

Figure 3.18 : Volume of vesicles and yield at 75 minutes for fractions sonicated at 10 microns.

For the vesicles sonicated at 12.5 microns, the maximum yield after 10 minutes occurs in fraction 3 but after 75 minutes there is a plateau between fractions 2 — 5 (Figures 3.15 and 3.16). Once again, these results can be well fitted to the surface area and total available volume of the vesicles. The earlier maximum produced for 12.5 than for 10 microns arises, because the higher power setting breaks down more of the multilamellar vesicles - those which are concentrated in the earlier fractions.

The volume effect is shown above in figure 3.20 and can be explained by the presence of large unilamellar vesicles in the solution sonicated at 12.5 microns, as presented in fractions 4 — 6 (Figure 3.10 (4 — 7)(ii)).

Large unilamellar vesicles have a larger internal volume (Figure 3.8) compared to the outer bilayer of multilamellar and the internal volume of small unilamellar vesicles (Figures 3.7 and 3.9), respectively. By having a greater volume of entrapped MES solution and a large surface area on which to concentrate the negatively charged AQDS, these vesicles have the ability to perform the reduction of AQDS longer. This is shown after 75 minutes, where the yields are comparable for fractions 2 — 5. The yield at

fraction 6 is higher than fraction 1 because the volume of entrapped MES^- is greater in fraction 6 than 1. Therefore, the presence of large unilamellar vesicles compensates for the dilution of the vesicles after fraction 3 for the solution sonicated at 12.5 microns after 75 minutes.

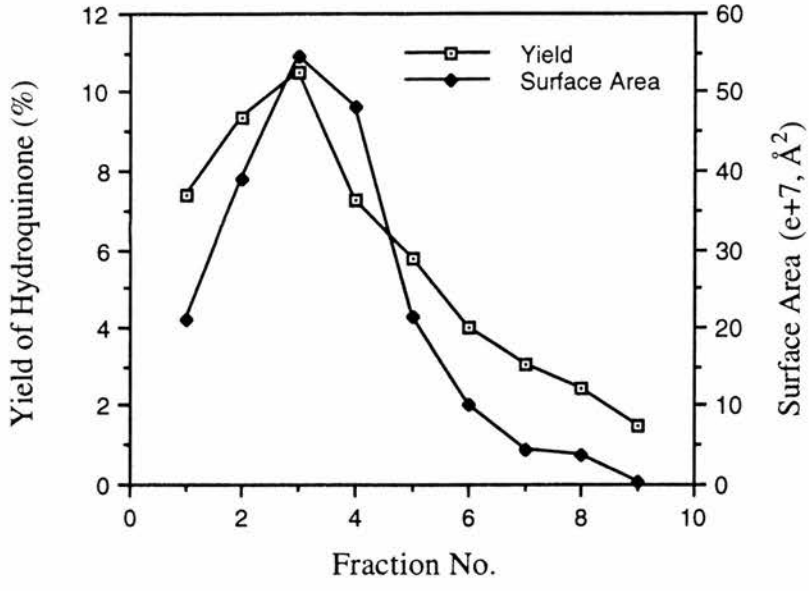

Figure 3.19 : Surface area of vesicles and yield after 10 minutes for vesicles sonicated at 12.5 microns.

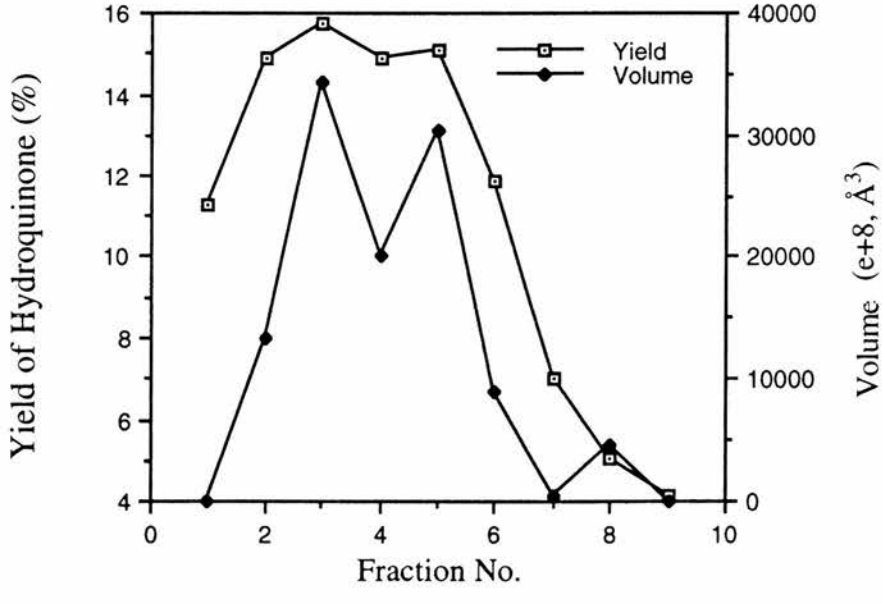

Figure 3.20 : Volume of vesicles and yield for 75 minutes for vesicles sonicated at 12.5 microns.

The yields produced from fraction 7, at 10 microns were identical to those for fraction 9, at 12.5 microns, which would indicate that the vesicles in both solutions were comparable in size (Figure 3.10 (7)(ii) and (I)) and concentration.

From the results presented in figures 3.17 — 3.20, we can conclude that the initial rate of production of $AQDSH_2$ is dependent upon the total surface area present in solution. This is because the [MES^-] is in excess and has not diminished enough to become rate limiting. However, over a period of time the MES^- becomes rate limiting since it is a sacrificial electron donor. The yield of $AQDSH_2$ under these circumstances is determined by the 'total available' volume of the vesicles.

References

1. P. Ekwall, *Adv. Liquid Cryst.*, 1975, **1**, 1.
2. J.M. Gebicki and M. Hicks, *Nature'*(London), 1973, **243**, 232.
3. J.M. Gebicki and M. Hicks, *Chem. Phys. Lipids*, 1976, **16**, 142; M. Hicks and J.M. Gebicki, *'Ibid'*, 1977, **20**, 243.
4. T. Kunitake and Y. Okahata, *J. Am. Chem. Soc.*, 1977, **99**, 3860.
5. T. Kunitake, Y. Okahata, K. Tamaki, F. Kumamaru and M. Takayanagi, *Chem. Lett.*, 1977, 387.
6. C.D. Tran, P.L. Klaki, A. Romero and J.H. Fendler, *J. Am. Chem. Soc.*, 1978, **100**, 1622.
7. A. Romero, C.D. Tran, P.L. Klan and J.H. Fendler, *Life Sci.*, 1978, **22**, 1447.
8. K. Kano, A Romero, B. Djermouni, H. Acheau and J.H. Fendler, *J. Am Chem. Soc.*, 1979, **101**, 4030.
9. Y.Y. Lim and J.H. Fendler, *J. Am Chem. Soc.*, 1979, **101**, 4023.
10. U. Herrman and J.H. Fendler, *Chem. Phys. Lett.*, 1979, **64**, 270.
11. J.H. Fendler, *Acc Chem. Res.*, 1980, **13**, 7.
12. M. Gratzel, '*Heterogeneous Photochemical Electron Transfer.*' C.R.C. Press Inc., Boca Ralon, 1989, Chap. 2.
13. C Tanford '*The Hydrophobic Effect*', Wylie, New York 1973; J.H. Fendler and E.J. Fendler, '*Catalysis in Miceller and Macromolecular Systems*' Academic Press, New York, 1975.
14. T,. Nagamura, S. Mihara, Y. Okahata, T. Kunitale and T. Matsuo, *Ber. Bensenges. Phys. Chem.*, 1978, **82,** 1093.
15. E.A.G. Aniansson, M. Almgren and S.N. Wall, '*Chemical and Biological Applications of Relaxation Spectrometry*', E.Wyn Jones Ed., Reidel. Dordrecht, Holland, 1975, 239.
16. S. Baral and J.H. Fendler '*Photoinduced Electron Transfer Part B*', M.A. Fox and M. Chenon Eds., Elsevier, 1988, Chap. 3.2.
17. E.A.G Anionsson, S.N. Wall, M Almgren, H. Hoffman, I. Kielmann, N. Ulbricht, R. Zana, J. Lang and C.J. Tondre, *J. Phys. Chem.*, 1976, **80**, 905.
18. K. Kalyanasundaram '*Photochemistry in Microheterogeneous Systems*', Academic Press, London, 1987.
19. A. Kumano, T. Kajiyama, M. Takayanagi and Y. Okahata, *Ber. Bunsenges Phys. Chem.*, 1984, **88**, 1216; D. Papahadjopoulos and W.J. Vail, *Ann. N.Y. Acad. Sci.*, 1978, **308**, 259.
20. H. Ringsdorf, B. Schlarb and J. Venzner, *Angew. Chem. Int. Ed. Engl.*,

1988, **27**, 113 and refs. therein.

21. J. Stefely, M.A. Markowitz and S.L. Regan, *J. Am. Chem. Soc.*, 1988, **110**, 7363 and refs. therein.
22. N. Higashi, T. Adachi,and M. Nina, *J.Chem. Soc, Chem. Commun.*, 1988, 1573 and refs. therein.
23. J. N. Israelachivili, '*Intermolecular and Surface Forces*', Academic Press, London, 1985.
24 P.M. Claesson, A.M. Carmona-Ribeiro and K. Kurihara, *J. Phys. Chem.* 1993, **93**, 917.
25. A.M. Carmona-Ribeiro and B.R. Midmore, *J. Phys. Chem.*, 1992, **96**, 3542.
26. A.M. Carmona-Ribeiro and B.R. Midmore, *Langmuir*, 1992, **8**, 801.
27. A.M. Carmona-Ribeiro, *Chem. Soc. Revs.*, 1992, 209.
28. J. N. Robinson, D.J.Cole-Hamilton, M.K. Whittlesey and P. Camilleri, *J. Chem. Soc. Faraday Trans.*, 1990, **86**, 2897.
29. R.A. Mortara, F.H. Quina and H. Chaimovich, *Biochem. Biophys. Res. Commun.*, 1978, **81**, 1080.
30. A. M. Carmona-Rebeiro and H. Chaimovich, *Biochem. Biophys. Acta.*, 1983, **733**, 172.
31. A.M. Carmona-Rebeiro, L.S. Yoshide, A. Sesso and H. Chaimovich, *J. Colloid, Interface Sci.*, 1984, **100**, 433.
32. S.V. Lymer, U.N. Parmonard and K.I. Zameraev, '*Topics in Current Chemistry*', 1991, **159**, 3.
33. J.H. Fendler, *Chem. Rev.*, 1987, **87**, 877.
34. J.H.Fendler, '*Membrane Mimetic Chemistry*', Wiley, New York, 1982.
35. T. Kajiyama, A. Kumano, M. Takayanagi, Y. Okahata and T. Kunitake, *Chem. Lett.*, 1979, 645.
36. C.D. Tran, P.L. Klahn, A Romero and J. H. Fendler, *J. Am. Chem. Soc.*, 1978, **100**, 1622.
37. E.A. Munn, *Meth. Enzym.*, 1974, **32**, 20.
38. L.Y.-C. Lee, J.K. Hurst, M. Polite, K. Kurimara and J.M. Fendler, *J. Am. Chem. Soc.*, 1983, **105**, 370.
39. L.T. Mimms, G. Zampighi, Y. Nozaki, C. Tanford and J.A. Reynolds, *Biochem.*, 1981, **20**, 833.

Chapter 4

Kinetic Studies on Vectorial Electron Transfer Across DODAB Vesicles Using BTDB

4.1 Introduction

Having established in the previous chapter that photochemical transmembrane electron transfer can be promoted by BTDB, we studied the reduction of AQDS by BTDB in a vesicle environment by examining the influence, each of the individual reagents had on the overall reaction. The aim was to present an accurate picture for the overall mechanism of photochemical electron transfer across a surfactant vesicle bilayer.

As a result of the various sonicating conditions employed in the previous chapter, the unsymmetrical vesicle solutions were prepared by sonicating them at 12.5 microns through a 0.5 mm titanium head probe for 15 minutes at 70°C (Section 6.2.2). This allowed the reaction to be studied using the maximum concentration of unilamellar vesicles, as shown in figure 3.10 (1 — 9)(ii), as it is unilamellar vesicles that are most commonly employed to study transmembrane electron transfer. The vesicle solution upon elution from the Sephadex column was collected to a total volume of 10 — 11 cm^3, after an initial volume of 14 — 16 cm^3 had been eluted (Section 6.2.2).

4.2 Mechanistic Studies

4.2.1 Light Intensity

The first variable to be studied was light intensity and the influence it had on the overall reduction of AQDS by BTDB. As before, the light intensity was varied by using various sizes of gauze and placing them in front of the light source. The percentage of transmitted light passed through each of the gauzes was determined using an I.R. machine, see section 6.1.10. The light intensity's finally used were 33, 52, 63, 73 and 100%. The overall yields achieved for each intensity are shown in figure 4.1 and the initial rates were determined and plotted in figure 4.2.

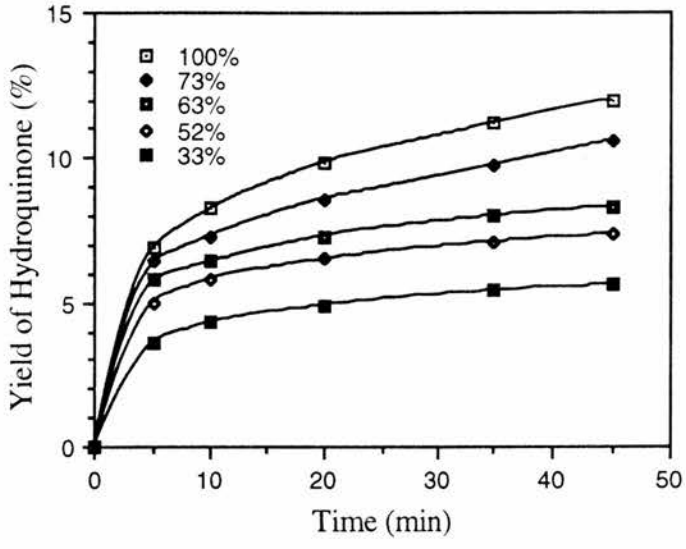

Figure 4.1 : Production of $AQDSH_2$ while varying light intensity in the presence of DODAB, MES^- and BTDB at pH 6.5.

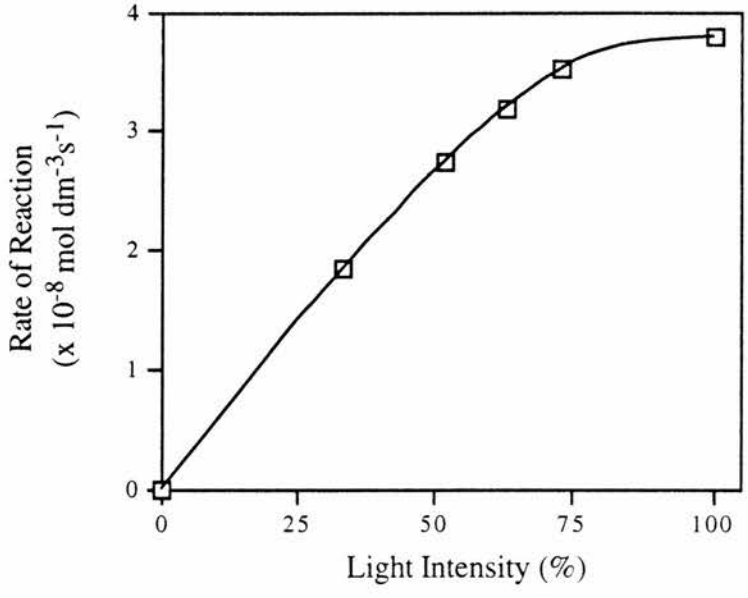

Figure 4.2 : Initial rates of reaction for the production of $AQDSH_2$ in the presence of DODAB, MES^- and BTDB at pH 6.5.

4.2.2 [MESH]

This set of experiments was concerned with the effect that the [MESH] had on the overall reduction of AQDS at various concentrations (0.0125, 0.025, 0.05, 0.075 and 0.1 mol dm^{-3}) (Section 6.2.2 (viii)). A control was employed where MESH was

absent with the yields and initial reaction rates for the production of $AQDSH_2$ are displayed in figures 4.3 and 4.4, respectively.

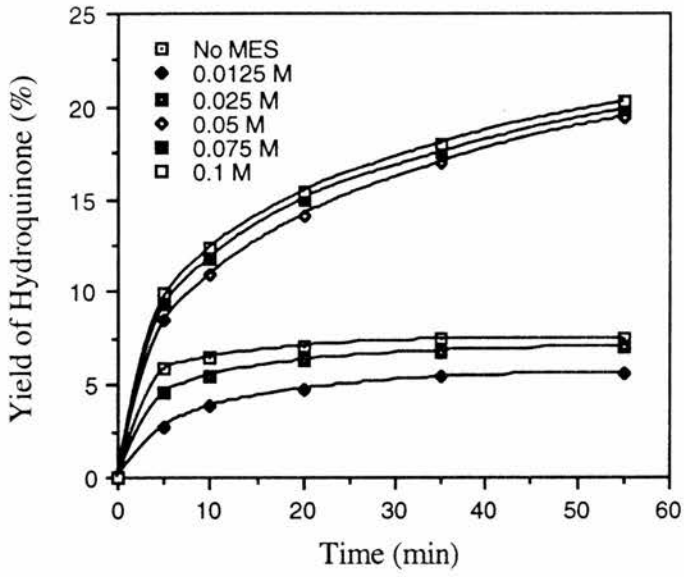

Figure 4.3 : Production of $AQDSH_2$ while varying [MESH] in the presence of DODAB and BTDB at pH 6.5.

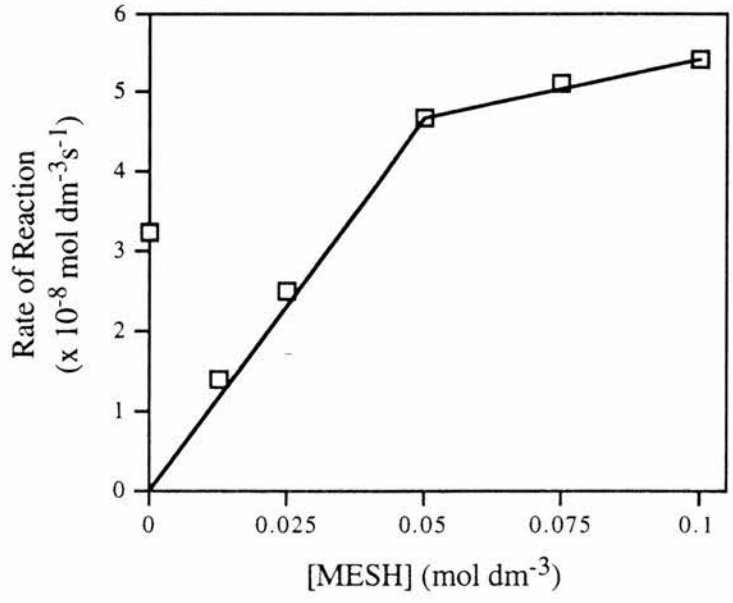

Figure 4.4 : Varying initial rates of production caused by varying [MESH] in the presence of DODAB and BTDB at pH 6.5.

4.2.3 [BTDB]

The next reagent to be studied was BTDB at various concentrations, which were 0.041, 0.083, 0.165, 0.248 and 0.33 mmol dm^{-3} (Section 6.2.2 (viiii)). The results of varying [BTDB] are shown in figures 4.5 and 4.6, showing yields and rates of reaction for the production of $AQDSH_2$, respectively.

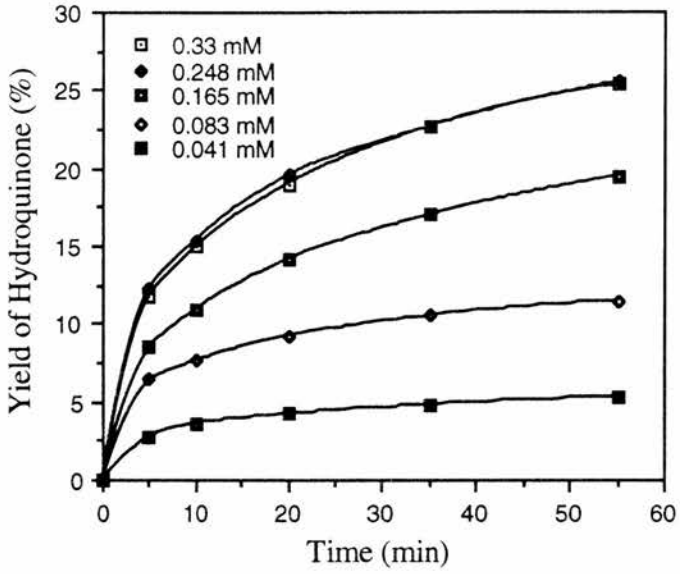

Figure 4.5 : Yields of $AQDSH_2$ while varying [BTDB] in the presence of DODAB and MES^- at pH 6.5.

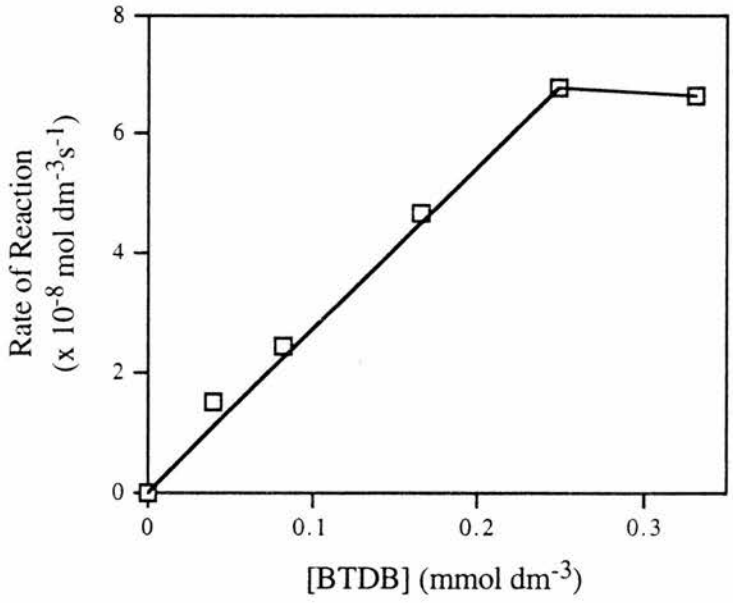

Figure 4.6 : Initial rates of reaction caused by varying [BTDB] in the presence of DODAB and MES at pH 6.5.

4.2.4 pH

The next effect studied was pH (Section 6.2.2 (vi)). A pH range from 4 — 11 was employed and the production of $AQDSH_2$ at each pH is presented graphically in figure 4.7 with the initial rates plotted against pH in figure 4.8 and these show an optimum rate at pH 6.5.

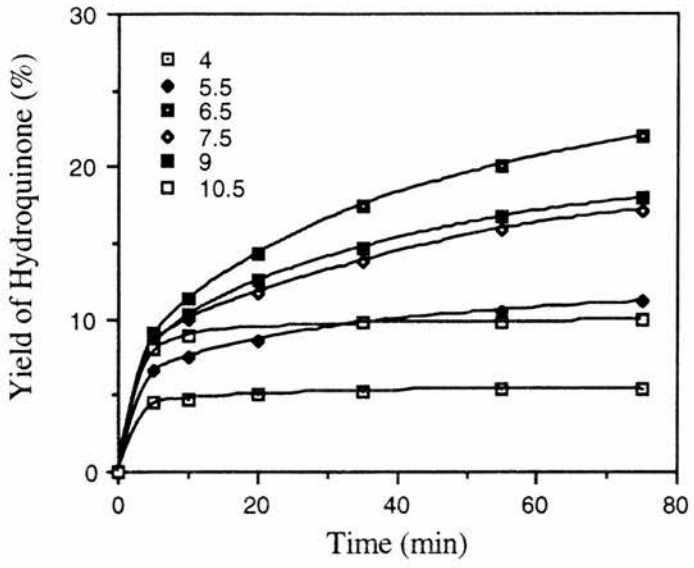

Figure 4.7 : Production of $AQDSH_2$ while varying pH in the presence of DODAB, MES^- and BTDB.

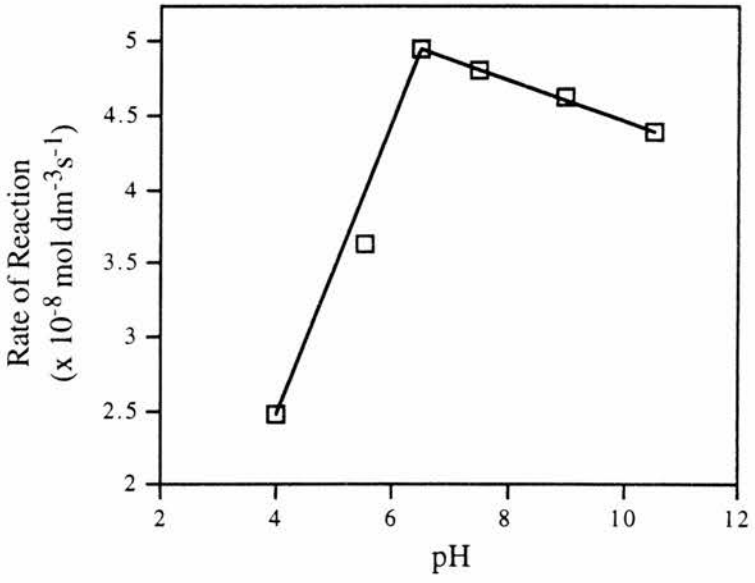

Figure 4.8 : Varying rates of reaction caused by changes in pH in the presence of DODAB, MES^- and BTDB

4.2.5 [AQDS]

The final reagent to be studied was AQDS (Section 6.2.2 (ix)) at concentrations from 0.041 — 0.33 mmol dm^{-3}. The effect these various concentrations had on the overall yield and initial rate of reaction for the reduction of AQDS is shown in figures 4.8 and 4.9, respectively.

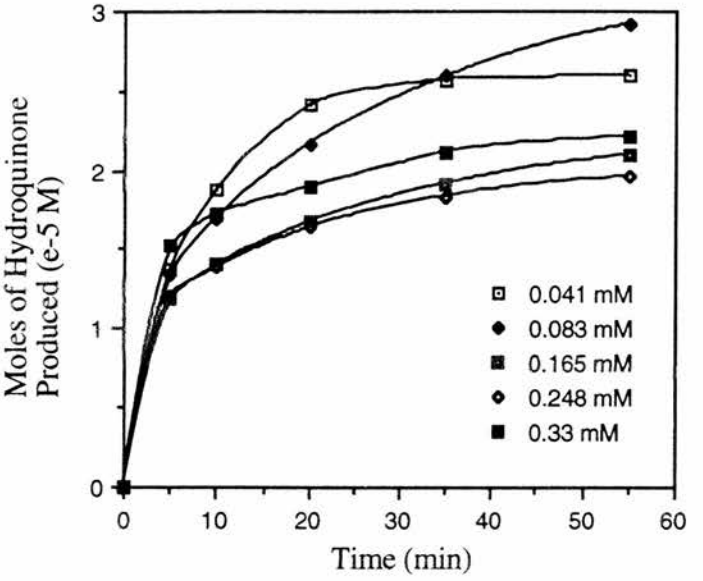

Figure 4.9 : Production of $AQDSH_2$ as a result of varying [AQDS] in the presence of DODAB, MES^- and BTDB at pH 6.5.

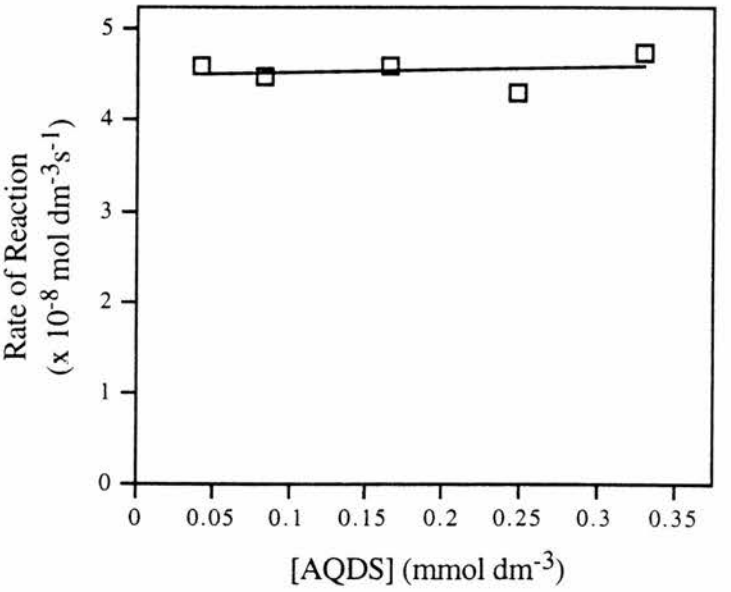

Figure 4.10 : Initial rates of reaction for the production of $AQDSH_2$ as a result of varying [AQDS] in the presence of DODAB, MES^- and BTDB at pH 6.5.

4.3 Discussion

Before the results presented in the previous section are discussed, the overall reaction mechanism for the reduction of AQDS by MES^- in the presence of BTDB will be presented and subsequently, a rate expression will be derived for the reaction, see figure 4.10, below. It is assumed that the rate of decomposition of $MES^{\cdot}$ and the disproportionation and protonation of $AQDS^{-\cdot}$ are fast compared with the other steps.

$$BTDB + I \xrightarrow{k_1} BTDB^*$$

$$BTDB^* \xrightarrow{k_2} BTDB$$

$$BTDB^* + MES^- \xrightarrow{k_3} BTDB_i^{-\cdot} + MES^{\cdot} \xrightarrow{Fast} \text{Decomposition}$$

$$BTDB_i^{-\cdot} \underset{k_{-4}}{\overset{k_4}{\rightleftharpoons}} BTDB_o^{-\cdot} \qquad \text{(Diffusion Across Vesicle)}$$

$$BTDB_o^{-\cdot} + AQDS \xrightarrow{k_5} BTDB + AQDS^{-\cdot} \xrightarrow[H^+]{Fast} {}^1/_2AQDSH_2 + {}^1/_2AQDS$$

$$\text{Rate} = k_5 [BTDB_o^{-\cdot}][AQDS]$$

$$\frac{d[BTDB_o^{-\cdot}]}{dt} = k_4 [BTDB_i^{-\cdot}] - k_5 [BTDB_o^{-\cdot}][AQDS] - k_{-4}[BTDB_o^{-\cdot}] = 0$$

$$\frac{d[BTDB_i^{-\cdot}]}{dt} = k_3 [BTDB^*][MES^-] - k_4 [BTDB_i^{-\cdot}] + k_{-4}[BTDB_o^{-\cdot}] = 0$$

$$\frac{d[BTDB^*]}{dt} = k_1 I[BTDB] - k_2[BTDB^*] - k_3[BTDB^*][MES^-] = 0$$

$$\text{Rate} = k_3[BTDB^*][MES^-]$$

$$[BTDB^*] = \frac{k_1 I[BTDB]}{k_2 + k_3[MES^-]}$$

$$\therefore \text{RATE} = \frac{k_3 k_1 I[BTDB][MES^-]}{k_2 + k_3[MES^-]}$$

Figure 4.11 : The reaction mechanism and the rate law expression for the BTDB catalysed reduction of AQDS within a vesicle environment.

From the final rate expression, the following predictions about the order of the

reaction with respect to individual reagents can be determined:

(1) 1st order with respect to Light Intensity (I),

(2) 1st order with respect to [BTDB],

(3) 1st order with respect to [MES^-] at low [MES^-] and zero-order at high [MES^-]

(4) Independent of [AQDS].

4.3.1 Light Intensity

The dependence of the initial rate of production of $AQDSH_2$ upon light intensity is shown in figure 4.2. As expected from the rate expression, the reaction shows first order dependence upon light intensity but less than first order at higher light intensity. This behaviour which is very similar to that observed in the micellar system, arises because the number of molecules present in solution is finite and is not uncommon for a photochemical reaction. Therefore, if all molecules are excited then any further increases in light intensity cannot excite greater numbers of molecules, resulting in no increase in the observed rate. It must be assumed that in our experiments we are moving towards this situation at higher light intensities. At the light intensity used for the majority of the reactions studied (100%), the reaction is essentially independent of the light intensity.

4.3.2 [MESH]

The effect of [MESH] upon the reduction of AQDS is shown in figure 4.4 and is again very similar to the behaviour observed in the micelles. The reaction follows first order kinetics at low concentrations and at higher concentrations the reaction tends to zero order. This result agrees with the rate expression derived in figure 4.11. However, when the sacrificial electron donor was absent from the system, the production of $AQDSH_2$ was observed (Figure 4.3) at a higher initial rate than at low [MES^-]. This result can be explained in terms of OH^- acting as the electron donor towards $BTDB^*$ (as has been observed for BTDN)[1] and upon the addition of MESH, which is in great excess compared with [OH^-]. The rate determining step becomes the rate of electron

transfer between MES^- and $BTDB^*$ (k_3), when all other reagents are constant at MESH concentrations between 0.01 and 0.05 mol dm^{-3}. However, at the concentration employed as standard (0.05 mol dm^{-3}) we observed very little dependence and this was confirmed upon doubling the concentration which showed little effect upon the rate of formation of $AQDSH_2$.

The rate becomes dependent upon the [MESH] because MES^- may be more strongly attracted to the internal surface of the vesicle bilayer and is in such excess compared with OH^- that, MES^- restricts the ability of OH^- to transfer its electron to $BTDB^*$.

4.3.3 [BTDB]

The effect of [BTDB] on the formation of $AQDSH_2$ is shown in figure 4.6. A first order dependence is observed up to 0.248 mmol dm^{-3} but at higher concentrations there is a tendency towards zero order dependence. This behaviour is quite different from that observed in micelles (purely first order) or expected from the rate expression derived in figure 4.11. It suggests that, whereas, the mechanism of figure 4.11 is adequate for explaining the behaviour of the system at low [BTDB], some other process may become rate determining at higher [BTDB].

4.3.4 [AQDS]

As for the micelle system (Figure 2.30), the rate expression for the vesicle system, (Figure 4.11), indicates that the initial rate should also be independent of [AQDS] which is confirmed by the graph presented in figure 4.10.

4.3.5 Charge Compensation Across Vesicle Bilayers

Although the rate expression derived in figure 4.11 is adequate for explaining the behaviour of the system for transbilayer electron transfer at low concentrations of all reagents, it clearly breaks down at higher concentrations and indeed the initial rate of $AQDSH_2$ formation is almost independent of [BTDB], [MESH], [AQDS] and light

intensity at the standard concentrations used for most of the experiments. It is also independent of which mediator (BTDB, BTDB or BTDE) is employed (Figure 4.12). This suggests that some other process must be rate determining under these conditions.

The process of transmembrane electron transfer is electrogenic; if charge transfer were to occur without any compensating ion migration, substantial trans-bilayer electrical potentials would soon develop, increasingly opposing and ultimately limiting the transbilayer redox reaction.[2] This did not occur during electron transfer which made it apparent that charge compensating transbilayer ion diffusion must be present in these systems.

We have shown that both MES and AQDS cannot permeate the vesicle bilayer of DODAB and since the diffusion of Na^+ or Br^- across the bilayer are both known to be very slow.[1] We conclude, that protons or hydroxide ions are almost certainly the active species involved in the charge compensation. Studies have revealed that both are relatively permeable across synthetic vesicle bilayers[3,5] (1000 times faster than bromide ion).[4]

Further support comes from the relatively unchanged pH of the bulk water phase of our asymmetric vesicle systems, which was measured before (pH 6.5) and after photolysis (pH 6.3). If diffusion of a counterion did not occur then it would be expected to observe a sharp rise in pH through the disproportionation and protonation of external $AQDS^{-\cdot}$ to $AQDSH_2$.

The zero order dependencies described above suggest that, the charge compensating diffusion of H^+ or OH^- across the vesicle may become rate determining at the higher concentrations of reagents used. In order to test whether this was the case and, if so, which of H^+ or OH^- was responsible, we have studied the effect of pH on the system.

4.3.6 Effect of pH

The effect of pH on the system is shown in figure 4.8 and below pH 6.5 parallels the

behaviour observed in micelles as the N atom of the MESH becomes protonated making it a poor electron donor.

Above pH 6.5, the results obtained in the vesicles show a fall off in reaction rate as the pH is increased. This in contrast to the results obtained in the micelles which showed that the reaction was independent of pH between pH 6.5 and 10.5.

The fall off in rate as the pH was increased in the vesicular system was good evidence that the reaction was dependent on $[H^+]$ in the pH range 6.5 — 10.5 and hence the charge compensation which we have already shown was rate determining involves H^+ migration from the inner to the outer water pools rather than diffusion of OH^- in the reverse direction. It is not clear, however, why the dependence upon $[H^+]$ should be logarithmic. Attempts to confirm this by adding a proton carrier such as vitamin K were frustrated because it caused coagulation of the vesicles.

The conclusions are that, the diffusion of $BTDB^{-\cdot}$ across the DODAB vesicle bilayer is the prominent mechanism by which BTDB mediates the transfer of electrons from entrapped MES^- to externally bound AQDS. The overall rate being controlled by the rate of H^+ migration. Therefore, the proposed overall mechanistic process within the DODAB vesicle is illustrated in figure 4.13.

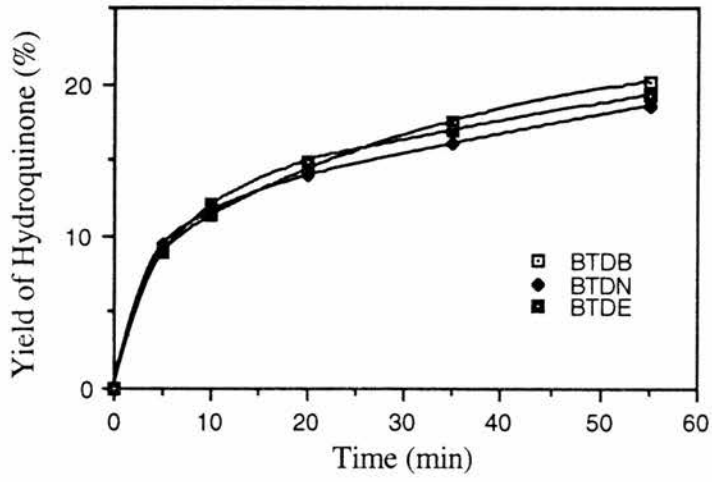

Figure 4.12 : Photochemical conversion of AQDS to $AQDSH_2$ in the bulk water with MES^- and BTDN, BTDE and BTDB in DODAB vesicles at pH 6.5.

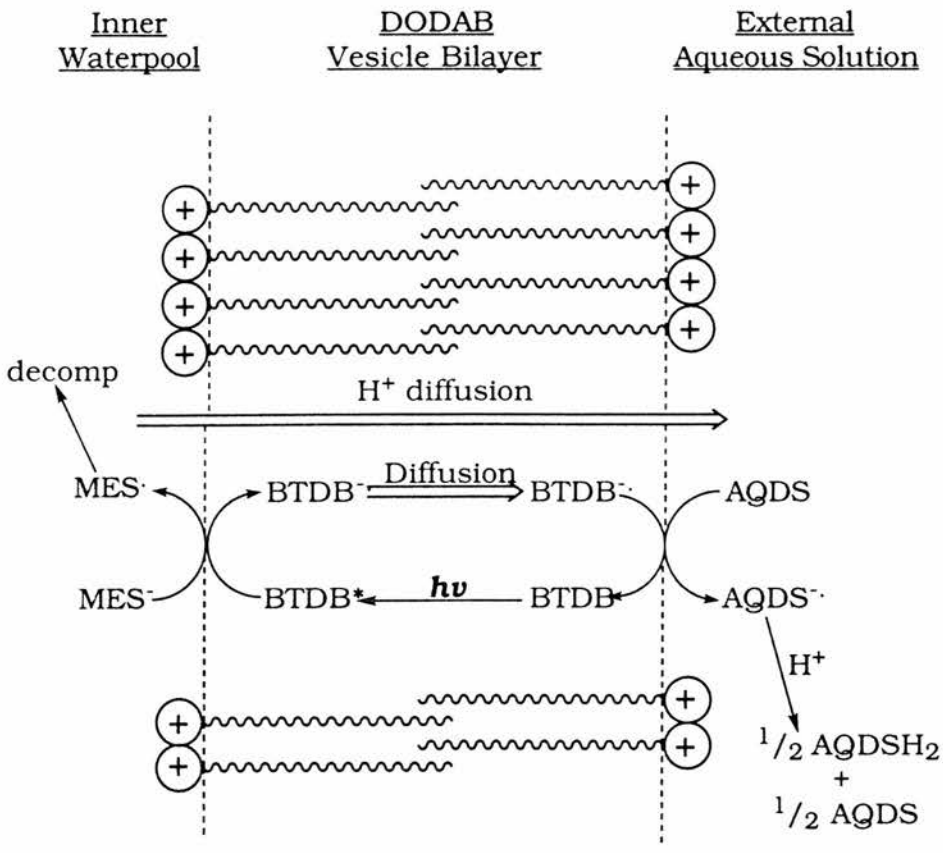

Figure 4.13 : Mechanistic process occuring in DODAB for the reduction of AQDS to $AQDSH_2$.

4.5 Attempted Photochemical Generation of $BTDB^{-\cdot}$

The first method employed in attempting to generate $BTDB^{-\cdot}$ involved photolysis and was achieved by omitting AQDS from the reaction described above. Upon photolysing the BTDB in the presence of DODAB and MES, under an argon blanket, a green/yellow colouration appeared with an absorption maximum at 400 nm. There was a corresponding reduction in the intensity of BTDB at 320 nm. When repeated in air the colouration appeared again but slower than under an inert atmosphere. This result was identical to that achieved upon photolysing BTDB within a micellar system (Section 2.7) and attempts to isolate the unknown species or to identify it by n.m.r. spectroscopy were again thwarted by the low concentration of BTDB in solution.

4.6 Preparation of Hydrogen Evolving Catalysts

4.6.1 Introduction

To attempt to couple the transbilayer electron transfer to hydrogen production, hydrogen activating catalysts such as the platinum group metals[10] or hydrogenase were used.[11-13] Hydrogenases are the most appropriate since they have a specific activity and the resources for their production are practically unlimited. However, low stability of these enzymes as compared with a chemical catalyst prevents wider application.

4.6.2 Metal Catalysts[14]

Colloidal systems have received special attention because in addition to providing extremely high surface area catalysts, they enable a quantitative study of the efficiency of the photoredox and catalytic steps. The most commonly used are colloidal platinum solutions prepared *via* the chemical reduction of Pt(IV) or (VI) salts with citrate, hydrazine or $NaBH_4$. Excess reductant and ions are removed via dialysis or ion exchange resin. The naked Pt^0 sols are protected against flocculation/coagulation by using inorganic or organic polymers such as carbowax or polyvinylalcohol. Platinum sols protected with carbowax are more stable and active than those protected with PVA. Alternatively, they can be deposited on solid supports, for example, semiconductor oxide dispersions such as TiO_2 or zeolites or protected by surfactant molecules.

4.6.3 Determination of Platinum content and Particle size

The method of preparation and stabilisation of the colloidal platinum catalyst was based on the procedure by Gratzel *et al.*[15-17] and the resulting colloids were found to be comparable (Section 6.7.3). The platinum content was determined by atomic absorption spectroscopy and gave a value of 2.5 mg Pt per 25 cm^3 (5.1×10^{-4} M). The size of the platinum particles was determined by transmission electron spectroscopy (TEM) and showed that the platinum particles were 30 — 60 Å in diameter.

4.6.4 Hydrogenase

Hydrogenases are members of a class of iron-sulfur enzymes found in a variety of bacterial species (aerobic, anaerobic and facultative) and some eukaryotic algal species. The possession of iron-sulfur centres is a universal feature of hydrogenases but there is a great diversity in molecular composition, electron carrier specificity, sensitivity to oxygen and cellular localisation.[11-13]

Hydrogenases (oxidoreductases) catalyse the production or consumption of hydrogen gas in bacteria according to the equation;

$$2H^+ \longrightarrow H_2 + 2e^-$$

Hydrogen production provides a means whereby an organism can dispose of excess reductant (i.e. excess electrons) in the absence of suitable electron acceptors other than protons e.g. some fermentative, anaerobic bacteria produce hydrogen via hydrogenase in order to oxidise electron carriers that have been reduced during fermentation. This allows the carriers to be recycled so that a continuous supply of ATP can be generated.

A second division are those that are bound to a membrane and those that are not with the former being difficult to purify. A third division covers those with and without nickel. The role of nickel varies depending on the function of the hydrogenase, but in general the nickel appears to confer greater stability against oxygen compared with those containing only iron-sulfur clusters. It is accepted that the nickel centre represents the hydrogen binding and activating site. Non-nickel containing hydrogenases have a specialised iron-sulfur cluster which acts as the hydrogen binding site. Oxygen rapidly inactivates hydrogenases (in the cell free state) but the nickel protein may be activated again by exposure to strong reductants.[18]

The enzymes being employed for these studies are *Desulfovibrio Desulfuricans* (Norway strain) (Fe)[19-21] and *Desufovibrio Gigas* (Ni)[22-24] and appear to exist in three different states. In addition to the catalytically active form (active state) there exists two catalytically inactive states termed the ready and the unready states. These

two inactive states were discovered when the effects of different reductants upon activation of deactivated hydrogenase were studied.[22]

4.6.5 Protein Determination

Determining the grammes of protein per cm^3 of enzyme was achieved using the Bradford assay with bovine serum albumin as standard,[25,26] (Section 6.5.2). From the absorbance of the standards employed, we were able to plot a standard curve shown in figure 4.14, below.

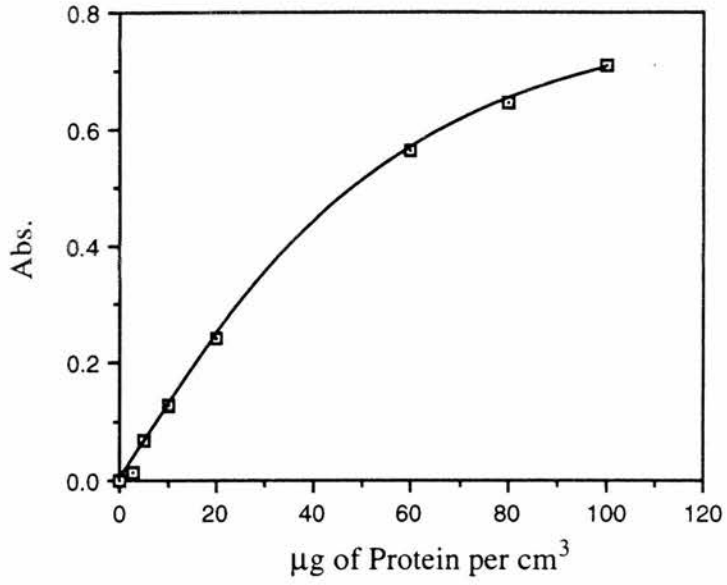

Figure 4.14 : Coomassie standard curve for determination of grammes of protein per cm^3 of enzyme.

From this graph we were able to determine the grams of protein for each batch of enzyme (Section 6.6.1). The concentration of the enzyme was determined using the Beer-Lambert Law ($\varepsilon = 46000$)[23] see section 6.6.1 (iii). Subsequently, the activity of the enzyme could be determined using the hydrogen uptake assay.[28,27] The results of these tests are presented in table 4.1. Studies, by Tagi *et al.*[28] have shown that the ratio of the rate of hydrogen evolution to that of hydrogen uptake with methyl viologen as an electron carrier was about 1.5. Since the standard redox potential of methyl

viologen (-0.44 V vs NHE) is slightly more negative than that for H_2—H^+ half cell (-0.42 vs NHE, pH 7), it is reasonable that the rate of hydrogen evolution was slightly higher than that of hydrogen uptake.

Protein	mg of protein per cm^3 of Enzyme	Protein Concentration	Hydrogenase Assay : Hydrogen Uptake (mmol H_2 consumed min^{-1} mg $protein^{-1}$)
Batch 1 - D. Gigas	3.4	467 µM	3.0
Batch 2 - D. Gigas	3.6	200 µM	4.0
Batch 3 - D. Desulfuricans	40	1.11 mM	6.0
Batch 4 - D. Desulfuricans	35	289 µM	2.9
Batch 5 - D. Desulfuricans	12	533 µM	2.0

Table 4.1 : Showing the quantity, concentration and activity for each of the separate batches of enzyme.

4.6.6 Methyl Viologen Assay[27]

This is a standard assay used to detect changes in the activity of the hydrogenase. In this assay (Section 6.6.1 (iv)), active hydrogenase catalyses the transfer of electrons from hydrogen gas (dissolved in buffer) to MV^{2+}. The MV^{2+} is reduced by a single electron to form $MV^{+\cdot}$ a blue coloured compound which absorbs at 604 nm (ε = 13900).[18]

$MV^{+\cdot}$ is able to reduce ready-state hydrogenase and converts the enzyme to the active state. Therefore, at the start of an assay any active-state molecules of enzyme will reduce MV^{2+} and the $MV^{+\cdot}$ formed will reduce ready-state hydrogenase (not unready state enzyme) to form the active state. So the proportion of hydrogenase in the ready and active states can be measured. The activity determined is shown above in table 4.1.

4.6.7 Use of Buffers for Enzyme/Vesicle System

The use of buffers is essential when employing an isolated enzyme to minimise the possibility of denaturation[29] which results in the loss of enzyme activity, decreased aqueous solubility and increased susceptibility to proteolytic degradation. Denaturation can be brought about by heat and by treatment with reagents such as acid and alkalis, detergents, organic solvents and heavy metal cations. Associated with denaturation is the loss of organised three dimensional structure and the exposure to the aqueous environment of numerous hydrophobic groups normally located within the folded structure. Therefore, a medium with adequate buffer capacity is essential along with clean glassware.

Initial studies involved the formation of vesicles by sonication in buffered solutions at various concentrations >40mM. The buffers employed were, Hepes, Trizma Base, Tris HCl, MOPSO, MOPS, BES, ACES, ADA, TES, acetate and phosphate. The result of these tests was that in each case the vesicle coagulated to form a gel.

Based upon the above results, it was decided to prepare the vesicles in the absence of buffer, (section 6.2.2), and add the buffer solution to the unilamellar vesicles. In practice, the buffer contained the enzyme and MV^{2+} if required. The buffers used previously were tested again but at weaker concentrations (<30 mM) and ACES (25 mM,pH 6) and BES (25mM, pH 7.0) were found not to cause the coagulation of the vesicles. An experiment was performed to confirm that neither ACES nor BES could act as sacrificial electron donors (Section 6.6.1 (iv)).

4.7 Hydrogen Evolution Studies with BTDB

4.7.1 Colloidal Platinum

Coupling of the electron transfer to H_2 evolution in micellar and vesicle environments was not achieved in the presence of colloidal platinum (5.1×10^{-4} M), supported and protected by Carbowax-20M or polyvinylalcohol (PVA, MWt. 14000). In addition experiments were performed where methyl viologen was present acting as an additional

electron relay between $BTDB^{-\cdot}$ and the colloidal platinum. In the micellar solution, the characteristic blue colour appeared for $MV^{+\cdot}$ with an absorbance at 604 nm. Despite the presence of the radical cation, which is widely known in the presence of a suitable catalyst to be virtually 100% efficient in evolving hydrogen from water, no hydrogen was detected by g.c.[16] The presence of $MV^{+\cdot}$ in the micellar solution could have been as a result of a reaction between MV^{2+} and MES^-. However, in the vesicle solution, no $MV^{+\cdot}$ was detected which was probably as a result of the cationic headgroups of the vesicle electrostatically repelling the MV^{2+} and that MES^- does not diffuse through the vesicle bilayer.

The possible reasons behind the failure of the colloidal platinum catalyst to catalyse the evolution of hydrogen are; the particle size was not small enough to maximise mass transport of the electroactive species, ie. the surface area per gram of catalyst employed was not large enough. The concentrations of Carbowax and PVA may have been too large thus inhibiting the access of the electron relay to the active sites and/or increasing the overpotential for hydrogen evolution. Attempts were made to try and eliminate some of these potential problems by varying the concentrations of colloidal platinum and polymeric support but these were also found to be unsuccessful.

Another reason for not observing H_2 production could be the inhibition of the catalytic process by the surfactant, causing the redox potential of methyl viologen being shifted more anodic, as was shown to occur for the chromophores in the presence and absence of CTAB, see section 2.10. We assume that the same effect would be observed in the presence of DODAB. Therefore, the actual redox potential in the CTAB solution for methyl viologen may not be sufficiently cathodic for hydrogen evolution.

Studies were also performed without the presence of CTAB or DODAB and as before, the evolution of hydrogen was not detected. This was probably as a result of BTDB complexing to the platinum. Benzothiadiazoles are known to complex strongly to metals[30], possibly through the sulfur, explaining the lack of activity. The characteristic blue colour of $MV^{+\cdot}$ was produced and so it is the onward electron

transfer to H^+ that is being inhibited in this system.

4.7.2 Hydrogenase from *D. Desulfuricans* and *D. Gigas*

The hydrogen evolution experiments involving the enzyme hydrogenase from *D. Desulfuricans* and *D. Gigas* were only performed in the DODAB system (Section 6.6.2). As with the studies involving colloidal platinum, the coupling of the electron transfer across the vesicle bilayer with the reduction of water and the subsequent generation of hydrogen was unsuccessful. Previous studies[31-33] have shown that electron carriers of methyl viologen or cytochrome c_3[34,35] are essential in the ability of hydrogenase to catalyse hydrogen evolution and if either are omitted from the solution then hydrogen was not produced. Therefore, if the methyl viologen was unable to be reduced by $BTDB^{-\cdot}$ because it was electrostatically repelled by the cationic headgroups of the vesicle, or because the redox potential had become less cathodic, then methyl viologen could not act as a relay and the enzyme would be rendered inoperative. The experiments were not operated at the ideal temperature 30°C because at that temperature the DODAB vesicles undergo phase transitions (Section 3.4) which may affect their ability to retain MES^- within the inner waterpool.

4.7.3 Future Work

The problems experienced with the hydrogen evolution studies may be overcome if for example, propylsulfonate-viologen (PVS) was employed as the electron relay between $BTDB^{-\cdot}$ and the catalyst, as PVS is neutral in the oxidised form and negatively charged in the reduced form. Therefore, it will be easier for $BTDB^{-\cdot}$ to transfer the electron to PVS which will not be electrostatically repelled like MV^{2+}. Instead of employing a viologen as the electron relay between chromophore and catalyst, cytochrome c_3 could be used. Also, we could employ a non-ionic surfactant micelle or vesicle, in which to perform vectorial electron transfer which would allow the continued use of the known systems used above. Another alternative would be to replace the thiadiazole ring for a furazan ring on the chromophore because without the presence of sulfur the

chromophore would not complex with and deactivate the platinum catalyst.

A possible reaction scheme for the photo-production of hydrogen from water is shown in figure 4.15.

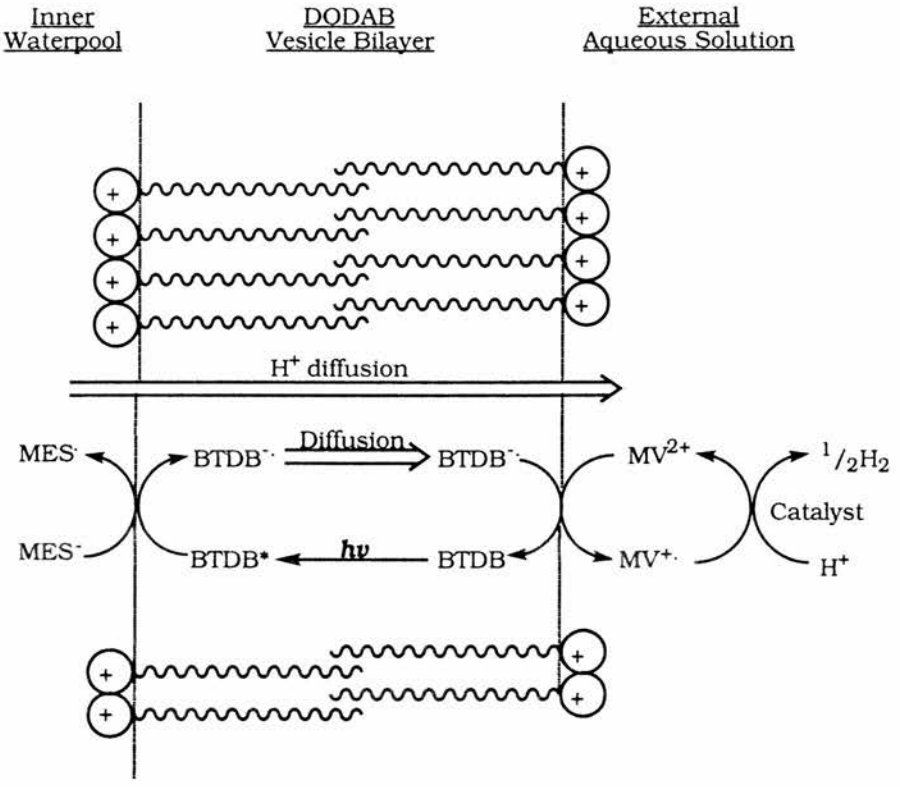

Figure 4.15 : Possible reaction scheme for the photo-production of hydrogen from water.

References

1. J.N. Robinson, D.J. Cole-Hamilton, M.K. Whittlesey and P. Camilleri, *J. Chem. Soc. Faraday Trans.*, 1990, **86**, 2897.
2. L.Y.-C. Lee and J.K. Hurst, *J. Am. Chem. Soc.*, 1984, **106**, 7411.
3. D. Papahadjopoulos, K. Jacobson, S. Nir and T. Issac, *Biochim. Biophys. Acta*, 1975, **311**, 330.
4. R.D. Ricke and S.E. Bales, *J. Am. Chem. Soc.*, 1974, **96**, 1775.
5. C.D. Tran, P.L. Klaki, A. Romero and J.H. Fendler, *J. Am. Chem. Soc.*, 1978, **100**, 1622.
6. M. Takeishi, M. Nakatsugawa and M. Kikuchi, *Die. Angew. Makromol. Chem.*, 1993, **204**, 73.
7. S.S. Anderson, I.G. Lyle and R. Peterson, *Nature (London)*, 1976, **259**, 147.
8. J.J. Grimaldi, S. Boileau and J.M. Lehn, *Nature (London)*, 1977, **265**, 229.
9. M.I. Montenegro et al. (eds), *'Microelectrode: Theory and Applications'* Kluwer Academic, Netherlands, 1991.
10. A. Mills, *Stud. Inorg. Chem.*, 1991, 302 and refs therein.
11. R. Cammack, D.O. Hall and K. Krishna Rao, *Microbial Gas Metabolism:Mechanistic, Metabolic and Biotechnological Aspects*, 1985, Chp.4, p. 75.
12. M.W.W. Adams, L.E. Mortensen and J.-S. Chen, *Biochim. Biophys. Acta.*,5 1981, **594**, 105 and refs. therein.
13. M.W.W. Adams, *Biochim. Biophys. Acta.*, 1990, **1020**, 115 and refs. therein.
14. D.J. Cole-Hamilton and D.W. Bruce,*'Comprehensive Coordination Chemistry'*, G.Wilkinson, R.D.Gillard and J. A. McCleverty Eds., Pergamon Oxford, 1987, vol. 6, p. 487 and refs. therein.
15. J. Kiwi and M. Gratzel, *Nature (London)*, 1979, **281**, 657.
16. E. Borgarello, J. Kiwi, E. Pelizzetti, M. Visca and M. Gratzel, *Nature (London)*, 1981, **289**, 158.
17. P.-A. Brugger, P. Cuendet and M. Gratzel, *J. Am. Chem. Soc.*, 1981, **103**, 2923.
18. R. Cammack, V.M. Fernandez and E.C. Hatchikan, *Methods in Enzymology*, 1994, **243**, 43.
19. E.C. Hatchikan, N. Forget, V.M. Fernandez, R. Williams and R. Cammack, *Eur. J. Biochem.*, 1992, **209**, 357.
20. R. Rieder, R. Cammack and D.O. Hall, *Eur. J. Biochem.*, 1984, **145**, 637.

21. L.H. Eng, M.B.-M. Lewin and H.Y. Neujahr, *J. Chem. Tech. Biotechnol.*, 1993, **56**, 317.
22. V.M. Fernandez, E.C. Hatchikan and R. Cammack, *Biochim. Biophys. Acta.*, 1985, **832**, 69.
23. E.C. Hatchikan, M. Bruschi and J. Le Gall, *Biochem. Biophys. Res. Commun.*, 1978, **82**, 451.
24. S. Pulvin and C. Bourdillon, *Enzyme Microb. Technol.*, 1986, **8**, 137.
25. M.M. Bradford, *Anal. Biochem.*, 1976, **72**, 248.
26. O.H. Lowy, N.J. Roserough, A.L. Farr and R.J. Randall, *J. Biol. Chem.*, 1951, **193**, 265.
27. E.C. Hatchikan, A.S. Traore, V.M. Fernandez and R. Cammack, *Biochim. Biophys. Acta.*, 1985, **832**, 69.
28. T. Yagi, A. Endo and K. Tsuji, *'Hydrogenases: Their Catalytic Activity, Structure and Function'*, E. Goltze and K.G. Gottingen (Eds.) 1978, p.109.
29. K. Wilson and K.H. Goulding (Eds), *'A Biologists Guide to priciples and Techniques of Practical Biochemistry'*, 3rd. Edition, 1989.
30. V.G. Pesin, *Russ. Chem. Rev.*, 1970, **39**, 923 and refs. therein.
31. I. Okura, *J. Mol. Catal.*, 1979, **6**, 227.
32. I. Okura, *Coord. Chem. Revs.*, 1985, **68**, 53.
33. I. Okura, S. Kusonki, N. Kim-Thuan nd M. Kobayashi, *J. Chem. Soc., Chem. Commun.*, 1981, 56.
33. T. Kamachi, T. Hiraishi and I. Okura, *Chem. Lett.*, 1995, 33.
35. M.W.W. Adams, L.E. Mortenson and J.S. Chen, *Biochim. Biophys. Acta.*, 1981, **594**, 105.

Chapter 5

Studies of Benzofurazan-4,7-dicarbonitrile (BFDN) in a Micelle and Vesicle System

5.0 Introduction

It is known that benzothiadiazoles can complex to metals through the sulfur atom of the heterocyclic ring[1] and hence may poison, for example, the colloidal platinum catalyst intended to be used for hydrogen evolution. Therefore, we proposed that by employing key substituted benzofurazans as chromphores/electron mediators, it should be possible to eliminate the possibility of poisoning the catalyst. The reason being, that benzofurazans possess an oxygen atom within the heterocylic ring and this should complex much less strongly to the platinum catalyst. We have synthesised the dicarbonitrile species of benzofurazan (BFDN) which allowed direct comparisons to be made with the dicarbonitrile species of 2,1,3-benzothiadiazole (BTDN).

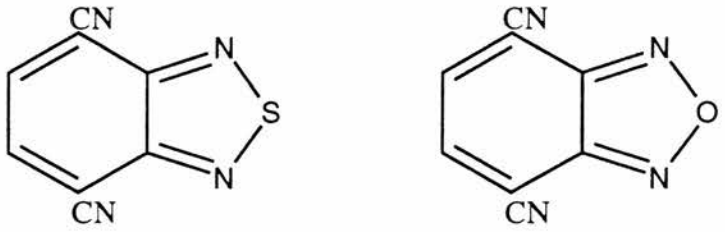

BTDN BFDN

Figure 5.1 : Structures of 2,1,3-benzothiadiazole-4,7-dicarbonitrile (BTDN) and benzofurazan-4,7-dicarbonitrile (BFDN).

5.1 Synthesis of BFDN

5.1.1 Method 1[2-5]

The initial stage was the double nitration of 1,4-dibromobenzene in the 2,3 position. This proved difficult as those positions were the least favoured on which to perform a double nitration due to steric hinderance caused by the bromine atoms but nitration at the 2,6 and 2,5 positions was more favourable. The final product contained three different isomers which required separation and individual identification and was

achieved by recrystallising the isomers from glacial acetic acid and by using n.m.r. and g.c.m.s. The empirical equation $\delta_H = 7.27 + \Sigma z_i$ was employed,[6] for estimation of the proton chemical shifts in substituted benzenes for all three isomers. Σz_i is the sum of the chemical shift values of the substituents and δ_H is the final proton shift value. The calculated chemical shift values do not accurately match the observed values but the differences between them are similar, see table 1 below.

Compound	2,3-dinitro	2,5-dinitro	2,6-dinitro
Calculated ^{1}H Shift value	8.01	8.58	8.7
Observed ^{1}H Shift value	7.7	8.03	8.17

Table 5.1 : Calculated and Observed ^{1}H n.m.r. Chemical shifts for 1,4-dibromo-2,3-dinitrobenzene.

The n.m.r. in figure 5.2, was from a sample obtained after only one recrystallisation. This shows the predominance of the desired 2,3 dinitro substituted compound (resonance at 7.7 p.p.m.) and corresponded to the major peak on the g.c. trace.

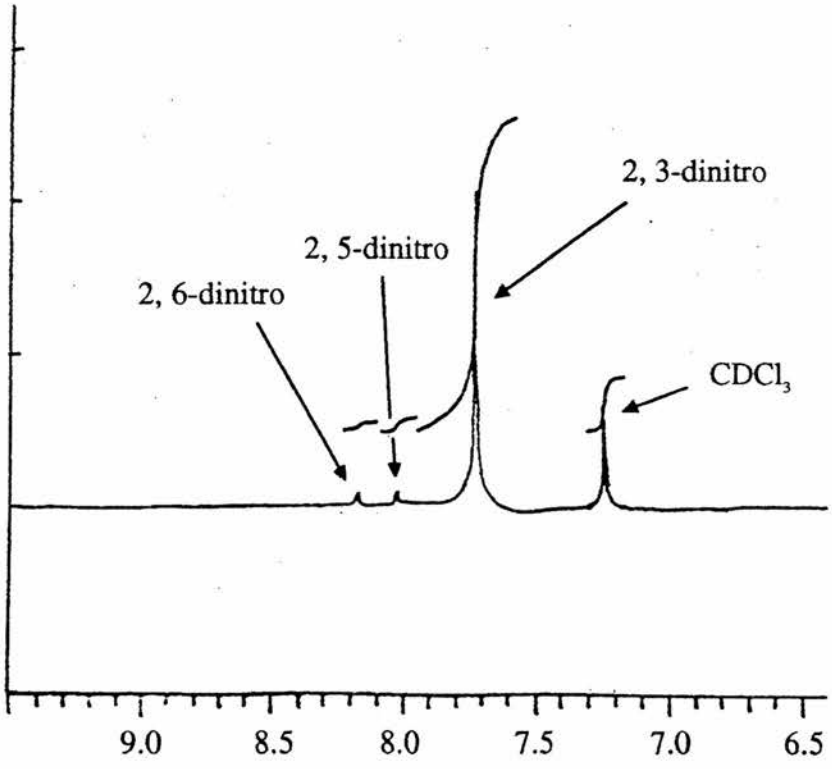

Figure 5.2 : ^{1}H n.m.r. spectrum of the 3 isomers of dibromodinitrobenzene.

The next stage was the formation of 3,6-dibromo-2-nitroaniline by refluxing a solution of 2,3 dinitrobenzene in ethanol while ammonia gas was bubbled through the solution for three hours. This procedure was repeated on the same solution after being held at room temperature for 48 hours and no experimental difficulties were observed. The following step involved the preparation of the azide by the diazotization of the nitroamine. The mass spectrum of the azide indicated that dinitrogen was lost first to give the base peak.

Ring closure was obtained by the thermal decomposition of the o-nitroazide to produce 4,7-dibromobenzofurazan oxide. According to g.c.m.s. analysis, this stage was successful but purification of the oxide was required before proceeding to the last two stages. Purification was achieved using dry column chromatography in toluene-n-hexane (1:1 v/v) on alumina, following evaporation, the product was obtained as yellow prisms.

The penultimate stage, was the reduction of the furazan oxide with hydroxylamine hydrochloride and potassium hydroxide, followed by steam distillation of the alkaline solution. This gave a yellow solution from which 4,7-dibromobenzofurazan was extracted along with some impurities. It was purified by recrystallisation from petroleum ether 40/60:ethyl acetate (3:1 v/v).

The final reaction, was the replacement of the bromine atoms for nitrile groups using cuprous cyanide in dimethyl formamide[5] at elevated temperatures for 1.5 hours to yield the 4,7-benzofurazandicarbonitrile in moderate yield. Purification of the compound was achieved by recrystallising from petroleum ether 40/60. Figure 5.3 presents, the overall reaction scheme for the above preparation of BFDN.

However, due to the length of time required and the low yield of BFDN produced by this method we began to investigate other potential routes. The most successful alternative was *via* tetrabromotetrahydrobenzofurazan and this method for the preparation of BFDN is described in the following section.

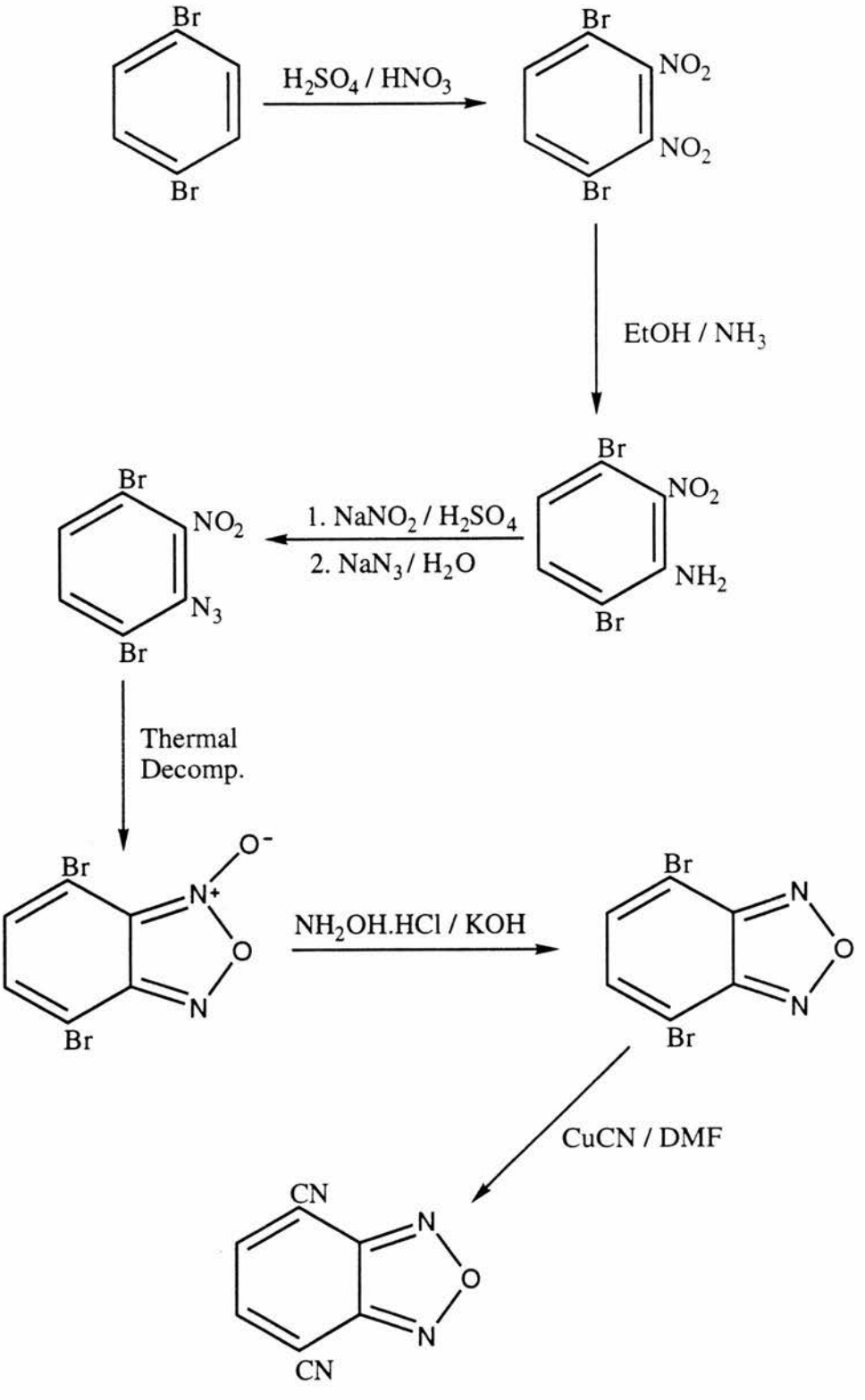

Figure 5.3 : Formation of 4,7-benzofurazandicarbonitrile from 1,4-dibromobenzene (Method 1).

5.2.2 Method 2[5,7]

The first stage involved the formation of tetrabromotetrahydrobenzofurazan oxide by a free radical addition of bromine to benzofurazan oxide. This was followed by the removal of two molecules of hydrogen bromide to form dibromobenzofurazan oxide. The final two stages were exactly the same as steps 5 and 6 of method one (see 6.12.5). For an overall reaction scheme of method two, see figure 5.4. This method took less time and allowed the reaction to be scaled up to practical and manageable quantities of reactants.

BFDN was fully characterised by g.c.m.s., accurate mass analysis, elemental analysis and ^{1}H and ^{13}C n.m.r. spectroscopy. Figure 5.5 shows the mass spectrum for BFDN with a molecular ion peak with an m/e value of 170, as expected and figure 5.6 shows the ^{13}C n.m.r. spectrum.

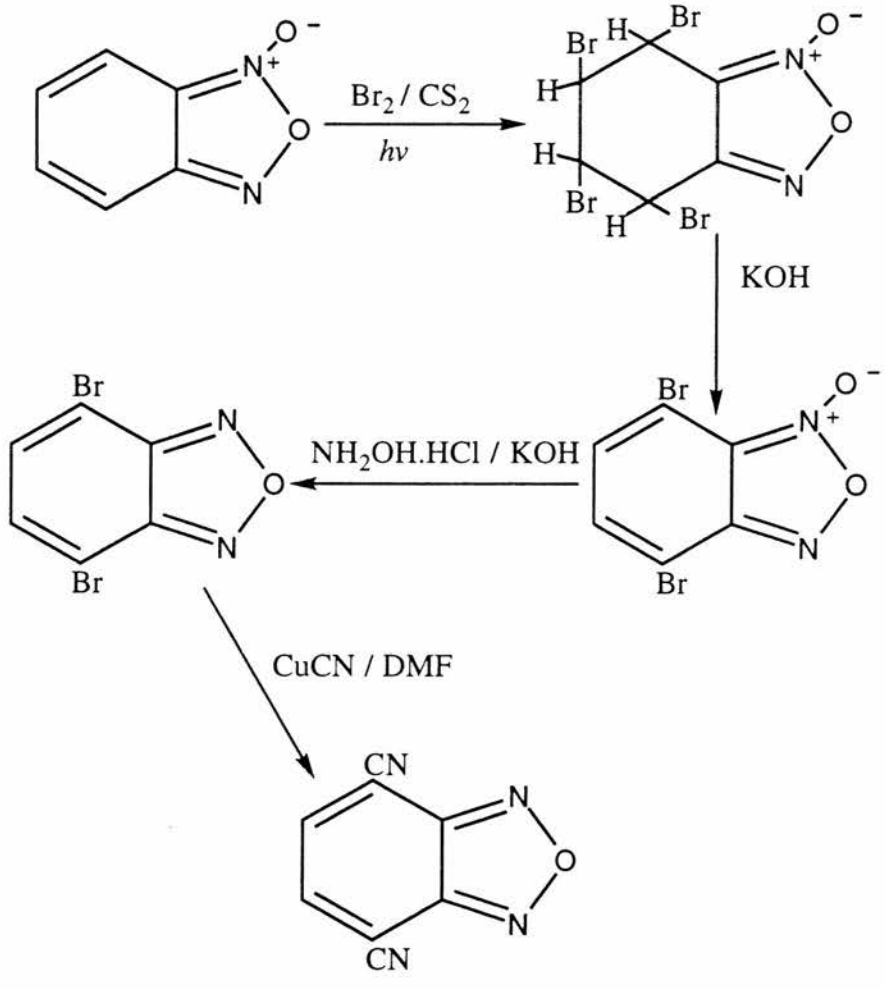

Figure 5.4 : Formation of benzofurazan-4,7-dicarbonitrile by method 2.

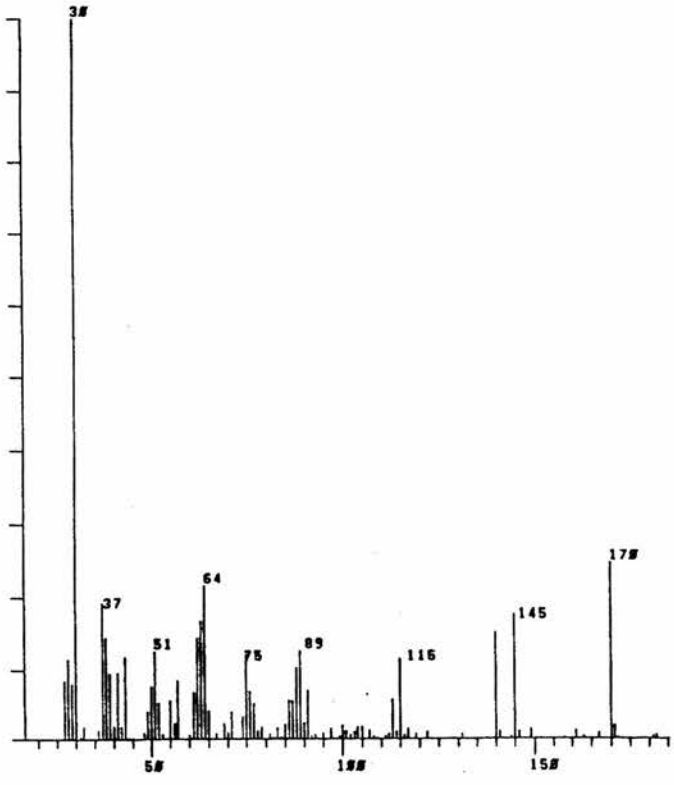

Figure 5.5 : Mass Spectrum of BFDN.

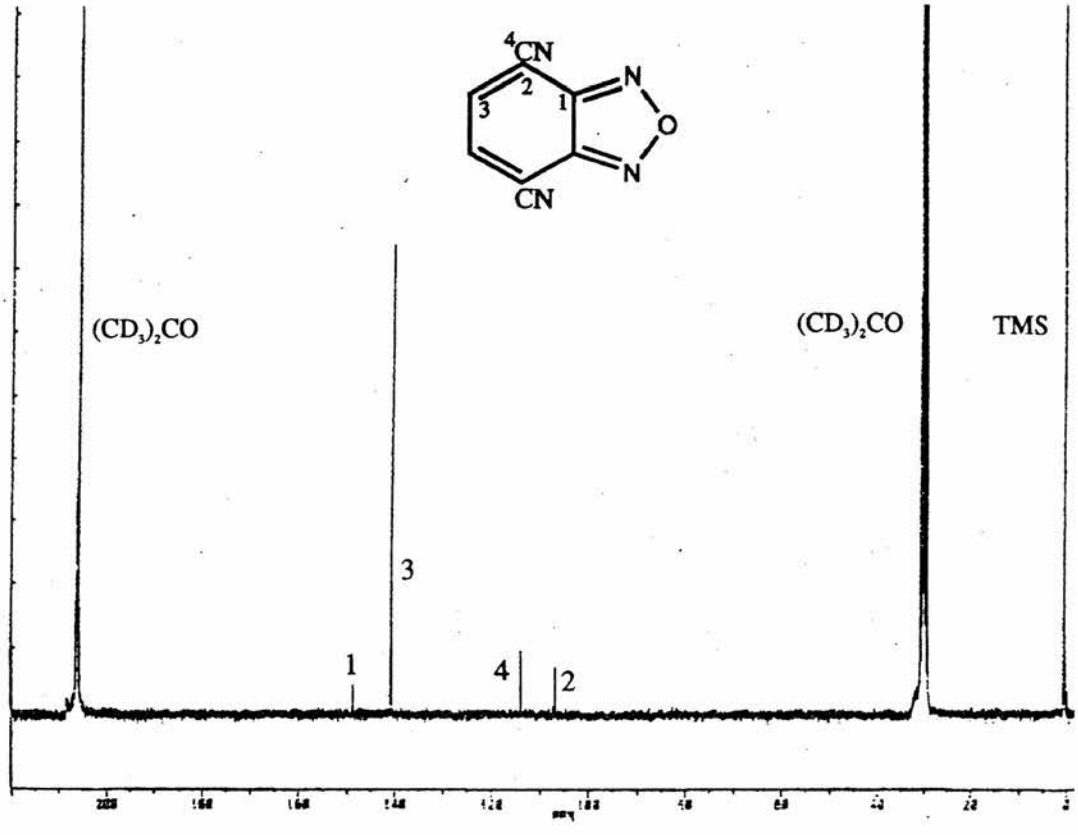

Figure 5.6 : ^{13}C n.m.r. spectrum of BFDN in $(CD_3)_2CO$.

5.2 Photolysis Studies in a Micellar and Vesicle Environment

These studies were concerned with investigating the efficiency of $BFDN^{-\cdot}$ as a combined chromophore and electron transfer agent (Section 6.2.1 (i) and 6.2.2 (iii)) and a comparison of its performance with that of BTDN. As with BTDB, we were interested in determining whether BFDN was capable of enhancing the reduction of AQDS to $AQDSH_2$. Therefore, continuous photolysis was performed and the results are presented in figure 5.7;

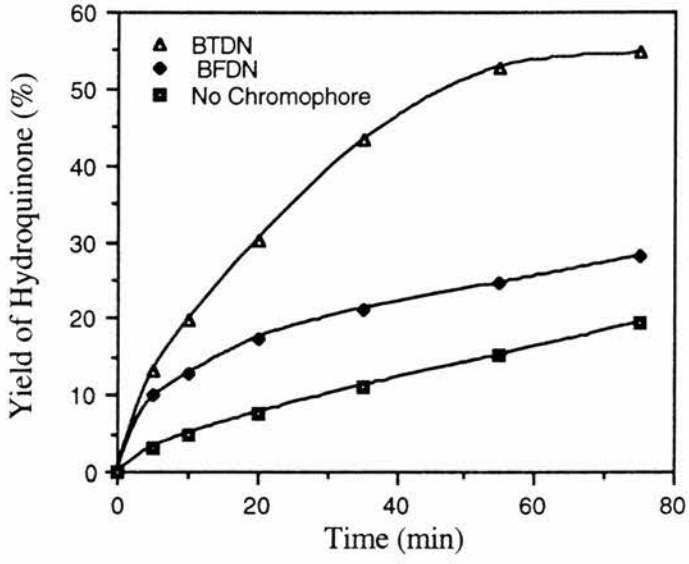

Figure 5.7 : Production of $AQDSH_2$ in CTAB, with MES in the presence and absence of BFDN & BTDN at pH 6.5.

Figure 5.7 shows, that it is possible to achieve enhanced electron transfer from MES^- to AQDS in a micellar system with the benzofurazan species but that its efficiency is well below that of BTDN.

A possible explanation for the lower yield of $AQDSH_2$ using BFDN may be that some competing reaction was occuring, since an unidentified species was observed by u.v.-visible spectroscopy while monitoring the growth of $AQDSH_2$ after only 5 minutes. In contrast, when BTDN was employed the growth of another species occured after 55 minutes and from the u.v.-visible spectrum it was concluded to be the stable radical anion, $BTDN^{-\cdot}$.

Studies in the DODAB environment were unsuccessful as we observed the presence of an unknown product, which we recorded on the initial u.v.-visible spectrum, with a peak at 440 nm and upon photolysis, no $AQDSH_2$ was produced.

5.3 U.V.-Visible Spectroscopy

Upon investigating the light absorbing properties of BFDN in comparison with those of BTDN, we discovered that, BFDN had a much lower extinction cofficient than BTDN (Table 5.2, Figure 5.8).

Therefore, from these results we can conclude that fewer quanta of light can be absorbed by BFDN than by BTDN so that less energy can be transferred in a given time.

Chromophore	$\varepsilon_{325}/10^4 dm^3 mol^{-1} cm^{-1}$	$\varepsilon_{400}/10^4 dm^3 mol^{-1} cm^{-1}$
BTDN	1.8	0.02
BFDN	0.9	0

Table 5.2 : Extinction coefficients for BFDN and BTDN at 325 and 400 nm.

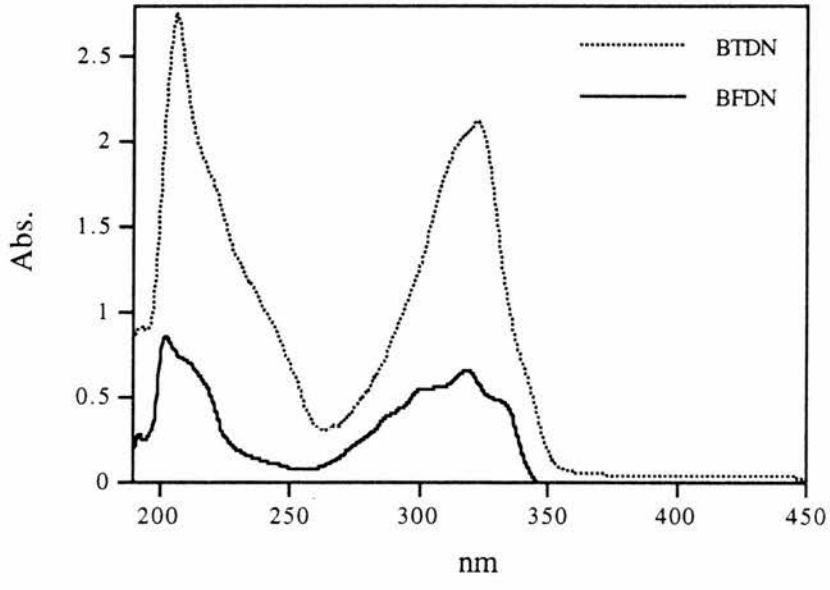

Figure 5.8 : U.v.-visible spectrums of BFDN and BTDN.

5.3 Partition Coefficient

These studies provided an indication of the environment in which the majority of the chromophore was located during photolysis experiments in the micellar and vesicle systems. The results obtained showed that BFDN has a lower partition coefficient than BTDN, the values obtained were 3 and 9, respectively. This shows that BFDN will be found predominately, as in the case of BTDN, in the bulk aqueous environment to a greater degree than BTDN. Having such a low partition coefficient may make it extremely difficult for $BFDN^{-\cdot}$ to be taken up and stabilised by the micelles.

5.4 Attempted Photochemical Generation of $BFDN^{-\cdot}$

Having shown that BFDN can act as an electron transfer agent, we attempted to generate $BFDN^{-\cdot}$ by photolysis, simply omitting AQDS from the reaction mixture. The experiment was performed in the presence of CTAB and MES^- in a buffered aqueous solution (pH 6.5) under a blanket of nitrogen. Upon photolysis a blue colouration appeared as a function of the period of photolysis with absorption maximum at 385 and 590 nm and upon the addition of air the colouration remained. The u.v.-visible spectrum obtained for the unidentified species (blue colouration) is shown in figure 5.9. Figure 5.9 shows the u.v.-visible spectrum obtained upon photolysing a solution of BTDB and BFDN in the presence of CTAB and MES^- at pH 6.5. The peaks produced below 350 nm, for both species, correspond to unreacted BTDB and BFDN, respectvely. The spectrum for BTDN has been determined as that of the radical anion.[8] The compound that produced the spectrum for the BFDN has not been identified.

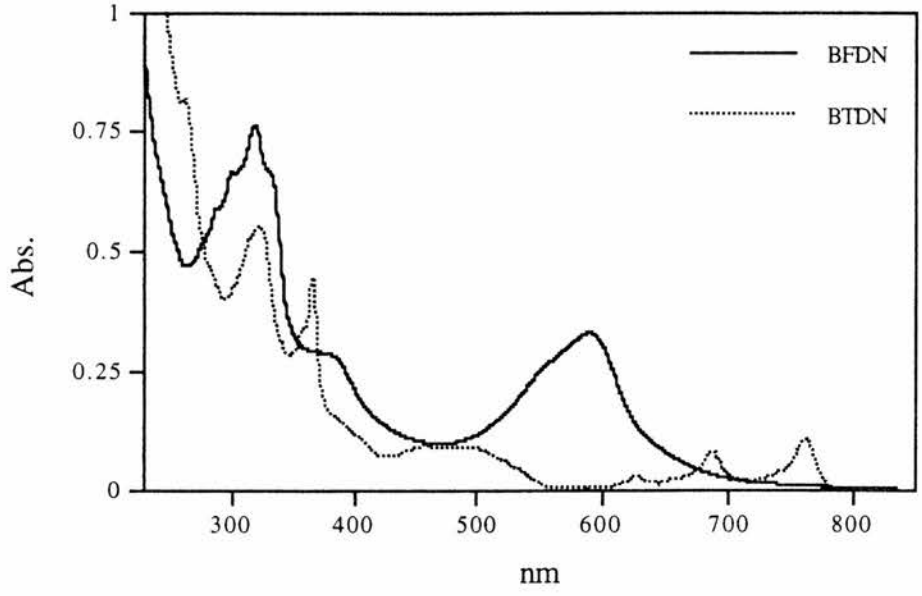

Figure 5.9 : U.v.-visible spectrum produced for BTDN and BFDN while attempting to generate the radical anion.

5.5 Cyclic Voltammetry Studies

5.5.1 Aqueous and Micellar System

These studies were concerned with observing the effect, if any, the replacement of a sulfur atom with an oxygen atom had on the redox couples and the electrochemical processes of BFDN. All peak positions were referenced against a saturated calomel electrode (+241.5 mV vs NHE) and by using the Hickling equation,[9] we determined that the process involved one electron transfer.

We were also interested in studying the effect that CTAB had on the redox couples, in the case of BFDN, and based on the partition coefficient, there may be little or no change in the peak positions. Initial studies were performed in an acetate buffered solution (0.14 M, pH 6.5) without the presence of CTAB (Section 6.4 (v)), while subsequent studies were performed in the presence of CTAB (0.8% w/w). The results of these studies are presented in tables 5.3 and 5.4, respectively.

	Redox Couple (1)		Redox Couple (2)	
Chromophore	$E^{C}_{p_1}$ (mV)	$E^{A}_{p_1}$ (mV)	$E^{C}_{p_2}$ (mV)	$E^{A}_{p_2}$ (mV)
BTDN	-752	-669	-1097	No Peak Observed
BFDN	-570	-469	-947	No Peak Observed

Table 5.3 : Showing the peak positons for BTDN and BFDN in acetate buffer solution (pH 6.5, 0.14 M) recorded against SCE (+241.5 mV v NHE) at 100 mVs^{-1} using a glassy carbon working electrode (3 mm diameter).

	Redox Couple (1)		Redox Couple (2)	
Chromophore	$E^{C}_{p_1}$ (mV)	$E^{A}_{p_1}$ (mV)	$E^{C}_{p_2}$ (mV)	$E^{A}_{p_2}$ (mV)
BTDN	-569	-475	-884	-794
BFDN	-430	-329	-822	-685

Table 5.4 : Showing the peak positons for BTDN and BFDN in the presence of CTAB (0.8% w/w) at pH 6.5, recorded against SCE (+241.5 mV v NHE) at 100 mVs^{-1} using a glassy carbon working electrode (3 mm diameter).

The results obtained from the studies in the absence of CTAB (Table 5.3) show that BFDN is more readily reduced than BTDN. The first redox couple of BFDN showed that much of the reduction product was lost through an ec mechanism before re-oxidation occured. The same was true of the first redox couple of BTDN. The second redox couple showed similar behaviour to that of BTDN, in being irreversible. The possible reactions that BFDN was undergoing in an aqueous environment are shown in figure 5.9:

$$BFDN + 1e^- \rightleftharpoons BFDN^{-\cdot}$$

$$BFDN^{-\cdot} \longrightarrow \text{Unknown Product}$$

$$BFDN^{-\cdot} + 1e^- \rightleftharpoons BFDN^{2-}$$

$$BFDN^{2-} \longrightarrow \text{Unknown Product}$$

Figure 5.9 : Reaction scheme for BFDN in an aqueous environment during cyclic voltammetry studies.

Upon the addition of CTAB (0.8% w/w) we observed that the peak position values have shifted anodically compared with the potentials obtained in the absence of CTAB. However, the potentials obtained when studying BFDN have shifted less positively than those of BTDN. This may be a further indication of the more hydrophilic nature of BFDN because the benefit of CTAB in the case of BTDB (hydrophobic), was that the surfactant may have introduced BTDB to the electrode through solubilisation within the micelle and/or by reducing the hydrophilic nature of the surface of the electrode thus reducing the overpotential required to reduce BTDB. An interesting observation is the existence of an anodic wave for the second redox couple for both BTDN and BFDN (Figure 5.11) which is probably a result of $BTDN^{-\cdot}$ solubilisation within the micelle[8] where the radical anion is stabilised thus allowing the species to be electrochemically reduced (Figure 5.10). From the similar structural characteristics of BFDN and BTDN (discussed later) we would assume that BFDN behaves in a similar manner. Further evidence of the similar behaviour, is that both species appear to undergo chemical reactions, possibly through protonation but BFDN appears to be more reactive than BTDN.

$$BFDN + 1e^- \rightleftharpoons BFDN^{-\cdot}$$

$$BFDN^{-\cdot} \longrightarrow \text{Unknown Product}$$

$$BFDN^{-\cdot} + \text{micelle} \rightleftharpoons BFDN^{2-}.\text{micelle}$$

$$BFDN^{2-}.\text{micelle} \longrightarrow \text{Unknown Product}$$

Figure 5.10 : Reaction scheme for BFDN during cyclic voltammetry studies in a micellar environment.

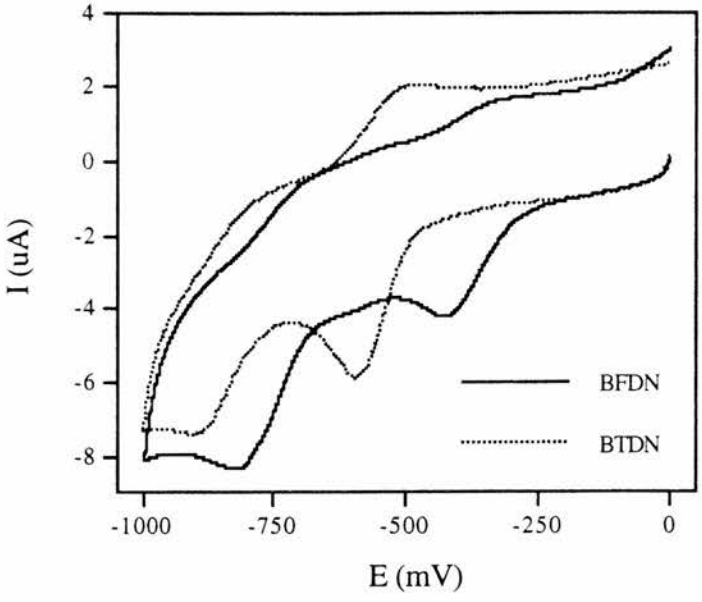

Figure 5.11 : Cyclic voltammogram of an aqueous buffered solution (pH 6.5) of BFDN and BTDN in the presence of CTAB (0.8% w/w) referenced to SCE (241.5 mV vs NHE) at 100 mVs^{-1}.

5.5.2 Non-Aqueous System

Acetonitrile was employed as the solvent which allowed an extended potential window to be employed for studying the cyclic voltammograms of BTDB and BFDN. All peak positions were referenced against a silver/silver chloride (Ag/AgCl) electrode (+222 mV vs NHE) and by using the Hickling equation,[9] we determined that the process involved one electron transfer. The results obtained at a sweep rate of 100 mVs^{-1} are shown in table 5.5 and an example of the cyclic voltrammograms obtained for BFDN in acetonitrile at various sweep rates are presented in figure 5.12.

	Redox Couple (1)		Redox Couple (2)	
Chromophore	$E^{C}_{p_1}$ (mV)	$E^{A}_{p_1}$ (mV)	$E^{C}_{p_2}$ (mV)	$E^{A}_{p_2}$ (mV)
BTDN	-606	-530	-1436	-1352
BFDN	-408	-330	-1296	-1224

Table 5.5 : Showing the peak positons for BTDN and BFDN in acetonitrile, recorded against Ag/AgCl (+222 mV v NHE) at 100 mVs^{-1} using a glassy carbon working electrode (3 mm diameter).

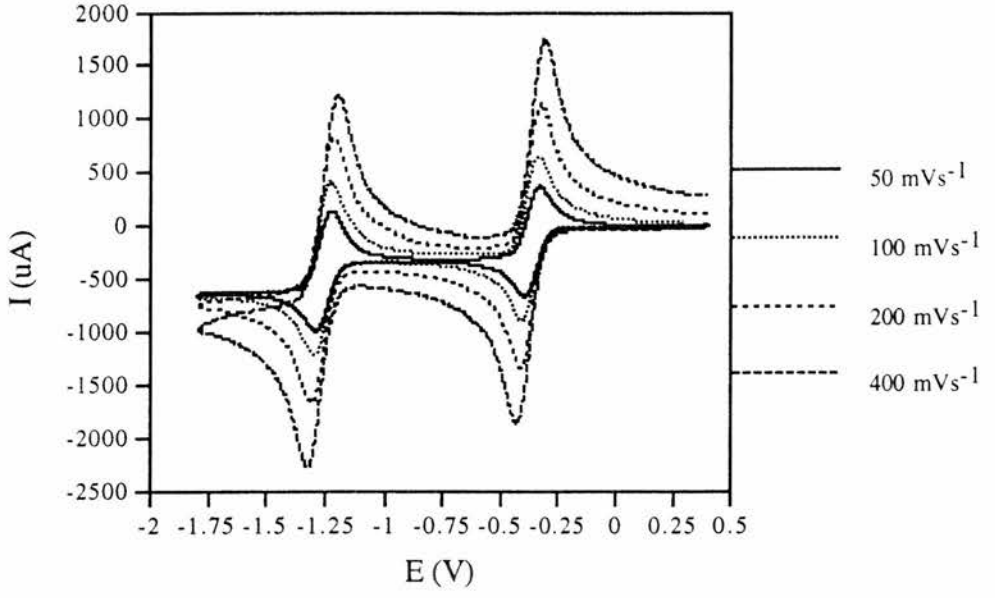

Figure 5.12 : Successive cyclic voltammograms for BFDN in acetonitrile at increasing sweep rates referenced against Ag/AgCl (222 mV vs NHE).

BFDN undergoes chemically reversible and quasi-reversible electrochemical processes where both redox couples show electrochemical reversibility at low sweep rates and increasing the sweep rate, the separation between the peaks begins to increase, indicating quasi-reversibility. A plausible reaction scheme for the electrochemical reactions that BFDN undergoes in a acetonitrile is shown in figure 5.13.

$$BFDN + 1e^- \rightleftharpoons BFDN^{\cdot-} \quad (E_{p1}^C)$$

$$BFDN^{\cdot-} + 1e^- \rightleftharpoons BFDN^{2-} \quad (E_{p2}^C)$$

$$BFDN^{2-} - 1e^- \rightleftharpoons BFDN^{\cdot-} \quad (E_{p2}^A)$$

$$BFDN^{\cdot-} - 1e^- \rightleftharpoons BFDN \quad (E_{p1}^A)$$

Figure 5.13 : Reaction scheme of the redox reactions for BTDB during cyclic voltammetry studies in acetonitrile.

The electrochemical studies show that both BTDN and BFDN undergo the same electrochemical processes with the only significant difference being the potential at which these processes occur. We believe that the difference in the potentials is related to the lower energy LUMO of the BFDN species based on calculations using MNDO,[10] AM1[11] and PM3[12] methods using version 6.0 of the MOPAC[13] system (Section 6.1.20). The results of these calculations are presented in table 5.6.

Method	BTDN (eV)	BFDN (eV)
MNDO	-2.30	-2.38
AM1	-2.23	-2.43
PM3	-2.68	-2.61

Table 5.6 : Energy levels for the LUMO of BTDN and BFDN, calculated by MNDO, AM1 and PM3.

The results presented in table 5.6, show that two of three methods indicate that the LUMO for BFDN is of a lower energy than that of BTDN. The difference between the orbitals as determined by AM1 is very similar to the potential difference achieved experimentally. It was shown that the LUMO was delocalised over the ring and appeared to be concentrated on the N atom.[14] These studies subsequently led onto more calculations to discover if there were any significant structural differences that would affect the abiliity of BFDN to perform as well as BTDN as an electron transfer agent.

5.6 MOPAC Calculations on BFDN and BTDN

There is much debate regarding which canonical form of 2,1,3-benzoxadiazole (benzofurazan) and its sulfur and selenium analogues accurately represents these compounds. The usual representation, by analogy to quinone, is the *ortho*-quinoid form, I (Figure 5.14).

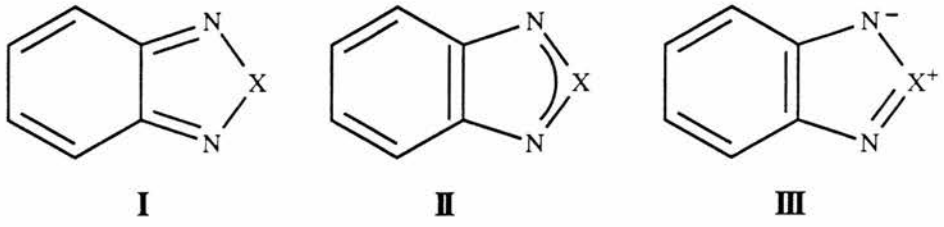

Figure 5.14 : Canonical forms for 2,1,3-benzoxadiazole and its sulfur and selenium analogues (X = O, S, Se).

The relative importance of these structures has been investigated experimentally. If the o-quinoid form predominates, there will be double-bond fixation and diene-like reactivity, otherwise, benzenoid characteristics should be observed. Evidence for both has been found and therefore not one structure fits all the data[15,16] and may be a result of the LUMO being delocalised over the ring which allows these molecules their flexibility to react with either benzenoid or dienoid character.[14]

Previous studies[17] using ^1H n.m.r. have concluded that the sulphur compound has the most benzenoid character because this compound had the smallest difference between the two JHH (ortho) coupling constants. However, dipole measurements (Figure 5.15) indicate that the selenium containing compound has the lowest dipole moment of the series and this has been interpreted as indicating that the selenium and sulfur compounds have the most benzenoid character.[18]

	O	> S	> Se
D	4.37	1.73	0.94

Figure 5.15 : Dipole moments for benzo-oxa/thia/selena-diazole.

On the other hand X-ray measurements[19] indicate that the oxygen compound has the most benezenoid character, whereas ESR studies[20] have indicated that despite the possibility of sulfur and selenium using *d*-orbitals in $d\pi$—$p\pi$ bonding, the *d*-orbitals have relatively little importance in these compounds. ^{13}C n.m.r. spectroscopy measurements[21] demonstrate that the selenium compound is most electron withdrawing towards the 5-membered ring, with sulfur showing a slightly smaller effect but both much larger than oxygen.

In order to try and gain further information regarding the effects of the different heteroatom, we have carried out calculations using 3 methods (MNDO, AM1 and PM3)[10-13] on the neutral species of BTDN and BFDN.

Our results (see Appendix) indicate that the structures have strong bond fixation. There is no evidence for the sulfur species expanding its valence shell using *d*-orbitals in agreement with the ESR and ^{13}C studies on the benzo-oxa/thia/selena-diazoles. The results would suggest a closed πp-system comprising of six electrons to give a quinoid formulation.

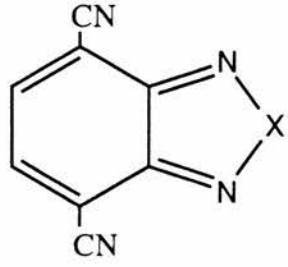

Figure 5.16 : Proposed quinoid structure for benzofurazan and benzothiadiazole species based upon MOPAC calculations (X = O or S)

Calculations were also carried out on the radical anion, also optimised to C_{2v} symmetry, with the unpaired electron in a π-orbital delocalised over the whole bycyclic system. The overall bond orders show significant differences from those in the neutral molecule. In particular, there is extensive delocalisation over all of the bicyclic periphery, except for the bonds to the heteroatom. While the bond orders calculated by the different methods differ in detail (Appendix, Table 1 and 2) the overall conclusions for each of the neutral and anionic molecules and the difference

between them are similar except that the N—S bonds are much more polar than the N—O bonds.

The differences in the bond order for the neutral and anionic molecules of BTDN and BFDN calculated, occur in the bonds denoted **c** and **d** (Appendix, Table 1). These are readily intelligible in terms of the form of the SOMO, a π type orbital which is bonding in **d** and anti-bonding in **c**. It is not possible to give a simple pictorial representation of the electronic structure of the anion but the structure presented in figure 5.17 can all be regarded as contributors. Where **A** will be the major form of the radical anion based upon bond orders and atomic charges of the neutral species.

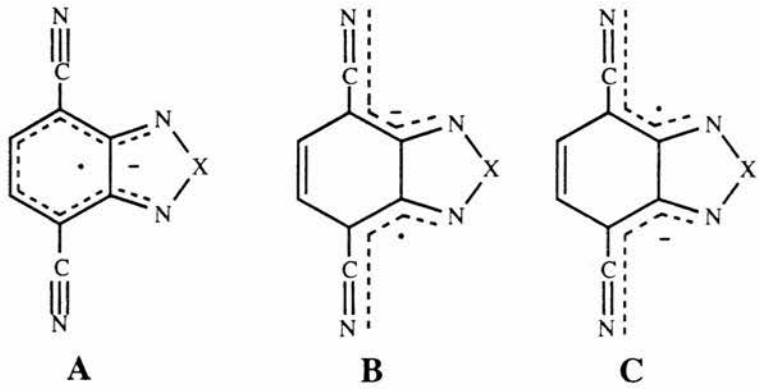

Figure 5.17 : Possible electronic structures for the radical anion of BTDN and BFDN (X = 0, S).

Therefore, from these calculations, we can conclude that the heteroatom plays no significant part in the determining if the structure is quinoid or benzenoid. However, to provide more conclusive evidence for the structure of the dicyano species of benzofurazan and benzothiadiazole, accurate X-ray crystal data is required and should form part of the future work of this interesting project. From the studies so far it would appear the reason why BFDN is poorer at transfering electrons and its susceptbility to undergo a competing reaction and the fact that it has very poor light absorbing properties. The synthesis of diester species based on benzofurazan would be of interest where the light absorbing properties might be enhanced (c.f. BTDN and BTDB).

References

1. V.G. Pesin, *Russ. Chem. Rev.*, 1970, **39**, 923 and refs. therein.
2. C.L. Jackson and D.F. Calhane, *Am. Chem. J.*, 1902, **28**, 451.
3. C.J. Sunde, G. Johnson and C.F. Kade, *J. Org. Chem.*, 1939, 548.
4. W. Moje, *J. Org. Chem.*, 1964, **29**, 3722.
5. K. Pilgram and M. Zupan, *J. Het. Chem.*, 1974, 813.
6. D.H. Williams and I. Fleming, *Spectroscopic Methods in Organic Chemistry* (4th. Ed), McGraw-Hill, London, 1989.
7. D.L. Hammick, W.A.M. Edwardes, *J. Chem. Soc.*, 1932, 3308.
8. J.N. Robinson, Ph.D.Thesis, University of St. Andrews, 1989.
9. P.L. Allen and A. Hickling, *Trans. Faraday Soc.*, 1957, 1627.
10. M.J.S. Dewar and W. Thiel, *J. Am. Chem. Soc.*, 1977, **99**, 4899.
11. M.J.S. Dewar, E.G. Zoedirsch, E.F. Heady and J.J.P. Stewart, *J. Am. Chem. Soc.*, 1985, **107**, 3902.
12. J.J.P. Stewart, *J. Comp. Chem.*, 1989, **10**, 209.
13. J.J.P. Stewart, *J. Comp.- Aided Molecular Design*, 1990, **4**, 1.
14. M.C. Wrin and M.A. Whitehead, *J. Chem. Soc. Faraday Trans.*, 1992, **88**, 2641.
15. R.M. Paton, *Comprehensive Heteroyclc Chemistry*, Pergamon Press, London, 1984, Vol.6, p.393.
16. L.M. Weinstock and I. Shinkai, *Comprehensive Heterocyclic Chemistry*, Pergamon Press, London, 1984, Vol. 6, 513.
17. N.M.D. Brown and P. Baldon, *Spectrochim Acta.*, 1968, **29A**, 1869.
18. R.W. Hill and L.E. Sutton, *J. Chim. Phys.*, 1949, **46**, 244.
19. V. Luzzati, *Acta Crystallogr.*, 1951, **4** , 193.
20. G.T. Strom and G.A. Russell, *J. Amer. Chem. Soc.*, 1965, **87**, 336, N.M. Atherton, J.N. Ockwell and R. Dietz, *J. Chem. Soc.*, 1967, 771.
21. G.W.H. Cheeseman and C.J. Turner, *Organic Magnetic Resonance*, 1974, **6**, 430.

Appendix

In this appendix, we present, bond lengths, bond orders (Table 1 & 2) and net charges on atoms (Table 3) for the neutral and anionic species of BTDN and BFDN, determined using MNDO, AM1 and PM3 methods using the MOPAC system Version 6.0.

Table 1

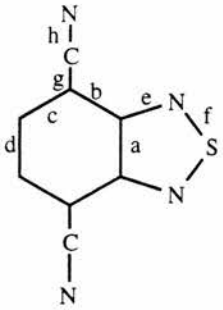

Bond Lengths

	Neutral			Anion		
Bond	MNDO	AM1	PM3	MNDO	AM1	PM3
a	1.483	1.492	1.460	1.500	1.514	1.468
b	1.460	1.438	1.441	1.437	1.421	1.413
c	1.378	1.371	1.366	1.417	1.403	1.400
d	1.454	1.425	1.432	1.402	1.385	1.389
e	1.329	1.339	1.335	1.336	1.339	1.354
f	1.622	1.630	1.711	1.638	1.664	1.733
g	1.425	1.420	1.422	1.417	1.412	1.418
h	1.162	1.103	1.159	1.165	1.166	1.163

Bond Orders

	Neutral			Anion		
Bond	MNDO	AM1	PM3	MNDO	AM1	PM3
a	1.074	1.105	1.113	1.012	1.011	1.073
b	1.038	1.089	1.076	1.136	1.172	1.218
c	1.708	1.627	1.663	1.300	1.290	1.344
d	1.110	1.182	1.161	1.415	1.449	1.421
e	1.626	1.508	1.577	1.555	1.495	1.426
f	1.155	1.225	1.178	1.050	1.072	1.047
g	1.002	1.005	1.021	1.024	1.030	1.037
h	2.900	2.889	2.888	2.850	2.839	2.847

Table 2

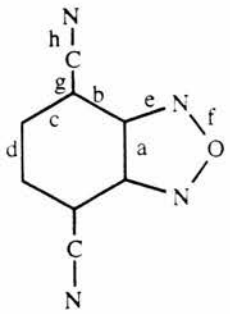

Bond Lengths

	Neutral			Anion		
Bond	MNDO	AM1	PM3	MNDO	AM1	PM3
a	1.469	1.491	1.456	1.485	1.508	1.466
b	1.450	1.434	1.438	1.429	1.415	1.414
c	1.382	1.330	1.365	1.422	1.405	1.403
d	1.456	1.433	1.438	1.402	1.388	1.390
e	1.354	1.353	1.336	1.357	1.357	1.346
f	1.298	1.326	1.370	1.312	1.345	1.407
g	1.423	1.419	1.421	1.415	1.410	1.413
h	1.152	1.163	1.159	1.165	1.167	1.164

Bond Orders

	Neutral			Anion		
Bond	MNDO	AM1	PM3	MNDO	AM1	PM3
a	1.123	1.085	1.098	1.050	1.016	1.047
b	1.054	1.071	1.066	1.143	1.157	1.179
c	1.696	1.661	1.685	1.278	1.290	1.325
d	1.119	1.152	1.144	1.438	1.438	1.424
e	1.578	1.585	1.631	1.520	1.525	1.519
f	1.155	1.141	1.119	1.063	1.044	1.029
g	1.003	1.006	1.022	1.027	1.034	1.047
h	2.901	2.890	2.889	2.847	2.835	2.834

Table 3

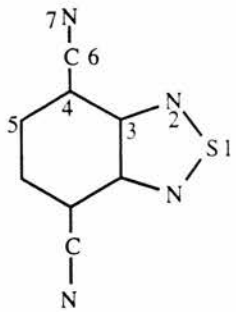

Net Charge on Atoms

	Neutral			Anion		
Atom	MNDO	AM1	PM3	MNDO	AM1	PM3
1	+0.539	+0.659	+0.389	+0.310	+0.307	+0.136
2	-0.302	-0.302	-0.172	-0.390	-0.351	-0.315
3	-0.015	-0.070	-0.059	+0.049	-0.002	+0.003
4	+0.070	+0.063	+0.096	-0.114	-0.102	-0.043
5	-0.004	-0.084	-0.059	-0.061	-0.131	-0.121
6	-0.056	-0.100	-0.109	+0.028	-0.030	-0.011
7	-0.046	-0.001	-0.017	-0.201	-0.149	-0.175

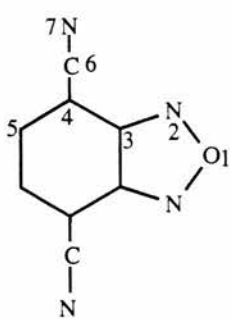

Net Charge on Atoms

	Neutral			Anion		
Atom	MNDO	AM1	PM3	MNDO	AM1	PM3
1	0.059	+0.019	+0.002	-0.035	-0.084	-0.095
2	-0.030	+0.034	+0.042	-0.174	-0.110	-0.140
3	-0.064	-0.104	-0.099	+0.009	-0.038	-0.020
4	+0.079	+0.065	+0.108	-0.117	-0.11	-0.071
5	0.000	-0.074	-0.055	-0.059	-0.129	-0.118
6	-0.063	-0.109	-0.117	+0.026	-0.034	-0.009
7	-0.037	+0.014	-0.007	-0.200	-0.148	-0.186

Chapter 6

EXPERIMENTAL

6.1 Equipment and Instrumentation Used

6.1.1 N.M.R. Spectroscopy

Both ^{1}H and ^{13}C n.m.r. spectra were recorded on a Brucker AM 300 spectrometer at room temperature with (for ^{13}C) noise proton decoupling. The chemical shifts for ^{1}H spectra were referenced to tetramethylsilane (TMS). ^{13}C resonances were referenced to residual solvent, usually $CDCl_3$, 77 p.p.m. or $(CD_3)_2CO$, 30.2 and 205.1 p.p.m. or CD_2Cl_2, 54 p.p.m. Chemical shift values are quoted relative to TMS.

6.1.2 Gas Chromatography - Mass Spectroscopy Analysis

The g.c.m.s. spectra were recorded on an INCOS 50 g.c.m.s. system with a Hewlett Packard 5890 Gas Chromatograph, fitted with a Hewlett Packard silica capillary column with a cross - linked 50% Phenyl Methyl Silicone phase.

The g.c. gradient was 60 — 300°C / 20°C per minute with the g.c. being held at 300°C for 10 minutes. Samples were run in methylene chloride.

6.1.3 IR Spectroscopy

Infra-red spectra were obtained on a Perkin Elmner 1710 Infra-red Fourier Transform Spectrometer in the range 4000 — 400 cm^{-1}. The spectra were recorded as nujol mulls between KBr plates.

6.1.4 U.V./Visible Spectroscopy

U.v.-visible spectra of solutions were recorded on a Pye-Unicam 720 u.v.-visible Spectrophotometer and a Shimadzu UV-2101PC u.v.-visible Scanning Spectrophotometer against a blank of solvent or aqueous buffer solution in a matched 1 cm quartz cell held at a constant temperature of 25°C.

U.v.-visible spectra of solutions used for protein determination and activity

assays were recorded on a Pye Unicam SP8-100 Ultraviolet Spectrophotometer against a blank of aqueous buffer solution in a matched 1 cm quartz cell held at a constant temperature of 25°C.

6.1.5 Photolysis Studies

Air sensitive solutions were placed in a 4 cm^3 quartz u.v. cell (1 cm pathlength) fitted with a vacuum-tight tap and wrapped on three sides with aluminium foil (Figure 6.1). The solution was degassed by bubbling N_2 for 0.5 hr. The resulting solutions were photolysed using white light from a Thorn EMI 500 W tungsten halogen lamp focused onto the sample through a glass lens. The sample was held at 13°C by placing it in a circulating Pyrex water bath.

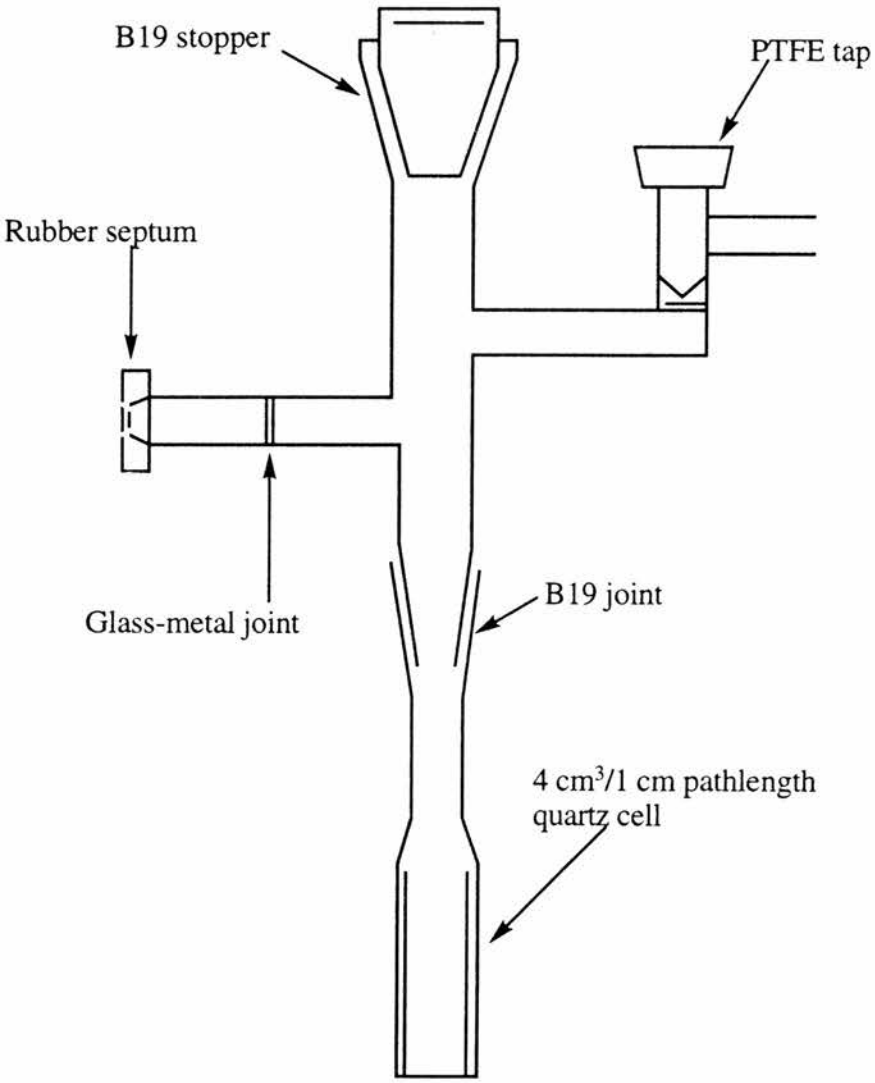

Figure 6.1 : Photolysis Cell

6.1.6 Determination of Extinction Coefficients

Each chromophore (0.33 mmol dm^{-3}) was dissolved in ethanol, placed in a 4 cm^3 quartz cuvette and the u.v.-visible spectrum recorded against a blank. The extinction coefficient was then calculated using Beers Law.

6.1.7 Measurement of Partition Coefficients

The chromophore was dissolved in octan-1-ol and its uv-visible spectrum measured. An equal volume of water was added, the solution was shaken which gave an emulsion. The solution was then left to settle back into, two distinct phases. The solutions were then separated and the visible spectra of the two layers were recorded. The partition coefficient was obtained as the ratio of absorbances of the two solutions at λ max.

6.1.8 pH Measurement

The pH was measured on a Pye Unicam 292 pH meter at 20 °C with a Russell Electrodes glass electrode. The pH electrode was calibrated using Fisons pH tablets at pH 4 and 9.2.

6.1.9 Elemental Analysis

C-H-N microanalysis were performed on a Carlo Erba MOD1106 elemental analyser at St. Andrews University.

6.1.10 Measurement of Light Filters

Metal gauzes of different mesh size were used as light filters and the percentage of light which they allowed to pass through was determined using a Perkin Elmer 1330 Infrared Spectrophotometer. The machine was set to 100% on the absorption scale with no gauze present in the beam. Each gauze was then individually placed in the beam and the deflection on the absorption scale gave a direct reading for the percentage of light absorbed by each filter.

6.1.11 Determination of Reaction Rates and Kinetics

From the results obtained in chapters 2 and 4, we can determine the rate of reaction and therefore acquire the order of the reaction. The rates of reaction were determined by obtaining the slope of the tangent to the percentage conversion - time curve at t = 0. The slope was taken at time zero because at that time the concentration for all the reactions, apart from the reagent being varied, was the same for all solutions. The reaction rates were determined for each run and these values were then plotted against the variable. From the slope of the plot, the order of the reaction can be determined.

6.1.12 Vacuum Lines

The vacuum work was performed on a Schlenk line with greased taps, ball and socket compression joints, using catheter tubing techniques. 'White spot' nitrogen was dried by passing it through a column containing chromium (II) absorbed on silica.

6.1.13 Preparation and Regeneration of Chromium (II) Drying Catalyst

Chromium trioxide (CrO_3, 20g) was dissolved in distilled water (500 cm^3) and to this suspension was added silica (M60, 400g). The water was decanted off and the catalyst dried in an oven (*ca.* 170°C) overnight. The catalyst was then transferred to a glass tube (80 cm long x 4 cm wide) fitted with Youngs taps at either end. The column was heated to 500°C in a tubular oven for 30 minutes with an in and out flow of oxygen until the catalyst turned, golden brown. The flow of oxygen was then replaced by a flow of carbon monoxide (15 — 30 mins.) until the catalyst turned blue. Once blue, the column was purged with nitrogen, sealed and allowed to cool before connecting to the vacuum line.

6.1.14 Measurement of Water Conductivity

Performed using a Whatman Pure H_2O μ-Sensor (0.1—99.9 μS/cm)

6.1.15 Transmission Electron Microscopy

(a) Vesicle Preparation — (i) Duration of Sonication

A solution of Dioctadecyldimethylammonium bromide (DODAB, Kodak) (0.0505g, 8 mmol dm^{-3}) in distilled water, was sonicated using a Sanyo Gallenkamp Plc MES Soniprep 150 Ultrasonic Disintegrator for 5 and 15 minutes at 70°C while operating at 12.5 microns using a 9.5 mm titanium head probe. The vesicle solution was then passed down a Sephadex G-50 medium column (10 cm x 2 cm in diameter) and after the elution of 13 — 15 cm^3 of the bulk solution, the unsymmetrical vesicle solution was collected (10 cm^3).

(ii) Power of Sonication

The method is the same as that above except that the solutions were sonicated for 15 minutes at the power settings of 10 and 12.5 microns. The vesicle solutions were then passed down a Sephadex G-50 medium column (10 cm x 2 cm in diameter) and after the elution of 13 — 15 cm^3 of the bulk solution, the unsymmetrical vesicle solutions (18 cm^3) were collected in sample tubes, each to a volume of 2 cm^3.

(b) TEM Sample Preparation

A drop of each vesicle solution fraction was applied to a copper mesh grid coated with a pioloform/carbon coated film and allowed to sit for a few minutes before being drained dry. A uranyl acetate solution (2%) was then applied in a similar manner. The electron micrographs of the fractions were obtained using a Philips Transmission Electron Microscope 301(60kV), at a magnification of 45 000 (actual magnification 38 400).

6.1.16 Calculation of Volume and Surface Area of DODAB Vesicles

The photographs presented in chapter 3, were used as a gross representation of the vesicle content per fraction and from these photographs, the magnification of the vesicles was determined. This allowed the diameters of each vesicle to be calculated

in angstroms. These measurements allowed the nature of the vesicle to be determined i.e. was the vesicle multilamellar, large and/or small unilamellar. The sizes that determined classification were (a) multilamellar, >1750 Å, (b) large unilamellar, 500 — 1750 Å and (c) small unilamellar, <500 Å.

Total surface area was determined using $4\pi r^2$, assuming that all the vesicles were spherical.

The total available volume of MES solution was determined for unilamellar vesicles (both large and small) by : (1) subtract 45 Å (thickness of bilayer) from the radius, (2) calculate the volume for each vesicle using $^4/_3\pi r^3$ and add together.

For multilamellar veicles, the entrapped volume between the outer two bilayers for each vesicle was calculated by : (1) subtract 45 Å (thickness of bilayer) from the radius, (2) subtract 61 Å (outer bilayer thickness + thickness of MES solution) from the radius, (3) calculate the volume for (1) and (2) using $^4/_3\pi r^3$, (4) subtract the value for (2) from (1) to give the volume of MES solution, finally (5) add final values for multilamellar vesicles together. For vesicle fractions containing both multi- and unilamellar vesicles, add both totals together.

6.1.17 Gas Analysis

For detecting the presence of oxygen in the hydrogen evolution experiments a Pye Unicam Series 204 Chromatograph with chart recorder and a Carbosphere 80/100 mesh column (Alltech) at 120°C, with Nitrogen employed as the carrier gas.

6.1.18 Optical Bench

To ensure good reproducibility of light intensity an optical bench was employed. Attached to the bench was the tungsten lamp (500W), lense, circulating bath and clamp to hold the sample during photolysis. The cuvette containing the sample was 0.5 cm from the wall of the Pyrex circulating bath. The circulating bath was 26.5 cm from the front of the lense and the back of the lense was 21 cm from the bulb of the lamp. Each piece of equipment was securely clamped to the bench.

6.1.19 Determination of Speciation Curve

Diagram showing speciation (%) v pH, were constructed with the program SPE[1] from the literature value of pKa for MES[2] and printed on a HP postscript laser printer using GWBASIC program and SPEPLOT.

6.1.20 MOPAC by MNDO, AM1 and PM3 Methods

All calculations were made by MNDO[3], AM1[4] and PM3[5] methods using version 6.0 of the MOPAC system[6] ; atomic parameters were taken from published sources.[3-5,7] All important geometric variables were simultaneously optimised and UHF wavefunctions were used for open-shell species ; the convergence criterion adopted throughout was GNORM = 0.01.

6.2 Photolysis Studies

6.2.1 Micelle Systems

(i) Photo-assisted Reduction of Anthraquinone Salts

The heterocycle (0.33 mmol dm^{-3}) was dissolved in acetate buffer (0.14 mol dm^{-3}, 100 cm^3), containing CTAB (0.8g) and AQDS (0.33 mmol dm^{-3}). Immediately prior to irradiation, an aliquot (4 cm^3) was taken, the electron donor added (0.05 mol dm^{-3}) and the pH suitably adjusted using A.R. grade sodium hydroxide solution (2.5 M) (MESH, pH 6.5). After degassing, a u.v.-visible spectrum was recorded against a blank (acetate buffer) as background and the solution irradiated with further spectra being taken at set time intervals.

(ii) Determination of the Extinction Coefficient (ε) for 1,5-$AQDSH_2$

The method above was repeated with AQDS at 0.165 mmol dm^{-3}. The reaction was performed until the production of 1,5-$AQDSH_2$ ceased (monitored at 392 nm). It was assumed that all AQDS had been converted to $AQDSH_2$ (0.165 mmol dm^{-3}). The extinction coefficient was then calculated using Beers Law ($A = \varepsilon cl$) and was

determined to be 17500 $dm^3mol^{-1}cm^{-1}$ at 392 nm. Therefore, yields of 1,5-$AQDSH_2$ were determined from the absorbance at 392 nm (ε = 17500 $dm^3mol^{-1}cm^{-1}$).

(iii) Effect of Light Intensity in the Photo-assisted Reduction of AQDS

The method employed was the same as in (i) but with this set of experiments, light filters (6.1.10) were used to determine the effect of light intensity upon the rate of conversion of AQDS to $AQDSH_2$. Yields of 1,5-$AQDSH_2$ were determined as in (i).

(iv) Effect of [MESH] in the Photo-assisted Reduction of AQDS

The method used for this set of experiments was the same as in (i) but here we were looking at the effect of varying the [MESH] upon the rate of conversion from AQDS to $AQDSH_2$. Concentrations used were 0.025, 0.05, 0.075 and 0.1 mol dm^{-3}, respectively. A control was employed at each [MESH] where BTDB was absent. The yields of 1,5-$AQDSH_2$ being determined as before.

(v) Effect of [BTDB] in the Photo-assisted Reduction of AQDS

The method employed was the same as in (i) except that we were varying [BTDB]. The concentrations used were 0.165, 0.333, 0.5 and 0.666 mmol dm^{-3}, respectively. A control without BTDB was employed and the yields of 1,5-$AQDSH_2$ were determined as before.

(vi) Effect of [CTAB] in the Photo-assisted Reduction of AQDS

This set of experiments was concerned with studying the effect the [CTAB] has on the reduction of AQDS. The method was the same as in (i) and the [CTAB] used were 0.017, 0.034 (c.m.c.), 0.052, 0.1, 0.2 and 0.8% w/w respectively. A control was employed where CTAB was absent.

(vii) Effect of pH in the Photo-assisted Reduction of AQDS

The method and conditions used for this set of experiments were identical to (i) but the pH of the solution being photolysed was varied within a range of 4 — 12 using A.R. grade c. hydrochloric acid and sodium hydroxide (2.5 M). No control was employed.

(viii) Effect of [AQDS] in the Photo-assisted Reduction of AQDS

The method and conditions used for this set of experiments were identical to (i) but the [AQDS] employed was 0.083, 0.165, 0.33, 0.495 and 0.66 mmol dm^{-3}, respectively. Yields of $AQDSH_2$ were determined as before and no control was employed.

6.2.2 Vesicle Systems

(i) Vesicle Preparation

Aqueous solutions (10 cm^3) containing DODAB (0.0505g, 8 mmol dm^{-3}), MESH (0.05 mol dm^{-3}) and BTDB (0.333 mmol dm^{-3}) were sonicated for 15 minutes at 70°C with a Sanyo Gallenkamp Plc. MES Soniprep 150 Ultrasonic Disintegrator, operating at 12.5 microns through a 9.5 mm titanium head probe.

For studies, investigating the effects of vesicle formation on the reduction of AQDS (Chapter 3), the method given above was followed except the solutions were sonicated for only 5 and 15 minutes at 12.5 microns and for 15 minutes at 10 and 12.5 microns, respectively.

(ii) Preparation of Unsymmetrical Vesicles

The vesicles were separated from the bulk aqueous solution and its contents by passage down a *freshly* prepared column of Sephadex G-50 medium, (50 — 150 μ, Aldrich) 10 cm long by 2 cm diameter. The vesicles (10 — 12 cm^3) were collected from the column after 14 — 16 cm^3 had eluted to give a mixture of unilamellar and multilamellar vesicles, with MESH trapped in the inner water pool and BTDB contained within the bilayer.

Note : For BTDN, BTDE and BFDN, the chromphore was added after the preparation of the unsymmetrical vesicles.

(iii) Photo-assisted Reduction of AQDS in Unsymmetrical Vesicles

To the solution of unsymmetrical DODAB, MESH and BTDB (2 cm^3) was added the 1,5-anthraquinone salt (AQDS, 0.33 mmol dm^{-3}) in distilled water (2 cm^3). The solution was placed in a 4 cm^3 quartz u.v. cell (Figure 4.1) wrapped on 3 sides with aluminium foil and degassed by bubbling N_2, through the solution for 15 mins. Before photolysis a u.v-visible spectrum was recorded against a blank (distilled water). The solution was then photolysed, while being held at a constant temperature. The yields of $AQDSH_2$ were determined as before for the micelle experiments.

(iv) Determination of MESH & AQDS Leakage Across DODAB Bilayers

(a) The method and conditions used in 6.2.2 (iii) were employed. The solution was photolysed for 75 minutes and then passed down a freshly prepared Sephadex G-50 column (10 cm long x 2 cm diameter) where the vesicle and bulk water fraction were collected. U.v.-visible spectrum were recorded of both solutions. The solutions were rephotolysed, with the yield of $AQDSH_2$ being determined as in section 6.2.1(i).

(b) Control Experiment

As in 6.2.2.(iii), the method and conditions employed were the same except that BTDB was not present in solution.

(vi) Effect of pH in the Photo-assisted Reduction of AQDS

The method employed for this set of experiments was the same as in 6.2.2(iii) while altering pH over a range of 4 — 10.5 using A.R. grade conc. hydrochloric acid and sodium hydroxide (2.5 M) after chromatography. Yield of $AQDSH_2$ was determined as before.

(vii) Effect of Light Intensity in the Photo-assisted Catalysed Reduction of AQDS

The method used for this set of experiments was the same as in 6.2.2(iii) with light filters used to alter the light intensity, as in section 6.2.1 (ii). A control was employed

in which the solution was not photolysed. Yields of $AQDSH_2$ was determined as before.

(viii) Effect of [MESH] in the Photo-assisted Reduction of AQDS

The method used for this set of experiments was the same as in 6.2.2(iii) while varying [MESH]. The concentrations employed were 0.0125, 0.025, 0.05, 0.075 and 0.1 mol dm^{-3}. A control was employed with MESH absent. Yields of $AQDSH_2$ were determined as before.

(viiii) Effect of [BTDB] in the Photo-assisted Reduction of AQDS

The method used was the same as in 6.2.2(iii) except that the variable was [BTDB]. The concentrations employed were 0.041, 0.083, 0.165, 0.248, 0.33 mmol dm^{-3}. A control was employed where BTDB was absent. Yields of $AQDSH_2$ were determined as before.

(ix) Effect of [AQDS] in the Photo-asssited Reduction of AQDS

The method used for this set of experiments was the same as in Section 6.2.2(iii) but we are studying the effect of varying [AQDS]. The concentrations employed were 0.041, 0.083, 0.165, 0.248 and 0.33 mmol dm^{-3}. The yield of $AQDSH_2$ were determined as before.

6.3 Enhancement of Electron Transfer across Vesicle Bilayers

These experiments were concerned with determining if charge compensating diffusion of H^+ or OH^- was the rate determining step in the overall mechanism of electron transfer across the vesicle bilayers. The use of Vitamin K_3 (10^{-5} — 10^{-3} mol dm^{-3}) in the vesicle solution caused the precipitaion of the vesicles. This occured if the Vitamin was added before sonication or to the bulk aqueous phase after the unsymmetrical vesicles were prepared.

6.4 Cyclic Voltammetry

Electrochemical measurements were performed using an EG & G PARC (Model 273A) potentiostat/galvanostat with EG & G PARC electrochemical software controlled by an IBM compatible PC. The experiments utilised a 3 and 2 electrode system in a cell where the cell configuration allowed a minimal distance between the reference and working electrode to be achieved. A platinum gauze counter electrode was used and all experiments were referenced to SCE (Russell Electrodes, +0.2415 V v SHE) and Ag-AgCl reference electrode (0.222 V v SHE) without correcting for liquid junction potentials. IR compensation was employed and the potential measured was corrected accordingly. The cell was continuously purged with argon between and during electrochemical experiments. Electrochemical measurements were made at room temperature (*ca.* 293 K). The working electrode was polished between successive CV scans and sonicated in distilled water for 10 minutes. The cell was placed in a Faraday cage to minimise noise interference.

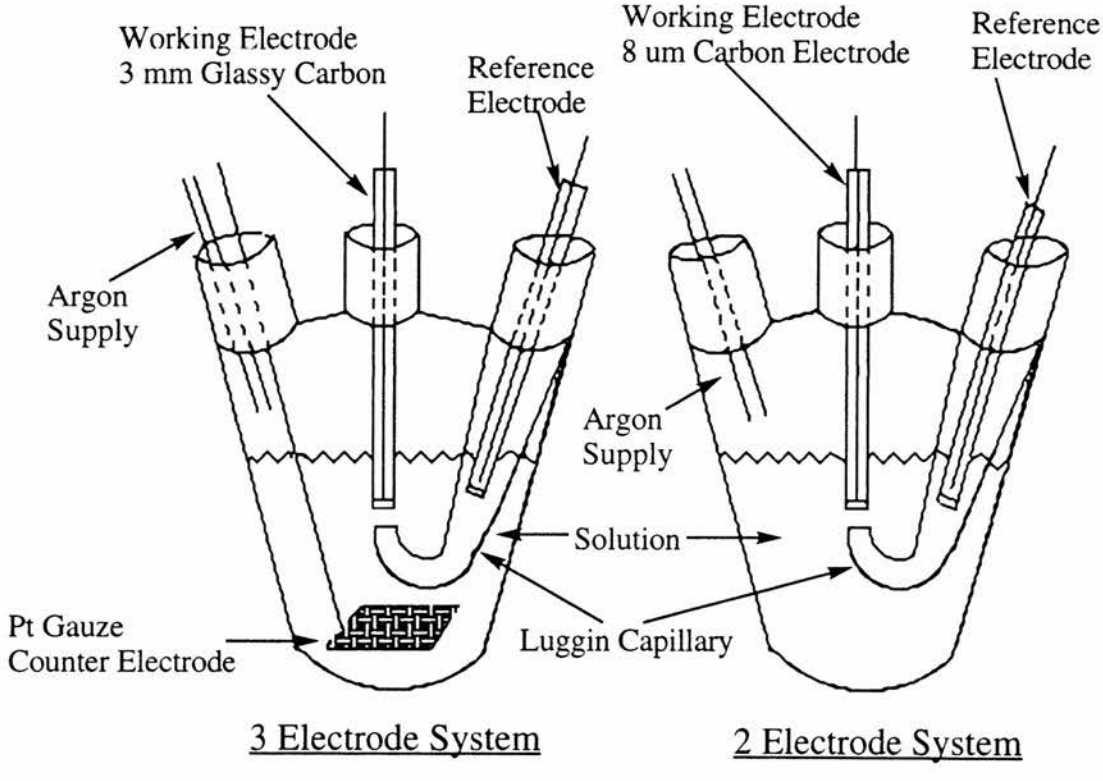

Figure 6.3 : Cyclic voltammetry cell for 3 and 2 electrode system.

(i) Construction of Glassy Carbon Electrode[8]

The working electrodes were constructed from 3 mm diameter glassy carbon. The glassy carbon was sealed to teflon with epoxy resin and a connection was made to a stainless steal rod by silver epoxy. The carbon was polished with successively finer grades of alumina (Beuhler) suspended in water or non-aqueous solvent on chemically resistant polishing cloths (Beuhler), followed by rinsing and sonication until a mirror finish was attained.

(ii) Construction of Microelectrode[8]

The micro-working electrodes were prepared by rapidly collapsing glass onto a carbon fibre or platinum wire of appropriate diameter (8 μm and 25 μm, respectively), followed by cutting to reveal the micro-disk. Electrical contact for the carbon fibre was made by connecting a 0.5 mm copper wire to the microwire *via* a silver loaded epoxy resin. For the micro-platinum electrode, electrical contact was made to the 0.5 mm copper wire *via* solder or a lead plug.

The electrodes were polished with alumina (Beuhler) of decreasing sizes (1μm, 0.3 μm and 0.05 μm) suspended in water or non-aqueous solvent on chemically resistant cloth (Beuhler), followed by sonication and rinsing. The diameter of the micro-disk was confirmed by scanning electron microscopy (SEM) analysis and the quality of the disk after polishing was checked microscopically.

(iii) Construction of Ag-AgCl Reference Electrode[9]

One end of a 13 cm length of 1.0 mm diameter Ag wire (99.99%, Advent) was swirled briefly in a 1:1:1 mixture of H_2O: c.HNO_3: c.HCl to a depth of about 2 — 3 cm. The surface became tarnished with a thin layer of AgCl. The electrode was then rinsed quickly and thoroughly with distilled water.

One end (2 cm) of a 12 cm section of an 8 mm o.d. glass tube was heated and narrowed to 4 mm o.d. This end was then sealed using a Vicor glass Frit held in place with heat shrinking teflon.

A saturated solution of KCl was prepared (5 cm^3) to which 1 — 2 drops of an $AgNO_3$ (0.1 M) solution was added. The KCl/$AgNO_3$ solution was then added to the glass tube, to a depth of about 7 — 8 cm. The wire was inserted, with the tarnished end approximately 1 cm above the Vicor frit. The wire was secured in place by insertion through an n.m.r. subaseal, to give an air tight seal that minimised the leakage of KCl solution. The electrode was immersed in the test solution to the same level as the meniscus of the KCl solution ensuring that any residual leakage was diffusion controlled and negligible.

(iv) Determination of Electrochemical Stability Window

Before commencing with electrochemical studies, control experimenets were performed in the absence of the heterocycle to determine the potential range over which the solvent, acetate buffer, CTAB, DODAB and electrolyte were electrochemically stable. The procedure is given in the following two sections.

(v) Aqueous Systems with Macro & Micro Electrodes

The heterocycle (0.33 mmol dm^{-3}) was dissolved in acetate buffer (0.14 mol dm^{-3}, 100 cm^3) containing CTAB (0.8 g) and electrolyte (Analar KCl, 0.1 mol dm^{-3}). The pH was adjusted to 6.5, the solution (10 cm^3) was placed in the cell to cover the electrodes. The solution was degassed for at least 0.5 h. The electrolyte used was A.R. grade potassium chloride (KCl, 0.1 mol dm^{-3}) and the internal standard employed was A.R. grade potassium ferrocyanide (K_4FeCN_6, 0.33 mmol dm^{-3}) in cell volume. Experiments were also performed with CTAB absent from solution.

Studies involving DODAB vesicles were unsuccessful because the surfactant vesicles precipitated from solution upon the addition of electrolyte.

(vi) Non-Aqueous Systems with Macro & Micro Electrodes

The procedure was the same as that employed for the aqueous system except that acetonitrile was employed as the solvent. The increased solubility of the heterocycles

mean't that more defined cyclic voltammograms were obtained with typical heterocycle concentrations of 3.3 mmol dm^{-3}. The electrolyte employed was tetrabutylammoniumhexafluorophosphate (0.1 mol dm^{-3}) in cell volume (10 cm^3). The internal standard used was ferrocene (3.3 mmol dm^{-3}) in cell volume (10 cm^3).

6.5 Photochemical Generation of Radical Anions

6.5.1 E.S.R. Studies

All esr spectra were recorded on a Brucker ER200-SRC spectrometer (K band). *In situ* generation of radicals by photolysis was achieved by irradiating solutions in a 1 mm diameter quartz/silicone capillary from a 500 Watt 'super pressure' mercury arc lamp.

(i) Aqueous Systems

An acetate buffered solution (pH 6.5, 4 cm^3) of the heterocycle (0.33 mmol dm^{-3}), TEOA or MES (0.05 mol dm^{-3}) and CTAB (0.8% w/w) was placed in an esr capillary and degassed with N_2 for 0.5 hr. After degassing, the esr spectrum of the solution was measured before, during and after photolysis.

(ii) Non- Aqueous Systems

The non-aqueous solvent (4 cm^3) containing the heterocycle (0.01 mol dm^{-3}) and TEOA (0.05 mol dm^{-3}) was placed in an esr capillary and degassed with N_2 for 0.5 hr. Again the esr spectrum was recorded before, during and after photolysis.

6.6.2 Laser Flash Photolysis with Uv-visible Detection

A Lambda Physic EMG-50 excimer laser operated at 308 nm (XeCl 40 ns pulse-width, 30 mJ $pulse^{-1}$ at a 32 kV discharge) was employed. The laser was routinely operated at a 1 Hz repetion rate and had an output beam with dimensions of 2 cm x 1 cm at the cavity exit. This was focused down to 1 mm diameter before the sample, so that the beam had a diameter of 5 mm at the sample. The sample compartment was housed in an Applied Photophysics laser kinetic spectrometer with a 250 W Xe arc

lamp (which can be pulsed for timescales less than 100 μs) as a white light source. The white beam was focussed and passed through the sample at 180° to the excitation pulse, thus ensuring maximum beam overlap. The transmitted white light was then focused into the monochromator which was coupled to a photomultiplier. The response of the photomultiplier was wavelength dependent and was normalised by manual variation of the supply voltage. The low wavelength limit for detection was set at 350 nm by cut-off filter, positioned so as to prevent back reflections from the laser entering the monochromator. The high wavelength limit was set at 900 nm by the use of a R928 photomultiplier tube. The output from the photomultiplier was connected to a Tektronix TDS 520 digital oscilloscope via a variable terminator resistor. The oscilloscope was triggered by diverting a small proportion of the laser output to a photodiode. The oscilloscope collected 2500 data points with a maximum resolution of 0.001 V and a limiting sampling rate of 2 ns $point^{-1}$. Any number of shots could be averaged at the oscilloscope before all 2500 data points were transferred via a GPIB interface to a Dell PC using software developed by Davor Dukic at York University. The Dell has a dedicated timing board and controls the opening of shutters and the firing of the laser and the arc lamp pulse. Decays were converted to absorbance units by entering the voltage value at 'infinite' time. First or second-order plots were analysed by linear least-squares regression. Standard errors were converted to 95% confidence limits.

(i) Studies in a Micellar Environment

The heterocycle (3.3×10^{-4} mol dm^{-3}) was dissolved in acetate buffer (0.14 mol dm^{-3}, 100 cm^3) containing CTAB (0.8% w/w) and electron donor (MES, 0.05 mol dm^{-3}) with the pH adjusted to 6.5 for MES. The solution was stored in the dark until required. An aliquot was taken, placed in a cuvette and the u.v.-visible spectrum was recorded to observe the absorbance at 308nm. Satisfactory values were between 0.5 and 1.0. If >1 then the solution required dilution and when <0.5 the solution was too weak. Once completed a uv-visible spectrum was recorded as the background and the

solution was then photolysed by a XeCl laser operating at 308 nm. The absorbance (ΔAbs.) was determined at 10 nm intervals over a range of 350 — 750 nm and at wavelengths of maximum ΔAbs, recordings were taken at 5 nm intervals. The samples were studied under atmospheric and inert atmospheres by degassing for 15 minutes with argon and with and without the presence of AQDS.

(ii) Studies in a Unsymmetrical Vesicle Environment

The vesicle solutions were prepared as before in Section 6.2.2 (i & ii). The solution was stored in the dark until required. The procedure was then the same as for the studies in a micellar environment, see previous section. However, these studies were inconclusive because no significant amount of $BTDB^{-\cdot}$ was formed within the duration of the laser pulse.

6.7 Production and Identification of Unknown 'Green' Species

The unknown species could be generated in a micellar (6.2.1 (i)) or vesicle (6.2.2 (iii)) solution without the presence of AQDS. The growth of the species was monitored by u.v.-visible spectroscopy at 395 — 401 nm.

Therefore, to identify the unknown species attempts were made to isolate it species by generating it *in situ* within a quartz n.m.r. tube. The micellar solution (2 cm^3) was employed which contained excess BTDB and D_2O (2 drops). The solution was degassed with N_2 for 0.5 h., cathetered into a degassed quartz n.m.r. tube, to a depth of 4 cm^3 and sealed. An n.m.r was then recorded before photolysis. The solution was then photolysed for 6 hours during which the solution became green in colour and after photolysis, an n.m.r was recorded overnight. A change in the n.m.r. spectra was observed but as a result of being in such low concentration, no accurate determination of structure could be made.

6.8 Preparation and Analysis of Potential H_2 Producing Catalysts

Hydrogenase from *Desulfovibrio Desulfuricans ATCC7757* (Norway Strain) and *Desulfovibrio Gigas*

Samples of hydrogenase from the bacteria, *D. Desulfuricans* and *D. Gigas* were kindly donated by Prof. R. Cammack of King's College, London and stored at -78°C when not in use.

6.8.1 Protein Concentration[10,11]

The protein concentration (mg of protein per cm^3 of enzyme) was determined by the Bradford method using bovine serum albumin as standard.

(i) Preparation of Bradford Reagent[10]

Coomassie Brilliant Blue (50 mg) was dissolved in ethanol (25 cm^3 95%) and left for 1 hr. To this solution was added phosphoric acid (50 cm^3 of 85% (w/v)), followed by distilled water, to give a final volume of 500 cm^3. The solution was filtered twice, stored in a dark bottle and placed in the fridge. With age, the dye began to precipitate and this precipitate was removed by filtration.

(ii) Method for Bradford Assay[10]

(1) Protein dilutions were made from a stock solution of 1 mg/cm^3 protein standard (1 cm^3, Bovine Serum Albumin, Sigma) in Hepes (9 cm^3, 50 mmol dm^{-3}, pH 8). From this stock solution, an aliquot was taken and diluted to the appropriate concentration, see table 1, below. The solutions were allowed to sit for at least 2 minutes but not longer than 1 hr before recording the absorbance.

Protein Standard (cm^3)	Diluent (cm^3)	Protein Conc($\mu g/cm^3$)
1	9	100
4	1	80
3	1	60
2	1	40
1	1	20
1	1	10
1	1	5
1	1	2.5

Table 1 : Shows volume taken from stock solution (100 $\mu g/cm^3$) and dilution required to give Protein Conc. Standard.

(2) Distilled water was used as a standard zero reading against which an absorbance background of buffer:dye (1:1 v/v) was recorded.

(3) The absorbance of the standard protein solutions were measured and the background subtracted to give the final absorbance.

(4) A standard curve was plotted of final absorbance against protein concentration ($\mu g/cm^3$).

(5) To x μl of unknown enzyme was added the appropriate volume of buffer to give a volume of 1 cm^3 and to this was added Bradford reagent (1 cm^3) to give a final volume of 2 cm^3. The absorbance was recorded and from the standard curve the protein concentration was determined for each batch of enzyme, taking into account the dilution factor.

(iii) Determination of Molarity[12]

This was achieved by adding 1 μl of enzyme solution to a solution of Hepes (1 cm^3, 50 mM, pH 8) and recording the absorbance. Employing the Beer-Lambert law and a known extinction coefficient for the enzyme (ε = 45000 $dm^3\ mol^{-1}\ cm^{-1}$), the molarity was determined, taking into account the dilution factors.

(iv) Methyl Viologen Assay[13]

The methyl viologen hydrogen-uptake assay is the standard assay employed to detect changes in the activity of the hydrogenase. The buffers employed caused no coagulation of the vesicles. They were ACES (pH 6.5), BES (pH 7.0 & 7.5) and TES (pH 8.0) at a concentration of 25 mM.

To confirm that neither of these buffers acted as sacrificial electron donors, a solution of each was made (0,05 mol dm^{-3}), to which AQDS (0.33 mM) was added. An aliquot was taken and placed in a cuvette (Section 6.1.5) and degassed by passing nitrogen through the solution for 15 minutes. A u.v.-visible spectrum was taken and the sample was photolysed, with u.v.-visible spectrum being recorded at regular time intervals. No $AQDSH_2$ was produced.

Method for Methyl Viologen Assay[13]

A stock solution of the ACES (25 mM) and methyl viologen (100 mM) was degassed and saturated with wet H_2 for 45 minutes. H_2 saturated buffer solution (1.98 cm^3) was added to a degassed cuvette (fitted with quickfit joint and subaseal). An aliquot of the methyl viologen solution (20 µl) was added and the resulting solution degassed for a further 15 minutes.

Enzyme solution (10 µl) was added to buffer (90 µl) and activated (reduced) by passing wet H_2 gas ***over*** the solution for 30 — 40 minutes for *D. Desulfuricans* and 6 — 8 hours for *D. Gigas*. From the enzyme solution x µl were taken and added to the cuvette containing the methyl viologen solution which was equilibrating at 30°C in the uv-visible spectrophotometer and shaken. A blue colour appeared and the absorbance was recorded at 604 nm. A blank experiment omitting the enzyme was carried out and showed no generation of the blue colour of $MV^{+\cdot}$.

From the gradient of the curve of absorbance against volume of enzyme added it was possible to determine the specific activity for that enzyme i.e. 1 unit of enzyme converts 1 µmol of substrate per minute.

6.8.2 Procedure for Hydrogen Evolution Employing Hydrogenase

The unsymmetrical DODAB solution containing BTDB and MES was prepared as before in section 6.2.2 (i—iii). An aliquot (1.5 cm^3) of this solution was taken and added to a cuvette (6.1.5) and degassed with argon for 15 minutes.

A buffered solution (1 cm^3, ACES, 25mM, pH 6) containing MV^{2+} (10^{-5} — 10^{-3} mol dm^{-3}) was degassed with argon for 10 minutes. To this buffered solution was injected Hydrogenase (10^{-7} — 10^{-5} mol dm^{-3}) from *D. Gigas* or *D. Desulfuricans* which had been activated by passing *wet* H_2 gas over the enzyme for 1 and 8 hours respectively. Before the enzyme was injected into the buffered MV^{2+} solution, the enzyme was purged to remove the traces of H_2, by passsing argon over the enzyme for 30 minutes.

The buffered solution was then transfered, under argon, to the vesicle solution. The cuvette was then wrapped on three sides with foil and photolysed for 6 — 8 hours. Gas samples (1 cm^3) were taken every 0.5 h. and analysed by g.c. The cuvette was held at a constant temperature of 27°C by placing it in a circulating Pyrex water bath.

Note : Enzyme concentrations in excess of 10^{-4} mol dm^{-3}, result in the precipitation of the vesicles.

6.9.3 Colloidal Platinum

(i) Preparation of Colloidal Platinum[14,15]

Fresh H_2PtCl_6 (12 — 100 mg Pt dm^{-3}, Pt content 37.50%, Aldrich) depending on the platinum concentration to be used, was dissolved in distilled water (450 cm^3, 1.3 μs cm^{-1}) contained in a round-bottom flask. Sodium Citrate (50 cm^3 of a 1% aq. solution) was slowly added with stirring. The solution was refluxed for four hours during which time the solution turned from pale yellow to dark grey-brown. The solution was then cooled in an ice bath.

At this stage, the catalyst consisted of citrate-protected colloidal particles and was stored in a cool, dark place until required over the next few weeks. If an

alternative protective agent was needed the excess citrate was removed by passing the solution down an 'Amberlite MB-3A' (Aldrich) ion exchange resin column (15 cm long x 2 cm diamter) until the conductivity was less than 2 $\mu s\ cm^{-1}$. The solution was warmed, the protective agent was added with stirring and the solution was allowed to equilibrate for an hour. A ratio of 2:1 for Pt : Carbowax-20M or PVA (MW 14000) gave the best catalytic activity and stability.

(ii) Determination of Platinum Content and Particle Size

The platinum content of the solution was initially determined by atomic absorption spectroscopy and confirmed plasma emmission spectroscopy. Aliquots of the various platinum protected solutions were treated with aqua regia for several hours until clear solutions were obtained. Calibration was by standard addition to each of the solutions, in order to make allowance for the effects of the various protective species on the nebulisation and atomisation processes.

The size of the platinum particles was determined using a Philips Transmission Electron Microscope 301, 60kV, at a magnification of 34 000. The solutions were concentrated by centrifugation at 15000 rpm for 30 minutes. A drop of each solution was applied to a copper mesh grid coated with a pioloform/carbon coated film and allowed to sit for a few minutes before being drained dry.

(iii) Platinum Catalyst Assay - H_2 Reduction of MV^{2+}

A weak buffer (6 cm^3, 0.02 mol dm^{-3}, sodium acetate pH 6) containing MV^{2+} (0.514 mg, 2 x 10^{-4} mol dm^{-3}, 2 cm^3) was placed in a 25.5 cm^3 Schlenk tube. The solution was degassed by bubbling N_2 for 30 minutes. On the addition of the degassed catalyst solution (2 cm^3), the solution was again degassed for 15 minutes. After 1 minute of H_2 bubbling in the presence of the catalyst it was apparent from the blue colour that $MV^{+\cdot}$ was present. Oxygen was not detected in the system by g.c. analysis.

6.10 Procedure for Hydrogen Evolution Employing Colloidal Pt Catalyst

(i) In Aqueous Solution

BTDB (0.33 mM) was dissolved in weak and strong acetate buffer (50 cm^3, 0.02 and 0.14 mol dm^{-3}) with the aid of an ultrasonic bath. Prior to irradiation, 8 cm^3 was taken and methyl viologen dichloride (2 mmol dm^{-3}) and MES (0.05 mol dm^{-3}) were added. The platinum containing solution (2 cm^3) was added and adjusted to pH 6. The solution was placed in a 25.5 cm^3 Schlenk tube with a stirrer bar, thoroughly degassed by bubbling N_2 for 15 minutes and then irradiated for several hours. A blue colouration appeared due to low levels of $MV^{+\cdot}$ being produced ($>10^{-4}$ mol dm^{-3}). After each 30 mins., a 1 cm^3 sample of gas was taken from above the solution and analysed by g.c. The pH of the solution remained constant with photolysis. The presence of oxygen in the sytem would have been detected by the g.c. analysis.

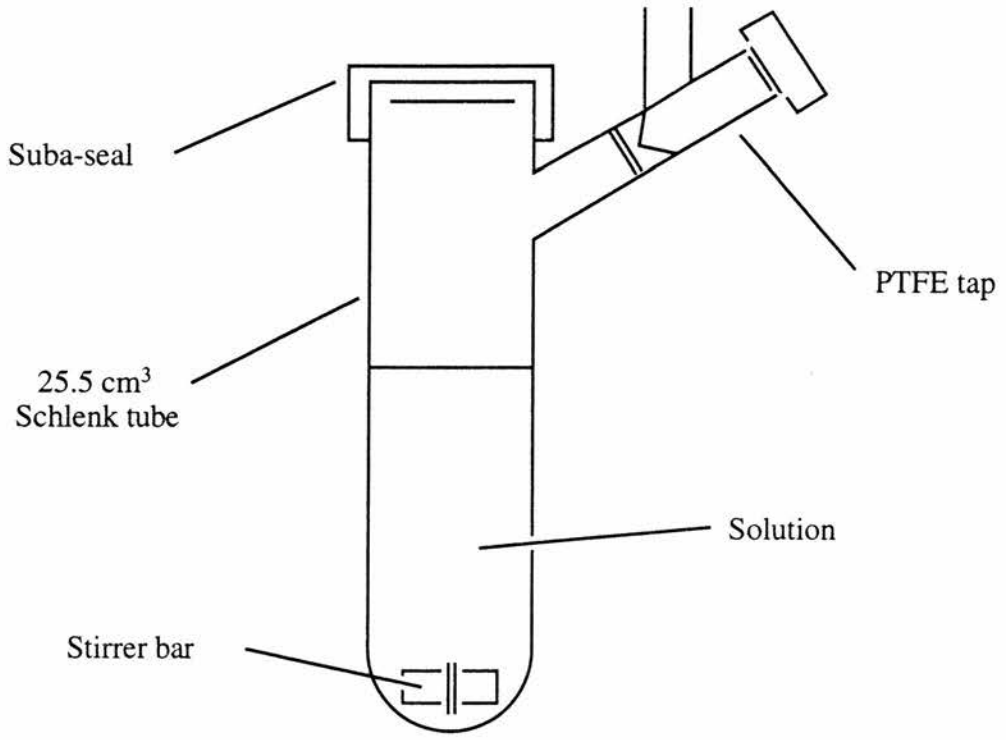

Figure 6.4 : 25.5 cm^3 Schlenk tube.

(ii) In a Micellar Environment with Methyl Viologen

BTDB (0.33 mmol dm^{-3}) was dissolved in acetate buffer (100 cm^3, 0.07 mol dm^{-3}), containing CTAB (0.8 g) and methyl viologen (0.2 mmol dm^{-3}). An aliquot (2 cm^3) was taken to which the appropriate platinum solution (2 cm^3) and electron donor (MES, 0.05 mol dm^{-3}) was added and the pH adjusted to 5.5 — 6. The solution was then added to a cuvette as shown in section 6.1.5 and degassed with N_2 for 0.5 h. The cuvette was wrapped on three sides with foil and photolysed, with gas samples (1 cm^3) being taken every 0.5 h for 6 — 8 hours and sampled by g.c. A blue colouration appeared due to low levels of $MV^{+\cdot}$ being produced (>10^{-4} mol dm^{-3}).

In addition to this, we stirred the micellar solution, by increasing the solution volume and the weight of MESH and MV^{2+}, two fold. The reaction was performed in a Schlenk tube under a N_2 atmosphere.

A control experiment was prepared and performed as above with BTDB absent. A blue colouration appeared due to low levels of $MV^{+\cdot}$.

(iii) In a Vesicle Environment with Methyl Viologen

The unsymmetrical DODAB solution containing BTDB and MES was prepared as before in section 6.2.2 (i—iii). An aliquot (2 cm^3) of this solution was taken to which was added the appropriate platinum catalyst and methyl viologen (2 x 10^{-4} mol dm^{-3}) solution (2 cm^3) which was buffered with ACES (25 mM) at pH 6. The solution was then added to a cuvette as shown in section 6.1.5 and degassed with N_2 for 0.5 h. The cuvette was then wrapped on three sides with foil and photolysed for 6 — 8 hours. Gas samples (1 cm^3) were taken every 0.5 h. and sampled by g.c. No blue colouration due to the production of $MV^{+\cdot}$, was observed.

Control experiments were performed where (a) methyl viologen and (b) BTDB were absent and no blue colouration was observed.

6.11 Preparation of Buffers

(i) Acetate Buffer

The acetate buffer (0.14 mol dm^{-3}) was prepared by dissolving sodium acetate (19.1 g) in distilled water (800 cm^3), adjusting the pH to *ca.* 5.5 with glacial acetic acid and adding further distilled water, up to a total volume of 1 litre.

(ii) Phosphate Buffer

KH_2PO_4 (17.1g) and Na_2HPO_4 (17.75g) were dissolved in distilled water (400 cm^3), the pH was adjusted to *ca.*7 with an 85% solution of H_3PO_4. The solution was then made up to 500 cm^3 by the addition of distilled water.

6.12 Preparation of Compounds

All chemicals were used as supplied and were of reagent grade.

6.12.1 Preparation of 2,1,3-benzothiadiazole-4,7-dibromide[16]

A mixture of 2,1,3-benzothiadiazole (10g, 0.007 mol., Aldrich) and hydrobromic acid (92 cm^3, 47% solution in water) was heated under reflux while hydrogen peroxide (60 cm^3, 30% solution in water) was added. After six hours the reaction mixture was quenched in ice water, filtered, washed with water (300 cm^3) and dried to give 2,1,3-benzothiadiazole-4,7-dibromide (18.94g, 0.064 mol, 75%).m.p. 181 — 183°C, lit. 184 — 185°C.

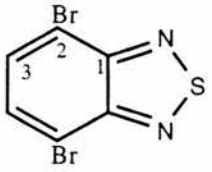

^1H n.m.r. ($CDCl_3$) δ 7.8 ppm. ^{13}C n.m.r. ($CDCl_3$) δ 113.9 (C(2)), 132 (C(3)), 152.9 (C(1)).

6.12.2 Preparation of 2,1,3-benzothiadiazole-4,7-dicarbonitrile[17]

A mixture of 2,1,3-benzothiadiazole-4,7-dibromide (29.4g, 0.1 mol) and cuprous cyanide (20g, 0.223 mol) in DMF (300 cm^3), was heated under reflux overnight and

then concentrated under reduced pressure, the black residue was then suspended in concentrated hydrochloric acid (60 cm^3).

Hydrogen peroxide (25 cm^3, 30%) was added dropwise with stirring. The addition was exothermic and the temperature of the reaction mixture was controlled to 40 °C by external cooling. The mixture was stirred for forty-eight hours and filtered. Both filtrate and filter cake were extracted with boiling toluene (600 cm^3) by a soxhlet extraction. The combined extracts were washed with water and concentrated to give 2,1,3-benzothiadiazole-4,7-dicarbonitrile plus impurities.

Chromatography of the yellow/orange solid on silica using petroleum ether 40/60:ethyl acetate (3:1 v/v), eluted BTDN as a yellow band. The petroleum ether 40/60:ethyl acetate was removed *in vacuo* and the solid recrystallised from petroleum ether 40/60:ethyl acetate (3:1 v/v) at -78°C to yield BTDN (2g, 0.011 mol 15%) mp 187 — 189°C, lit. 189 — 191°C.

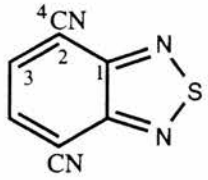

The I.R. spectrum of BTDN has a sharp peak at 2236 cm^{-1} due to the two cyano substituents. ^1H n.m.r. ($(CD_3)_2CO$) δ 8.2 ppm. for the aromatic hydrogens. ^{13}C n.m.r. ($(CD_3)CO$) δ 111.2 (C(2)), 115.5(C(4)), 137.9 (C(3)), 153.8 (C(1)).

6.12.3 Preparation of the Dibutyl Ester of 2,1,3-benzothiadiazole-4,7-dicarboxylic acid (BTDB)[18]

A solution of BTDN (1g, 5.4 mmol dm^{-3}) in aqueous NaOH (20 cm^3, 25% solution) was heated under reflux until the evolution of NH_3 had ceased (18 hours).

Acidification with HCl, afforded a brown solid, the dicarboxylic acid, which was filtered and oven dried. The dicarboxylic acid was then treated with refluxing thionyl chloride (40 cm^3) for twenty-four hours and after cooling, filtering and evaporation of the filtrate gave the crude dicarboxylic acid dichloride (0.44g). The acid dichloride was then added to a solution of pyridine (0.25g) in butanol (5 cm^3)

which was refluxed for three hours to produce a red/brown solution. Butanol was evaporated *in vacuo* and to ensure complete removal, petroleum ether 40/60 (15 cm^3) was added then removed *in vacuo* to leave a red oil of BTDB plus impurities.

Chromatography of the oil was performed by absorbing the oil onto alumina (Type II-III) and placing on top of a dry alumina column (12 cm x 2 cm). The impurities were eluted as a yellow band using petroleum ether 40/60, to leave BTDB still absorbed to the alumina at the top of the column. The alumina was then removed and washed with ether to extract the BTDB, the ether was removed *in vacuo*, to leave BTDB as a red/orange oil.

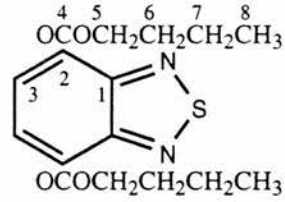

^1H n.m.r. ($CDCl_3$) δ 1.05 (CH_3, t), 1.55 (CH_2, m), 1.85 (CH_2, m), 4.50 (OCH_2, t), 8.40 (2H, aromatic protons, s). ^{13}C n.m.r. ($CDCl_3$) δ 13.7 (C(8)), 19.2 (C(7)), 30.7 (C(6)), 65.9 (C(5)), 127.2 (C(2)4ry), 131.6 (C(3)), 152.7 (C(1)), 164 (C(4)). Found m/z 336.1139 . Empirical requires 336.1144. Microanalysis Found: C, 56.9; H, 6.06; N, 8.44; $C_{16}H_{20}O_4N_2S$ Requires: C, 56.1; H, 5.99; N, 8.33%.

6.12.4 Preparation of the Diethyl Ester of 2,1,3-benzothiadiazole-4,7-dicarboxylic acid (BTDE)[18]

A solution of BTDN (2g, 0.011 mol.) in aqueous NaOH (20 cm^3, 25% solution) was heated under reflux until the evolution of NH_3 had ceased (18 — 24 hours).

Acidification with HCl, afforded a brown solid, the dicarboxylic acid, which was filtered and oven dried. The dicarboxylic acid was then treated with refluxing thionyl chloride (75 cm^3) for twenty-four hours and after cooling, filtering and evaporation of the filtrate gave the crude dicarboxylic acid dichloride (1.2g). The acid dichloride was then added to a solution of pyridine (0.9g) in ethanol (15 cm^3) which was refluxed for three hours. Ethanol was evaporated *in vacuo* and to ensure complete removal, petroleum ether 40/60 (15 cm^3) was added then removed *in vacuo*

to leave a yellow solid of BTDE plus impurities.

Chromatography of the solid was performed by absorbing the solid onto alumina (Type II-III) and placing on top of a dry alumina column (10 cm x 2 cm). The impurities were eluted as a yellow band using petroleum ether 40/60, to leave BTDE still absorbed to the alumina at the top of the column. The alumina was then removed and washed with ether to extract the BTDB, the ether was removed *in vacuo*, to leave BTDE as a yellow solid. The solid was then recrystallised from petroleum ether 40/60:ethyl acetate (3:1 v/v) at -78°C. The pale yellow solid was then filtered to give BTDE (0.75g, 2.7 x 10^{-3} mol, 58%), m.p. 62.5 — 64°C, lit. m.p. 65°C.

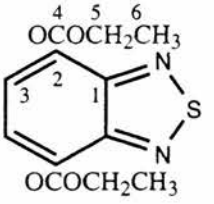

^{1}H n.m.r. ($CDCl_3$) δ 1.45 (CH_3, t), 4.55 (CH_2, q), 8.37 (CH, s). ^{13}C n.m.r. ($CDCl_3$) δ 14.3 (C(6)), 62.1 (C(5)), 127.2 (C(2)), 131.7 (C(3)), 152.8 (C(1)), 163.9 (C(4)).

6.12.5 Preparation of 4,7-Benzofurazandicarbonitrile

STEP 1 - Preparation of 2,3-dinitro-1,4-dibromobenzene [19,20]

1,4-dibromobenzene (30g, 0.127 mol) was dissolved in fuming nitric acid (110 cm^3) and mixed with sulfuric acid (110 cm^3, concentrated). The mixture was warmed and allowed to boil gently for three hours in a flask closed with a porcelain crucible after which the oil was allowed to cool. Before the oil solidified it was poured into water (600 cm^3), in an evaporating dish for ease of removing the solid. The solid was filtered and washed with water then dried over silica gel, overnight. The desired compound was separated from the other two isomers by a two stage crystallisation using glacial acetic to produce white needles. Yield 2g (6.13 x 10^{-3} mol, 5%) m.p. 158 — 160°C, lit. 159 — 160°C.

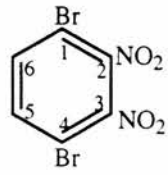

^{1}H n.m.r. ($CDCl_3$) δ 7.7 (2H, s).

STEP 2 - Preparation of 3,6-dibromo-2-nitroaniline [21]

Anhydrous ammonia was bubbled through a suspension of 2,3-dinitro-1,4-dibromobenzene (4.60g, 0.014 mol) in refluxing absolute ethanol (150 cm^3) for three hours. After 48 hours at 25°C, the orange solution was refluxed for an additional three hours while ammonia was passed through the solution. Evaporation gave an orange solid which on recrystallising from ethanol, gave 3,6-dibromo-2-nitroaniline (3.86g, 0.013 mol) as yellow needles, 84%, m.p. 72—74°C, lit. 75°C.

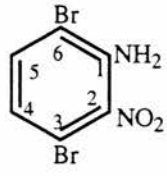

^{1}H n.m.r. ($CDCl_3$) δ 6.9 (1H, d), 7.4 (1H, d). ^{13}C n.m.r. ($CDCl_3$) δ 110.1 (C(5)), 114.8 (C(4)), 122.8 (C(6)), 135.4 (C(3)), 136.4 (C(1)), 140.1 (C(2)).

STEP 3 - Preparation of azidodibromonitrobenzene [21]

Finely pulverised sodium nitrite (1.37g, 0.02 mol) was gradually added to concentrated sulfuric acid (9.5 cm^3) with stirring at 0°C. The suspension was heated to 50°C and held at this temperature until the sodium nitrite dissolved. The solution was cooled and a finely divided suspension of 3,6-dibromo-2-nitroaniline (4.80g, 0.015 mol) in glacial acetic acid (49 cm^3) was added gradually with stirring while the temperature was maintained below 15°C.

After the diazotisation was complete, the pale yellow suspension was added dropwise to a solution of sodium azide (1.36g, 0.021 mol) in water (23.5 cm^3) with vigorous stirring at 10 °C. The resulting precipitate was filtered, washed with water and recrystallised from n-hexane to give pale yellow needles of 1-azido-3,6-dibromo-2-nitroaniline. Yield 3.50g, (0.011 mol, 70%).m.p. 67 — 69°C, lit. 71.5 — 72.5°C.

STEP 4 - Preparation of 4,7-dibromobenzofurazan oxide [21]

This compound was prepared by the thermal decomposition of the corresponding o-nitroazide. A solution of 1-azido-3,6-dibromo-2-nitrobenzene (3.50g, 0.011 mol) in anhydrous toluene (80 cm^3) was refluxed for 29 hours. Evaporation gave a tan solid. Dry column chromatography in toluene-n-hexane (1:1 v/v) on alumina gave a yellow band which eluted steadily to yield 4,7-dibromobenofurazan oxide which crystallised from 95% ethanol, to form yellow prisms. m.p. 128 — 130°C, lit. 132°C. The yield was 2.21g (7.52 mmol, 42%).

^1H n.m.r. ($CDCl_3$) δ 7.3 (CH, s), 7.4 (CH, s). ^{13}C n.m.r. ($CDCl_3$) δ 105 (C(4)), 110.7 (C(7)), 131.7 (C(5)), 134.9 (C(6)), 150.(C(9)), 151.9 (C(8)).

STEP 5 - Preparation of 4,7-dibromobenzofurazan [21]

The dibromobenzofurazan was prepared by reduction of the furazan oxide with hydroxylamine followed by distillation of the alkaline solution of the dioxime. A solution of 4,7-dibromobenzofurazan oxide, (2.21g, 0.007 mol) in hot ethanol (100 cm^3, 95%) was cooled rapidly in an ice bath to produce a finely divided suspension. A solution of hydroxylamine hydrochloride (0.83 g, 0.009 mol) in water (4.6 cm^3) was added followed by aqueous potassium hydroxide (25%) with stirring and cooling until nitrogen evolution ceased. Distillation of the deep red alkaline solution produced a yellow solution from which the final product was extracted using methylene chloride. The methylene chloride was then removed *in vacuo* to give a yellow solid which was recrystallised from petroleum ether 40/60 : ethyl acetate (3:1 v/v) to give 4,7-dibromobenzofurazan (1.02g, 3.66 x 10^{-3} mol, 52%), m.p. 109 — 111°C, lit. 113°C.

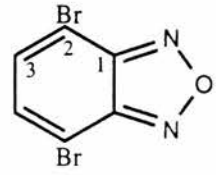

^1H n.m.r. ($CDCl_3$) δ 7.5 (2H's, s). ^{13}C n.m.r. ($CDCl_3$) δ 108.7 (C(2)), 134.2 (C(3), 149.4 (C(1))

STEP 6 - Preparation of 4,7-benzofurazandicarbonitrile (BFDN)[22]

A solution of 4,7-dibromobenzofurazan (1.02g 0.003 mol) and cuprous cyanide (0.68g) in DMF (4.55 cm^3) was stirred and heated at 150 — 155°C for 1.5 hours. DMF was removed under reduced pressure and the residue was extracted several times with boiling xylene. After evaporation of the xylene, the crude dinitrile was recrystallised from petroleum ether 40/60 at -78°C and filtered to give yellow-brown crystals of BFDN, 0.35g (2.06 mmol, 56%) m.p. 182 — 185°C, lit. 185 — 188°C.

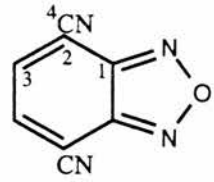

^1H n.m.r. ($CDCl_3$), δ 8.4 ppm. ^{13}C n.m.r. ((CD_3)CO), δ 106.7 (C(2)), 113.9 (C(4)), 140.6 (C(3)), 148.7 (C(1)). Found : m/z 170.0226. Empirical requires 170.0229. Microanalysis Found: C, 56.51; H, 1.38 ; N, 31.64 $C_8H_2N_4O$ Requires: C, 56.43 ; H, 1.20 ; N, 32.90%.

6.12.6 Method 2 - Preparation of 4,7-Benzofurazandicarbonitrile

STEP 1 - Preparation of Tetrabromotetrahydrobenzofurazan oxide[23]

Benzofurazan oxide (10g, 0.074 mol., Aldrich) was dissolved in carbon disulphide (100 cm^3) to which was added bromine (12g) in carbon disulphide (20 cm^3). The solution was illuminated by white light from a 500 W Tungsten Halogen Lamp for 8 hours. Evaporation of the carbon disulphide gave tetrabromotetrahydrobenzofurazan oxide and impurities and upon recrystallisation from ethanol (95%) gave white crystals. (15g, 0.022 mol, 30%) m.p.169°C, lit. 170°C.

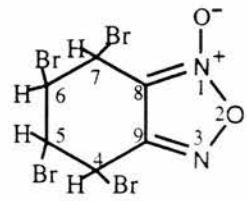

^1H n.m.r. (CD_2Cl_2) δ 4.75—5.1 (2H's, m), 5.3—5.75 (2H's, m), ^{13}C n.m.r. (CD_2Cl_2) δ ,35.1 (C(5)), 35.3 (C(6)), 47.4 (C(4)), 47.9 (C(7)), 151.9 (C(9)), 152.2 (C(8)).

Note : Using the same experimental conditions as above, with benzofurazan, resulted in the final 'product', upon analysis by g.c.m.s., being shown to be unreacted benzofurazan.

STEP 2 - Preparation of 4,7-Dibromobenzofurazan oxide[23]

Tetrabromotetrahydrobenzofurazan oxide (15g) was added to potassium hydroxide soluiton (5 M) with stirring. HBr was liberated and a yellow solid (11.5g) was produced. Recrystallisation from ethanol afforded yellow crystals of dibromobenzofurazan oxide (10g, 77%) m.p. 129 — 131°C, lit. 132°C.

STEP 3 - Preparation of 4,7-Dibromobenzofurazan[21]

See section 6.7.6, step 5.

STEP 4 - Preparation of 4,7-Benzofurazandicarbonitrile[21]

See section 6.7.6, step 6.

6.12.7 Preparation of Benzofurazan[21]

Benzofurazan oxide (30g, 0.22 mol., Aldrich) was dissolved in hot ethanol (510 cm^3, 95%), then rapidly cooled in an ice bath to produce a finely divided suspension. A solution of hydroxylamine hydrochloride (11.2 g) in water (61.2 cm^3) was added with stirring followed by potassium hydroxide solution (25%) with cooling until the evolution of N_2 ceased. Steam distillation of the deep red alkaline solution produced a

yellow solution from which the final product was extracted using methylene chloride. The methylene chloride was then removed *in vacuo* to give a yellow solid which was recrystallised from ethanol (95%) to give benzofurazan (21 g, 0.175 mol., 70%), m.p. 52 — 54°C, Lit. 53 — 55°C.

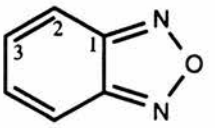

^{1}H n.m.r. ($CDCl_3$) δ 7.45 (2H's), 7.96 (2H's). ^{13}C n.m.r. ($CDCl_3$) δ 116.31 (C(3)), 131.52 (C(2)), 148.98 (C(1)4^{ry}).

References

1. *Determination and use of Stability Constants*, A.E. Martell and R.J. Motekaitis (pub. VCH), 1988.
2. N.E. Good, D. Winget, W. Winter, T.N. Connolly, S. Izawa and R.M.M. Singh, *Biochem.*, 1966, 5, 467.
3. M.J.S. Dewar and W. Thiel, *J. Am. Chem. Soc.*, 1977, **99**, 4899.
4. M.J.S. Dewar, E.G. Zoedirsch, E.F. Heady and J.J.P. Stewart, *J. Am. Chem. Soc.*, 1985, **107**, 3902.
5. J.J.P. Stewart, *J. Comp. Chem.*, 1989, **10**, 209.
6. J.J.P. Stewart, *J. Comp.- Aided Molecular Design*, 1990, **4**, 1.
7. M.J.S. Dewar and Y.-C. Yuan, *Inorg. Chem.*, 1990, **29**, 3881.
8. A.M. Christie, University of St. Andrews, PhD Thesis, 1995.
9. M.K. Ahn, D.J. Reuland and K.D. Chadel, *J. Chem. Educ.*, 1985, 74.
10. M.M. Bradford, *Anal. Biochem.*, 1976, **72**, 248.
11. O.H. Lowry, N.J. Roserough, A.L. Farr and R.J. Randall, *J. Biol. Chem.*, 1951, **193**, 265.
12. R. Cammack, V.M. Fernandez and E.C. Hatchikan, *Methods in Enymology*, 1994, **243**, 43.
13. E.C. Hatchikan, A.S. Traore, V.M. Fernandez and R. Cammack, *Biochim. Biophys. Acta.*, 1985, **832**, 69.
14. P.-A. Brugger, P. Cuendet and M. Gratzel, *J. Am. Chem. Soc.*, 1981, **103**, 2923.
15. K. Aika, L.L. Ban, I. Okura, S. Namba and J. Turkevich, *J. Res. Inst. Catalysis Hokkaido Univ.*, 1976, **24**, 54.
16. K. Pilgram, M. Zupan and R. Skiles, *J. Het. Chem.*, 1970, **7**, 629.11.
17. K. Pilgram, *J. Het. Chem.*, 1974, **11**, 777.
18. K. Pilgram, *J. Het. Chem.*, 1974, **11**, 835.
19. C.L. Jackson and D.F. Calhane, *Am. Chem. J.*, 1902, **28**, 451.
20. C.J. Sunde, G. Johnson and C.F. Kade, *J. Org. Chem.*, 1939, 548.
21. W. Moje, *J. Org. Chem.*, 1964, **29**, 3722.
22. K. Pilgram and M. Zupan, *J. Het. Chem.*, 1974, 813.
23. D.L. Hammick, W.A.M. Edwardes, *J. Chem. Soc.*, 1932, 3308.